Biomechanical study of the action of compression bandages on the lower leg

Fanette Chassagne

N°d'ordre NNT : 2017LYSEM015

THESE de DOCTORAT DE L'UNIVERSITE DE LYON
opérée au sein de
l'Ecole des Mines de Saint-Etienne

Ecole Doctorale N° 488
Sciences, Ingénierie, Santé

Spécialité de doctorat :

Mécanique et Ingénierie

Soutenue publiquement le 19/06/2017, par :

Fanette CHASSAGNE

Étude biomécanique de l'action des bandes de compression sur le membre inférieur

Biomechanical study of the action of compression bandages on the lower leg

---

Devant le jury composé de :

Président :	SCHACHER, Laurence	Professeur, ENSISA, Muhlouse
Rapporteurs :	MITTON, David	Professeur, IFSTTAR, Lyon
	GEFEN, Amit	Professeur, Tel Aviv University, Israel
Examinateurs :	PARTSCH, Hugo	Professeur, Medical University, Vienna, Austria
	DUBUIS, Laura	Maître de conférences, UCBL, Lyon
Directeur de thèse :	MOLIMARD, Jérôme	Professeur, Mines Saint-Etienne
Co-directeur de thèse :	GIRAUX, Pascal	Professeur, UJM, Saint-Etienne
Encadrant :	BADEL, Pierre	Maître-assistant, Mines Saint-Etienne
Invité :	CONVERT, Reynald	Directeur R&D, Thuasne, Saint-Etienne

Spécialités doctorales	Responsables :	Spécialités doctorales	Responsables
SCIENCES ET GENIE DES MATERIAUX	K. Wolski Directeur de recherche	MATHEMATIQUES APPLIQUEES	O. Roustant, Maître-assistant
MECANIQUE ET INGENIERIE	S. Drapier, professeur	INFORMATIQUE	O. Boissier, Professeur
GENIE DES PROCEDES	F. Gruy, Maître de recherche	SCIENCES DES IMAGES ET DES FORMES	JC. Pinoli, Professeur
SCIENCES DE LA TERRE	B. Guy, Directeur de recherche	GENIE INDUSTRIEL	X. Delorme, Maître assistant
SCIENCES ET GENIE DE L'ENVIRONNEMENT	D. Graillot, Directeur de recherche	MICROELECTRONIQUE	Ph. Lalevée, Professeur

EMSE : Enseignants-chercheurs et chercheurs autorisés à diriger des thèses de doctorat (titulaires d'un doctorat d'État ou d'une HDR)

ABSI	Nabil	CR	Génie industriel	CMP
AUGUSTO	Vincent	CR	Image, Vision, Signal	CIS
AVRIL	Stéphane	PR2	Mécanique et ingénierie	CIS
BADEL	Pierre	MA(MDC)	Mécanique et ingénierie	CIS
BALBO	Flavien	PR2	Informatique	FAYOL
BASSEREAU	Jean-François	PR	Sciences et génie des matériaux	SMS
BATTON-HUBERT	Mireille	PR2	Sciences et génie de l'environnement	FAYOL
BEIGBEDER	Michel	MA(MDC)	Informatique	FAYOL
BLAYAC	Sylvain	MA(MDC)	Microélectronique	CMP
BOISSIER	Olivier	PR1	Informatique	FAYOL
BONNEFOY	Olivier	MA(MDC)	Génie des Procédés	SPIN
BORBELY	Andras	MR(DR2)	Sciences et génie des matériaux	SMS
BOUCHER	Xavier	PR2	Génie Industriel	FAYOL
BRODHAG	Christian	DR	Sciences et génie de l'environnement	FAYOL
BRUCHON	Julien	MA(MDC)	Mécanique et ingénierie	SMS
CAMEIRAO	Ana	MA(MDC)	Génie des Procédés	SPIN
CHRISTIEN	Frédéric	PR	Science et génie des matériaux	SMS
DAUZERE-PERES	Stéphane	PR1	Génie Industriel	CMP
DEBAYLE	Johan	CR	Sciences des Images et des Formes	SPIN
DEGEORGE	Jean-Michel	MA(MDC)	Génie industriel	Fayol
DELAFOSSE	David	PR0	Sciences et génie des matériaux	SMS
DELORME	Xavier	MA(MDC)	Génie industriel	FAYOL
DESRAYAUD	Christophe	PR1	Mécanique et ingénierie	SMS
DJENIZIAN	Thierry	PR	Science et génie des matériaux	CMP
DOUCE	Sandrine	PR2	Sciences de gestion	FAYOL
DRAPIER	Sylvain	PR1	Mécanique et ingénierie	SMS
FAUCHEU	Jenny	MA(MDC)	Sciences et génie des matériaux	SMS
FAVERGEON	Loïc	CR	Génie des Procédés	SPIN
FEILLET	Dominique	PR1	Génie Industriel	CMP
FOREST	Valérie	MA(MDC)	Génie des Procédés	CIS
FOURNIER	Jacques	Ingénieur chercheur CEA	Microélectronique	CMP
FRACZKIEWICZ	Anna	DR	Sciences et génie des matériaux	SMS
GARCIA	Daniel	MR(DR2)	Sciences de la Terre	SPIN
GAVET	Yann	MA(MDC)	Sciences des Images et des Formes	SPIN
GERINGER	Jean	MA(MDC)	Sciences et génie des matériaux	CIS
GOEURIOT	Dominique	DR	Sciences et génie des matériaux	SMS
GONDRAN	Natacha	MA(MDC)	Sciences et génie de l'environnement	FAYOL
GRAILLOT	Didier	DR	Sciences et génie de l'environnement	SPIN
GROSSEAU	Philippe	DR	Génie des Procédés	SPIN
GRUY	Frédéric	PR1	Génie des Procédés	SPIN
GUY	Bernard	DR	Sciences de la Terre	SPIN
HAN	Woo-Suck	MR	Mécanique et ingénierie	SMS
HERRI	Jean Michel	PR1	Génie des Procédés	SPIN
KERMOUCHE	Guillaume	PR2	Mécanique et Ingénierie	SMS
KLOCKER	Helmut	DR	Sciences et génie des matériaux	SMS
LAFOREST	Valérie	MR(DR2)	Sciences et génie de l'environnement	FAYOL
LERICHE	Rodolphe	CR	Mécanique et ingénierie	FAYOL
MALLIARAS	Georges	PR1	Microélectronique	CMP
MOLIMARD	Jérôme	PR2	Mécanique et ingénierie	CIS
MOUTTE	Jacques	CR	Génie des Procédés	SPIN
NIKOLOVSKI	Jean-Pierre	Ingénieur de recherche	Mécanique et ingénierie	CMP
NORTIER	Patrice	PR1	Génie des Procédés	SPIN
O CONNOR	Rodney Philip	MA(MDC)	Microélectronique	CMP
OWENS	Rosin	MA(MDC)	Microélectronique	CMP
PERES	Véronique	MR	Génie des Procédés	SPIN
PICARD	Gauthier	MA(MDC)	Informatique	FAYOL
PIJOLAT	Christophe	PR0	Génie des Procédés	SPIN
PINOLI	Jean Charles	PR0	Sciences des Images et des Formes	SPIN
POURCHEZ	Jérémy	MR	Génie des Procédés	CIS
ROBISSON	Bruno	Ingénieur de recherche	Microélectronique	CMP
ROUSSY	Agnès	MA(MDC)	Microélectronique	CMP
ROUSTANT	Olivier	MA(MDC)	Mathématiques appliquées	FAYOL
SANAUR	Sébastien	MA(MDC)	Microélectronique	CMP
STOLARZ	Jacques	CR	Sciences et génie des matériaux	SMS
TRIA	Assia	Ingénieur de recherche	Microélectronique	CMP
VALDIVIESO	François	PR2	Sciences et génie des matériaux	SMS
VIRICELLE	Jean Paul	DR	Génie des Procédés	SPIN
WOLSKI	Krzystof	DR	Sciences et génie des matériaux	SMS
XIE	Xiaolan	PR1	Génie industriel	CIS
YUGMA	Gallian	CR	Génie industriel	CMP

Mise à jour : 12/12/2016

Un jour j'irai vivre en Théorie,
parce qu'en Théorie tout se passe bien.

Remerciements - *Acknowledgments*

Oulalalala! Difficile tâche que d'écrire ses remerciements ...
Après plusieurs kilomètres de bandes de compression et quelques milliers d'heures de calculs cluster, voici la fin d'une aventure scientifique, mais surtout humaine. Le moment est donc venu de remercier toutes les personnes qui, d'une manière ou d'une autre, ont contribué à cette aventure, le tout dans un ton plus léger que la rédaction (plutôt caustique et rempli d'ironie). Avant tout, je tiens par avance à m'excuser pour d'éventuels oublis.

Afin d'être fidèle au schéma classique, je vais commencer par la fin de l'histoire : la soutenance (ce moment tant attendu ...), où 3 ans de travail sont donc résumés en 45 minutes de présentation.
So! (pour toi Boris ;)), I first want to thank Pr. David Mitton and Pr. Amit Gefen for the review of my manuscript (a lot to read) and all the relevant questions you asked during my dissertation. I also would like to thank Pr. Hugo Partsch for coming all the way from Austria. It's been a real honor for me and a very interesting discussion about compression bandages.
Passons maintenant au côté féminin de ce jury. Pr. Laurence Schacher, merci d'avoir accepté de présider ce jury, mais aussi, merci pour tout ce que j'ai appris en co-encadrant avec vous ma toute première stagiaire.
Dr. Laura Dubuis, merci d'avoir accepté de participer à ce jury et pour toutes tes questions très intéressantes pendant la soutenance. Tu as surement dû me transmettre la passion des mollets en TD de MMC ;)

Avant d'en arriver à la fin de l'histoire, il m'a fallu l'aide précieuse de mes encadrants. Commençons par Pierre, puisque tu étais dans mon encadrement depuis le début de mon stage... Soyons honnête, je ne ferai pas aussi bien que toi lors de ma soutenance, mais je vais essayer... Tout d'abord je veux vraiment te remercier pour ta disponibilité et ton efficacité, surtout au début de mon stage, mais aussi au fur et à mesure de ma thèse (pour des problèmes Abaqus ou pour apprendre à rédiger un article). Ta passion pour la bioméca et surtout son application clinique m'a motivée à poursuivre en thèse. J'étais ravie de partager avec toi cette passion pour le chocolat ;)
Après avoir pris la folle décision de démarrer ma thèse (toujours motivée par la passion des mollets), s'est rajouté à mon encadrement mon directeur de thèse. Jérôme, merci pour tout ce que tu m'as appris en mécanique expérimentale (aussi bien d'un point de vue technique que sur la manière dont on construit un plan expérimental). En tant que directeur de thèse, tu as su me laisser la liberté de faire mes propres choix tout en me guidant. Cela peut paraître assez bateau, mais je pense que cette liberté m'a aidée à grandir en tant que *bébé chercheur* :)
Merci à tous les deux pour toutes nos discussions et questionnements "Sciences", mais aussi toutes les discussions politique et sport (ou blessure ;)). Pour sûr, avoir travaillé avec vous deux n'a fait que renforcer mon envie de continuer dans la recherche. Pour terminer, mention spéciale à la grande qualité de vos jeux de mots!

En plus de l'expérience *labo* (qui sera plus longuement détaillée par la suite), tout a commencé à Thuasne. Reynald je te remercie pour l'opportunité de stage que tu m'as offerte, sans laquelle je n'aurais jamais fait cette thèse. Merci pour toutes les connaissances en ingénierie textile que tu as pu me transmettre. Que ce soit en stage ou en thèse, tu as toujours su donner une ligne directrice à ce projet et je te remercie de m'avoir donné les moyens (humains, techniques et financiers) de mener à bien ce projet.
Le dernier environnement de cette histoire est l'hôpital, ou la rencontre de deux mondes. Pascal, merci d'avoir apporté une touche médicale à cet encadrement, ce qui fut très enrichissant, et merci de m'avoir permis de réaliser une étude clinique. Cette étude a été une super expérience, scientifique, mais surtout humaine. Et aussi merci pour avoir trouvé ce nom tellement génial pour cette étude : Superbande!
Stéphane, tu n'étais pas dans mon encadrement, mais je tenais à te remercier pour ton aide et ton soutien tout au long de mon cursus.

Au début, il y a les encadrants, puis est venu le moment terrible où je suis moi-même devenue encadrante ... Emilie, Adèle et Clothilde, je tenais à vous remercier pour votre implication dans ce projet. Vous avez eu la patience d'échanger avec moi sur des sujets que je ne connaissais pas ou peu. Vos différents travaux ont particulièrement aidé à l'avancée du projet et j'ai beaucoup appris en travaillant avec vous.

Repartons maintenant depuis le début de l'histoire... avec les premières personnes que j'ai côtoyées, c'est à dire, mes co-bureaux et co-burettes! Et comme j'ai eu un nombre non négligeable de bureaux, la liste est plutôt longue ...

Commençons par mon premier bureau à Thuasne: le bureau des stagiaires !
Merci à Mathilde (qui m'a aussi suivie dans le bureau R&D), Mathilde et Marco pour toutes nos discussions et pique-niques au parc. Après ça, nous avons migré chez les "grands" avec Mathilde, Laure et Frédéric (j'ai particulièrement apprécié travailler avec toi sur cette campagne de mesures de pression :)). Ensuite est arrivé Romain (oh yes Biomécanique!). Merci pour tous ces échanges boulot (Matlab est ma passion), ou moins boulot (anciens combattants de la ME). Grégoire (l'avant dernier arrivé), merci d'avoir rehaussé le niveau humour de ce bureau (ce commentaire est aussi valable pour Romain) et puis Florian, le dernier arrivé, qui a fini de donner un aspect *testostérone* à ce bureau ;)

Mon deuxième bureau était donc celui du CIS ...
Rebecca, merci pour toutes ces discussions et échanges sur la thèse (mais pas que), qui m'avaient permis de me décider pour cette longue aventure de 3 ans et aussi merci d'avoir "essuyer les plâtres" ("Comment je fais ? -> Fais comme Rebecca ;)")
David (Oh Grand Maître Abaqus !!), merci beaucoup pour toute l'aide apportée sur le côté geek de ma thèse, merci pour ta patience (que ce soit pour le temps passé à m'expliquer comment marchait le cluster, ou pour supporter nos blagues *décoratives* et plutôt roses avec Klervi). D'un point de vue beaucoup moins professionnel, tu étais quand même l'autre *un peu* auvergnat passionné de rugby (et de mêlée nocturne :)), de pâtes et avec un talent caché pour le mannequinat ;). En tous cas, je te souhaite beaucoup de réussite pour ton nouveau projet de capitaliste (comme dirait sylvain:)).
Dans notre bureau est ensuite arrivée ma co-burette Klervi (précédemment citée pour ses goûts en matière de déco rose)! Première coureuse à pied (je me rappelle encore juste avant la course où tu me disais "mais pourquoi je t'ai suivie ?!"), amatrice de pringles au paprika et de Causette, je dois souligner la qualité de tes déguisements! Tu as été une parfaite co-burette (;)), mais pas que !

Et enfin Sabri. Très discret au début, mais beaucoup moins à la fin ;)
Après un déménagement, un nouveau co-bureau. Witold, merci pour toutes ces discussions (faut quand même dire qu'on a tendance à plus papoter dans un bureau à 2). On avait un peu de mal à se croiser, donc quand on se voyait on avait plein de choses à raconter :)

Maintenant, passons à mon dernier bureau, aussi appelé l'*openspace*. Merci Oscar, pour ce super repas que tu avais organisé, pour la bonne humeur que tu as amenée et pour l'aide apportée à Clothilde. Je suis très fière de t'avoir convertie aux pauses café!
La deuxième occupante de ce bureau était Caro (1ère du nom). D'un point de vue professionnel, un immense merci pour toute l'aide que tu m'as apportée (même si t'oubliais toujours qu'on avait rdv ;)), pour avoir détaillé ce que voulaient dire toutes ces abréviations, pour tes grandes capacités de persuasion et pour être quand même venue voir une fois ce que je faisais!
D'un point de vue moins professionnel, je ne sais pas si je dois te remercier pour l'ambiance musicale de ce bureau ou pour tes super règles de vie (pour plus de détails, veuillez vous adresser directement à l'intéressée) ;) En tout cas, tu t'es intégrée comme une cheffe dans le milieu des *ingénieurs* !

Pendant ces 3 ans, j'ai travaillé dur, mais rarement toute seule ;)
Nico, un immense merci pour ta patience et ton efficacité, et pour tout ce que tu as apporté à cette thèse! Mille mercis aussi pour toute l'aide que tu as apportée à Adèle :)
Dans ces grands projets de conception mécanique, il y avait Fanny (ou plutôt devrais-je dire Mamie ;)). Membre du club des fétichistes du mollet et grande féministe, j'ai vraiment adoré partager toutes ces séances de compression du mollet avec toi (c'est quand même une super déclaration que je fais là...).
Etienne (geek en devenir), merci pour ta patience, pour avoir répondu à toutes mes questions stupides, et m'avoir permis de comprendre le fonctionnement (plutôt obscur au début) du service. En tout cas, j'ai beaucoup appris, au niveau médical, humain et scientifique (surtout en stat') et j'espère t'avoir transmis ma passion pour Matlab ;) Je te souhaite beaucoup de réussite pour cette aventure qu'est la "thèse de sciences" comme vous dites! (Et n'oublie pas, le secret, c'est la pause café ;))

Betty, Amélie et Françoise, je tiens à vous remercier pour votre gentillesse et votre grande efficacité. De même, Thierry (Louvancourt), Olivier, Jérôme et toutes les personnes du service Informatique de Thuasne, un très grand merci pour votre disponibilité et pour avoir solutionné nombre de mes problèmes.
Diana, merci pour ton aide précieuse et ton efficacité pour la rédaction du protocole (et aussi pour m'avoir accueillie plus d'une fois pour un café :)). Adeline et Marion, je voulais vous remercier de m'avoir guidée dans le monde obscur des études cliniques.

Un immense merci à tous les doctorants que j'ai pu côtoyer, et comme la tradition l'impose, on commence par les plus vieux ;).
Pierre-Yves Rohan (ancien membre du club des fétichistes du mollet), j'ai été ravie de t'avoir croisé à ma première conf' dans le Nord, merci beaucoup pour ta bonne humeur, ton aide et tes conseils au début de mon stage. On s'est pas croisé très longtemps mais j'espère qu'on se recroisera dans d'autres conf' ;)
Baptiste (1er du nom), mon premier encadrant de projet de biomécanique quand j'étais petite. Merci pour ton aide scientifique ou pour chercher des postdocs, pour m'avoir fait découvrir ce en quoi consistait "faire le sanglier" et pour cette visite matinale de Pittsburgh ("mais Baptiste, il fait encore nuit là !?!").
Merci aussi à Laura, la reine des pub quizz, à Aaron et Benjamin pour votre accueil ainsi qu'à

Manu pour tous ces footings qui m'ont permis de découvrir Sainté !
Sareh, je tiens à te remercier pour ta spontanéité, ta gentillesse et tes remerciements de thèse au top! Je tiens aussi à souhaiter bon courage aux nouveaux (plus si nouveaux que ça en fait), Cristina, Romain, Sophie, Radha, Aymeric, Moshein, Solmaz et les futurs nouveaux Nicolas et Joseph (ou Junior).
Un immense merci à ceux du bâtiment C, Estelle, Antoine, Coach Jules et Andréa pour tous les footings et soirées et aussi à ceux de l'ASEC, Clothilde, Laura et Guillaume :)

Après, il y avait ce groupe emblématique, dont j'étais la plus fidèle groupie : 3 ou 4 ans plus tard ;) Le bassiste (David) et la guitariste (Fanny) étant déjà cités, il reste tout de même le chanteur, le batteur et le guitariste. Omar, le littéraire du groupe, un immense merci pour tous nos longs échanges et discussions (plutôt sérieux :)) et pour nous avoir fait découvrir le Liban! Baptiste (2ème du nom) (ou Papa Charbo), merci pour ta sagesse et pour avoir été un super papa: tu sais cuisiner des pâtes et tu amenais des kinders quand on allait voir des dessins animés ;) Boris, capable d'écrire 10 lignes sur une salade de pâtes et dessinateur de fémur en série, merci pour ta passion pour les déguisements toujours au top, pour l'organisation des We Ski, et pour tes capacités dansistiques inégalables (surtout sur Tunak-Tunak ;)). Se sont ensuite ajoutés au groupe, devenu "A billig" : Sylvain (cité plus loin) et Piou-piou, amateur de dessins animés et expert à *Cards against humanity* (mélange surprenant quand même ...). Toujours dans la musique, merci à Gwen, ma meilleure élève en danse classique ;)
A quand le prochain concert?!

Travailler c'est bien, mais soyons honnêtes je n'ai pas fait que ça ... J'ai aussi beaucoup couru (en mode salon de thé, hein Sylvain ?!) et jamais toute seule (c'est pas marrant, on ne peut pas parler ...).

Armelle (ou Copine), merci pour toutes nos longues discussions, pour nous avoir fait découvrir la fête de la bière (un grand moment ;)) et pour les courses qu'on a faites ensemble :)
Maman Agathe, étrangère du bâtiment C, toujours motivée pour bouger et fan du "rice & curry"! Merci pour ton dynamisme et ta *positive attitude* pendant nos différents week-ends et vacances ainsi que pour ton aide précieuse le week-end et le lendemain de ma thèse ;)
Dans le groupe des *coureurs de l'extrême* nous pouvons ajouter les Martin-Gestin. Sylvain inventeur du concept de la sortie "salon de thé", adepte des marcels (passion partagée avec Roro et Pierrot) et fan de Magic System; Mathilde, la deuxième bretonne du groupe, capable de courir avec un bras presque cassé (on t'avait dit que le trampo c'était dangereux :)). Viennent ensuite, Thierry et Pierrot. Thierry, maniaque des siphons de lavabo et organisateur de la course à la saucisse, merci pour toutes ces discussions boulot (ou pas) pendant des pauses café toujours très courtes (euh...), ces nombreuses courses et WE, ainsi que tes récits ou aventures toujours aussi incroyables :) Pierrot (la plus belle des fées), amateur de déguisements et de perruques, compagnon des footings matinaux avec Fanny et Copine l'année d'après, merci pour ton dynamisme et nos longues discussions autour d'un café ou pendant un footing :) Éclate-toi au pays des karibous !
Jo, merci d'avoir eu cette idée géniale pour notre premier défi :) (c'est promis on en trouvera d'autres ;)) Merci aussi aux autres *coureurs de l'extrême*, Ana & Benjamin, pour nous avoir accompagnés dans ces projets légèrement stupides.

Après la course à pied, il y avait quand même un deuxième truc essentiel: le café!
Un immense merci à toutes les personnes avec qui j'ai pu échanger autour d'un café (et d'un carré de chocolat:)).
Au CIS, Claire, Woo-Suck, Laurent, Afafe, David & Jérémy, Coralie, Lara, Nathalie, Valérie,

Clémentine, Francesca, Olfa, Victor et Jamal.
Je tiens aussi à remercier Joao (prend bien soin de mon appart ;)), Brieuc, Jie, Xavier, Maxym, Olivier, et Jessie pour m'avoir si souvent accueillie au C3 :)

Merci aussi à mes compagnons de café du MPR, Caro (2ème du nom) & Alex. Caro, merci pour ta bonne humeur et pour ton soutien en juin ;) Alex, merci beaucoup pour ton accueil dans le service et pour nous avoir permis (avec Boris) de découvrir le côté nocturne d'un congrès (et merci aussi à Tata ;)).
Je tiens aussi à remercier très chaleureusement toutes les personnes que j'ai côtoyées au MPR pour leur accueil.
Un immense merci à toutes les personnes de la R&D de Thuasne, Jérémy, Nicolas, Fanny, Sabrina G et Sabrina M, Céline, Louise, Aurélia, Nathalie et Laurence, pour votre accueil, pour m'avoir beaucoup appris sur le textile et pour être venu assister à ma soutenance (ça m'a fait très plaisir :)).
Je tiens aussi à remercier les gens du J3 et ceux de mon cours d'allemand (faut l'avouer, on était super fort!), pour votre accueil et votre bonne humeur: Loïc, Jean-Marc, Michal, Laure et Jérémy.

Une dernière chose importante pendant ces 3 ans était le pipeau!
Merci à toutes les personnes que j'ai cotoyées au Noac (ou Orchestre Massenet) pour votre accueil et votre bonne humeur que ce soit pour les répèt', les concerts ou les temps moins musicaux. Valérie, merci beaucoup pour votre patience, et pour tout ce que j'ai appris durant ces 3 ans de cours avec vous.
En dehors de Sainté, un grand merci à Agathe, pour ton accueil pendant l'ESB (mais pas que) et nos longues discussions (parfois sur la thèse quand même ;)).
Jean (Merci bonus d'être venu à ma soutenance :)), Gio, Vanessa, Adrien, Béné et Ravit, merci pour tous nos week-end rando et ski de fond ou week-end tout court et d'avoir supporté mes longues tirades sur mon quotidien de doctorante ;) Merci aussi à Charlène, Estelle, Élise et Alicia pour nos soirées entre filles :)

Et pour finir (last but not least), Maman, Papa, Sylvain, un très grand merci pour votre soutien pendant ces longues études (promis maintenant c'est fini!). Merci à vous 3 ainsi que Simone, Rinou et Clarisse pour le pot de thèse de folie que vous avez organisé !

A tous ceux cités précédemment, et à tous ceux que j'aurais oubliés :

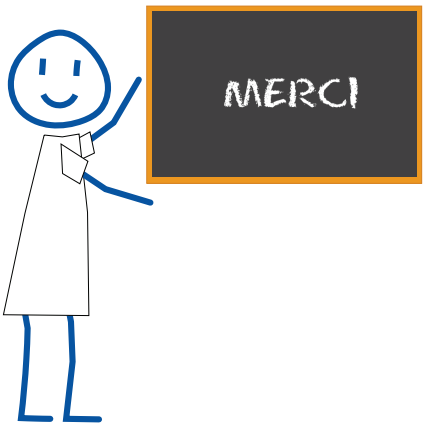

Contents

List of Figures

List of Tables

Chapter 1

Introduction Générale - *General Introduction*

L'insuffisance veineuse est une pathologie chronique qui va de la sensation de "*jambe lourde*" à l'ulcère veineux, sa forme la plus sévère. Une des modalités de traitement la plus courante pour ces pathologies est la compression du membre inférieur. Ce traitement compressif, dont l'efficacité clinique est largement admise, est réalisé grâce à des chaussettes ou des bandes de compression. Ces dernières sont le plus souvent utilisées au début du traitement ou pour traiter des pathologies sévères. En effet, le traitement des pathologies les plus sévères requiert un haut niveau de pression ($> 40\ mmHg$) qui peut être atteint avec une seule bande ou en superposant plusieurs bandes. De plus, à la phase initiale du traitement, la morphologie de la jambe peut rapidement évoluer (réduction rapide de l'œdème) et une seule bande peut s'adapter à différentes morphologies alors que différentes tailles de chaussettes sont nécessaires pour des morphologies variables.
Les bandes sont enroulées sur la jambe, avec un allongement donné, le plus souvent en spirale à 2 ou 3 recouvrements, c'est à dire que la jambe est couverte par 2 ou 3 couches de bandes (pour une application à 2 ou 3 recouvrements la bande est recouverte à la moitié ou au tiers de sa hauteur).

Les chaussettes ou les bandes de compression appliquent une pression sur la surface externe de la jambe, appelée pression d'interface, qui est ensuite transmise aux vaisseaux via les tissus mous (tissus musculaires et adipeux). Cette pression d'interface, principe actif du traitement, impacte directement l'effet thérapeutique mais aussi l'observance du traitement.
Pour les bandes de compression, cette pression d'interface dépend de différents paramètres liés à la bande elle-même (propriétés mécaniques du textile, technique de pose de la bande, ...) ou au patient (morphologie du membre inférieur, ...). Il est donc essentiel d'évaluer l'impact de ces paramètres sur la pression afin d'adapter le traitement à chaque patient et à sa pathologie.
A ce jour, la méthode la plus courante pour prédire les pressions appliquées par un bandage est la Loi de Laplace. Cette équation purement théorique, dont l'utilisation est remise en question, considère la pression comme étant directement proportionnelle à la tension de la bande (i.e. la force nécessaire pour allonger la bande) et au nombre de recouvrements mais inversement proportionnelle au rayon de courbure local de la jambe. Bien que personnalisée (à minima), cette méthode repose sur de nombreuses hypothèses et reste trop imprécise.
Une autre méthode, mise en œuvre plusieurs fois pour la prédiction des pressions exercées par des chaussettes de compression, est la simulation numérique. Cependant, cette méthode est parfois complexe à mettre en œuvre et coûteuse en temps.

L'objectif de cette thèse est de mieux comprendre les mécanismes influençant la pression exer-

cée par les bandes de compression sur le membre inférieur, dans le but d'être capable de prédire les pressions d'interface de manière personnalisée. L'approche proposée est divisée entre une part expérimentale (mesures de pression d'interface) et une part numérique (modélisation de la pose d'une bande).

Ce projet de recherche est réalisé dans le cadre d'une collaboration entre :

- le Centre Ingénierie et Santé de l'École des Mines de Saint-Étienne, via le département STBio qui travaille sur la biomécanique des tissus mous,
- la société Thuasne, fabricant de nombreux dispositifs médicaux textiles dont des bandes de compression,
- le Service de Médecine Physique et de Réadaptation du CHU de Saint-Étienne, cadre de la partie clinique de ce projet.

Le **Chapitre 2** présente le contexte clinique et biomécanique de ce projet. Après une brève description des pathologies veineuses, l'impact clinique du traitement par bandes de compression est détaillé. Une revue de la littérature permet d'émettre l'hypothèse que la pression d'interface exercée par un bandage (i.e. le principe actif du traitement) dépend :

- des bandes composant le bandage,
- de leurs propriétés mécaniques,
- de la technique de pose,
- de l'allongement des bandes une fois posées,
- de la morphologie de la jambe du patient,
- d'autres paramètres tels que les propriétés mécaniques des tissus mous de la jambe du patient, sa position, les interactions entre les différentes couches de bandes, etc.

Les différentes études ayant évalué l'impact de ces paramètres sur la pression d'interface sont répertoriées dans la suite de ce chapitre. La dernière partie concerne les différentes modélisations développées pour la prédiction de la pression appliquée par une chaussette ou une bande de compression. Suite à cette revue de la littérature, le positionnement de l'étude est précisé.

Le **Chapitre 3** présente deux études préliminaires. Pour la première étude expérimentale, les pressions exercées par différentes bandes posées à 2 ou 3 recouvrements sont mesurées pour 30 sujets. Ces mesures permettent d'évaluer l'impact des propriétés mécaniques des bandes, de la technique de pose, mais aussi de la morphologie de la jambe sur les pressions d'interface. La deuxième étude préliminaire concerne le développement d'une première simulation éléments finis personnalisée de la pose d'une bande. Cette méthode, basée sur la géométrie de la jambe obtenue par un scanner optique, permet d'obtenir la distribution complète des pressions sur la jambe.
Ces deux études ont soulevé des interrogations quant à l'impact des propriétés mécaniques des tissus mous de la jambe et des interactions de surface entre les bandes sur la pression d'interface.

Ainsi le **Chapitre 4** décrit les deux méthodes développées pour la caractérisation de ces deux paramètres. La première est une méthode expérimentale, couplée à une modélisation éléments finis, permettant de caractériser les propriétés mécaniques des tissus mous de la jambe à partir

d'une simple compression de ces tissus par un cylindre. Cette méthodologie a été développée en collaboration avec Fanny Frauziols, travaillant sur la caractérisation des tissus mous de la jambe.
La deuxième méthode permet de caractériser le coefficient de frottement bande-bande, dans des conditions proches de leurs conditions d'utilisation (allongement et pression variables). Cette méthode est basée sur l'adaptation du *Kawabata Evaluation System* qui permet de caractériser le *toucher* d'une étoffe.

Dans le **Chapitre 5**, une nouvelle simulation éléments finis de la pose d'une bande est présentée. La réduction de ce modèle, couplée à une description paramétrique de la géométrie de la jambe, permet de créer un outil de prédiction personnalisée de la pression d'interface appliquée par un bandage. Cette méthode de prédiction, dont la mise en œuvre ne prend que quelques minutes (contre quelques jours pour une simulation éléments finis), est ensuite confrontée aux mesures de pression expérimentales.

Après les études expérimentales et numériques de la pression exercée par une seule bande, le **Chapitre 6** présente les résultats d'une étude clinique sur les pressions appliquées par la superposition de deux bandes de compression. Ces mesures, effectuées sur les deux jambes de 25 patients, permettent d'évaluer l'impact sur la pression des composantes du bandage, mais surtout de l'ordre dans lequel elles sont appliquées. Il est aussi possible de tester le lien entre la pression appliquée par chacune des composantes seules et celle résultant de leur superposition. La méthode de caractérisation des propriétés mécaniques des tissus mous de la jambe, préalablement détaillée dans le Chapitre 3, a été mise en œuvre pour les deux jambes de 24 patients en position assise et debout. L'identification de ces propriétés mécaniques permet d'évaluer leur impact sur les pressions d'interface.

Enfin, les résultats obtenus sont synthétisés et les limites des différentes études sont détaillées. Les perspectives et développements possibles de cette étude sont présentés.

Chaque chapitre est précédé d'un résumé étendu en français rappelant les principales motivations, résultats et conclusions du chapitre.

Chapter 2

Contexte - *Context*

This first chapter describes the clinical and scientific context of this work. A quick overview of venous pathologies is first proposed and is followed by a chapter on compression therapy, either performed thanks to stockings or bandages. From the state of the art on the biomechanics of compression bandages, the positioning of the study but also the main hypothesis are detailed.

Contents

2.1 Résumé

L'état de l'art a montré le besoin de nouveaux outils ou méthodes pour prédire les pressions exercées par un bandage. De nombreux travaux se sont intéressés aux mécanismes d'action des chaussettes de compression ainsi qu'à la transmission de la pression qu'elles exercent sur la jambe vers les veines, via les tissus mous (tissus musculaires et adipeux). Cependant, même si de nombreuses études ont montré l'intérêt clinique des bandes de compression, les mécanismes mis en jeu dans ce traitement sont encore que partiellement compris.

De ce fait, l'objectif de ce travail était de mieux comprendre la pression exercée par une bande de compression sur le membre inférieur, grâce à une approche biomécanique. Cette approche, à la fois expérimentale et numérique, était divisée entre des mesures des pression d'interface et le développement d'une simulation de la pose d'une bande. Cette étude était uniquement focalisée sur la distribution des pressions d'interface. Ainsi, ni les mécanismes de transmission de cette pression via les tissus mous, ni son impact sur l'efficacité du traitement n'ont été étudiés.

Deux études préliminaires, expérimentale et numérique, ont montré que l'approche classique, basée sur la loi de Laplace, était insuffisante pour expliquer la distribution des pressions d'interface. Suite aux questionnements et problématiques soulevés dans ces deux études, le travail a été divisé entre les étapes suivantes :

- le développement d'une nouvelle méthodologie pour la caractérisation personnalisée des propriétés mécaniques des tissus mous du mollet, puisqu'il a été montré que les déformations des tissus mous induites par l'application de la bande devaient être prises en compte,
- la conception d'une méthode de caractérisation du coefficient de frottement bande-bande, car il est possible que ce paramètre ait un impact sur les pressions d'interface,
- la simulation numérique de l'application d'une bande sur la jambe, avec une cinématique d'enroulement réaliste,
- la mesure des pressions d'interface couplée à la caractérisation des propriétés mécaniques des tissus mous de la jambe, dans le cadre d'une étude clinique, pour valider la simulation numérique mais aussi étudier la pression appliquée par la superposition de deux bandes de compression.

Principaux choix et hypothèses.

Les mesures de pression d'interface ont pour objectif de comprendre comment la pression d'interface est générée. Cependant, par simplification, toutes les mesures de cette étude étaient statiques. De plus, elles ont été prises dans un très court intervalle de temps et ne rendent pas compte du comportement à long terme des bandes de compression. La pression a été mesurée à hauteur des points de mesure B1 et C (Figure 2.7). Ces deux points ont été choisis suite aux recommandations d'un article de consensus [Partsch 06]. Le point de mesure B n'a pas été pris en compte dans cette étude car cette région du membre inférieur est essentiellement composée d'os et de tendons.

Parallèlement, une simulation éléments finis 3D de la pose d'une seule bande a été développée. Cette simulation est basée sur des géométries de jambe personnalisées, obtenues avec un scanner optique 3D. L'anatomie de l'intérieur de la jambe était donc inconnue. Les tissus mous de la jambe, composés de tissus musculaires et adipeux, ont été modélisés comme un

seul matériau homogène quasi-incompressible, dont le comportement était hyperélastique. Les muscles ont toujours été considérés comme étant dans un état passif. Les bandes de compression ont été considérées comme un matériau orthotrope dont le comportement mécanique a été modélisé par une loi de comportement élastique linéaire. Le modèle de la jambe est resté simple car le développement de la simulation était principalement focalisé sur la simulation de la pose d'une bande. L'objectif de cette simulation était d'abord d'étudier quels étaient les paramètres qui impactaient la pression d'interface mais aussi de proposer un outil pour la prédiction personnalisée des pressions d'interface.

2.2 Venous pathologies

2.2.1 Anatomy of the lower leg

The *lower leg* is defined as the leg segment from the ankle joint to the knee joint.
The skeleton structure of this segment is composed of two bones: the *tibia* and the *fibula* (Figure 2.1 - B). These two bones are tightly linked by the inter-osseous membrane (Figure 2.1 - C) and surrounded by four muscular groups (Figure 2.1 - C):

- the anterior compartment, composed of the *tibialis anterior*, the *extensor hallucis longus*, the *extensor digitorum longus* and the *peroneus tertius*,
- the lateral comportment, composed of the *peroneus longus* and the *peroneus brevis*,
- the deep posterior compartment, composed of the *tibialis posterior*, the *flexor digitorum longus*, the *flexor hallucis longus* and the *popliteus*,
- the superficial posterior compartment, composed of the *gastrocnemius*, the *soleus* and the *plantaris* [Kamina 09].

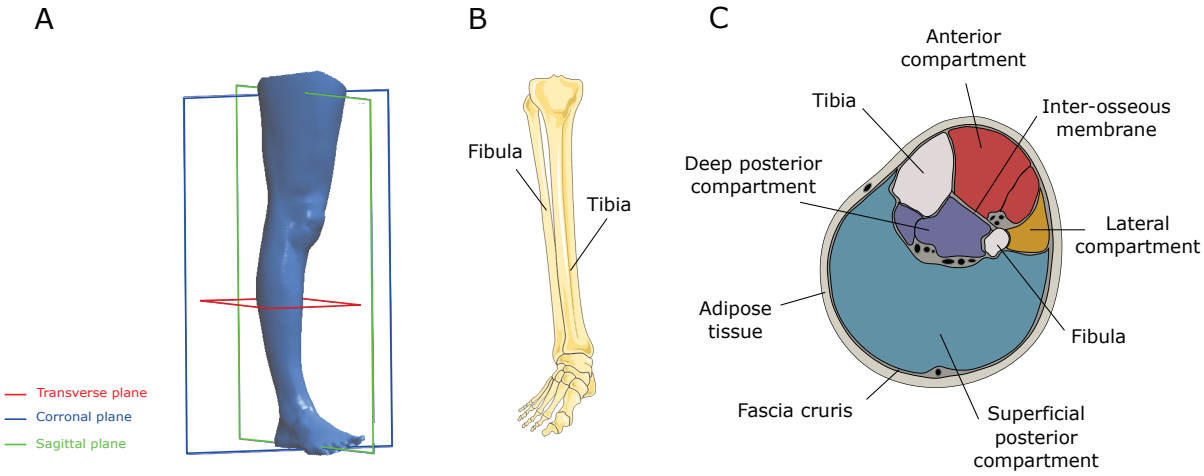

Figure 2.1: A - Anatomical planes, B - Bones in the lower leg, C - Cross section of the lower leg (adapted from [Braus 21])

The *fascia cruris* is a dense connective tissue enclosing the four muscular compartments (Figure 2.1 - C). Eventually, *adipose tissue* is located above this connective tissue and beneath the skin.

2.2.2 Venous system and venous return

Veins are non-pulsatile vessels, whose role is to bring blood back to the heart. They represent a much larger blood reservoir than the arteries: the capacity of the whole venous system is about 4,700 mL whereas it is only about 800 mL for the arterial system [Kamina 09].
The veins start from the capillaries which are the location of water, oxygen, carbon dioxide and nutriments exchange between the blood and the tissues. The venous system is divided in two networks, the superficial one and the deep one (Figure 2.2 - A). The superficial veins, which in the lower leg contain 1/10 of its blood volume, are linked to the deep veins via the perforating veins (Figure 2.2 - A).
The veins diameter is variable, which gives them the ability to store the blood and to adapt to

pressure variations. Their diameter mainly depends on the transmural pressure, P_{Tm}, which is the difference between the inside and the outside pressure of the vein, respectively P_{V1} and P_O (Figure 2.2 - B):

$$P_{Tm} = P_{V1} - P_O. \tag{2.1}$$

In the lower leg veins, this pressure can vary from 5 mmHg in the supine position to 75 mmHg in standing position [Gardon-Mollard 06]. To counteract gravity, veins have valves (Figure 2.2 - B) which prevent venous blood to fall down. If the pressure upstream in the valves (P_{V1}) is lower than the pressure downstream in the valves (P_{V2}), the valve is closed (Figure 2.2 - B). And when the pressure upstream in the valves (P_{V1}) is higher than the one downstream (P_{V2}), then the valve opens and the blood can flow to the heart. This mechanism is helped by muscle contraction.

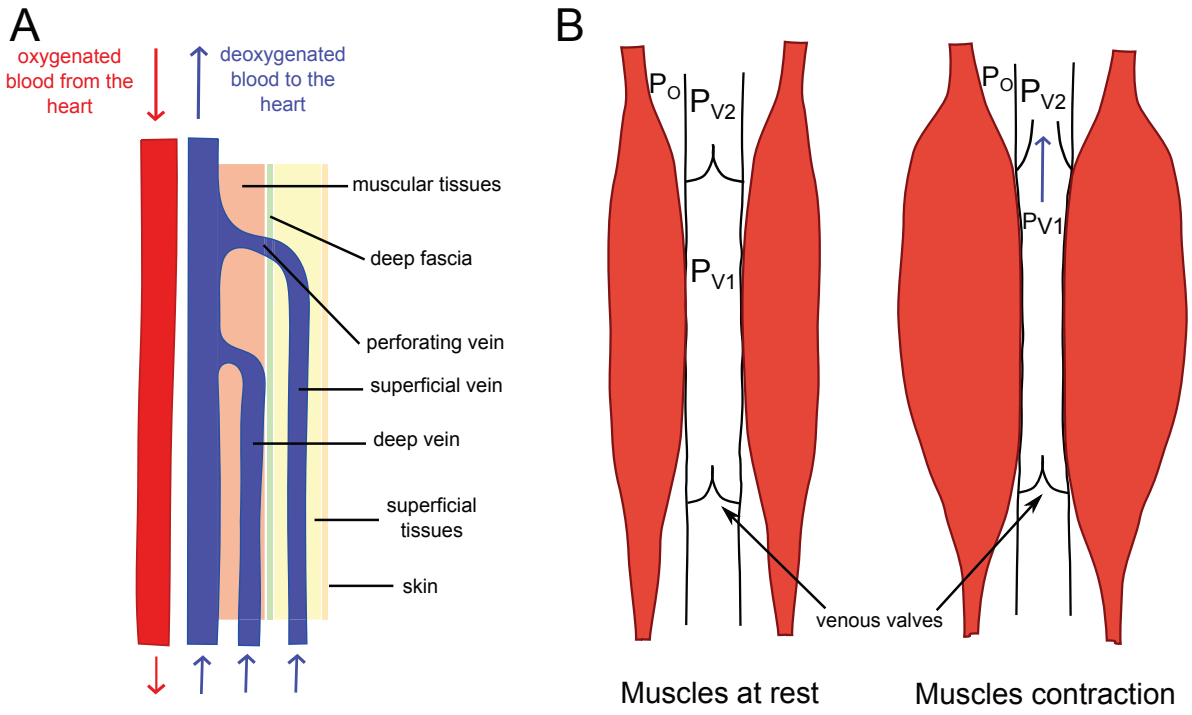

Figure 2.2: A - Venous system topography; B - Venous muscular pump

2.2.3 Pathologies

The starting point of venous pathologies in the lower leg is an hyper-extensibility of the venous wall [Gardon-Mollard 06]. By increasing venous blood pressure, the vein diameter is excessively enlarged [Gardon-Mollard 06]. Consequently, the valves become incontinent which leads to blood reflux and stasis. These phenomena are responsible for a change in the veins wall mechanical properties and consequently for venous pathologies [Gardon-Mollard 06].
The evaluation of the venous reflux can be performed with air-plethysmography [Nicolaides 93]. This technique helps to measure blood volume. First, the patient is set in the supine position, with the leg raised, in order to empty the veins (Figure 2.3). Then the patient is asked to stand up, his body weight on the opposite leg. The *Venous Volume* (VV) is measured once the leg volume is stable.

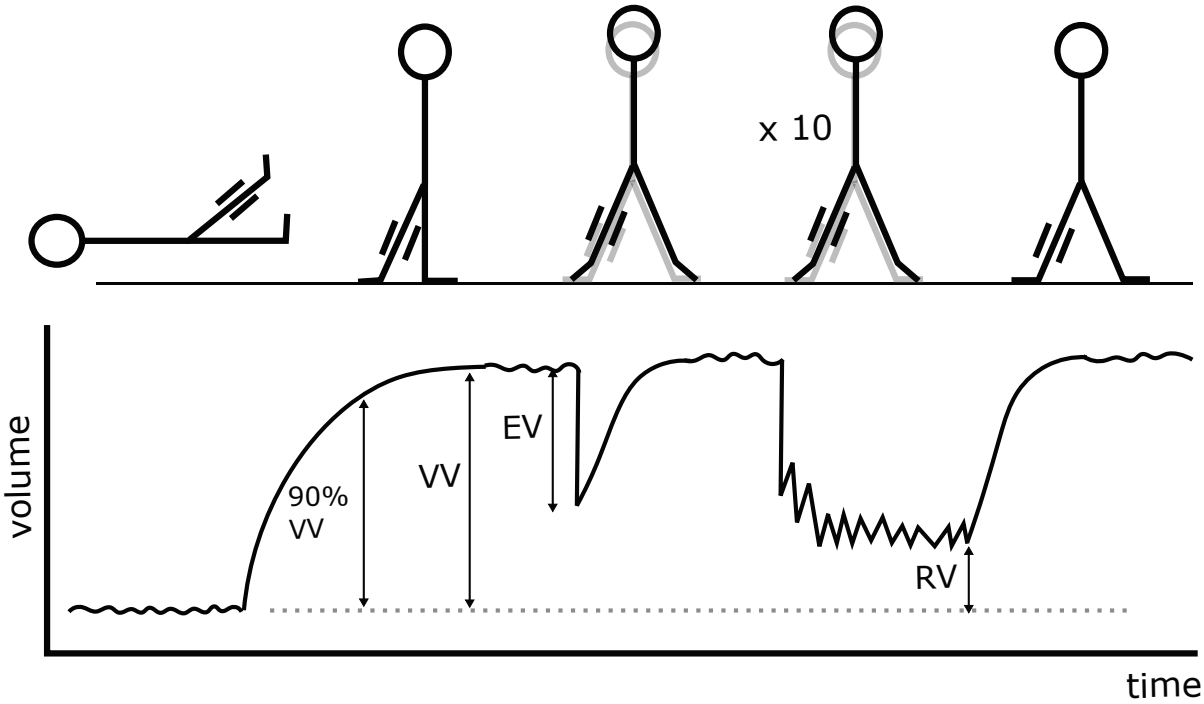

Figure 2.3: Measurement protocol of Venous Volume (VV), Ejection Volume (EV) and Residual Volume (RV) - Adapted from Nicolaides et al. [Nicolaides 93]

The *venous filling index* is the ratio between 90% of venous volume and the time needed to reach this filling volume:

$$\text{Venous Filling Index (VFI)} = \frac{90\%\ \text{VV}}{90\%\ \text{VV Filling time}} \tag{2.2}$$

The *Ejection Volume* (EV) consists in the blood volume reduction with one tip toe movement [Nicolaides 93] (Figure 2.3). The *Ejection Fraction* (EF) is defined as the ratio between the *Ejection Volume* (EV) and the *Venous Volume* (VV). After ten tip toe movements, the remaining blood volume is the *Residual Volume* (RV). All these measurements help to evaluate venous reflux, first to assess the severity of the patient's pathology but also to evaluate the efficacy of a treatment on the venous return.
Indeed, it was observed that patients suffering from Chronic Venous Insufficiency (CVI) have a statistically lower venous ejection fraction and ejection volume than healthy subjects [Mosti 08a]. There is also a correlation with venous pathologies and Venous Filling Index. Patients with Venous Filling Index lower than 2 mL/s have no significant venous reflux. However, an index higher than 7 mL/s is associated with skin changes, chronic swelling and ulceration [Christopoulos 88].
Venous pathologies go from the *heavy legs* feelings to the most severe form: venous ulcers. They are graded in the Classification for Venous Disorders, named CEAP (Table 2.1).

Age, pregnancy and obesity are risk factors for CVI [Beebe-Dimmer 05] [Carpentier 04] as well as CVI family history. For example, a patient has a 9-in-10 chance to develop varicose veins if both of his/her parents suffered from this pathology [Cornu-Thenard 94]. This drops to 4-in-10 chance for men and 6-in-10 for women if only one parent was affected and 2-in-10 if none of the parents was affected. This also showed that women have higher chance to be affected by CVI than men. Also, prevalence of CVI is more important in developed countries [Beebe-

Classification	Clinical signs
C_0	no visible or palpable sign of venous disease
C_1	telangiectasies or reticular veins
C_2	varicose veins
C_3	oedema
C_4a	pigmentation or eczema
C_4b	lipodermatosclerosis or *atrophie blanche*
C_5	healed venous ulcer
C_6	active venous ulcer

Table 2.1: CEAP classification - [Eklöf 04]

Dimmer 05]. Eventually, CVI is worsened with reduced mobility [WUWHS 08].
However, the exact prevalence of CVI is complex to determine. Estimations go from 1 to 60% for women and to 2 to 56% for men [Robertson 08]. Venous pathologies represent a major health problem. For example, in France in 1991, 2.6 % of health expenses were dedicated to these pathologies [Lafuma 94]. Moreover in 1996, about a third of the population was affected by venous pathologies [Floury 96]. However, 70% of the pathological population suffered from a light or moderate venous disease.
In addition to financial cost, CVI impacts the patients' quality of life, which decreases with increased severity of the pathology [Andreozzi 05].

2.3 Compression therapy

One of the treatment for different stages of CVI is compression of the lower limb, whose efficacy is admitted [Musani 10] [Amsler 09] [Agu 99] [Lattimer 14]. This compression treatment can be performed either with compression socks or stockings, compression bandages [Brizzio 10] [Mosti 13] or intermittent pneumatic compression devices. This study will only be focused on textile medical compression devices.
These devices apply a pressure on the external surface of the limb called *interface pressure*. This pressure is then transmitted, through internal soft tissues (adipose and muscle tissues), to the veins [Rohan 15] [Partsch 05a]. This treatment tends to decrease veins transmural pressure P_{Tm} by increasing the pressure outside of the vein P_O (Equation 2.1) [Gardon-Mollard 06]. Consequently, it is likely that a better control of interface pressure will lead to a better controlled treatment, as interface pressure consists in the therapeutic dosage of the treatment.
Though it was observed that compression stockings enhance venous return, the action mechanisms of compression therapy are not fully understood [Lattimer 14]. Indeed, the treatment or prevention efficiency of compression depends on the interface pressure applied at rest, but also while walking [Partsch 06].

2.3.1 Introduction to fabric mechanics

Medical compression bandages consist in a stretched fabric material wrapped around the limb. Fabrics can either be woven or knitted. Weaving is the orthogonal interlacing of two types of

yarns: the warp yarns, in the longitudinal direction of the fabric and the weft yarns, in the transverse direction of the fabric (Figure 2.4 - A). Knits are composed of interlaced threads (Figure 2.4 - B).
Two of the fabrics characteristics were of interest in this study:

- the mechanical properties,
- the frictional properties.

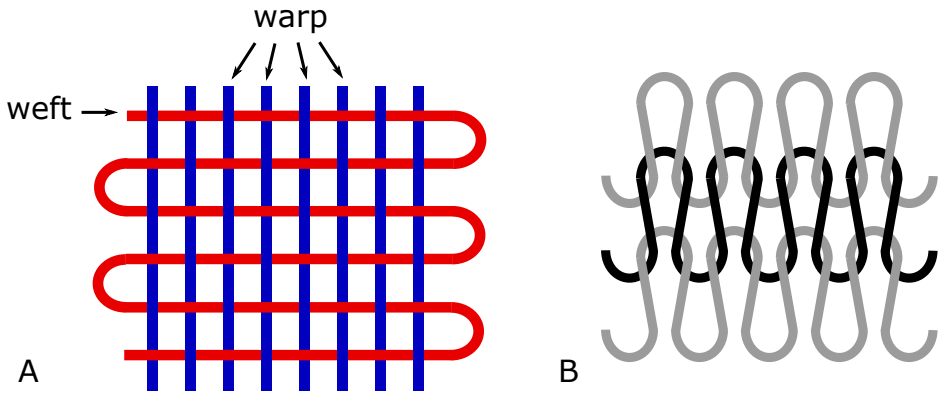

Figure 2.4: Illustration of a fabric (A) and a knit (B)

2.3.1.1 Mechanical properties of fabrics

In the case of compression textile devices (lumbar belts, compression stockings, ...), the fabrics tensile mechanical properties are of high interest because they directly impact the success of the treatment. However, textile material mechanical behaviour differs from the "conventional engineering materials" [Hu 04]: they are inhomogeneous and often submitted to very large strain. They also show a non linear mechanical behaviour and large hysteresis (difference between the loading and unloading).
Woven fabrics are considered as sheet/shell whose mechanical behaviour can be described as orthotropic (because of the symmetries of their structure (Figure 2.4 -A)). Thus, assuming a linear response, their orthotropic in-plane mechanical behaviour can be described thanks to a Hookean constitutive law:

$$\begin{bmatrix} \epsilon_{11} \\ \epsilon_{22} \\ \epsilon_{12} \end{bmatrix}_{\perp} = \begin{bmatrix} \frac{1}{K_1} & -\frac{\nu_{12}}{K_1} & 0 \\ -\frac{\nu_{12}}{K_2} & \frac{1}{K_2} & 0 \\ 0 & 0 & \frac{1}{G} \end{bmatrix}_{\perp} \begin{bmatrix} N_{11} \\ N_{22} \\ N_{12} \end{bmatrix}_{\perp} \tag{2.3}$$

with ϵ_{11} and ϵ_{22} the strains in the in-plane directions, N_{11} and N_{22} the section forces in the in-plane directions, ϵ_{12} and N_{12} the shear strain and section force. K_1 and K_2 are the elastic moduli in the in-plane directions, ν_{12} is the Poisson's ratio and G the shear modulus.
The tensile properties of fabrics K_1 and K_2 can be derived from uni-axial traction tests in both in-plane directions. There are three ways to obtain an elastic modulus from non linear stress-strain curves:

- the secant modulus (Figure 2.5 - A), which is the slope of the curve drawn from the origin to a chosen stress/strain point,

- the tangent modulus (Figure 2.5 - B), which is the tangent at a chosen stress/strain point,
- the chord modulus (Figure 2.5 - C), which is the slope of the curve drawn between two stress/strain points.

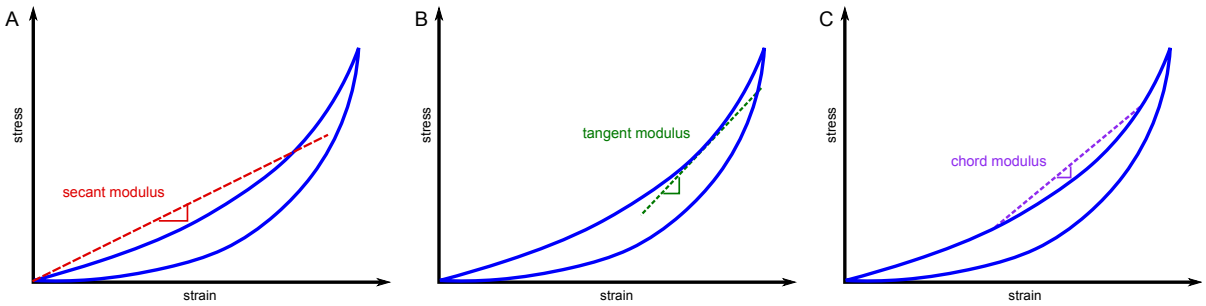

Figure 2.5: Illustration of a stress-strain curve and the different elastic moduli: Secant modulus (A) - Tangent modulus (B) - Chord modulus (C)

On the other hand, the out-of-plane mechanical behaviour can be described as follows:

$$\begin{bmatrix} M_{11} \\ M_{22} \\ M_{12} \end{bmatrix}_{\perp} = \begin{bmatrix} F_1 & \tilde{0} & 0 \\ \tilde{0} & F_2 & 0 \\ 0 & 0 & \tau_{12} \end{bmatrix}_{\perp} \begin{bmatrix} \kappa_{11} \\ \kappa_{22} \\ \kappa_{12} \end{bmatrix}_{\perp} \tag{2.4}$$

with M_{11}, M_{22} and M_{12} the section moments and κ_{11}, κ_{22} and κ_{12} the bending strains.
Most of fabric-material show a different mechanical behaviour between loading and unloading phases (Figure 2.5). This hysteresis effect [Kumar 13a] is to be considered in compression therapy as most of the compression fabrics are first stretched and relaxed to be applied on the skin (compression bandagse or lumbar belts).
The mechanical behaviour of fabrics over time may also play a role in compression therapy. Most of compression bandages are viscoelastic materials [Kumar 13b]. Once stretched, they exhibit a loss of tension over time, which may lead to a decrease in interface pressure [Kumar 13c].

The compression bandages are stretched then wrapped on the leg. During and after the wrapping process, bandage layers interact with each other, hence the need to characterize the frictional properties of compression bandages.

2.3.1.2 Fabric frictional properties

Once a bandage is wrapped around a limb, different bandage layers are in interaction as well as the skin and the bandage. These interactions may play a role in interface pressure generation, by preventing bandage slippage for example [Ghosh 08]. The frictional interactions are usually described with Amonton's law (also called Coulomb's law):

$$|F| = \mu |N| \tag{2.5}$$

with $|F|$ the tangential force, $|N|$ the normal force and μ the friction coefficient. This friction coefficient can either be static, prior to motion initiation, or dynamic, during sliding.
Different "contact measurement methods" were developed to characterize either the static or dynamic friction coefficient of fabrics [Gupta 08]. The first one is dated from 1955 as part of

the "cloth profile recorder" [Butler 55].
The simplest method for the evaluation of the static friction coefficient is the inclined plane (Figure 2.6 - A). A mass is set on a plane. This plane is inclined with an increasing angle α until the mass starts to slide. The angle α_0, at which the sliding is initiated, provides the static friction coefficient μ_{static}:

$$\overrightarrow{R} + \overrightarrow{F}_{grav} = \overrightarrow{0} \Rightarrow R_N = F_{grav}\, cos(\alpha_0) \text{ and } R_F = F_{grav}\, sin(\alpha_0) \Rightarrow \frac{R_F}{R_N} = tan(\alpha_0) = \mu_{static} \tag{2.6}$$

The second method (Figure 2.6 - B) helps to measure the dynamic friction coefficient. It consists in a plane surface moved on top of another plane surface. The force needed to move the plane surface F is measured by a load cell. Then it is possible to compute the dynamic friction coefficient $\mu_{dynamic}$:

$$\mu_{dynamic} = \frac{F}{F_{grav}} \tag{2.7}$$

with F_{grav} the normal force due to gravity and F the tangential force. The static friction coefficient μ_{static} can also be computed with this method from the force F required to initiate the motion. This method is often used, either for fabric-to-fabric [Ajayi 92b] [Kothari 94] or fabric-to-metal or polymer [Das 05] [Hermann 04] friction characterization.
Other studies were focused on the development of methods to characterize the *touch* of a fabric, i.e. a human finger touching a fabric. Ramkumar et al. designed a polymeric human finger to measure the finger-to-fabric friction coefficient [Ramkumar 03]. Also, Kawabata developed a four-instruments rig to characterize the fabric "hand" [Kawabata 80], the Kawabata Evaluation System (KES). One of the four instruments is dedicated to the measurement of the fabric friction coefficient, thanks to a metal "finger" and was used in previous studies [Bertaux 07] [Harwood 08].
The fabric frictional properties depend on fabric structure and composition [Das 05] [Ajayi 92a] [Moorthy 15] but also on environmental conditions [Arshi 12], such as humidity or temperature. Other studies were more specifically focused on the interactions between fabrics and human skin [Van Der Heide 13]. It was observed that the skin frictional properties were correlated with its hydration [Gerhardt 08] and may vary with its surface lipid content, which leads to large variations among individuals [Derler 11]. Also stick-slip phenomena were observed [Derler 13] which may question the use of Coulomb's law to describe skin-to-fabric interactions.

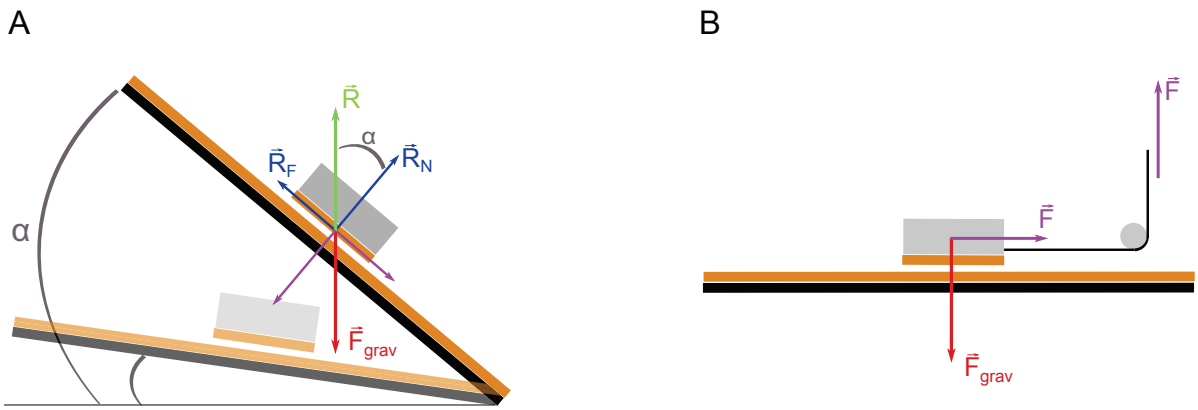

Figure 2.6: Methods for friction coefficient measurement: A - Inclined plane ; B - Characterization of dynamic friction coefficient

2.3.2 Compression stockings and bandages

Compression stockings consist in tubular fabrics (often knitted). They are sized to fulfil the stretch requirements, in order to apply the indicated pressure.
Several countries have divided compression stockings into classes, with regards to the interface pressure they apply at measurement point B (Table 2.2 and Figure 2.7).

Compression class	USA	UK	France	Germany
I	$15-20$	≤ 20	$10-15$	$18-21$
II	$20-30$	$21-30$	$15-20$	$23-32$
III	$30-40$	$31-40$	$20-36$	$34-46$
IV	> 40	$41-60$	> 36	> 49

Table 2.2: Pressures at measurement point B for different compression classes and for different countries - [Rabe 08]

On the other hand, bandages consist in a stretched fabric wrapped around the leg. Most often, unlike stockings, the same bandages are applied on legs with very variable geometries. Bandages and stockings have complementary use. Compression bandages are indicated at the very beginning of the compression treatment [Allaert 15], as they can easily accommodate to the changes in morphology due to the quick reduction of the oedema. Once the oedema is stable, stockings can be prescribed. Moreover, bandages are preferred when the patient's pathology prevents the wear of stockings, for example, after a knee-arthroplasty. Also, bandages are often more easily applied by caregivers than stockings.

In France, physicians (non-hospital physicians) prescribe mainly long-stretch bandages (elastic bandages) (50.8% of the prescriptions) or stockings (40%) for the treatment of venous ulcers [Begarin 14]. Multi-layer bandages are rarely prescribed (7.7%). This type of bandages and mono-layer short-stretch bandages (elastic bandages) were respectively known by 38.9% and 45.8% of the physicians who took part in this study.
The Bonn Vein study [Rabe 13] reported that 60% of patients with pathologies graded C3-C6 (Table 2.1) did not receive any compression treatment (stockings or bandages), though it was proven that compression was an effective treatment [Mosti 12a]. Almost 3/4 of the patients who received a compression treatment reported an improvement of their symptoms. Finally, the observance of medical compression stockings was found to be about 75%.

2.3.3 Interface pressure as therapeutic dosage

The *interface pressure* applied by compression bandages or stockings is the key aspect of the therapy and has to be adapted to patients' pathology [Vicaretti 10]. However the recommended amount of pressure for the treatment of different venous pathologies is not clearly defined.
It was proven that higher pressures help to cure venous leg ulcers [Milic 10]. However, increasing the pressure makes the treatment less bearable for the patients [Milic 10] and thus reduces the observance. Also if the applied pressure is too high, the treatment can induce skin damages (as pressure ulcers) [Mosti 10b], especially with patients suffering from mixed arterial-venous diseases. Nevertheless, it was observed that venous pumping could be significantly improved with inelastic bandages applying low resting pressure (about 20 $mmHg$) [Mosti 10b]. But higher

pressures (until 60 $mmHg$) would lead to greater improvement of venous pumping. In France, the *French National Authority for Health (Haute Autorité de Santé (HAS))* recommends to apply the highest pressure the patient can tolerate [HAS 10]. For venous leg ulcers, it was proven that a pressure over 40 mmHg helps to a rapid improvement [Blair 88]. Also, interface pressure may vary between a *passive* state (with relaxed leg muscles) and an *active* state (with active muscles) [Dissemond 16]. These pressures are called *resting pressure* and *working pressure*. The differentiation between these pressures is essential to understand the action mechanisms of compression therapy.

2.3.3.1 Measurement of interface pressure

Interface pressure can simply be evaluated by direct measurements, thanks to sensors located between the skin and the bandage or stockings.

For the standardization of such measurements, measurement points were identified on the lower leg [Partsch 06] [Prestandard 01] (Figure 2.7).

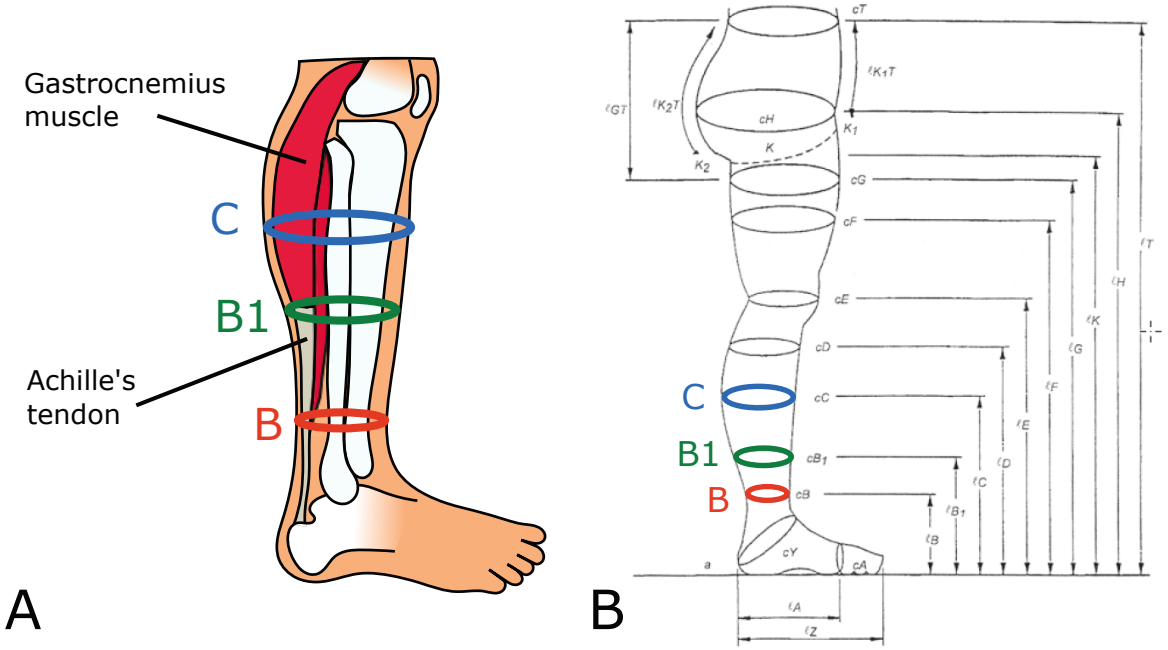

Figure 2.7: Locations of measurement points on the leg; 1 - Anatomy ; 2 - Standard [Prestandard 01]

Measurement point B is at the height corresponding to the smallest circumference of the lower leg, right above the ankle. Measurement point B1 is located at the height at which the Achilles tendon turns into the gastrocnemius muscles (Figure 2.7 - A). Eventually, measurement point C is at the height of the largest circumference of the calf.
Measurement point B is the reference point for stockings manufacturers. This area is of high interest because 80% of leg ulcers starts from there [Callam 87], but is mainly composed of bones and tendons.
Manufacturers very often use wooden leg (so called Hohenstein leg) to check pressure applied by the stockings at the area of measurement point B [Afnor 86]. These legs have a circular shape, whereas human leg is closer to an elliptic shape in this area [Veraart 97]. It was later

suggested that measurement point B1 should be included in all *in vivo* pressure measurements [Partsch 06]. The change in circumference from the supine to standing position or during dorsiflexions is very large, thus it is possible to observe large interface pressure variations [Stolk 04] [Partsch 05b].

2.3.3.2 Prediction of interface pressure: Laplace's Law

For now, there is only one method to compute or predict interface pressure applied by compression bandages or stockings. Laplace's Law states that pressure is directly proportional to the fabric tension T and inversely proportional to the local radius of curvature r_C. In case of bandages, this ratio is multiplied by the number of layers of the bandage n [Thomas 03a].

$$P = n * \frac{T}{r_C}, \quad T > 0, \; r_C > 0. \tag{2.8}$$

This law can be derived for a two dimensional problem [De Bruyne 76]:

$$P = \frac{T_1}{r_{C1}} + \frac{T_2}{r_{C2}} \tag{2.9}$$

with T_1 and T_2 respectively the tension in the sagittal/coronal and transversal planes and r_{C1} and r_{C2} respectively the radius of curvature in the sagittal/coronal and transversal planes (Figure 2.1 - A). However, the radii of curvature in the sagittal and coronal planes are much larger than the ones in the transverse plane:

$$r_{C1} \gg r_{C2} \rightarrow \frac{T_1}{r_{C1}} \ll \frac{T_2}{r_{C2}}. \tag{2.10}$$

Consequently, for the lower leg, Laplace's Law is most often used in its simplest form (Equation 2.8).
Moreover, the local radius of curvature is very variable in a leg cross section (Figure 2.8). Thus it is essential to compute interface pressure using the local radius of curvature and not a global estimation of this radius (leg circumference for example).
The use of this law in the medical field is wide [Basford 02], either for the prediction of pressure applied by different compression devices (lumbar belt, stockings, ...) or for physiological phenomena such as pulmonary physiology or hypertension for example.
Even though many attempts were made to improve this law, by considering the radius of curvature modification due to the fabric thickness for example [Al Khaburi 12], its use for interface pressure computation is called into question [Schuren 08].

2.3.4 Degressivity or progressivity

Most of compression stockings are so-called degressive stockings. This means that the pressure decreases from the ankle to the knee. This pressure profile can also be the result of a bandage applied with a constant stretch on the leg.
However a different type of compression profile, called progressive, was tested lately. Contrary to degressive compression, the interface pressure increases from the the ankle to the knee.
Even though the efficacy of degressive compression treatment has been proven, many studies have investigated the therapeutic effect of progressive compression, either performed with stockings [Mosti 11] or bandages [Mosti 12b]. It was observed that the efficacy of progressive stockings for the treatment of non-severe pathologies was not lower than degressive stockings [Couzan 09]. This type of stockings was also found to be easier to put on for patients [Couzan 12].

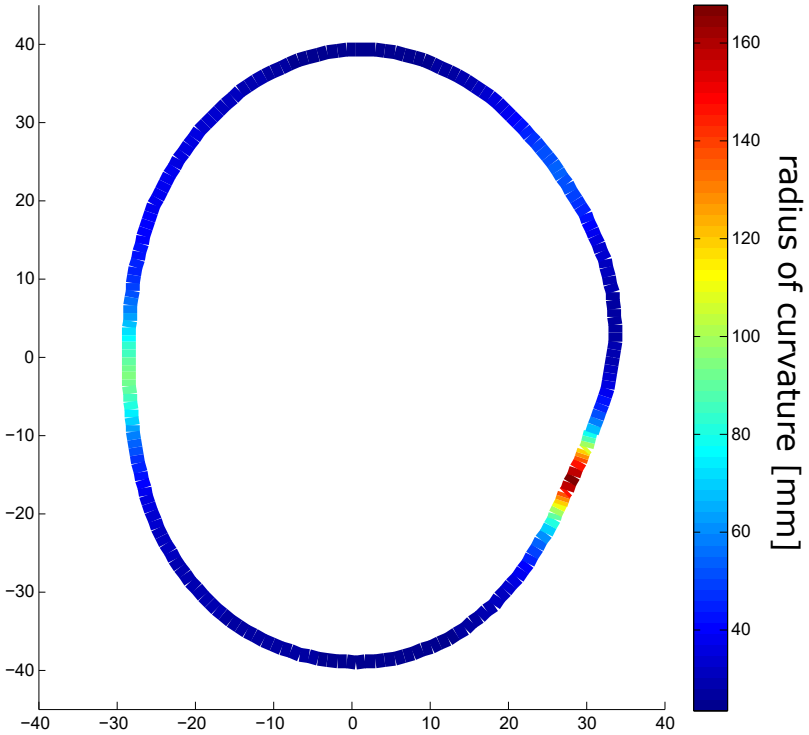

Figure 2.8: Illustration of the variations of the radius of curvature for a leg cross section

Other studies investigated the effect of progressive compression on venous return. They noticed an increase in venous ejection fraction for compression stockings [Mosti 11] and bandages [Mosti 12b] compared to degressive compression. Also, an increase in ankle interface pressure while maintaining the calf interface pressure does not seem to increase venous ejection fraction [Mosti 14].
However, these studies consisted in short-term experiments and long-term effects of progressive compression therapy should be further investigated [Shepherd 16].

2.3.5 Compression with bandages

Pressure applied by compression bandages, which could seem to be rather simple devices, is the result of complex phenomena [Clark 03] [Melhuish 00]. This pressure depends on the different materials applied on the limb and their mechanical properties, the amount of stretch in this material (*stretch = actual bandage length/initial bandage length*), the application technique (i.e. wrapping technique) and the interaction between the bandage layers [Ghosh 08]. But interface pressure also depends on parameters related to the patients: their leg morphology and their position for example.

2.3.5.1 Bandages materials

Compression bandages consist in fabrics or knits, whose composition can vary. However in practice, they are divided into 3 groups, depending on their *elasticity* [Partsch 08].
For medical compression bandages, *elasticity* is not exactly defined as the capacity of a material to return to its original shape after being stretched [Clark 03]. The criterion of interest to classify bandages material is the bandage stretch under a given applied force (10 N/cm - [61632 09]) or extensibility [Partsch 08] (Table 2.3).

	Inelastic		Elastic
	Rigid	Short-Stretch	Long-Stretch
Maximal stretch at 10 N/cm bandage width	0 - 10	10 - 100	> 100

Table 2.3: Classification of the *elasticity* of compression bandages [Partsch 08]

Bandages are described as *short-stretch* or *long-stretch*, depending on their stretch under a certain amount of force. Usually, a connection is made between the extensibility of the bandage and its elastic properties [Partsch 08]: *long-stretch* bandages are associated with *elastic* properties and *short-stretch* bandage are associated with *inelastic* properties. This terminology is not related to conventional terminology used in the field of mechanics.
More than impacting the tension in the bandage, mechanical properties influence the interface pressure variation between different body positions. Compression bandages are applied on the leg in supine position. Leg volume varies from supine to sitting or standing position, as well as muscle state (relaxed or contracted). On the one hand, long-stretch bandage will tend to adapt to this change in leg volume and will result in low pressure increase from supine position to standing position. On the other hand, short-stretch bandage will result in high pressure increase [Clark 03] [Partsch 05c].
Compression bandages usually show a different mechanical behaviour between the loading and unloading phases, called hysteresis (Figure 2.9). Most often, bandages mechanical properties are characterized during the loading phase [61632 09]. However, as many textile compression devices [Bonnaire 15], bandages are first stretched then applied on the leg, which corresponds to the unloading phase. Thus it is essential to consider the unloading phase for mechanical characterization.

This difference in mechanical properties of elastic/non-elastic fabrics is the cornerstone of the difference between compression and contention. *Compression* consists in the effects induced on the leg by an elastic fabric (active action of the fabric), whereas *Contention* is defined as the action of a non elastic fabric on the leg [Gardon-Mollard 06]. The action of contention is passive; the fabric will resist to the leg volume increase while standing for example. For the compression, the elastic forces due to the stretch actively apply a pressure on the leg.
Eventually, it is important to notice that contention stockings can not exist, because it would be impossible to put on non-elastic socks. From a clinical point of view, the differences in bandage mechanical properties seem to impact ulcer healing. On the one hand, a study has showed that elasticity has a positive impact on ulcer healing [Danielsen 98a]. On the other hand, studies have observed that ejection fraction was better improved with short-stretch bandages than with long-stretch bandages [Mosti 08a] but also that short-stretch bandages have a more pronounced effect on venous reflux than long-stretch bandage [Partsch 99].

2.3.5.2 Bandage *Stiffness* and *Static Stiffness Index*

As the notion of *elasticity*, the *stiffness* of bandages does not exactly corresponds to its mechanical definition.
In mechanics, stiffness is defined as follow:

$$stiffness = \frac{\text{applied force}}{\text{displacement}} \tag{2.11}$$

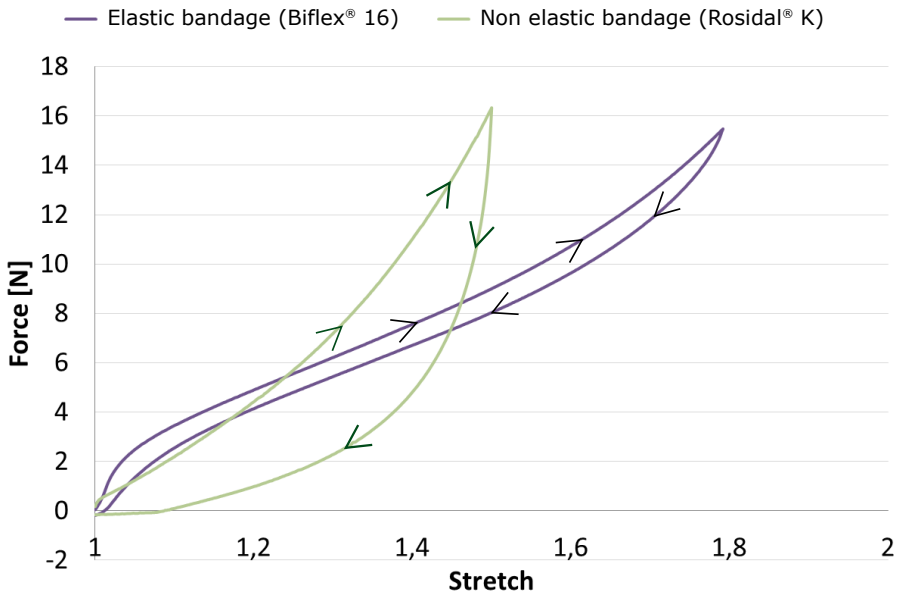

Figure 2.9: Examples of force = f(stretch) curves for elastic and non elastic bandages

For medical compression bandages, *stiffness* was defined as the pressure increase (in mmHg) per centimeter of leg circumference increase [Prestandard 01]. It can be measured thanks to *in vitro* tensile tests on bandages or specifically designed systems [Hirai 11b]. However, this *stiffness* can also be evaluated *in vivo* thanks to the pressure changes from supine to standing position [Partsch 05c]. This pressure variation between two static states is called *Static Stiffness Index* (*SSI*) [Partsch 05b] [Partsch 16] and is measured at the height of measurement point B1 on the medial side of the leg.
In standing position, leg volume increases as blood is flowing down and muscle groups tend to fall down, due to gravity. If the bandage is not stiff, then it will easily adapt to this change of leg geometry and volume. This type of bandage will result in a very low pressure increase or very low *SSI*. On the other hand, if the bandage is very stiff, then it will strongly counteract the geometry and volume change and it will result in a very high pressure increase. This is how the *Static Stiffness Index* can be used as an evaluation of the bandage stiffness. Elastic bandages show lower *SSI* ($SSI < 10\ mmHg$) than non-elastic bandages ($SSI \geq 10\ mmHg$) [Partsch 05c] [Partsch 05b] [Mosti 07]. A study showed that the lower the bandage elasticity (in a medical sense), the higher the pressure increase from supine to standing position [Lee 06]. Moreover, SSI can help to evaluate the *stiffness* of multi-component bandages, which can be composed of layers with different mechanical properties (the superimposition of elastic and inelastic bandages for example) [Mosti 08b].
However, this index has to be used with caution because it can also be influenced by patient related parameters, such as muscle force, venous filling [Schuren 13] or leg morphology.

2.3.5.3 Application technique

Bandages can be wrapped on the leg either in a spiral pattern or in a 'figure-of-eight' pattern (Figure 2.10). The type of application technique will result in differences in interface pressure [Coull 06], and more especially in pressure variation between the different body positions [Lee 06].
In addition to the wrapping pattern, the overlapping of the bandage (the number of layers)

impact interface pressure.

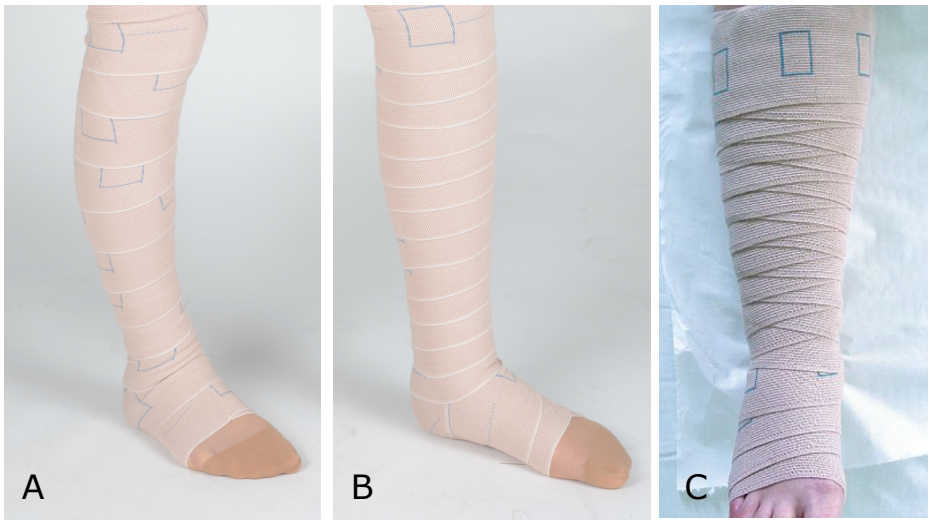

Figure 2.10: Different application techniques: A - 2-layer spiral pattern (i.e. 50% overlapping); B - 3-layer spiral pattern (i.e. 66% overlapping); C - Figure of eight [Benigni 08]

2.3.5.4 Limitation of bandage application

The bandage is wrapped on the limb with stretch, controlled by the operator. This stretch will directly impact the interface pressure (by changing the tension in the bandage), which is the therapeutic effect of the treatment. Thus it is essential to control the applied stretch.

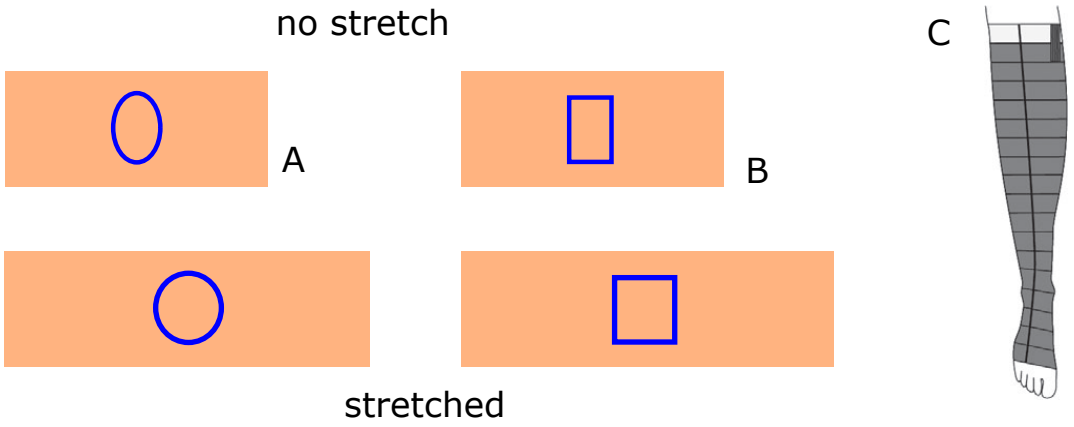

Figure 2.11: I
llustration of two types of calibration markers: A - a circle, B - a square; Compression bandages Presscise [Wiklander 16]

However, a large variation in bandage application was observed [Williams 99] [Logan 92], especially for different operators [Hafner 00b] [Bhattacharya 12], even though they were experienced bandagers [Keller 09]. Despite these differences, it was observed that a bandager tends to be constant and repeatable in bandage application [Thomas 03b] [Raj 80].

To improve stretch control, manufacturers have set up different strategies:

- the use of a calibration marker, a geometrical shape (rectangle, oval) which is deformed with the increasing stretch and which takes a regular geometrical shape (square or circle) once the recommended stretch is reached (Figure 2.11 - A and B),
- the use of bandages mechanical properties: the recommended stretch is the maximum stretch,
- the use of lines printed on the bandage, in a way that the bandage should be applied so that the lines on the different bandage layers are aligned (Figure 2.11 - C) [Wiklander 16].

The first two strategies aim to apply the bandage with a constant stretch over the leg and independently from the leg geometry, whereas for the third one, the bandage stretch can be variable over the leg and dependent on the leg geometry.
Even though these strategies seem to have a positive effect on stretch control [Hanna 08], the uncertainty of bandage application may lead to a lack of control of the therapeutic dose [Partsch 05c].

2.3.5.5 Multi-component systems

Medical compression bandages can be either mono-layer (i.e. the bandage is composed of one component) or multi-layer bandages (i.e. the bandage is composed of several components). Manufacturers offer a large diversity of multi-component systems, from 2 to 4 components [Moffatt 02] [Wong 12a] [Hanna 08]. These bandages systems are often composed of:

- a padding layer, applied with low or no stretch
- one or two compression layers
- a fixation layer: often a cohesive bandage.

The aim of the padding layer is to homogenize the leg geometry, in order to smooth sharp areas (tibia area for example) and to fill hollow areas. By superimposing the bandages, it is possible to increase the interface pressure. These types of bandages are regularly used in clinical practice [Hafner 00a] [Milic 10] and showed a larger positive effect on ulcer healing than single component bandages [O'Meara 12]. However, the pressure applied by the superimposition of two bandages is not the sum of the pressure applied by each bandage separately. This might be due to the thickness of the bandages [Al Khaburi 11b] but also to the morphology modification due to bandage application. The *stiffness* of the bandage is also modified by the superimposition of bandages. For example, the superimposition of two elastic bandages may exhibit larger stiffness than one elastic bandage [Partsch 06]. Also, adding one inelastic component to the bandage, even if all the other components are elastic, seems to have a pronounced effect on *stiffness* [Hafner 00a] [Hirai 11a].

2.3.5.6 Pressure variation over time

Interface pressure varies with body position but also over time [Wong 12b]. Bandages can be kept several days. The applied pressure tends to decrease due to the loss of tension in the bandage materials [Kumar 13b] (due to the viscoelastic behaviour of the fabrics). This pressure decrease was found to be lower for bandages composed of elastic yarns [Kumar 13b]. However, the viscoelastic behaviour of compression bandages is not the only reason of pressure variation over time. Bandages may slide down over the leg (because of ankle rotation for example) but also, the leg volume may change over time as the limb oedema is reduced thanks to compression therapy [Damstra 08] [Raj 80].

2.3.5.7 Different *schools of compression*

The numerous possibilities of compression bandages or stockings might be the consequence of differences in the use of compression therapy within countries. These differences do not only concern the standards on interface pressures (Table 2.2).
For example, French practitioners usually prescribe elastic (long-stretch) compression stockings and bandages [Gardon-Mollard 06]. These devices apply low interface pressures, which tend to be better observed by patients.
In Germany and Austria, compression bandages and stockings are also the standard treatment of chronic venous insufficiency [Gardon-Mollard 06]. However, contrary to France, inelastic (short-stretch) bandages are usually prescribed. Stockings will be preferred for very first stages of venous pathologies.
In England, venous leg ulcers are usually treated with the so-called *four-layer bandage* [Blair 88]. This bandage is composed of a wool bandage, a creped bandage and an elastic bandage applied in a figure-of-eight pattern. Eventually, these three layers are covered by a cohesive layer [Moffatt 02]. This bandage applies a pressure equal to 40 mmHg at the ankle and 20 mmHg below the knee and it is well observed by patients who can wear this bandage during several days.
In the Netherlands, venous ulcers are either treated thanks to non-elastic compression bandage or thanks to intermittent pneumatic compression devices, such as Unna boots for example [Gardon-Mollard 06]. To prevent the recurrence of ulcers, patients can wear thigh-length compression stockings.
However, in the USA, practitioners do not prescribe any compression bandages and compression stockings are spraringly used after varicose veins sclerotherapy or as the treatment of chronic venous diseases [Gardon-Mollard 06]. Even though these habits are changing, they are still very different from the European ones.

2.4 State of the art - Biomechanics of compression bandages

2.4.1 Interface pressure measurements

Interface pressure, measured between the skin and the bandage, is one of the key aspects of compression treatment and directly impacts the success of the treatment [Milic 10] [Partsch 05a]. A simple method to better understand compression therapy is to measure this pressure. Several measurements campaigns were performed in order to evaluate the impact of various parameters on interface pressure. Also, many pressure sensors are commercially available, whose performances were evaluated.

2.4.1.1 Measurements campaign

Interface pressure measurement is the simplest method to evaluate compression bandages. More than a simple evaluation, it also helps to understand the dependence of this pressure to different parameters. Interface pressure applied by a bandage may vary with [Melhuish 00]:

- the bandage components,
- the mechanical properties of its components,
- the application technique (spiral pattern or figure-of-eight),
- the stretch of its components,
- the patient's leg morphology,
- other parameters like the patient's leg mechanical properties, the patient's position, the friction between the different bandage layers, etc.

An overview of the influence of these parameters and associated previous work is proposed in what follows.

Mechanical properties of bandages

Interface pressure measurements can help to differentiate compression bandages between the elastic bandages (or long-stretch) and the inelastic ones (or short-stretch) [Partsch 08]. These bandages mainly differ in the pressure variation from supine to standing position, their so-called *stiffness*.
Another important mechanical characteristics of bandages is their tension, which is the force needed to stretch them. This tension was found to directly impact interface pressure [Rimaud 14].
Comparing long-stretch and short-stretch bandage, it was observed that pressure loss over time for elastic compression bandage was lower than inelastic bandages [Danielsen 98b]. Also pressure peaks while walking were similar for both bandages. This result contradicts the study of Hirai et al., who found that short-stretch bandages showed greater pressure peaks than long-stretch bandages [Hirai 98]. It was also observed that pressure increase from supine to standing position was higher for short-stretch bandages than for long-stretch bandages [Rimaud 14].
Bandage mechanical properties, tension and *stiffness*, strongly impact interface pressure and its variation with body position. Despite the strong correlation between bandage mechanical properties and interface pressure, the impact of a change of these properties on the pressure is

not fully understood.

Application technique

Interface pressure, but also *stiffness* [Lee 06], can be impacted by the bandage application technique, being either spiral or figure-of-eight pattern (Figure 2.10). A bandage applied in a figure-of-eight pattern tends to have a greater *stiffness* than a bandage applied in a spiral pattern [Benigni 08]. Also, the interface pressure was found to be higher for the figure-of-eight than for the spiral pattern in the lower areas (around the ankle) [Coull 06]. However, Rimaud et al. observed no difference at measurement points B1 and C between the pressures applied by the two bandages [Rimaud 14]. Also, the pressure applied by a 3-layer bandage (i.e. 66% overlapping) was about 1.8 time as high as the one applied by a 2-layer bandage. This results contradicts Laplace's Law (Equation 2.8), which states that pressure is directly proportional to the number of bandage layers. Indeed, according to this Law, the pressure applied by a 3-layer bandage should be 1.5 time ($= \frac{3}{2}$) as high as the one applied by a 2-layer bandage.
Differences in application techniques can be found in the application pattern or in the overlapping of the bandage. These differences in application technique induce pressure variation but also *stiffness* modifications, which supposes a potential impact of bandage friction.

Bandage stretch

The bandage stretch is a way to dose out the applied pressure. Thus it is essential to control the applied stretch while applying a bandage. However, only a few studies measured the stretch of the bandage [Coull 06]. This is a key issue of compression treatment with bandages. A single operator seemed to be consistent in his/her way to apply compression bandages [Raj 80] [Thomas 03b]. Nonetheless, large discrepancies can be observed in bandage application among different experienced bandagers [Keller 09].
The high operator dependence of bandage application and the fact that the bandage stretch is rarely measured represent an uncertainty about compression bandage therapy. This lack of stretch control may raise questions about the relevance of some clinical studies [Partsch 05c].

Bandage components

High interface pressures ($\geq 40 mmHg$ [Partsch 03b]) are required to treat severe venous pathologies. This high pressure level can be achieved thanks to multi-component bandages. The pressure applied by these multi-layer systems depends on their bandage components and the order in which they are applied on the leg. Hirai et al. measured the stiffness of different multilayer bandages *in vitro* [Hirai 09]. The bandages were composed of long and short stretch bandages. It was observed that the pressure applied by a short-stretch bandage applied on top of a long-stretch bandage was equivalent to the one applied by a long-stretch bandage applied on top of a short-stretch bandage. But, the *stiffness* of these two systems differed (depending on the initial applied pressure). Other *in vivo* pressure measurements were performed. Interface pressure applied by commercially available *kits* (i.e. multilayer bandages) was measured in several positions to evaluate their *stiffness* [Mosti 07]. Mosti et al. observed that super-imposing elastic compression bandages could lead to a *stiffness* equivalent to the one of inelastic bandages [Mosti 08b]. Others have investigated the pressure variation over time for different multi-component bandages [Hafner 00a]. Elastic multi-component bandages showed lower pressure loss compared to inelastic bandages. The impact of the number of components on pressure loss over time was evaluated for a four-layer bandage, a two-layer bandage and a single layer bandage [Jünger 09]. The two-layer bandage maintained over one week a pressure

level equivalent to the one of a four-layer bandage, and which was higher than a single bandage layer.
However, none of the pressure measurements campaigns have investigated the link between the pressure applied by one bandage and the one applied by the superimposition of two bandages. Moreover, as for the measurements of pressures applied by one bandage, never the stretch of the bandage was measured.

Patient's morphology

Interface pressure also depends on the patients' leg morphology. Contrary to stockings which are sized to the patient's morphology, bandages are identical for a wide range of morphologies. The lower limb geometry can vary with the patient's gender [Huston 08], but also with body position. Most often, interface pressure measurement campaigns do not differentiate women and men [Mosti 10a] [Mosti 13]. But most importantly, the change in morphology and leg soft tissue mechanical properties (muscle contraction for example) is the main cause of pressure increase from supine to standing. The change in morphology from supine to standing can be the consequence of the muscle groups falling down (due to gravity), the muscle contraction, but also the blood falling down [Meissner 07].
The pressure changes with regards to the patient's leg morphology should be further investigated. This would require precise morphological measurements to evaluate lower limb geometry changes within different patients but also within different body positions.

2.4.1.2 Pressure sensors

A large diversity of pressure sensors is commercially available [Bonnaire 14]:

- pneumatic sensors: Picopress®(Microlab, Padua, Italia), Kikuhime® (Meditrade, Soro, Denmark), SIGaT-Tester® (Ganzoni-Sigvaris, St. Gallen, Switzerland),
- electro-pneumatic sensors: Talley digital skin evaluator (Talley Group Ltd, Romsey, England),
- resistive sensors: Flexiforce™ (Tekscan, Boston, MA, USA),
- capacitive sensors: Pliance® X system (Germany-Novel Electronics, Munich, Germany).

The performance of pressure sensors can be evaluated thanks to the following parameters:

- measurement error: difference between the theoretical value and the measured one,
- repeatability or reproducibility: difference between two measurements taken in the same experimental conditions by the same operator in a very short time (repeatability) or by two operators within a longer time interval (reproducibility) ([21748:2010 10]),
- linearity of the measurement,
- hysteresis: difference between the measured value in the loading phase and the one in the unloading phase (Figure 2.12 - A),
- drift: measurement variation over time (the same loading is maintained over time) (Figure 2.12 - B).

Several studies have compared the performances of sensors for interface pressure measurements and have obtained various results (Table 2.4). However, the sensors used for the measurement

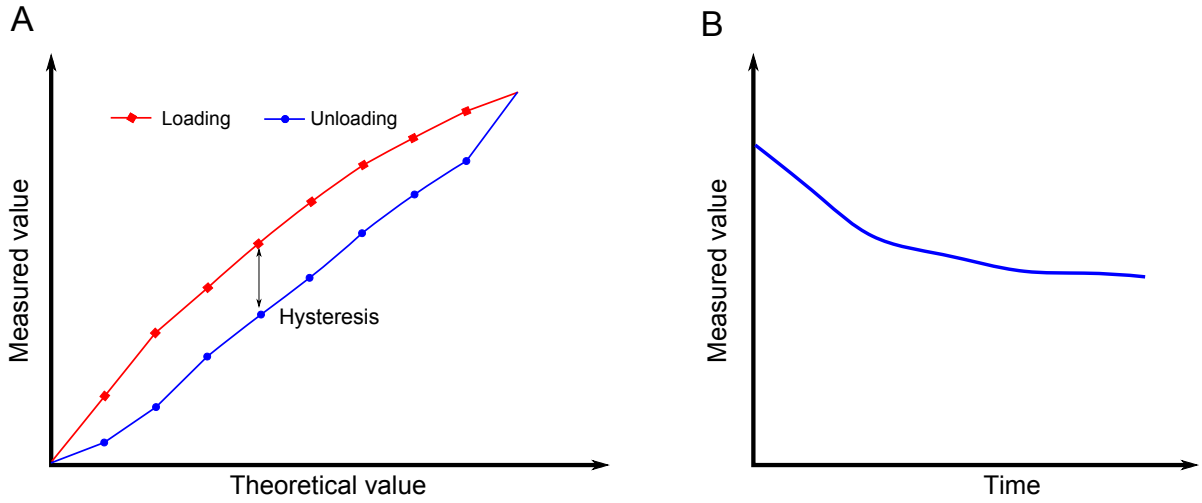

Figure 2.12: A - Illustration of a sensor response during loading and unloading phases; B - Illustration of the drift of a sensor

of pressure applied on the lower limb by compression devices have to be thin and flexible to adapt to the leg morphology [Partsch 06] [Rabe 08]. Thus, the measurement error of the sensor on a curved surface is also very important for this application. The measurement error observed on curved surfaces (Table 2.4) can be due to the bending of the sensor or to the local modification of the radius of curvature induced by the presence of the sensor [Vinckx 90]. From a general point of view, it is important to remember that a sensor placed at an interface always modifies this interface [Wolsley 00] (a measurement always modifies the measurand).
Despite the interrogations about the reliability of the sensor Picopress®, it was used in several studies lately [Damstra 13] [Lattimer 14] [Mosti 14] [Rimaud 14], like the pneumatic pressure sensor Kikuhime® [Mosti 08b] [Benigni 08] [Damstra 08].

Sensor	Type	Suface	Global error	Repeatability	Linearity	Hysteresis	Drift	Influence of curvature surface
Kikuhime®	pneum.	flat [Flaud 10]	4.3 %	0.6 mmHg ± 3.1 %	$R^2 = 0.99$			R=25 mm: -15 % ; R = 50 mm: - 14%
		curved [Partsch 10]	-1 - 6.5 mmHg	1.54 - 19.7 %	r = 0.99			
		flat and curved [Thomas 14]	0.38 ± 0.288 mmHg		$R^2 = 0.99$	very small hysteresis on curved surfaces		very large pressure overestimation for diameters from 41 to 110 mm
Picopress®	pneum.	curved [Partsch 10]	-5.5 - 1.5 mmHg	1.05 - 7.4 %	r = 0.99			
		flat + curved [Thomas 14]	0.02 ± 0.303 mmHg		$R^2 = 0.99$	very small hysteresis on curved surfaces		large pressure overestimation for diameters from 41 to 110 mm
Flexiforce™	resist.	flat [Ferguson-Pell 00]		2.3 - 6.6 %	1.9 - 9.9 %	5.4 %	1.7 - 2.5% /log. time	significant impact of curvature but suitable for measurement on surfaces with r > 32 mm
MST MKIII Salzmann	pneum.	flat [Flaud 10]	15.4 %	0.5 mmHg ± 2.0 %	$R^2 = 0.99$			R=25 mm: -18 % ; R = 50 mm: - 15%
SIGaT-Tester®	pneum.	curved [Partsch 10]	-12 - 3 mmHg	2.19 - 20.07%	r = 0.99			
Talley digital skin evaluator	electro. pneum.	flat [Flaud 10]	3.1 %	0.7 mmHg ± 2.9 %	$R^2 = 0.99$			R=25 mm: -27 % ; R = 50 mm: - 36%

Table 2.4: Characteristics of some pressure sensors used for the measurement pressure applied by compression devices on the lower leg

Pressure measurements are the first step for the evaluation of medical compression bandages. However, the second step is to link this interface pressure to the improvement of venous return. Also, pressure measurements consist in a retrospective approach to understand compression bandages. There is a possible prospective approach: the development of a numerical model of bandage application.

2.4.2 Model of the action of compression therapy

2.4.2.1 Introduction to soft tissue mechanics and modelling

The lower leg is mainly composed of muscle and adipose tissues surrounding two bones, the tibia and the fibula (Figure 2.1). Soft tissues are often submitted to large strains and have a non linear mechanical behaviour. More especially, muscle tissues show an orthotropic and viscoelastic mechanical behaviour [Van Loocke 06]. Very often, soft tissues are considered as hyper-elastic materials [Bouten 09]. Several constitutive equations were designed to describe the behaviour of hyper-elastic materials [Fung 93]. A simple constitutive equation, which describes the mechanical response of isotropic hyper-elastic material is the *neo-Hookean* strain energy density function:

$$\Psi = c_{10}(\bar{I}_1 - 3) \; + \; \frac{\kappa}{2}(J-1)^2 = \Psi_{isochoric} + \Psi_{volumetric} \text{ and } c_{10} = \frac{\mu}{2} \tag{2.12}$$

κ is the compressibility coefficient (or bulk modulus) and c_{10} is the elasticity coefficient, which is proportional to the shear modulus μ. This strain energy density function is composed of a isochoric part $\Psi_{isochoric}$ and a volumetric part $\Psi_{volumic}$, which is equal to zero for incompressible materials. This mechanical description of soft tissue was used for breast tissues [Chung 08], brain tissues [Kyriacou 98], lower limb soft tissues [Dubuis 12], residual limb soft tissues [Portnoy 08] or even to assess the impact of sitting position on human buttocks soft tissues [Linder-Ganz 07]. Eventually, it is possible to link the neo-Hookean constitutive parameters c_{10} and κ with the Hookean ones, for very small strains [Fung 01]:

$$\text{Neo-Hookean} \rightarrow \text{Hokean constitutive parameters} \quad E = \frac{18\kappa c_{10}}{3\kappa + 2c_{10}} \quad \text{and} \quad \nu = \frac{3\kappa - 4c_{10}}{6\kappa + 4c_{10}} \tag{2.13}$$

$$\text{Hookean} \rightarrow \text{neo-Hokean constitutive parameters} \quad c_{10} = \frac{E}{4(1+\nu)} \quad \text{and} \quad \kappa = \frac{E}{3(1-2\nu)} \tag{2.14}$$

2.4.2.2 Characterization of soft tissue mechanical properties

To build a numerical model of bandage application, it is essential to understand the mechanical behaviour of fabric materials, but also the behaviour of lower limb soft tissues. There are three methods for the identification of soft tissue mechanical properties.

The first one consists in *in vitro/ex vivo* mechanical testing. The tests are usually the same as for the identification of mechanical properties of other solid materials: tension and compression tests [Fung 93]. However, the extraction of soft tissues tends to degrade the samples. They are no more perfused and the hydration and temperature may vary. This method allows the differentiation of the tissues (between muscle and adipose tissue for example).

Another possibility is to characterize the mechanical properties of *in vivo* tissues by direct measurements. A recent method is elastography. Ultrasound elastography or magnetic resonance elastography provides elasticity maps of the tissues [Bercoff 04] [Bensamoun 08] [Frauziols 15b]. Thanks to this method it is possible to characterize the mechanical properties of muscle tissue

during contraction for example, which is not possible with *ex vivo* techniques. However, they very often consider soft tissue material as elastic material. Thus, it is not possible to identify the material parameters for complex constitutive laws.

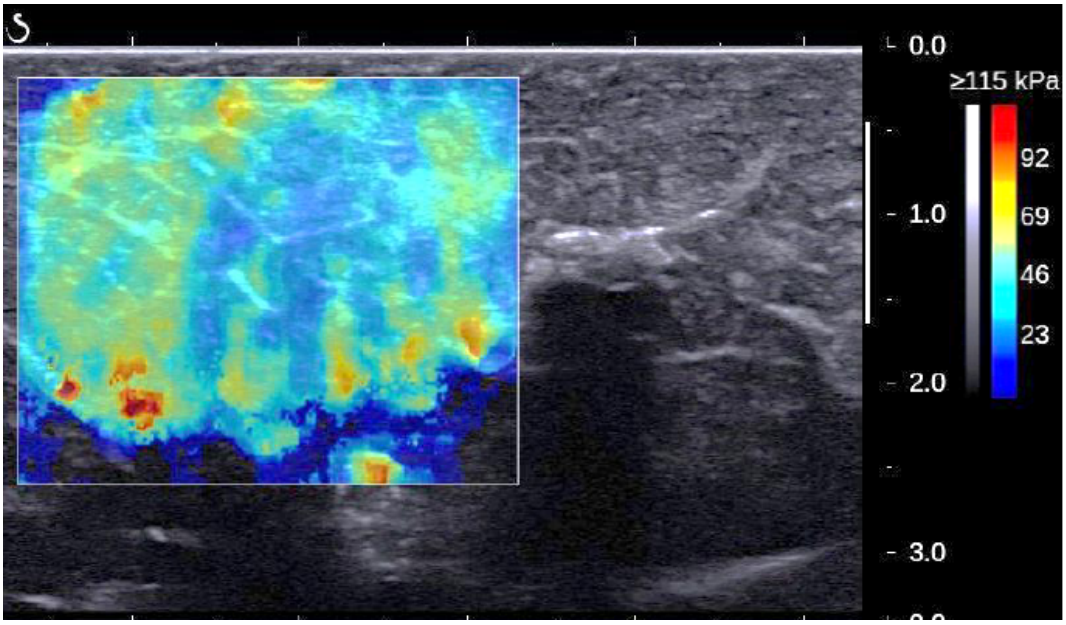

Figure 2.13: Illustration of an elasticity map obtained thanks to ultrasound elastography - [Frauziols 15a]

Eventually, a solution could be to associate *in vivo* experiments with numerical simulation. This method is called *inverse identification* and is suitable when the experimental technique is complex and/or the analysis can not be performed analytically. A numerical simulation is built to replicate an experimental test. The mechanical parameters to identify are set to initial values. The simulation is run and the numerical output is then compared with the experimental one. The mechanical parameters are modulated until the difference between the numerical and experimental outputs fulfil the stopping criterion (Figure 2.14). This method can identify material parameters for various constitutive laws and several types of soft tissues: skin [Boyer 13], brain tissue [Miller 00], arterial tissue [Franquet 12] or musculo-skeletal tissue [Takaza 13] [Chawla 08] [Affagard 15]. Inverse identification was very often used in soft tissue biomechanics when it is not possible to have a simple and perfectly controlled experiment.

2.4.2.3 Simulation of the action of compression therapy

The simulation of the action of compression therapy can help to understand the action mechanisms of the treatment when experiments are too limited to access some data or to make a distinction between competing phenomena for instance. It can also be used as a patient-specific method to predict the action of the treatment (predicting tool). The simulation can provide information that are not experimentally available, as the complete interface pressure distribution over the leg or hydrostatic pressure inside the soft tissues for example.

In existing previous studies, the investigation of the action mechanisms of compression therapy by numerical simulation can be divided in 3 steps:

- first, to better understand how interface pressure is distributed over the leg

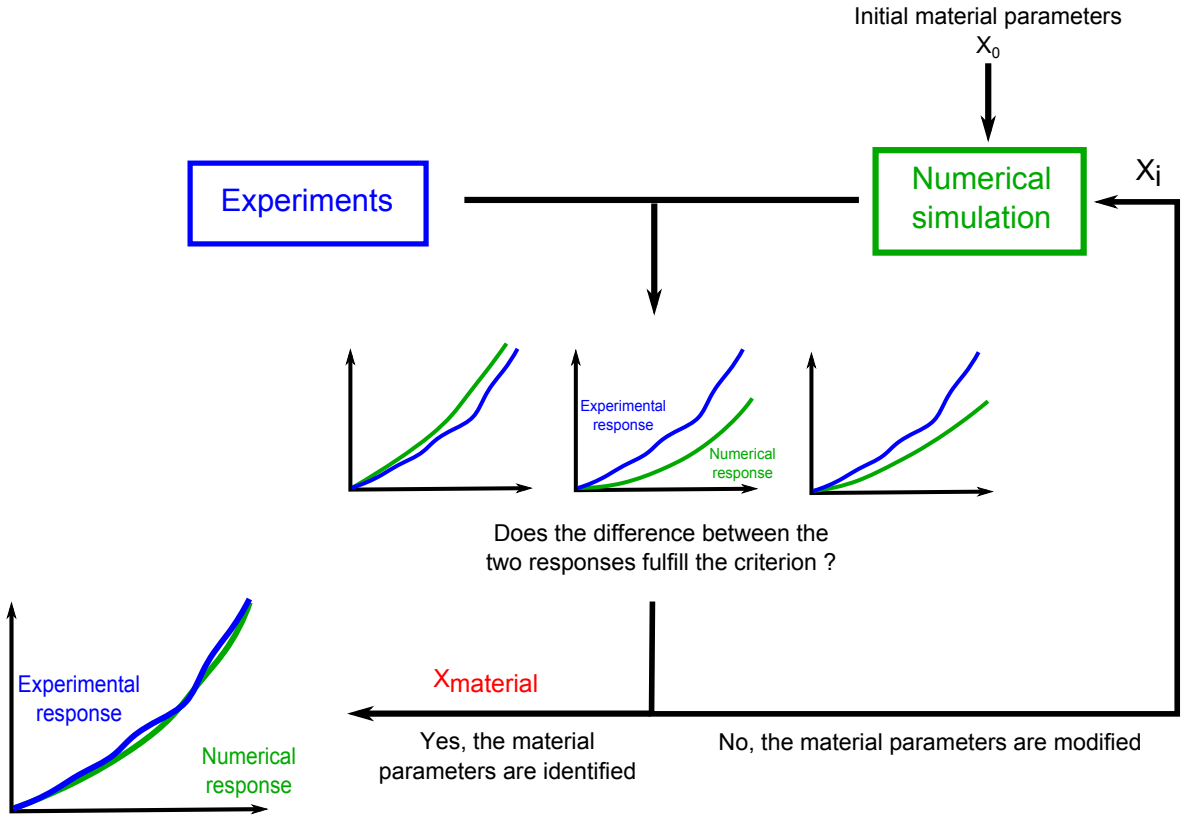

Figure 2.14: Inverse method for the identification of material parameters

- then, to investigate the pressure transmission from the external surface of the leg to the veins through soft tissues
- eventually, to understand how the pressure applied to the veins can enhance venous return.

Most of the studies were focused on the action mechanisms of compression stockings.

Simulation of the action of compression stockings

One of the first simulations designed to understand interface pressure distribution was a 2D model of a plastic leg whose geometry was obtained from a CT-scan [Uhl 05]. The stocking was first inflated and then relaxed to apply pressure on the leg section. The pressure given by the simulation showed trends in accordance with the pressure measured in the experiments. Also 3D models of stockings application were built [Dai 07] [Liu 06]. The stockings was pulled from the ankle to the top of the leg, whose geometry was obtained from MRI. This application technique was very realistic. Leg soft tissue were modelled as one homogeneous elastic material. Both models showed a good agreement with experimental pressure measurements.
Other 2D [Avril 10] [Bouten 09] and 3D [Dubuis 12] (Figure 2.15 - B) models of the action of compression stockings were designed in order to characterize the mechanical properties of leg soft tissues and hydrostatic pressure distribution in internal soft tissues. Both simulations differentiated muscle tissue from adipose tissue in the lower limb but *muscle* tissue was considered as a single homogeneous material. However, interface pressure applied on the external surface of the leg was obtained with Laplace's Law and the stockings was not modelled.

Finally, several 2D models investigated the pressure transmission through soft tissues to the veins [Narracott 09] [Rohan 15] [Wang 13] (Figure 2.15 - B). These complex models are composed of different muscle groups, adipose tissue and veins. They help to link interface pressure to therapeutic effects.

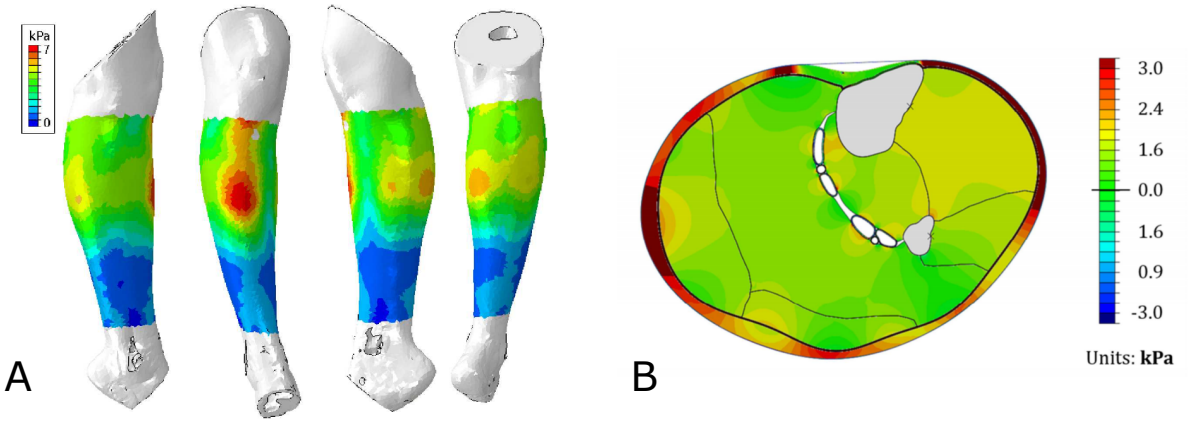

Figure 2.15: A - Illustration of pressure distribution applied by compression stockings over the leg [Dubuis 11]; B - Hydrostatic pressure in the leg soft tissues under elastic compression [Rohan 15]

Simulation of the action of compression bandages

Al Khabury et al. specifically developed a numerical model to compute interface pressure applied by compression bandages [Al Khaburi 11a] (Figure 2.16). The leg geometry was obtained thanks to a 3D scanner and the applied pressure was computed thanks to an improved Laplace's Law. Nevertheless, the bandage application was not modelled and thus soft tissues deformation induced by bandage application was not considered in this model.

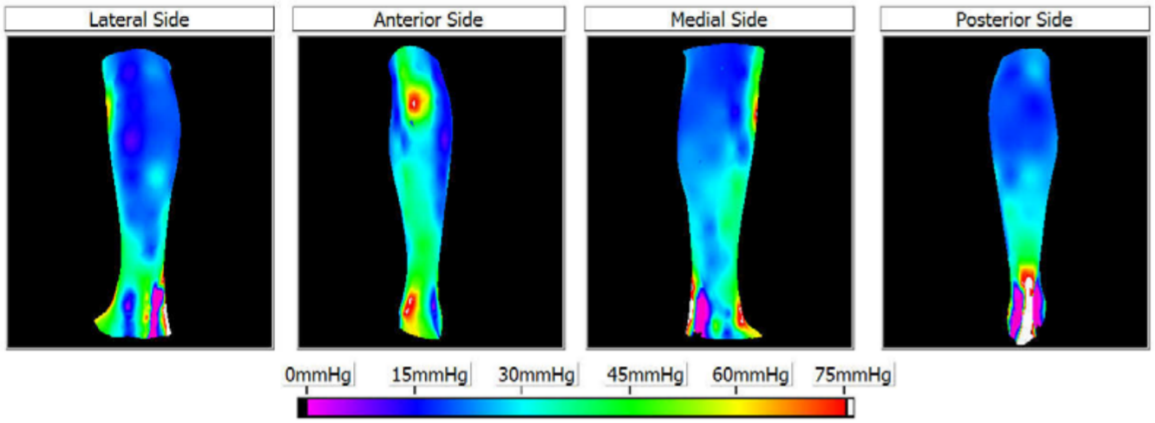

Figure 2.16: Pressure distribution applied by a compression bandage - [Al Khaburi 11a]

2.5 Synthesis and positioning of the study

This work is a collaboration between a medical devices manufacturer, the company Thuasne, a Biomechanics Laboratory, the *Centre Ingénierie et Santé* (Mines Saint-Etienne), and the University Hospital of Saint-Etienne.

The state of the art highlighted the need of new tools or methods to predict interface pressure applied by medical compression bandages. The action mechanisms of compression stockings but also the way interface pressure is transmitted through soft tissues to the veins were investigated in several studies. However, even though the clinical evidences of the positive impact of compression bandages are numerous, the mechanisms at stake in this treatment remain only partially understood [Partsch 03a].

The concept of evidence-based medicine is defined as *the conscientious, explicit, and judicious use of current best evidence in making decisions about the care of individual patients* [Sackett 96]. This concept requires strong research but also includes a patient-specific medicine. Consequently, a better understanding of the mechanisms of a treatment and its patient-specific modulation are the cornerstones of this concept. It will result in an improvement of practitioners' prescription and thus to a better observance of the treatment. In the meantime, it would also help manufacturers to design compression bandages.

Consequently, the objective of this work was to better understand interface pressure generation by compression bandages on the lower limb, thank to a biomechanical approach. This approach was divided between experimental pressure measurements and the development of a simulation of the application of compression bandages. This study was only focused on interface pressure distribution. Thus neither the transmission mechanism of this pressure through soft tissues nor the impact of interface pressure distribution on the treatment outcomes were investigated.

Preliminary experimental and numerical studies showed that a classical approach, based on Laplace's Law, is insufficient to describe interface pressure generation. From the questions and issues raised by these preliminary studies, the work was divided into the following steps:

- the development of a new methodology to characterize patient-specific calf soft tissue mechanical properties, as it was shown that leg soft tissue deformation induced by bandage application played a role in pressure generation,
- the design of a method to characterize the fabric-to-fabric frictional properties, as it may have an impact on interface pressure,
- the numerical simulation of bandage application based on realistic kinematics of bandage wrapping on the lower leg,
- experimental interface pressure measurements coupled with the characterization of calf soft tissue mechanical properties, through the design of a clinical study, with the aim to validate the numerical simulation but also to investigate the pressure applied by the superimposition of compression bandages.

Main choices and assumptions

Interface pressure measurements help to understand pressure generation. However, as a first and simpler approach, all measurements performed in this study were static measurements. Also, they were taken in a very short time scale, which makes it impossible to draw any conclusion about the long term behaviour of compression bandages. The measurements were taken at the height of measurement point B1 and C (Figure 2.7). These points were chosen following the recommendations of a consensus paper [Partsch 06]. Measurement point B was not considered in this study because this area is mainly composed of bones and tendons.

At the same time, a 3D numerical simulation of a single bandage application was developed. This simulation was based on patient-specific geometries, obtained from a 3D optical scanner. Thus, the internal geometry was not available. The leg soft tissues, composed of muscle and adipose tissues, were modelled as one quasi-incompressible homogeneous hyper-elastic material. Muscle tissues were always in a passive state. Compression bandages mechanical behaviour was simplified to an orthotropic linear elastic material. The leg model was simplified because the development of the simulation was mainly focused on the bandage application technique.
The aim of the simulation is first to highlight the main parameters impacting interface pressure but also to provide a patient-specific tool to predict interface pressure distribution.

Chapter 3

Etudes préliminaires - *Preliminary studies*

This third chapter describes the first experimental and numerical studies. The experimental studies consisted in interface pressure measurements, with the aim to evaluate the impact of several parameters on interface pressure (bandage mechanical properties, application technique, leg morphology, ...). This article was published in the Annals of Biomedical Engineering (vol. 43, no. 12, pp. 2967-2977, Dec. 2015). This first experimental study was combined with a first numerical simulation of bandage application. This study was published in the Annals of Biomedical Engineering (vol. 44, no. 10, pp. 3096-3108, Oct. 2016).
These two preliminary studies showed the limitations of the use of Laplace's Law to explain interface pressure generation.

Contents

3.1 Résumé

Ce deuxième chapitre regroupe deux études préliminaires sur les pressions exercées par des bandes de compression ou aussi appelées pressions d'interface.

La première est une campagne de mesure de pression. L'objectif de ces mesures était d'étudier l'impact de plusieurs paramètres sur la pression d'interface : les propriétés mécaniques des bandes, la technique de pose ainsi que la morphologie de la jambe.
Pour cela, des mesures de pressions ont été réalisées sur les jambes de 30 sujets sains (15 femmes - 15 hommes) sélectionnés en fonction de la circonférence de leur mollet à hauteur du point de mesure B1 [Partsch 06] (jonction entre le tendon d'Achille et le muscle gastrocnémien). Les mesures ont été effectuées en deux points, B1 et C (là où la circonférence du mollet est maximale) (Figure 3.1), sur la face médiale de la jambe avec le capteur Picopress®, en position allongée et debout. Deux bandes, Biflex® 16 et Biflex® 17 (Thuasne), ont été posées en spirale à deux ou trois recouvrements (c'est-à-dire, en recouvrant la bande sur la moitié ou les 2/3 de sa hauteur) (Figure 3.2). Ces deux bandes ont des structures semblables, mais des modules élastiques différents (Tableau 3.1). L'allongement des bandes une fois posées sur la jambe a été mesuré au niveau des points B1 et C. Tous les bandages ont été posés par le même expérimentateur.

La mesure de l'allongement des bandes à la pose a montré qu'il était proche, en moyenne, de celui préconisé par le fabricant (allongement = 1.3), mais variable sur la jambe (Figure 3.4 - A). Aucune différence significative n'a été observée entre les pressions mesurées sur les sujets féminins et celles mesurées sur les sujets masculins, sauf une très faible différence pour la variation de pression entre la position allongée et debout. Cependant, la pression mesurée était différente suivant la circonférence de la jambe (pression inférieure pour les grandes circonférences par rapport aux petites circonférences) (Figure 3.6). La pression exercée par les 4 bandages (2 types de bande et 2 types de pose) augmente significativement entre la position allongée et debout (Figure 3.5 - D). De plus, une très forte corrélation ($p < 0.00001$) a été observée entre le nombre de recouvrements et la pression d'interface (Figure 3.5 - B). Le ratio entre la pression exercée par une bande posée à 3 recouvrements et une posée à 2 recouvrements était égal à 1.52, ce qui était en accord avec la loi de Laplace :

$$Pression = \frac{\text{nb de recouvrements * tension de la bande}}{\text{rayon de courbure local}} \; donc \; \frac{P_{3\ recouvrements}}{P_{2\ recouvrements}} = \frac{3}{2} = 1.5 \tag{3.1}$$

Cependant, bien qu'une très forte corrélation ($p < 0.00001$) entre les propriétés mécaniques des bandes et la pression ait été observée (Figure 3.5 - A), le ratio entre les pressions exercées par 2 bandes ayant des propriétés mécaniques différentes n'est pas égal au ratio de leur tension (1.95 contre 1.48). Le fait que la pression ne soit pas directement proportionnelle à la tension de la bande montre donc la limite de la loi de Laplace.

La deuxième partie de ce chapitre décrit la construction d'un modèle numérique personnalisé de la pose d'une bande de compression sur la jambe.

Cette modélisation est basée sur la géométrie de la jambe obtenue avec un scanner optique 3D. La géométrie de la bande est ensuite construite à partir de cette géométrie et adaptée en fonction de la technique de pose (2 ou 3 recouvrements) (Figure 3.10). Le modèle de la bande est conçu de manière à être appliqué sur la jambe avec un allongement égal à 1.3 (conformément aux recommandations du fabricant). La bande est d'abord dilatée puis relâchée sur la jambe afin d'exercer une pression (Figure 3.11). Ces conditions limites sont semblables à celles utilisées

pour modéliser l'action d'une chaussette de compression sur la jambe [Rohan 13] [Bouten 09].

Les résultats de cette simulation, mise en œuvre pour 5 sujets féminins et 4 bandages (Biflex® 16 et Biflex® 17 (Thuasne), posées à 2 et 3 recouvrements), ont été comparés aux pressions mesurées expérimentalement ainsi qu'aux résultats obtenus avec la loi de Laplace (Figure 3.14). Cette comparaison a permis de montrer l'importance de la déformation de la jambe induite par la pose de la bande, qui n'est pas prise en compte par la loi de Laplace (Figure 3.15). Cependant, des écarts entre les pressions issues de la modélisation et les mesures expérimentales montrent qu'il est essentiel de développer une simulation plus réaliste de la pose d'une bande.

En plus d'avoir montré les limites de l'utilisation de la loi de Laplace, ces deux études ont mené à des interrogations quant au rôle des interactions bande-bande (frottement) dans la génération de pression. Ainsi il a été décidé de développer une méthode pour caractériser ce coefficient de frottement.
Parallèlement, l'étude numérique a mis en lumière l'importance des déformations de la jambe dues à l'application de la bande. Une méthodologie a été développée par la suite pour identifier les propriétés mécaniques des tissus mous de la jambe.

3.2 Experimental investigation of pressure applied on the lower leg by elastic compression bandage

Co-authored with Frédéric Martin, Pierre Badel, Reynald Convert, Pascal Giraux and Jérôme Molimard, from [Chassagne 15]

3.2.1 Introduction

Compression bandage is a common treatment for venous or lymphatic pathologies such as venous ulcers or lymphedema. In such diseases, bandages are preferred in the first step of the treatment by compression, instead of stockings. Indeed, during the first days of the treatment, the patients' leg shape changes a lot and the same compression bandage can be applied on the leg with different geometries, whereas a new stocking size would be needed to accommodate these changes. Once the leg shape is stable, the treatment by compression is usually performed with socks or stockings. Bandages are also used when the patient's pathology prevents the use of any other treatment (for example after a knee arthroplasty). Moreover, it is easier for a caregiver to apply bandages than stockings on patients' legs, especially with patients with impaired mobility. Consequently, compression bandage and stockings are complementary.
The bandage, tight on the limb, applies a pressure on the external surface of the limb which is then transmitted to the internal tissues and to the veins [Partsch 05a] [Rohan 15]. Numerous studies have proven the effect of compression therapy on venous and lymphatic system [Agu 99] [O'Meara 12] [Int. L. F. 12], whether compression is performed with bandage or stockings [Brizzio 10].
The efficacy of the treatment mainly depends on the level of pressure which is applied on the limb [Milic 10] [Partsch 06]. This level of pressure depends on several parameters such as:

- the bandage mechanical properties,
- the bandage components (padding layer, cohesive bandage, ...),
- the bandage stretch,
- the local curvature of the limb on which the bandage is applied,
- the application technique (spiral or figure of eight),
- other parameters such as friction between the different layers, mechanical properties of the limb soft tissues, ...

Better understanding how these parameters impact the level of applied pressure would lead to an improved treatment with compression bandage. A well-known theoretical relationship between the tension, T, of the bandage (force needed to stretch the bandage, which is given by the bandage mechanical properties and the applied stretch), the local curvature, r_C, of the limb and the locally applied pressure, P, is given by the Laplace's Law:

$$P = T/r_C \tag{3.2}$$

However, it has been shown that this law is not sufficient to explain the pressure distribution over a limb [Al Khaburi 12] [Thomas 03a], hence the need for an experimental investigation of the pressure applied by compression bandage on the lower leg.
Several measurements of the pressure applied by bandages were carried out, with various types of bandages, at different measurement points and on a wide range of subjects in different body positions [Damstra 13] [Danielsen 98b] [Mosti 13]. In order to standardize the way to

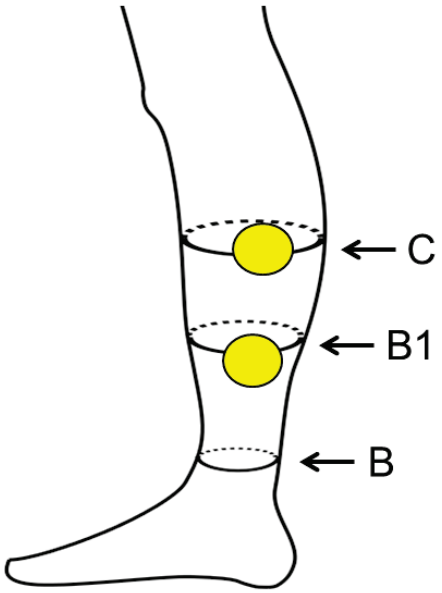

Figure 3.1: Location of measurement points B1 (where the Achilles' tendon turns into the gastrocnemius muscle) and C (where the calf circumference is the largest)

perform pressure measurements, recommendations have been published to proceed to interface pressure measurements [Partsch 06]. Measurement points have been identified on the lower leg [Partsch 06] such as (Figure 3.1):

- Measurement point B1: corresponding to the height where the Achilles' tendon turns into the gastrocnemius muscle
- Measurement point C: corresponding to the height where the calf circumference is the largest.

The pressure sensors used for the measurements should meet some requirements: for example to be thin and flexible [Partsch 06]. Different types of sensors exist but some have proven to be more reliable than others [Partsch 10] (Kikuhime® and Picopress® for example).
Most of the measurement campaigns which were performed on men and women did not take the gender difference into account [Mosti 13] [Mosti 10a]. However the leg morphology has an influence on the applied pressure. Indeed, the leg morphology varies from a subject to another and maybe even more especially from a female subject to a male subject [Huston 08].
Other groups investigated the impact of the application technique on the interface pressure [Coull 06] and they also measured the stretch of the applied bandage. However, as the aim of this previous study was to compare the pressure applied by different application techniques, it was carried out for a single bandage type. Other studies were focused on the influence of bandage mechanical properties and position (supine, standing, sitting) on the interface pressure [Danielsen 98b] [Hirai 09] [Benigni 08] [Rimaud 14], but as far as we know, none of them measured the stretch of the applied bandage, though it is one of the main parameters which controls the interface pressure.
This shows the need of performing other pressure measurements in order to simultaneously evaluate the influence of all following parameters on the interface pressure: bandage mechanical properties, application technique, subjects' gender and morphology and position (supine or

standing).
Within this context, the objective of the present study is to perform a complete campaign including bandage stretch and pressure measurements in order to test the following hypotheses:

- The applied pressure is proportional to the bandage elastic modulus (or the force needed to stretch the bandage),
- The applied pressure is proportional to the bandage overlapping (50% or 66% overlapping means that respectively 2 or 3 bandage layers cover the leg),
- The interface pressure significantly decreases when the subjects' leg circumference increases.

Moreover, these measurements result to a quantitative evaluation of the pressure differences among female and male subjects and of the pressure increase between the supine and the standing position.

3.2.2 Methods

Briefly, stretch and pressure measurements were performed on healthy male and female subjects in order to estimate the gender influence. Subjects were chosen in order to have a wide range of morphologies. Two different elastic bandages, with different mechanical properties, were applied on the subject's leg with two application techniques with the aim of evaluating the influence of mechanical properties, application technique and position (supine or standing) on the interface pressure.

3.2.2.1 Bandages

Two commercially available elastic bandages, which differ in their mechanical properties, were applied on the subjects' leg by the same experienced operator: the Biflex® 16 (B16) and the Biflex® 17 (B17) (Thuasne, Levallois-Perret, France) which is stiffer (Table 3.1). Bandage elastic modulus (K), in N/mm, is defined as follows:

$$K = \frac{\text{force to stretch the bandage}}{\text{bandage width } * \ (L - L_0)/L_0} \tag{3.3}$$

where L is the length of the stretched bandage and L_0 its initial length (Figure 3.2). Both bandages were 10 cm wide. They were applied on the leg with a target stretch of 1.3, in accordance with the manufacturer's recommendations and visual calibration marker (Figure 3.2). This visual calibration marker is a rectangle which turns into a square when the bandage stretch is equal to 1.3. It gives a visual indication to the bandager that the stretch is in accordance with the manufacturer's recommendations. The stretch is defined as the ratio between the length of the stretched bandage and its initial length ($stretch = L/L_0$). Bandage can be applied in the form of a spiral with a 50% or a 66% overlap, which means that at each turn, the bandage layer on top covers the bandage layer below respectively by 50% or 66% (Figure 3.2 and Figure 3.3). For a 50% or 66% overlapping technique, the leg is covered by respectively 2 or 3 bandage layers. The value of the overlap is usually prescribed by medical doctors. Lines were drawn on the bandage to help the bandager to apply the bandage with the correct overlap: one at 50% and one at 33% of the bandage width, for respectively a 50% and a 66% overlapping technique (Figure 3.2).

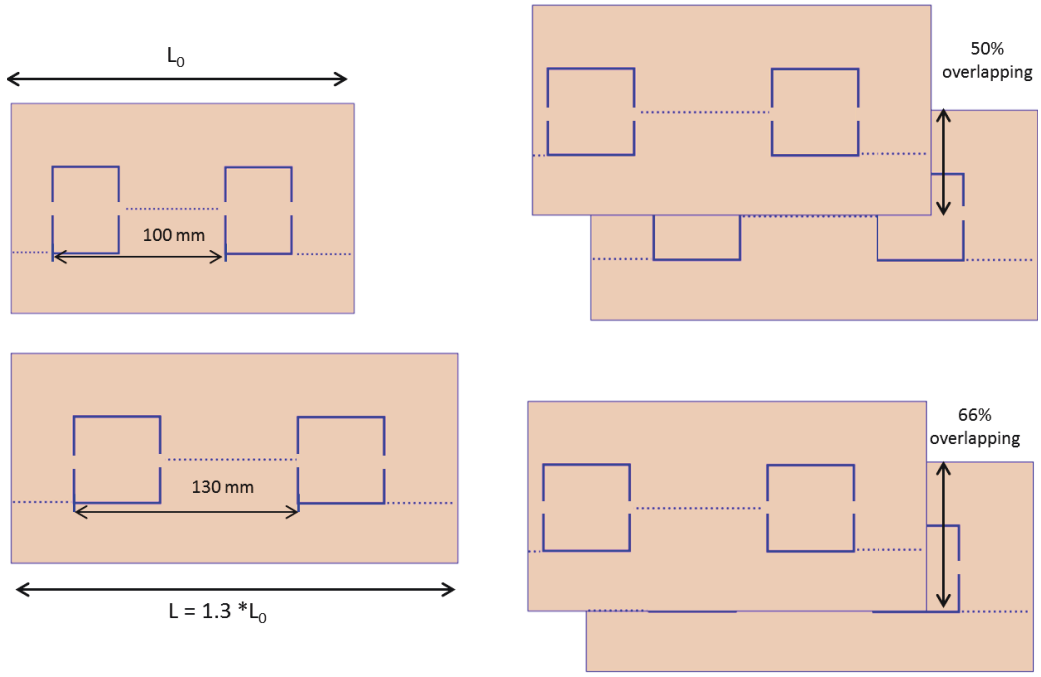

Figure 3.2: Bandage stretch and application technique in the form of a spiral; A visual marker (a rectangle which turns into a square when the bandage stretch is about 1.3) helps to apply the bandage with the correct stretch; Lines are drawn to help to apply the bandage with the correct overlap

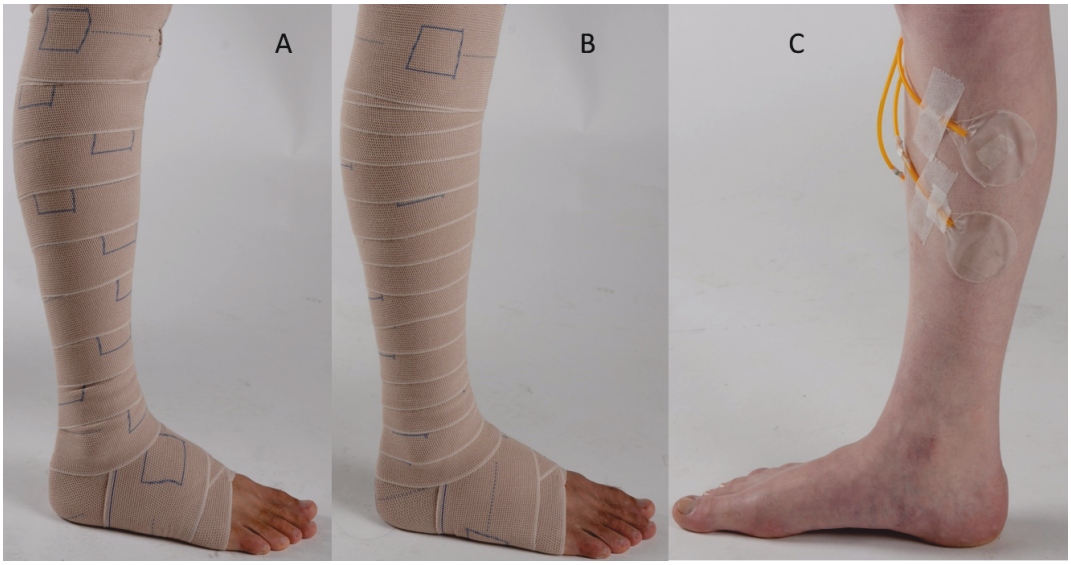

Figure 3.3: Bandage applied in the form of a spiral with a 50% (A) or 66 % (B) overlapping technique and locations of the sensors (C)

	Longitudinal elastic modulus $[N.mm^{-1}]$	Force at stretch = 1.3 $[N.mm^{-1}]$
Biflex® 16 (B16)	0.23	0.07
Biflex® 17 (B17)	0.44	0.13

Table 3.1: Mechanical properties of the two bandages used for the pressure measurements

3.2.2.2 Pressure sensors

The interface pressure was measured with pneumatic pressure sensors Picopress® (MicroLab Elettronica, Ponte S. Nicolo, Italy). This pressure sensor is a convenient device which was used in several previous pressure measurements studies [Damstra 13] [Lattimer 14] [Mosti 14].
As a preliminary study, the accuracy, the linearity and the hysteresis of the sensors were tested. To achieve this, the sensor was placed at the bottom of a water column. First, the column was filled with water and a measure was taken every 10 $mmHg$ (13.6 cmH_2O) from 0 to 147 $mmHg$ (199.9 cmH_2O). Then the column was emptied and a measure was taken every 10 mmHg. This allowed characterizing the hysteresis of the sensor, which is given by the following equation:

$$E_h = \underset{x_i}{mean}(\frac{|y_+(x_i) - y_-(x_i)|}{x_i} * 100) \tag{3.4}$$

where, $y_+(x_i)$ and $y_-(x_i)$ are the measured pressure value for a theoretical applied pressure equal to x_i, respectively during the loading and the unloading phases. The second test consisted in applying 20 different pressure values, which were randomly determined and allowed characterizing the sensor linearity. The coefficient of determination R^2 was used as the indicator of the linear dependence between the theoretical and the measured pressure. The closer to 1 the coefficient R^2 was, the more linear the sensor was.
These tests were performed for the Picopress® device and the two sensors which were used in the study (respectively at measurement points B1 and C).
The tests showed that R^2 was almost equal to 1 for both sensors ($R^2 = 0.9999$) and that the hysteresis was slightly higher for the sensor located at measurement point B1 (1.0%) than for the other sensor located at measurement point C (0.0%).
The tests performed on the sensors showed that these sensors were very reliable and, hence, suitable for the present work, which was in accordance with the tests conducted by Partsch et al. [Partsch 10].

3.2.2.3 Experimental Protocol

Subject selection

Pressure measurements were carried out on 30 healthy subjects, 15 women and 15 men, following informed consent (Table 3.2). This protocol was approved by the local ethics committee.
The subjects' selection was made with regards to their circumference at measurement point B1 (Figure 3.1) in order to be equally distributed in 3 groups of circumference at B1 height.
For this, a list of 205 women and one of 147 men were built and alphabetically ordered. Six groups (three for women and three for men) were created, depending on the subjects' circumference at measurement point B1:

	Age	Circumference at B1 [cm]	Circumference at C [cm]
Women	41.6 ± 1.3	31.4 ± 1.3	36.2 ± 1.6
Men	43.6 ± 1.1	30.4 ± 1.2	36.9 ± 1.4

Table 3.2: Age and morphological data (circumferences at measurement points B1 and C) of the subjects

- Circumference $\leq$ 29 cm,
- Circumference $>$ 29 cm & $<$ 32 cm,
- Circumference $\geq$ 32 cm.

Then 5 subjects were randomly selected in each group. The only criteria for subject selection were their gender and their circumference at point B1.
Once the subjects were chosen, the order in which they would take part in the study was randomly determined.

Pressure measurements

Two sensors were positioned on the medial side of the right leg at heights corresponding to the measurement points B1 and C (Figure 3.3). Measurement point B1 was chosen following the recommendations of a consensus paper on interface pressure measurements [Partsch 06] and measurement point C was chosen because it corresponds to a part of the calf which is mainly composed of soft tissues. All bandages were applied by the same trained operator. Four types of bandages were applied in the form of a spiral (Figure 3.3):

- B16 with a 50% overlap (B16 - 2 layers),
- B16 with a 66% overlap (B16 - 3 layers),
- B17 with a 50% overlap (B17 - 2 layers),
- B17 with a 66% overlap (B17 - 3 layers).

The order in which the bandages were applied was randomly determined for each subject.
The bandage was applied in the supine position, after a rest time of 5 to 10 minutes (time needed to set the sensors on the subject leg). Immediately after the bandage application, the stretch of the bandage around the measurement points B1 and C was measured thanks to a mark printed on the bandage every 100 mm (Figure 3.2). The distance between three consecutive marks (initially equal to 200 mm) was measured using a measuring tape once the bandage had been applied on the leg, around the locations of measurement points B1 and C, providing the stretch of the bandage (for example, if the distance was equal to 252 mm, the stretch of the bandage at this location was $252/200 = 1.26$).
After bandage application, the subject waited for two minutes in the supine position with the foot slightly raised in order to prevent any contact between the calf and the examination bed. After this time, three successive measurements were acquired. The mean value of the three measurements was considered as the pressure value.
Then the subject was asked to stand up and waited for 2 minutes before the measures were taken again.

3.2.2.4 Statistical Analysis

For all results, the values are given with their 95% confidence interval and all histograms represent the mean value and the 95% confidence interval.
Parametric tests (analysis of variance (ANOVA)) were used to evaluate all difference between two samples (whose size $n \geq 30$), except to analyse the effect of circumference on the pressure (the samples were too small: $n < 30$).
For the small samples ($n < 30$), the Kruskal-Wallis one-way analysis of variance was used and then the individual effects were tested with a Mann-Withney U test ($\alpha = \frac{0.05}{\text{number of tests}}$).

To evaluate the linear correlation between two samples, the coefficient of determination R^2 was computed, which equals the square of the Pearson correlation coefficient between the experimental data and the values from the linear regression. The variable t, which is approximately distributed as a Student's distribution with $n-2$ degrees of freedom for a zero correlation, was used to test the significance of the coefficient of determination R^2: $t = \sqrt{R^2 * \frac{n-2}{1-R^2}}$.

The coefficient of determination was used to characterize the linear correlation between the following parameters:

- the pressure applied by a B16 and the one applied by a B17
- the pressure applied by 2 layers and the one applied by 3 layers
- the pressure at measurement point B1 and the one at point C
- the pressure in the supine position and the one in the standing position.

Difference was considered as significant if $p < 0.05$.

3.2.3 Results

3.2.3.1 Bandage stretch

Considering all bandages together, mean stretch was equal to 1.30 ± 0.007, in accordance with the manufacturer's recommendations (Figure 3.4 - A). However, the results demonstrated that, irrespective of bandage type (B16 or B17), stretch at point B1 was significantly lower ($p < 0.0001$) than at point C. Mean stretch at point B1 was lower than recommended (1.27 ± 0.009). Conversely, at point C, mean stretch was higher than recommended (1.33 ± 0.008).
Also, B17 was applied with a significantly lower stretch than B16 ($p < 0.03$), respectively 1.29 ± 0.009 and 1.31 ± 0.01. No significant difference in stretch was observed at point C between bandage applied with 50% and 66% overlapping. Conversely, at point B1, bandages applied with 66% overlapping exhibit higher stretch compared to bandages applied with 50% overlapping ($p < 0.002$), respectively 1.29 ± 0.012 and 1.26 ± 0.012.

3.2.3.2 Pressure values for the different bandages

Considering all bandage types, body positions and measurement points, interface pressure increased significantly ($p < 0.0001$) with bandage overlapping. Interface pressure applied by bandage with 66% overlap were higher than pressure applied by bandage with 50% overlap (Figure 3.4 - B). Similarly, interface pressure increased significantly ($p < 0.0001$) with bandage elastic modulus: pressures applied by B17 were higher than pressures applied by B16 with the same application technique. There was no significant difference ($p > 0.05$) between interface pressure measured with B16 applied with 3 layers and B17 applied with 2 layers.

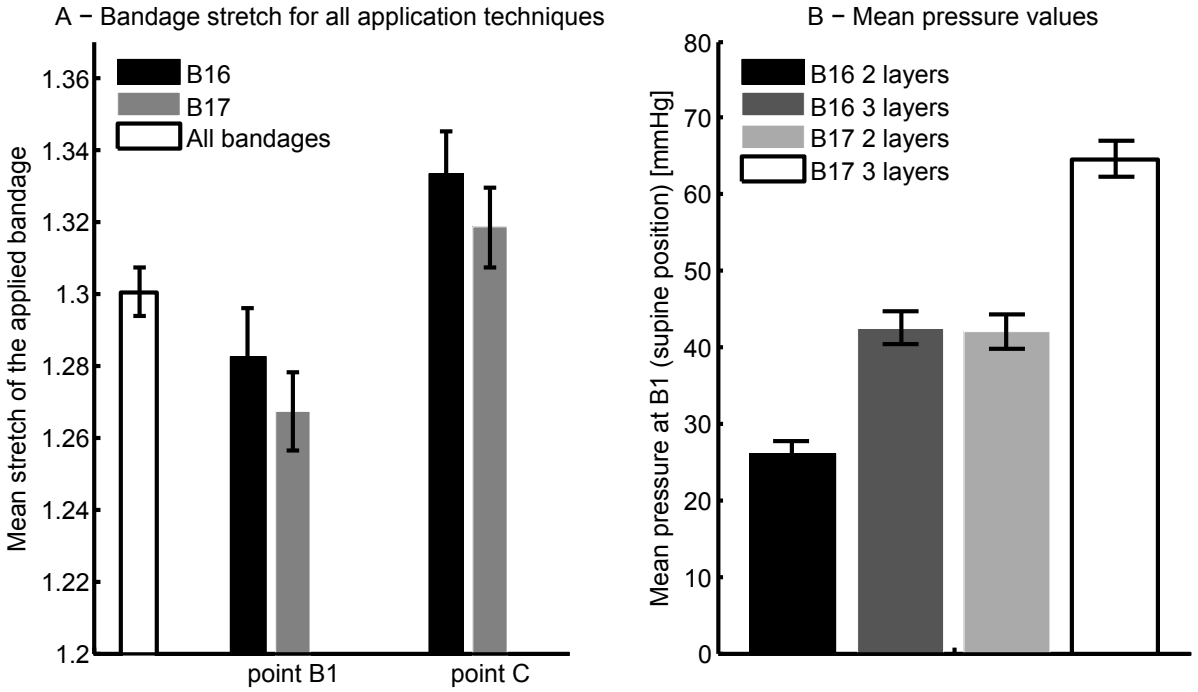

Figure 3.4: Stretch of the applied bandages (A) and mean pressure values (in the supine position) at measurement point B1 for the different bandages (B)

3.2.3.3 Gender influence

There was no overall significant difference between male and female in terms of pressure values and pressure gradient ($p > 0.05$). However, pressure variations between supine and standing positions were significantly different between male and female ($p < 0.01$). These variations were higher for males irrespective of bandage type and measurement point but the difference between sex remained low: the pressure variations between the two positions were +11% for women and +14% for men.

3.2.3.4 Influence of bandage mechanical properties

The correlations between the pressures exerted by the B16 and the B17 were significant at all measurements points, in all positions and for both application techniques ($p < 0.0001$) (Figure 3.5 - A). The pressure exerted by the B17 was about 1.5 times as high as the pressure exerted by the B16 whereas the ratio of elastic moduli was 1.95.

3.2.3.5 Influence of application technique

The correlation between the pressures exerted by any bandage applied with 66% overlap and the same bandage applied with 50% overlap was significant at all measurement points and in all positions ($p < 0.01$) (Figure 3.5 - B).

3.2.3.6 Influence of measurement point (degressivity)

The results demonstrated that, irrespective of bandage type, application method and body position, the elastic bandages followed the principle of pressure gradient along the length of the limb (Figure 3.5 - C). The measured pressures decreased significantly ($p < 0.0001$) from point

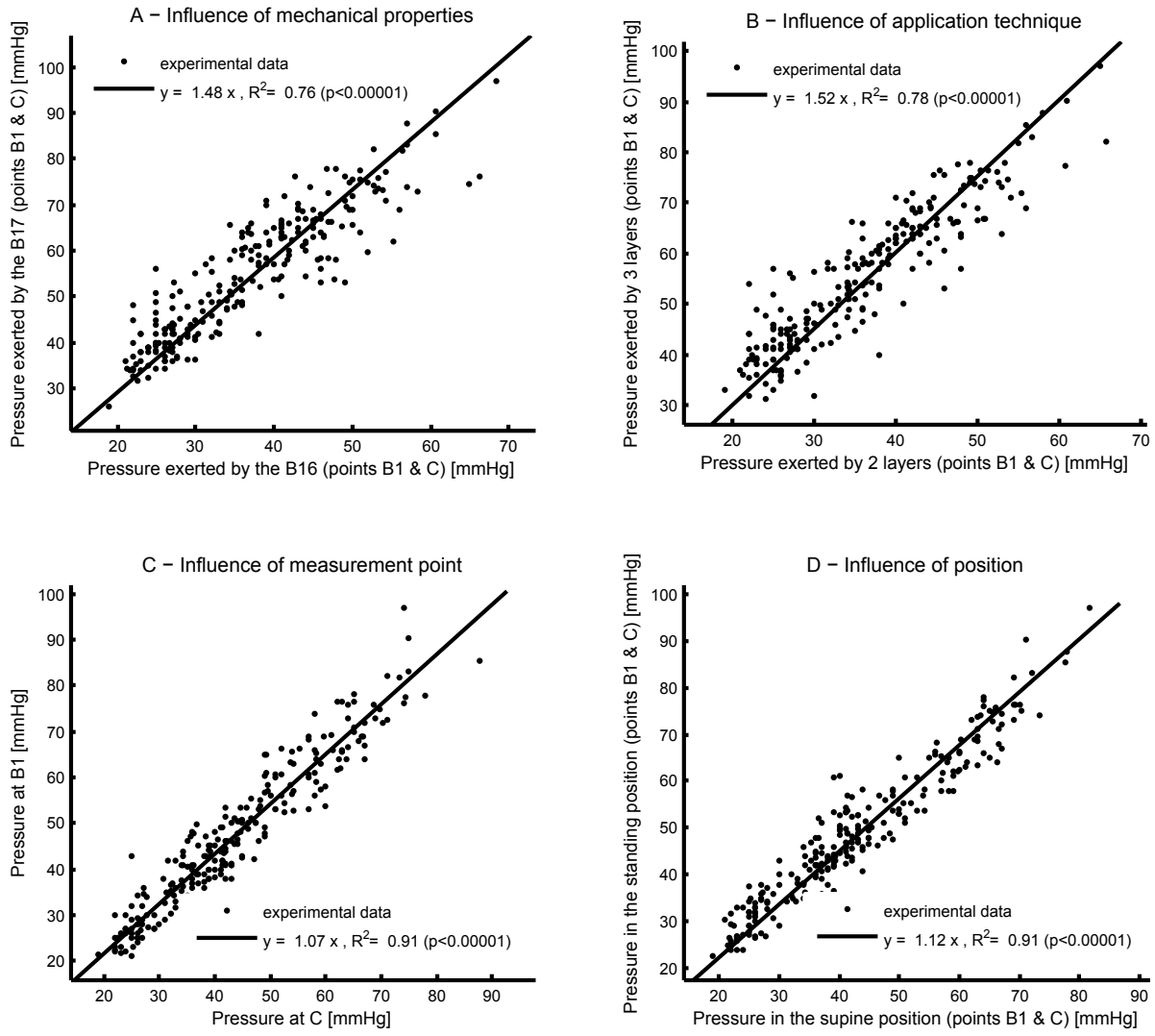

Figure 3.5: Evaluation of the influence on the applied pressure of the bandage mechanical properties (A), application technique (B), and position (D) considering both measurement points; Evaluation of the pressure difference between measurement points B1 and C (C)

B1 to point C, which means that bandages are degressive (decreasing pressure from the ankle to the knee). Pressures measured at point B1 were about 7% higher than pressures measured at point C.

3.2.3.7 Influence of position

The interface pressure increased significantly ($p < 0.0001$) from the supine position to the standing position, at point B1 and at point C, irrespective of bandage type and application method (Figure 3.5 - D). On average, interface pressures in standing position were 12% higher than in supine position.

3.2.3.8 Pressure and circumference

Irrespectively of bandage type, application method and body position, interface pressures tended to decrease when circumference at measurement point B1 increased (Figure 3.6). Differences were always significant ($p < 0.05$) between circumferences at B1 below 29 cm and over 32 cm.

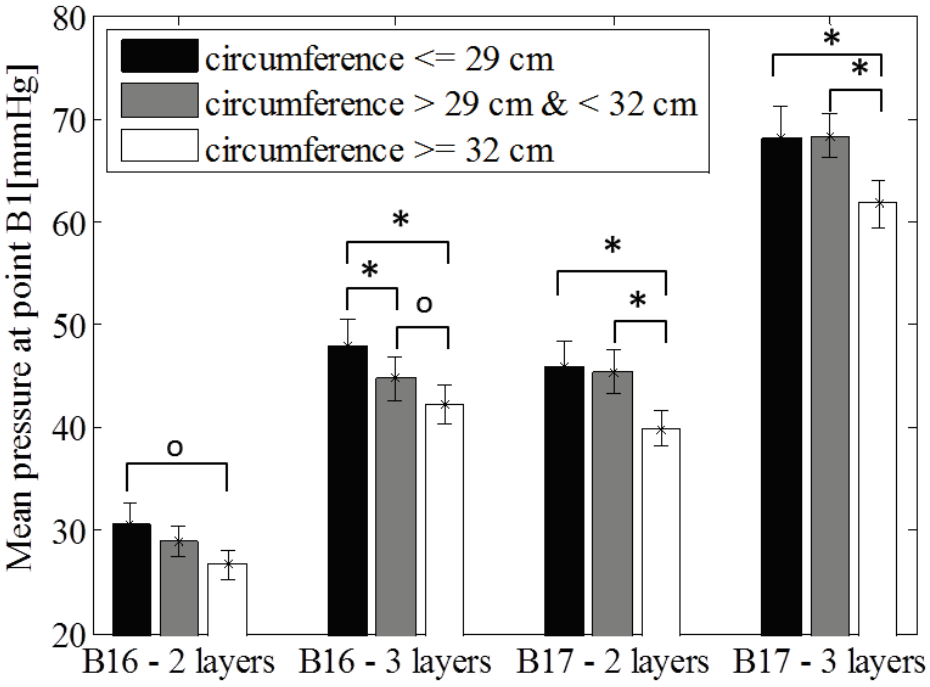

Figure 3.6: Influence of the leg circumference on the interface pressure at point B1 (o : $p < 0.05$, * : $p < 0.02$) - 3 groups of subjects were created regarding their leg circumference at measurement point B1

3.2.4 Discussion

The main strength of the study is to provide a unified investigation of the influence of several parameters on the applied pressure. It quantifies the influence of parameters which were

usually not taken into account. Among the most significant results, it was shown with our measurements that the bandage stretch is the key to a better control of the treatment. This data should be provided and considered in every future study on compression bandages. It was also shown that the relationship between applied pressure and elastic modulus of the bandage is not linear, which disputes once again Laplace's law in the context of compression bandages. The objective of the present study was to perform a complete campaign of stretch and interface pressure measurements carried on 30 subjects in order to test the following hypotheses:

- Hypothesis 1: the applied pressure is proportional to the bandage elastic modulus,
- Hypothesis 2: the applied pressure is proportional to the bandage overlapping,
- Hypothesis 3: the interface pressure significantly decreases when the subjects' leg circumference increases.

All bandages were applied by the same trained operator and the stretch of the applied bandage was close to the manufacturer's recommendations. It was noticed, however, that the actual stretch was not constant over the leg and was influenced by the bandage mechanical properties. It was shown that the interface pressure proportionally increased with the elastic modulus (Hypothesis 1) and the overlapping (Hypothesis 2) of the bandage and that it tended to decrease when the leg circumference increased (Hypothesis 3). Moreover, no significant difference was observed between men and women except for the pressure increase between the supine and standing position, which was larger for men. These results lead to a more detailed analysis of the quantified respective influence of the different parameters on the interface pressure, hence an improved understanding of the treatment. The following discussion is structured around three topics: the bandage itself, the subject and its position.
Even though the bandage stretch greatly impacts the level of interface pressure, it was noticed in previous studies [Bhattacharya 12] [Hafner 00b] that the bandage tension varied a lot with the bandager, even for experienced bandager. However each bandager seemed to be constant and repeatable in applying bandages [Thomas 03b] [Raj 80]. In this study, all bandages were applied by one trained bandager. This is why the observed trends only reflect one bandager's application technique and cannot be generalized straightaway.
Nevertheless, the maximum, minimum and mean stretches (respectively 1.45, 1.18 and 1.30) measured in the present study were in the vicinity of the target value of 1.3. This showed that the calibration marker (a rectangle which turns into a square when the stretch is equal to 1.3 (Figure 3.2) was effective in having a bandage stretch close to 1.3 [Hanna 08]. However, the stretch was not constant over the leg, with larger stretch at point C than at point B1, suggesting an influence of the leg's diameter on the bandager application technique. Moreover, the stretch was larger for the B16 than for the B17, which could be explained by the fact that the B16 was less stiff, so was easier to stretch, thus providing a different feedback to the operator. Measuring the stretch has shown that its control during bandage application can still be improved.

The results revealed a very strong correlation between the pressure and the bandage mechanical properties ($p < 0.00001$). The ratio between the pressure exerted by the B17 and that exerted by the B16 was about 1.5. This result raised an important question. Indeed, the ratio between the forces necessary for a 1.3 stretch was equal to 1.95 (force for the B16 = $0.069 N.mm^{-1}$; force for the B17 = $0.0135 N.mm^{-1}$), which should induce a ratio of 1.95 in pressure according to Laplace's Law as the pressure is supposed to be directly proportional to the force needed to stretch the bandage. Even though the measured stretch was lower for the B17 than for the B16, the relative difference in the stretch ($1.3 \pm 0.9\%$ of the stretch) is not sufficient to explain

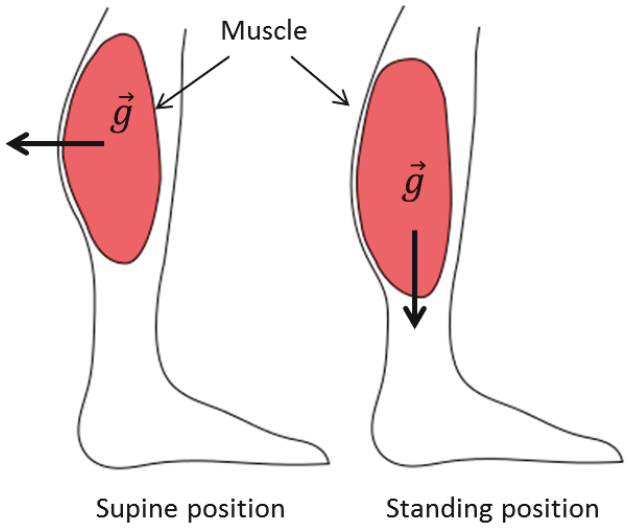

Figure 3.7: Difference in leg geometry between supine and standing position

the difference between the experimental ratio $(1.48, p < 0.00001)$ and the expected ratio (1.95), as this ratio is equal to 1.93 considering the slight difference in stretch. It is hypothesized that this difference is due to friction between the bandages and/or the application gesture. However, these are complex phenomena and need to be further investigated.
This study highlighted a strong correlation between the interface pressure and the bandage overlapping ($p < 0.00001$). The impact of the application technique on the pressure seemed to be in accordance with what was expected. Indeed, the ratio between the pressure applied by a 3-layer bandage and the one applied by a 2-layer bandage should be equal to $3/2 = 1.5$. The experimental ratio was about 1.5 ($p < 0.00001$), which is in accordance with the theory.
The second group of parameters which impacts the interface pressure is directly related to the subjects: their gender and morphology. In this study, pressure measurements were performed on both men and women subjects and the only significant difference between these two populations was for the pressure increase between the supine and the standing position. However the results were not treated separately for men and for women because it has been considered that the difference (3% of the pressure values) was small enough to merge the results. Nonetheless, it may be hypothesized that this small difference is due to the difference in musculature between men and women, which leads to a difference in the geometry variation between the supine and the standing position.
Considering both populations altogether, it was showed that the pressure tended to decrease when the leg circumference increased, which is in general agreement with the Laplace's law, as the pressure is supposed to be inversely proportional to the radius of curvature. Also, the circumference at point C was larger than the circumference at point B1, hence the fact that the bandage was degressive (the pressure at point B1 is higher than the pressure at point C). However, in the Laplace's law, only the local radius of curvature has an influence of the pressure. A larger circumference is only the sign of a global radius estimate but it does not consider local radius values. In that sense, our results showed that the level of pressure can vary significantly from a subject to another and that it depends on their leg geometry.

Eventually, the impact of the subject position was investigated: the pressure increased when moving from the supine to the standing position. Due to gravity, the leg geometry changes

from the supine to the standing position (Figure 3.7). The bandage is applied in the supine position. After bandage application, when the subject stands up, the leg circumference tends to increase [Mosti 07], which leads to an increase in the bandage stretch and induces a pressure increase. This change in geometry from the supine to standing positions may be a consequence of the muscle group tendency to fall down (because of gravity) and of the increase of hydrostatic blood pressure. The observed pressure difference can be used to characterize the stiffness of the bandage as described in the literature [Partsch 05c]. In this study, for which elastic bandages were used, the pressure increase is equal to 6.10 ± 0.54 $mmHg$. This is in accordance with the previous classification given by Partsch et al. [Partsch 05b], where elastic bandages should display an increase below 10 $mmHg$.

Limitations

The subjects in this study were all healthy subjects whose mean age was lower than the mean age of pathologic patients using compression bandage. An interesting perspective will be to carry out the same measurements on patients. Moreover, the pressure measurements were performed almost right after the bandage application, therefore neglecting the behaviour of compression bandage over time (slipping of the bandage, pressure loss, ...). Also, all measurements were static measurements.
All the tests that have been performed on the sensors were performed on a flat surface whereas they were used on a curved surface. This type of sensor was already tested on curved surface and showed some imprecisions: they tend to slightly overestimate pressure values [Thomas 14]. However, the largest radius of curvature used in this study was 55 mm whereas the approximated radius of curvature of the limbs in this study went from 40 to 70 mm (for measurement points B1 and C). The influence of curvature on the pressure measured by the pressure sensor Picopress®, in the range of limb curvature, should be further investigated.

Moreover, an on-going work aims to study the modification in the radius of curvature due to the sensor. Indeed, even though its thickness is very small, its 2 mL volume may induce a local variation in the radius of curvature, which may affect the local value of interface pressure.
All bandages were applied by the same person in order to prevent large variations in the bandage application. However, it would have been interesting to evaluate the variation in the application between different bandagers.

3.2.5 Conclusion

This study aimed at an objective evaluation of the influence of bandage mechanical properties, application technique and subject morphology on the interface pressure applied on the lower leg by elastic compression bandages and the influence of these parameters on the stretch actually applied by the bandager. It has revealed a very strong correlation between the applied pressure and the bandage mechanical properties but also between the pressure and the application technique. In a previous study [Partsch 05c], H. Partsch has raised the question of the control of the application technique and our study corroborates this claim. A better control of the stretch and the application technique will lead to a better control of the pressure applied by compression bandages. This study also shows the limit of the Laplace's law in explaining the level of interface pressure and raises some questions about parameters which have not been taken into account yet, such as the friction between the bandage layers. An interesting future direction will address dynamic measurements of the pressure applied by a single compression bandage or the superimposition of 2 compression bandages. These measurements could be

performed on pathologic subjects.

3.3 Numerical approach for the assessment of pressure generated by elastic compression bandage

Co-authored with Jérôme Molimard, Reynald Convert, Pascal Giraux and Pierre Badel, from [Chassagne 16]

3.3.1 Introduction

Compression of the lower leg is a common treatment for venous or lymphatic diseases [Coleridge-Smith 09] and can be performed either with elastic stockings or bandages [Brizzio 10]. Bandages are mainly used in the initial steps of the treatment of advanced stages of these pathologies such as legs ulcers or lymphedema [Allaert 15]. The treatment success depends on the pressure level which is applied on the leg in the supine and standing positions and while walking [Melhuish 00] [Partsch 06]. Even though the efficacy of this treatment, performed either with stockings or bandages, is admitted [Amsler 09] [Brizzio 10], its action mechanism and the pressure it applies on the leg remain poorly understood, especially in the case of bandages [Partsch 03a]. The pressure applied on a leg by compression bandage mainly depends on the following parameters:

- bandage components (crepes, padding layer, ...),
- mechanical properties of the different bandage components, such as elastic modulus,
- bandage stretch,
- application technique (spiral, figure-of-eight) and number of layers (overlap),
- leg morphology (local curvature of the limb),
- other parameters (soft tissue mechanical properties, friction between bandage layers, ...).

Different configurations are proposed to clinicians: application of "inelastic" or "elastic" bandages, 2 or 3 layers bandage application technique or combination of different types of bandages. The relevance and understanding of these various methodologies needs to be addressed.
For this, research on the mechanical action of elastic compression has been addressed using both experimental and modelling approaches, within the aim of understanding pressure generation and its effects on the leg soft tissues. An effort has been made to measure interface pressure applied by compression stockings or bandages [Amsler 09] [Danielsen 98b] [Hafner 00a] [Rimaud 14], though *in vivo* pressure measurements only provide localized information about the applied pressure. However, for now, local measurement methods are significantly more accurate than pressure mapping systems [Bonnaire 14], hence the lack of a convenient method to measure the complete pressure distribution over the leg.
A rough estimation of local pressure field can be obtained with Laplace's law (Equation 3.8) as a function of the local radius of curvature of the limb, the bandage tension and the number of layers. However this equation does not consider every aspect involved in the mechanism of pressure generation [Melhuish 00], such as shape changes due to bandage application or position variations. Despite many attempts to improve this law [Al Khaburi 12] [Thomas 03a], it remains insufficient to quantify the complete pressure distribution [Schuren 08].

Numerical simulations were introduced to achieve this goal. However, most of them sought to better understand the action mechanism of compression stockings which behave in a different way than bandage. Among these studies, a first 2D model was proposed considering a plastic leg, whose mechanical properties were known and whose geometry was obtained from

a CT-scan [Uhl 05]. Experimental pressure measurements were performed on the leg in order to be compared with the results given by the model. In this simulation strategy, the compression stocking was first inflated and then relaxed around the leg. The results they obtained had similar trends with experimental results. Later, 3D models were introduced in order to consider the heterogeneity and patient-specificity of the leg soft tissues [Dubuis 12]. The leg geometry was obtained from CT-scan images and the material parameters were identified by an inverse approach based on CT-scans of the patients wearing compression stockings. The main limitation of this simulation was that it did not model the stocking, the pressure applied on the leg being calculated using Laplace's law. Another more recent model was built in order to better understand how the pressure is transmitted through soft tissues and affects veins inside the leg [Rohan 13]. Its 2D geometry was obtained from MRI images to separate muscle compartments, main veins and adipose tissue.
To the authors' knowledge, only one attempt to simulate the action of compression bandage was proposed by Al Khaburi et al. [Al Khaburi 12]. The bandage was not modelled and the pressure exerted on the leg was computed using an improved Laplace's Law.

In short, to explain the action mechanism of compression bandage via the pressure distribution they generate, Laplace's law is not sufficient [Schuren 08]. On the other hand, local pressure measurements are not sufficient to understand the global action of compression bandages and there is, for now, no reliable technique for pressure mapping over the leg. As a consequence, clinicians and manufacturers currently have no reliable methods to predict pressure distribution applied by compression bandages, hence the need to develop new tools.

This study presents a first subject-specific numerical simulation to model the pressure distribution generated by compression bandages application. This simulation will lead to a more global approach of interface pressure generated by bandages, including 3D local curvature of the leg and its changes with bandage application, and soft tissue mechanical properties. The aim of the study was to validate the feasibility and reliability of a finite element (FE) simulation of lower-limb bandage in a simple case, in order to use it later with different bandage configurations.

The approach was based on experimental leg shape and pressure measurements on 5 female subjects for model generation and validation. For each subject, leg geometry was obtained with a 3D optical scanner and was then used to model the leg and the corresponding bandage. Bandage mechanical properties were measured experimentally. The results given by the simulation were then compared to the experimental pressure values. All results were compared to Laplace's Law, as it is, for now, considered as the reference method for interface pressure computation.

3.3.2 Methods

3.3.2.1 Experimental pressure measurements

Pressure measurements were performed on the medial and lateral sides of five female subjects' right legs with no known leg-related diseases, following informed consent (see Table 3.3).
Interface pressure was measured with pneumatic sensors Picopress® (Microlab Elettronica, Nicolò PD, Italy), whose diameter was 50 mm and discrimination threshold and resolution were 1 mmHg. Linearity and hysteresis were tested in a preliminary study and provided excellent results: linearity $R^2 > 0.9999$ and hysteresis $< 1.0\%$ [Chassagne 15]. However, the presence of this sensor modifies the real interface pressure (a measurement always modifies the

	Mean value	Standard deviation
Age	38.6 y.o.	7.8 y.o.
Circumference at point B1	32.4 cm	2.2 cm
Circumference at point C	36.9 cm	1.9 cm

Table 3.3: Principal characteristics of the 5 female subjects

measurand). A correction method was proposed and used to correct the interface pressure values measured in this study (see section below).
Four sensors gave local values of the pressure applied on the leg. They were placed at two different heights on the medial and lateral sides of the leg: two were located at the height of measurement point B1 (lower end of the calf) and two at the height of measurement point C (largest circumference of the calf) on both sides of the leg (Figure 3.8 - A). Measurement point B1 was chosen following the recommendations of a consensus paper [Partsch 06] while measurement point C was chosen because it is the fleshiest part of the calf. Then the bandage was applied and finally the foot was slightly raised in order to prevent any contact between the examination bed and the calf. After waiting for one minute in this position, pressure values were recorded.

All bandages were applied by the same trained operator in order to limit the discrepancy due to inter-operator variability: a bandager seems constant and repeatable in applying bandages [Raj 80] [Logan 92]. For each subject, four different bandages were applied on the leg in a spiral pattern (Figure 3.8 - B and C):

- Biflex® 16 (B16), a 100 mm wide bandage manufactured by Thuasne, with 2 and 3 layers (respectively 50% and 66% overlap),
- Biflex® 17 (B17), another 100 mm wide bandage manufactured by Thuasne, with 2 and 3 layers (respectively 50% and 66% overlap).

Both have the same textile structure but B17 has a higher elastic modulus than B16 (Table 3.5).
The manufacturer recommends applying these bandages with a 1.3 stretch ($stretch = L/L_0$, with L the applied bandage length and L_0 its initial length). To guarantee that this stretch is reached, a calibration marker was printed on these bandages every 10 cm by the manufacturer (Figure 3.8 - D). It consists in a rectangle which turns into a square when stretch is 1.3.

In this study, it was important to accurately measure the actual post-application bandage stretch because bandage application may be variable [Partsch 05c]. This was performed by a manual measurement of the distance between each printed marker:

$$\text{Stretch} = \frac{\text{distance between 2 markers after application}}{\text{distance between 2 markers before application (10 cm)}} \tag{3.5}$$

Prior to bandage application and actual stretch measurement, and within the aim of performing the subsequent simulation, the subject's leg geometry was scanned in standing position, with a structured light 3D scanner (Artec^{tm} MHT 3D scanner, Artec^{tm} Group), whose resolution is 0.5 mm. The experimental pressure measurement is to be compared with the pressure extracted from the simulation; the former corresponds to the average of the pressure over an

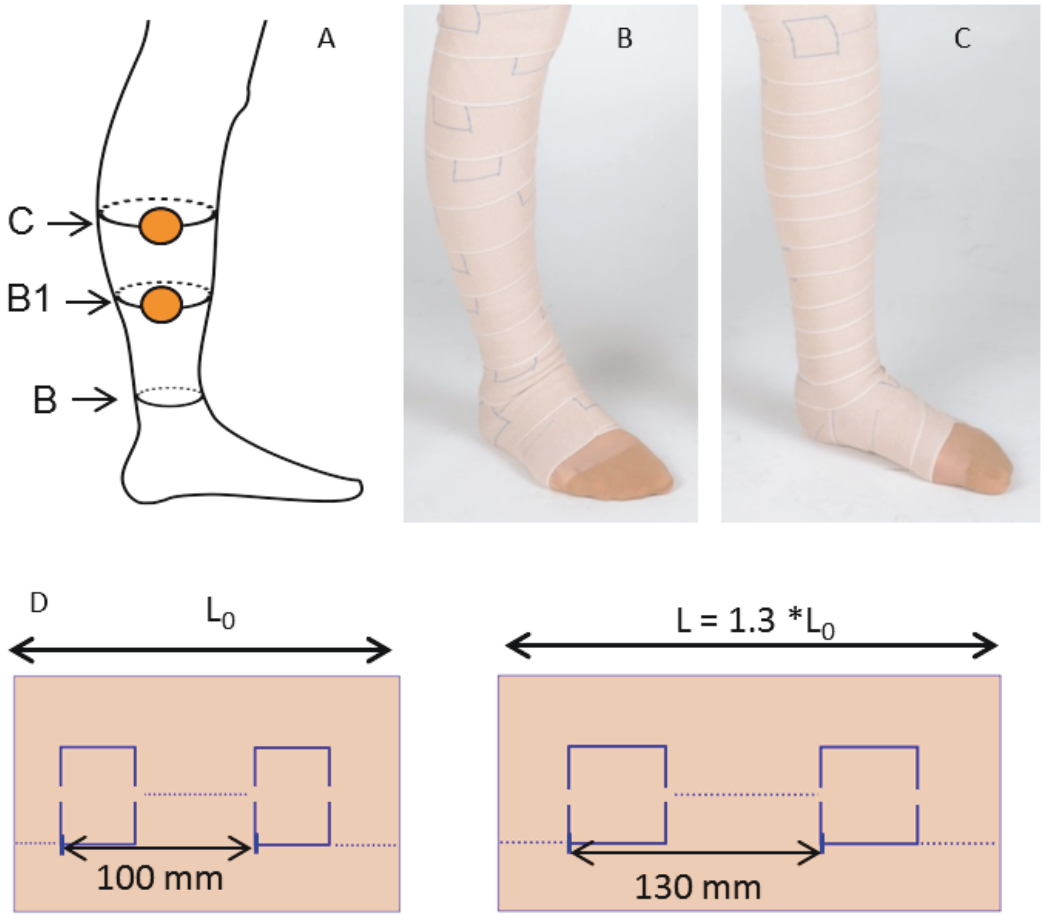

Figure 3.8: Location of measurement points (A) - Bandage applied with a 50% overlap (2 layers) (B) and a 66% overlap (3 layers) (C) - Bandage calibration marker (rectangle which turns into a square when the stretch is equal to 1.3) (D)

area corresponding to the sensor surface, and the latter has to be averaged over the same area. In order to accurately define the corresponding area, the sensor location was marked with a sticker that can be distinguished on the 3D scan of the leg without significantly modifying the leg geometry (Figure 3.10 - D).

3.3.2.2 Correction of the pressure measurement error due to the sensor volume

Although the pressure sensor is very thin, it can locally modify the curvature of the limb when inflated with the 2.0 mL air volume required. This curvature modification can then lead to a variation of the pressure applied by the textile.
In order to properly compare the experimental results with the simulation results (in which the sensor is not modelled), the local pressure variation due to the sensor was numerically investigated. For that, a 2D numerical model was built consisting of a disc representing the leg cross-section, whose radius varied from 30 to 70 mm, on which lied the sensor. The disc and the sensor were modelled as Neo-Hookean hyperelastic materials. The disc mechanical properties were the same as the living soft tissue mechanical properties used later in the simulation whereas the sensor mechanical properties were chosen in order to have very low shear stiffness and a high volumetric compression modulus (respectively $c_{10} = 4.0\ kPa$, $D_1 = 0.14\ MPa^{-1}$ and

$c_{10} = 4.0 * 10^{-3}\ kPa$, $D_1 = 0.14 * 10^{-3}\ MPa^{-1}$). The pressure was applied by a circular textile (modeled with linear beam elements) with a 1.3 stretch, whose stiffness varied from 0.46 MPa to 1.32 MPa (i.e. the equivalent range of elastic moduli used in this study (Table 3.5)). The friction coefficient between the disc and the sensor was 0.4 [Gerhardt 09].
The textile was inflated, then relaxed thus applying pressure on the disc and the sensor. The measured pressure was computed as the mean pressure on all nodes of the sensor. The reference pressure was the pressure at the opposite side of the disc, where there was no sensor (Figure 3.9 - A). The relative error was defined as follows:

$$\text{Relative Error } [\%] = \frac{\text{Measured pressure - Reference pressure}}{\text{Reference pressure}} * 100 \tag{3.6}$$

Thanks to this model, it was possible to quantify the measurement error due to the curvature modification (Figure 3.9 - B). A 3rd order polynomial correction profile was fitted on these results ($R^2 = 0.93$). It can be noticed that the higher the pressure, the lower the error. Indeed, as pressure increases, penetration of the sensor into soft tissues increases, so the curvature modification and the error decrease. All the experimental pressure values presented in this study were corrected according to this correction profile.

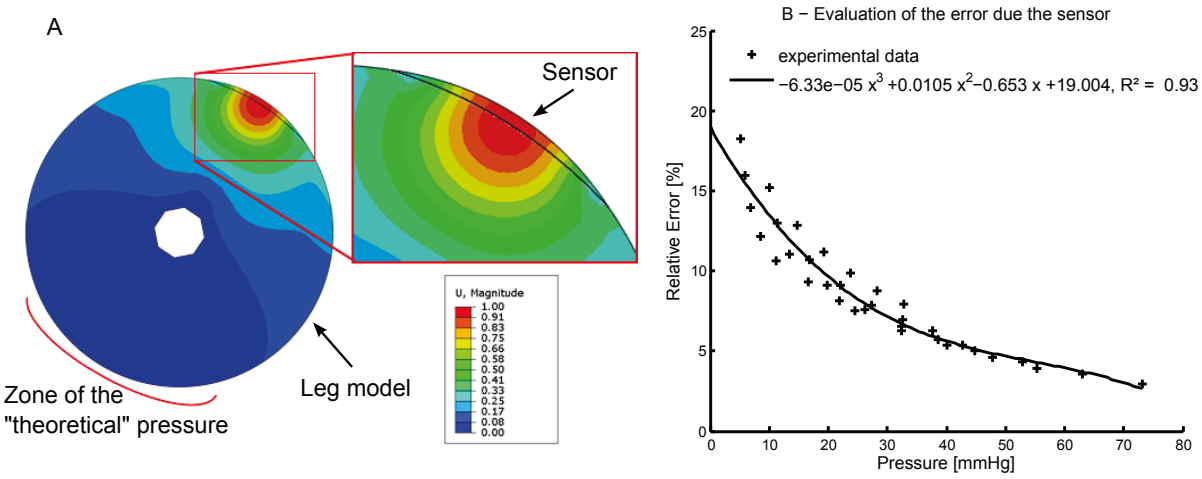

Figure 3.9: A -Numerical simulation used for the evaluation of the curvature modification due to the sensor; B - Relative error due to the sensor

3.3.2.3 Numerical simulation

A subject-specific simulation of bandage application was built, whose input data were the subject's leg geometry, the bandage mechanical properties and the application technique.

Leg geometry

The leg geometry was scanned with a structured light 3D scanner (Artec^{tm} MHT 3D scanner, Artec^{tm} Group) before bandage application (Figure 3.10 - A). The scan provided a cloud of points used to further reconstruct the external leg geometry model. The bone holes geometry was based on anatomical slices from the 'Visible Human Server' (Computer Science Department, Peripheral Systems Lab., Ecole Polytechnique Fédérale de Lausanne) (Figure 3.10 - A).

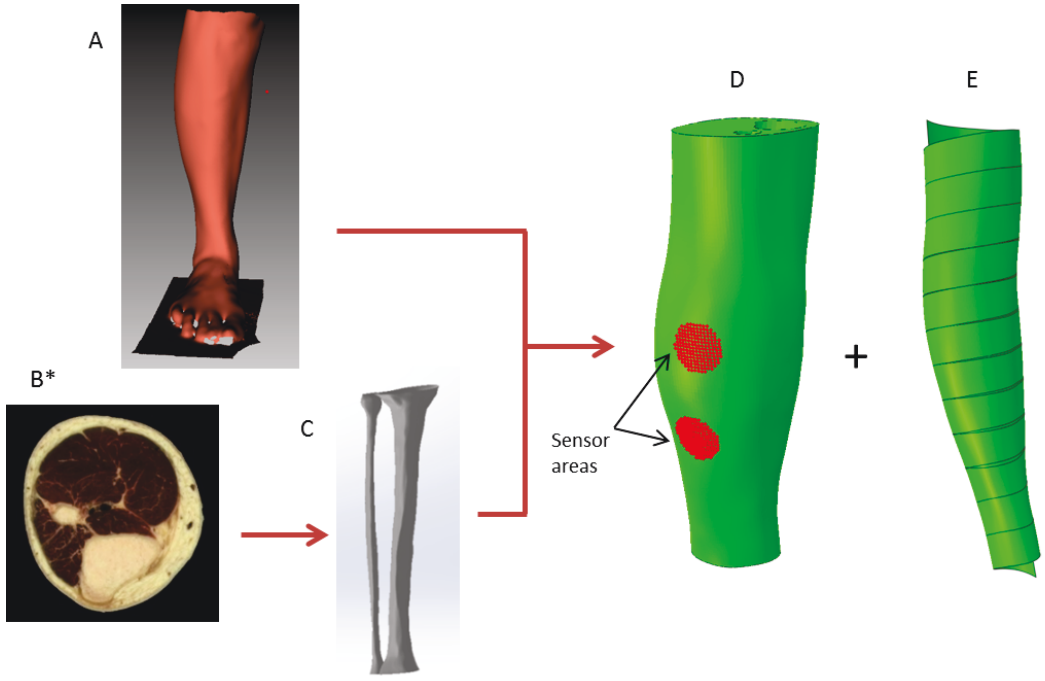

Figure 3.10: Building the model geometry: A - leg given by the 3D scanner; B - anatomic slice of a leg (* 'Visible Human Server', Computer Science Department, Peripheral Systems Lab., Ecole Polytechnique Fédérale de Lausanne); C - bones; D - leg geometry; E - bandage geometry

Leg soft tissue	$c_{10} = 4\ kPa \quad D_1 = 0.14\ MPa^{-1}$	$U = c_{10}\ (\bar{I}_1 - 3) + \frac{\kappa}{2}\ (J^{el} - 1)^2$

Table 3.4: Principal characteristics of the 5 female subjects

This bone geometry was scaled to fit the leg geometry and implanted in the leg volume using Boolean operations. These geometrical modelling operations were performed using the software SolidWorks®. It was verified in a preliminary study that little variation in the geometry of the bones had negligible influence on the pressure applied onto the skin. Bones being considered as non-deformable, the outer surface of soft tissues in contact with bones was assigned pinned boundary conditions (this mimics the presence of non-deformable material).

The complete leg was then meshed in Abaqus® with 4-node linear tetrahedron hybrid elements (around 600,000 elements, depending on subjects). Previously, a mesh convergence study was performed in order to determine the optimal element size of both parts: bandage and leg.

Last, leg soft tissues were considered as a single homogeneous material whose constitutive equation and parameters were taken from the literature (Table 3.4) [Dubuis 12]. A preliminary study confirmed that soft tissue mechanical properties had very little influence on pressure distribution in this simulation (mean variation: $0.20 \pm 3.33\%$, for $c_{10} = 1 - 35\ kPa$), justifying this choice.

Bandage geometry

The only known requirement for modelling the bandage is the 1.3 longitudinal stretch, once it is applied on the leg. The bandage model geometry, which preserves this 1.3-stretch condition, was built from the leg geometry obtained from the 3D scanner data (Figure 3.10 - E).
The shape of the bandage which is applied in a spiral pattern with respectively 50% or 66% overlap between successive layers consists in a helix. A custom meshing code (Matlab®) generated the FE mesh of any bandage knowing its width, the number of layers, the leg geometry, and ensuring a bandage stretch equal to 1.3 once the bandage is applied on the scanned leg geometry. The bandage was meshed with 4-node shell elements with reduced integration, whose size was determined by the mesh convergence study (about 55,000 elements, depending on subjects and number of bandage layers).
Bandage constitutive equation was considered as orthotropic linear elastic (Equation 3.7). Its parameters were characterized following the same methodology as described by Demanget [Demanget 12], combining different mechanical tests:

- several pure and plane strain tensile tests, to determine the in-plane orthotropic elastic behaviour of the fabrics and, thus, obtain the longitudinal and transverse elastic moduli (K_1 and K_2), the in-plane Poisson's ratio (ν_{21}), and the in-plane shear modulus G (see Equation 3.7);
- "nail tests", to determine the out-of-plane bending behaviour of the fabrics and, thus, estimate the longitudinal and transverse bending stiffnesses of the fabrics (F_1 and F_2).

All these parameters are linked by the following equation:

$$\begin{bmatrix}\epsilon_{11}\\ \epsilon_{22}\\ \gamma_{12}\end{bmatrix}_{\perp} = \begin{bmatrix}\frac{1}{K_1} & -\frac{\nu_{12}}{K_1} & 0\\ -\frac{\nu_{12}}{K_2} & \frac{1}{K_2} & 0\\ 0 & 0 & \frac{1}{G}\end{bmatrix}_{\perp} \begin{bmatrix}\sigma_{11}\\ \sigma_{22}\\ \sigma_{12}\end{bmatrix}_{\perp} \quad \text{and} \quad \begin{bmatrix}M_{11}\\ M_{22}\\ M_{12}\end{bmatrix}_{\perp} = \begin{bmatrix}F_1 & \tilde{0} & 0\\ \tilde{0} & F_2 & 0\\ 0 & 0 & \tau_{12}\end{bmatrix}_{\perp} \begin{bmatrix}\kappa_{11}\\ \kappa_{22}\\ \kappa_{12}\end{bmatrix}_{\perp} \tag{3.7}$$

with ϵ_{11}, ϵ_{22} and σ_{11}, σ_{22} the strains and the section forces in the in-plane directions, γ_{12} and σ_{12} the shear strains and section forces, M_{11}, M_{22} and M_{12} the section moments and κ_{11}, κ_{22}, κ_{12} the bending strains.

Simulation strategy

The simulation of bandage application was performed in 2 steps (Figure 3.11):

- Bandage dilatation, by imposing a radial displacement (Figure 3.11 - A);
- Activation of leg to bandage contact followed by bandage relaxation. First, only the radial displacement was relaxed (Figure 3.11 - B), then all displacement degrees of freedom were relaxed except both ends of the bandage which were pinned (Figure 3.11 - C).

The contact between the leg and the bandage allowed no penetration and had a friction coefficient equal to 0.4 [Gerhardt 09]. There was no contact between the different bandage layers.

3.3.2.4 Laplace's law

Laplace's law (Equation 3.8) is considered as the reference method for the computation of pressure applied by bandages. Hence, the experimental and simulated pressure values were

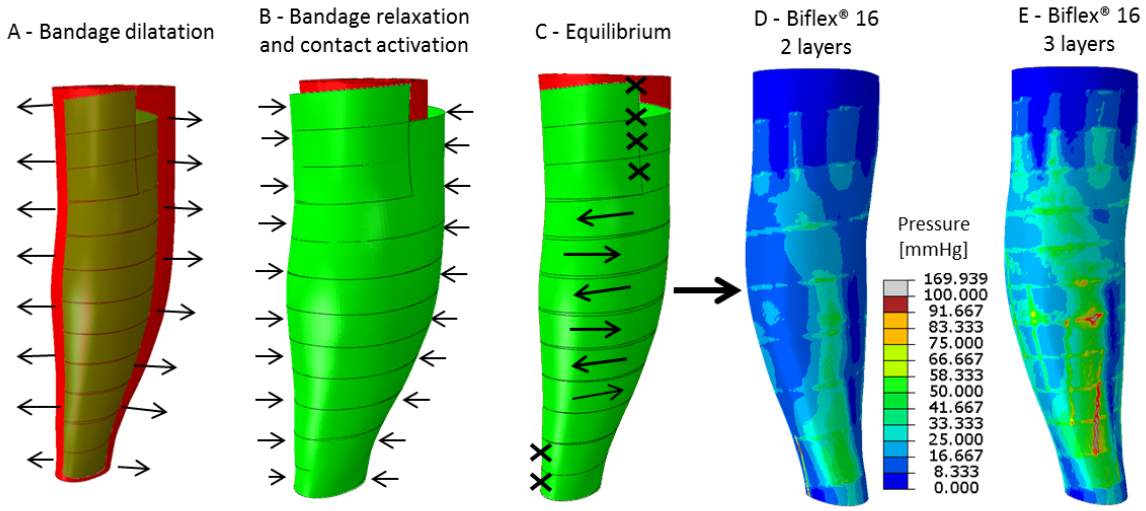

Figure 3.11: Different steps of the simulation A - B - C and examples of pressure distribution over the leg D - E

compared with those obtained using this law:

$$P = \frac{n\,T}{r}\ ,\ T\ >\ 0,\ r\ >\ 0 \tag{3.8}$$

with P the pressure ($N.mm^{-2}$), n the number of layers of the bandage, T the bandage tension (ratio between the force needed to stretch the bandage and the bandage width) ($N.mm^{-1}$) and r the local radius of curvature (mm).
To do so, transverse cross sections of the leg external surface were approximated by Fourier polynomials:

$$r(\theta, z) = r_0 + \sum_{k=1}^{n} a_k * cos(k\theta) + + \sum_{k=1}^{n} b_k * sin(k\theta). \tag{3.9}$$

where $r(\theta, z)$ is the local radius (in the transverse plane) for a given angle θ and a given height z (cylindrical coordinate system) and n is the degree of the polynomials ($n = 5$).
The radius of curvature was then computed using the following equation [Dubuis 12]:

$$R_C(\theta, z) = \frac{(r^2(\theta, z) + r'^2(\theta, z))^{2/3}}{r^2(\theta, z) + 2\ r'^2(\theta, z) - r(\theta, z)\ r''(\theta, z)} \tag{3.10}$$

with r' and r'' the first and second derivatives of the local radius of curvature.
The pressure given by Laplace's law is theoretically a function of the bandage tension in the transverse plane, T_1, and that in sagittal and coronal planes, T_2. Nevertheless, as the radius of curvature in the coronal/sagittal planes, R_2, is much larger than that in the transverse plane, R_1, the longitudinal component of Laplace's law was neglected:

$$P = \frac{T_1}{R_1}\ +\ \frac{T_2}{R_2}\ \ and\ \ R_2 \ggg R_1\ and\ \ T_1 \ggg T_2 \rightarrow\ \frac{T_2}{R_2} \ggg \frac{T_1}{R_1} \tag{3.11}$$

The pressure was computed from the leg geometry obtained from the scanner (non-deformed state) and the tension was computed knowing bandage stiffness, number of layers and bandage stretch.

3.3.2.5 Comparison of the different results

In order to compare the results obtained from the experiments, the simulation and Laplace's law, an attempt was made to fit a linear model on the three data sets. The linear model was inspired from Laplace's Law: $log(P) = log(n) + log(T) + log(C)$, with the local leg curvature, $C = \frac{1}{r}$. This linear model was modified with the aim of evaluating the linear effects a_i and the combined effects a_{ij} of each variable, which may explain the differences between the results sets:

$$\begin{aligned} log(P) = a_0 \ + \ a_1 \ log(n) \ + \ a_2 \ log(T) \ + \ a_3 \ log(C) \\ + \ a_{12} \ log(n) \ log(T) \ + \ a_{13} \ log(n) \ log(C) \ + \ a_{23} \ log(T) \ log(C) \end{aligned} \tag{3.12}$$

If the three data sets (given by the experiments, the simulation and Laplace's Law) were identical, then the identified coefficients a_i and a_{ij} should be equal for the different sets.
For the simulation, the local curvature (C) was that obtained at the end of the simulation (i.e. in the deformed state) whereas for the experience and Laplace's law the curvature was that in the non-deformed state (as the final geometry is unknown).
The tension (T) is a function of the bandage stretch. For the data computed with Laplace's Law, the stretch was 1.3. For the experiments and the simulations, the tension was computed with regards to the actual known stretch values. The three variables (tension, curvature and number of layers) were centred and scaled between -1 and 1 before fitting.

3.3.2.6 Statistical analysis

All the plotted histograms represent the mean value and the 95% confidence interval.
The linear correlation between two samples was evaluated using the coefficient of determination R^2, which is equal to the square of the Pearson correlation coefficient between the data (experimental or numerical) and the values given by the linear model. The significance of this coefficient R^2 can be tested thanks to the variable $t = \sqrt{R^2 \ \frac{n-2}{1-R^2}}$, with n the size of the sample. For a zero correlation, this variable t is approximately distributed as a Student's distribution with $n-2$ degrees of freedom. The differences between pressures applied by the different bandages (B16 - 2 layers, B16 - 3 layers, B17 - 2 layers, B17 - 3 layers) were tested with the Kruskal-Wallis one-way analysis of variance and the individual effects were tested with a Mann-Whitney U test ($\alpha = \frac{0.05}{\text{number of tests}}$). A non-parametric test for paired samples (Wilcoxon signed-rank test) was used to evaluate the differences between:

- stretches for the two bandages and around the two measurement points,
- pressures applied by 2-layer and 3-layer bandages and pressures applied by bandages B16 and B17 (for the experience and the simulation).

3.3.3 Results

The results given by the experiments and the simulation are respectively presented in Figure 3.12 and Figure 3.13. They were compared with the pressures computed using Laplace's law, as it is considered as the reference method for interface pressure computation.
The pressure given by Laplace's Law was obviously proportional to the bandage elastic modulus and the number of layers. Therefore the ratio between the pressure applied by the B17 and that applied by the B16 was equal to the ratio of bandage stiffnesses (Figure 3.12 - C and Figure 3.13 - B). Similarly, the pressure applied by a 3-layer bandage was 1.5 times as high as that applied by a 2-layer bandage (Figure 3.12 - D and Figure 3.13 - C). Eventually, the pressure at measurement point B1 was about 15% as high as that at point C (Figure 3.12 - E

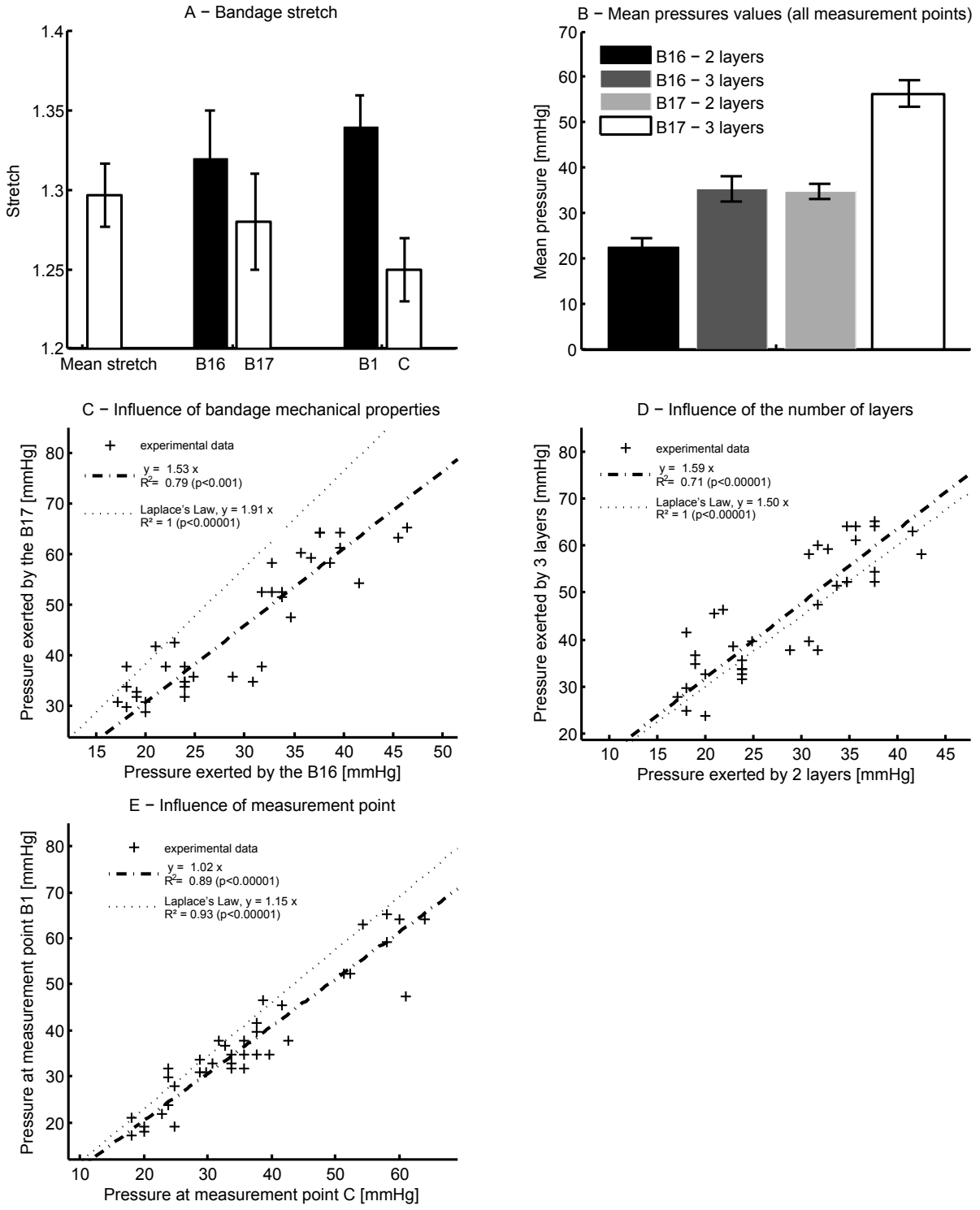

Figure 3.12: Experimental results: A - Mean bandage stretch for both bandages and around both measurement points B1 and C, mean bandage stretches for the two different bandages B16 and B16 and mean bandage stretches around measurement points B1 and C; B - Mean pressure values exerted by the four different bandages in supine position and for all measurement points and all subjects; C - Pressure applied by the B17 bandage vs. the one applied by the B16 bandage; D - Pressure applied by a 3-layer bandage vs. the one applied by a 2-layer bandage (for the same bandage); E - Pressure measured at point B1 vs the one measured at C (for the same bandage and application technique)

	Longitudinal and transverse elastic moduli	Poisson ratio and in-plane shear modulus	Longitudinal and transverse bending stiffnesses
Biflex® 16	$K_1 = 0.232\ N.mm^{-1}$ $K_2 = 0.417\ N.mm^{-1}$	$\nu_{12} = 0.072$ $G = 0.11\ N.mm^{-1}$	$F_1 = 0.13\ MPa$ $F_2 = 0.15\ MPa$
Biflex® 17	$K_1 = 0.444\ N.mm^{-1}$ $K_2 = 0.706\ N.mm^{-1}$	$\nu_{12} = 0.065$ $G = 0.21\ N.mm^{-1}$	$F_1 = 0.41\ MPa$ $F_2 = 0.25\ MPa$

Table 3.5: Bandage mechanical properties

and Figure 3.13 - D).

In the experiments, the measured mean stretch for all bandage applications was equal to 1.30 ± 0.02 (Figure 3.12 - A). However, stretches for the B16 and the B17 bandages differed ($p < 0.05$), with respective values of 1.32 ± 0.03 and 1.28 ± 0.03. In addition, the measured stretch was found to be different between the two measurement points ($p < 0.01$), with higher values at point C (mid-calf) than at point B1 (lower end of the calf) (respectively 1.34 ± 0.02 and 1.25 ± 0.02).

The pressure measurement error induced by the presence of the sensor was corrected for all the experimental results presented below. From a general point of view, it can be noticed that pressure increased with the number of layers of the bandage (Figure 3.12 - B and D) and with bandage elastic modulus (Figure 3.12 - B and C), as expected. Comparing the two types of bandages, the ratio between the pressure exerted by the B17 and that exerted by the B16 was about 1.5 at equal number of layers and with the hypothesis that stretches were equal (Figure 3.12 - C), whereas the ratio of their stiffnesses is 1.91 (Table 3.5). Eventually, the applied pressure varied along the leg: the pressure at measurement point C was slightly lower than at point B1 (Figure 3.12 - E).

Twenty different simulations were built: 5 female subjects and 4 bandages for each subject. Among these 20 models, 19 simulations reached convergence. An illustration of representative pressure maps is provided in Figure 3.11 - D and E. The pressure values which were extracted for comparison to the experimental data consist in the mean pressure over the areas corresponding to the sensors' locations (Figure 3.10 - D). These results are presented in Figure 3.13. Finale bandage stretch was 1.282 ± 0.008 when the target stretch was 1.3 (on the undeformed leg), which shows the validity of the bandage geometry used in the simulation and the applied boundary conditions.

The pressure increased with the number of layers ($p < 0.01$) and the bandage elastic modulus ($p < 0.01$) (Figure 3.13 - A, B and C). The pressure applied by the B17 (with the highest elastic modulus) was about 1.8 times as high as the pressure applied by the B16 (Figure 3.13 - B), at equal number of layers and with the hypothesis that bandages stretches were equal. However, the pressure applied by a bandage with a 66% overlap (3 layers) was about 1.4 times the pressure applied by a bandage with a 50% overlap (2 layers) (Figure 3.13 - C). Eventually,

the pressure increase between the measurement points C and B1 was about 11% (Figure 3.13 - D).

3.3.4 Discussion

This numerical approach proposed a new patient-specific simulation of compression bandage application, which is, to the authors' knowledge, the first one to model the bandage. This simulation provides the complete pressure distribution over the leg, with regards to the patient's leg morphology, the bandage mechanical properties and the application technique. The results given by the simulation need to be compared with the experiments.
In the experiments, bandage stretch was lower for the B16 than for the B17, which is due to the fact that the B17 is stiffer than the B16 (Table 3.5), thus harder to stretch. The experiments confirmed that the applied pressure increased with bandage elastic modulus. However, the pressure applied by the B17 was about 1.5 times as high as the pressure applied by the B16, while the B17 is 1.9 times as stiff as the B16 (hence the expected pressure ratio would be around 1.9). For this ratio, it was hypothesized that bandages' stretches were equal, which was not the case in the experiments (Figure 3.12 - A). Nevertheless, this difference in measured stretch does not explain such a large difference between the observed trend and the expected pressure value.

The ratio between the pressure exerted by 2-layer and 3-layer bandages was slightly higher than the expected ratio (1.5), even if the bandage stretch was about the same for both application techniques: 1.29 ± 0.03 for the 2-layer application technique and 1.30 ± 0.03 for the 3-layer application technique. Even though these pressure measurements were performed on only 5 female subjects, all these trends were in accordance with the results of a previous study [Chassagne 15], which was performed on 30 subjects (15 men - 15 women) and whose protocol was very close to that previously described. In short, the 3 data sets obtained from the experience, the simulation and Laplace's law showed different trends, especially regarding the influence bandage stiffness or number of layers. A simple way to compare the 3 data sets was to compare the pressure values at measurement point B1 on the medial side of the leg for all subjects (Figure 3.14). Although the differences between the data sets were almost never significant, the trends vary within the different bandages, hence the need to have an overall approach for the comparison of the different results.
For this a linear model was fitted on the different data sets. The linear effects a_i and the combined effects a_{ij} (Equation 3.12) were identified for the experiments, the simulation and Laplace's law (Figure 3.15).

The coefficient a_0 was not discussed because it consists in a constant value due to the conversion between pressure units.
As a first observation, these results showed that the effects of the different factors differ within the three data sets (Figure 3.15). Note, also, that all non-zero effects were significant ($p < 0.05$). The linear effects of the number of layers and the curvature, respectively a_1 and a_3, followed the same trends as the slopes showed in the previous results (Figure 3.12 - D and Figure 3.13 - C for the number of layers and Figure 3.12 - C and Figure 3.13 - B for the curvature). The number of layers had lower impact in the simulation than in the two other data sets. The curvature had larger influence on the pressure computed with Laplace's law than in the simulation and in the experience. This can be explained, at least in part, by the fact that Laplace's law does not consider the curvature modification due the soft tissue compression caused by bandage application.
Nevertheless, the linear effect of the bandage tension a_2 does not follow the same trends as

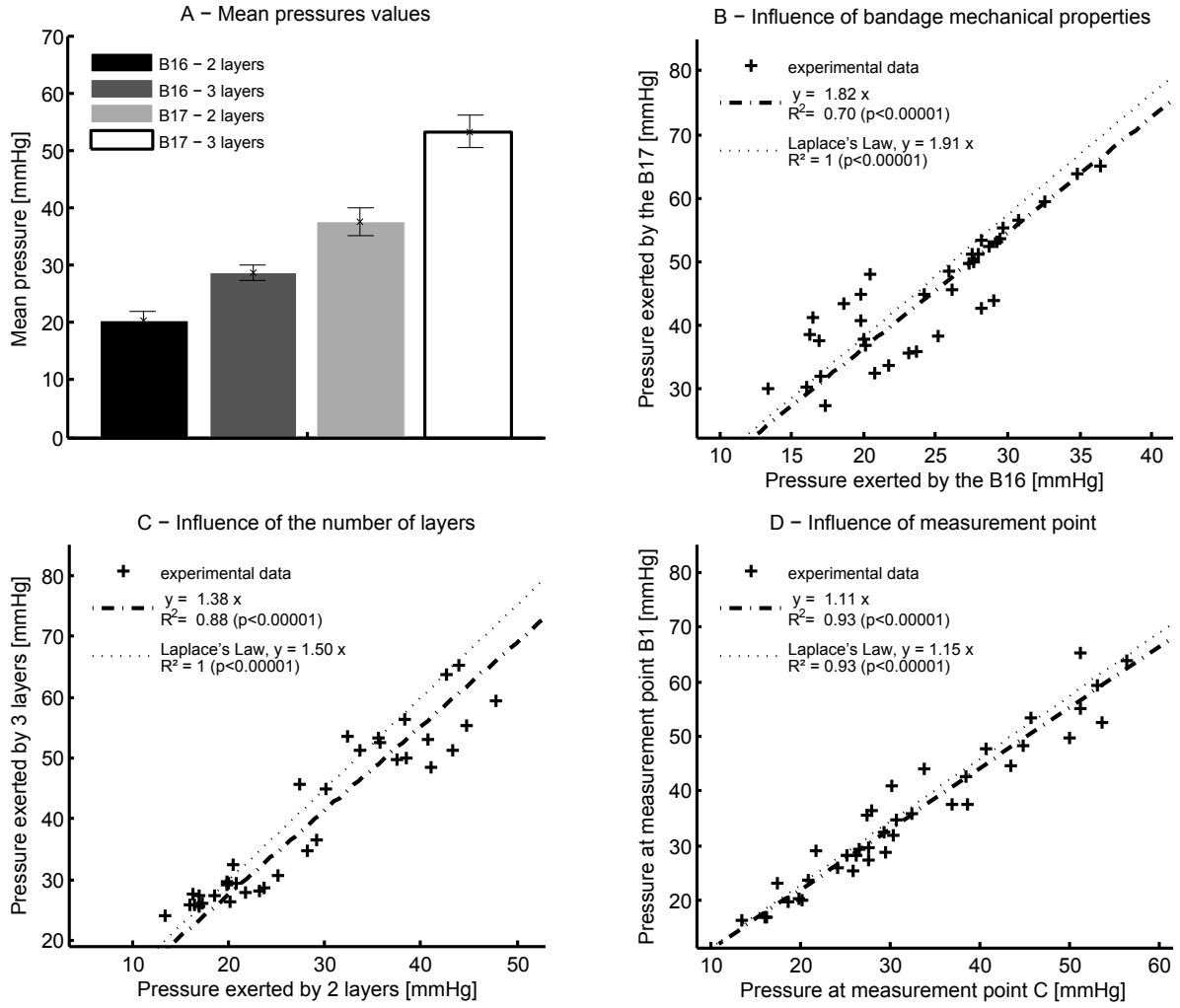

Figure 3.13: Results given by the simulation: A - Mean pressure values exerted by the four different bandages for all measurement points and subjects; B - Pressure applied by the B17 bandage vs. the one applied by the B16 bandage; C - Pressure applied by a 3-layer bandage vs. the one applied by a 2-layer bandage (for the same bandage); D - Pressure measured at point B1 vs the one measured at C (for the same bandage and application technique)

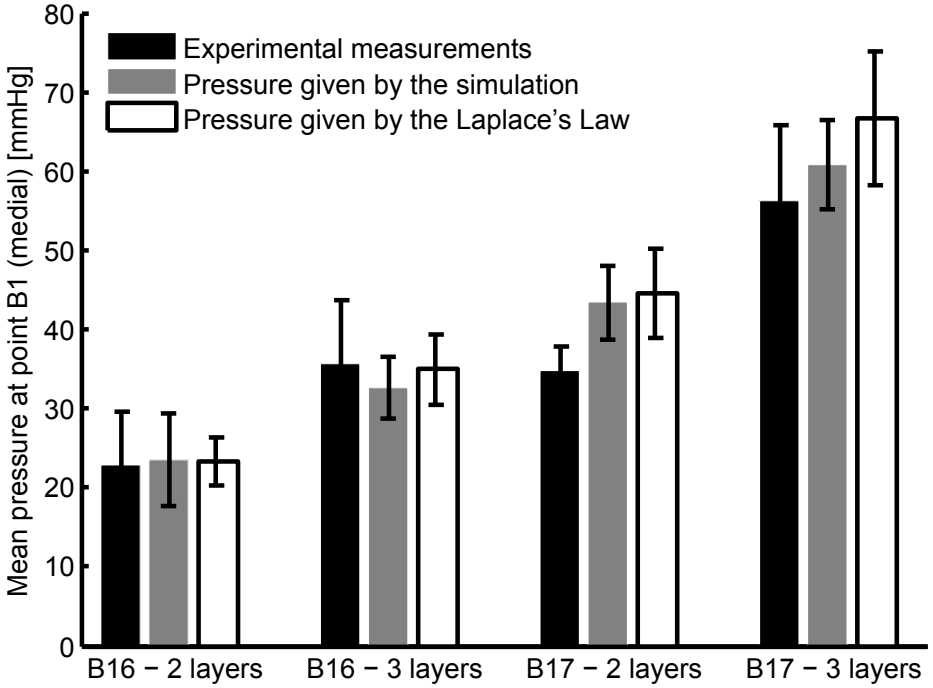

Figure 3.14: Comparison of the pressure given by the experiments, the simulation and Laplace's law, at measurement point B1 on the medial side of the leg for the 5 subjects and the 4 bandages

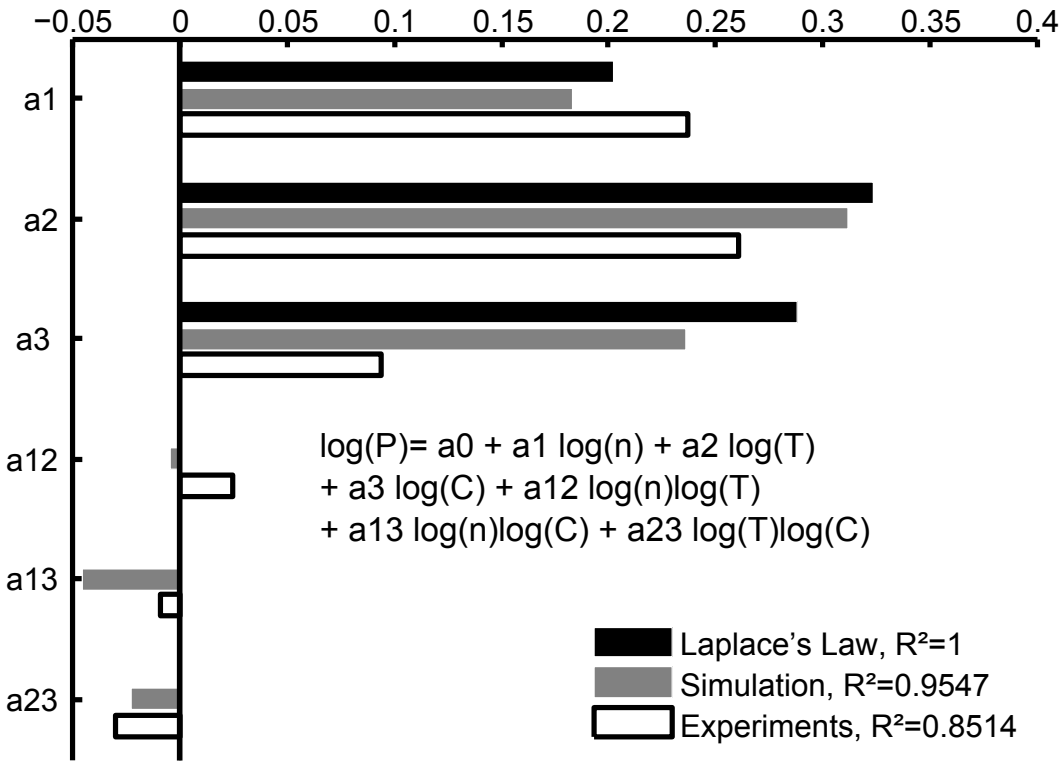

Figure 3.15: Coefficients of the linear model for the different data sets (n: number of bandage layers, T = bandage tension and C = leg curvature)

the slopes previously presented (Figure 3.12 - C and Figure 3.13 - B). Indeed, these slopes represent the ratio between the pressure applied by two bandages with different elastic moduli, applied with the same number of layers and with the hypothesis that their stretches were equal. However, the linear model did not consider the bandage elastic moduli but the bandage tension, which is a function of the bandage elastic moduli and stretch (Tension=(1-stretch)*elastic modulus). The stretch was constant in the simulation but varied in the experiments (Figure 3.12 - A). Therefore, this stretch variation can explain the difference between the linear effect of the bandage tension (Figure 3.15) and the trends previously observed in Figure 3.12 - C and Figure 3.13 - B.
More especially, as expected, no combined effect was found in Laplace's law. However, the combined effects of the curvature with the tension and the number of layers, a_{23} and a_{13}, play a role in the simulation and the experiments. This could be explained by the curvature modification due to bandage application, which is larger when the number of layers and the tension increase. The bandage applied on the leg tends to make the leg geometry rounder (radii of curvature are evened out).
Eventually, in the light of the coefficient of determination R^2 characterizing the correlation between the experiments and the linear model ($R^2 = 0.8514$), the limb curvature, the bandage tension and the number of layers are not the only parameters which impact on the interface pressure. Hence, Laplace's law cannot completely explain the pressure distribution applied on a leg by compression bandages.

Limitations

All pressure measurements were performed in a short time after bandage application, so they do not reflect bandage long-term or dynamic effects (over one-day or after walking).
The curvature modification due to the sensor was only numerically assessed. Several studies have investigated the performance of the pneumatic sensor Picopress, but their conclusions differ [Partsch 10] [Thomas 14] . However, one of them confirmed that the low pressure values tend to be overestimated when the radius of curvature is too small [Thomas 14].
The interaction between the different bandage layers may play an important role during bandage application. However, it was not taken into account in the simulation. An interesting perspective would be to add bandage to bandage interactions in future simulations. In this regard, the simulation of the real wrapping process, i.e. new boundary conditions, would likely be more suitable to account for these interactions.

Soft tissue mechanical properties used in the simulation were taken from the literature [Dubuis 12] and were identical for the 5 female subjects. As a preliminary study showed, the impact of these properties on the generated pressure is limited. Nevertheless, their effect on pressure transmission through soft tissues is of higher importance, for instance for vein closure [Frauziols 15b]. For this reason, it would be relevant to use subject-specific soft tissue mechanical properties.

3.3.5 Conclusion

Under the more general background of studying different possible bandage configurations, the aim of this study was to propose a patient-specific finite element model of bandage application to assess pressure distribution applied by elastic compression bandages. A major improvement over Laplace's law was that this simulation models leg shape changes due to bandage application, whereas Laplace's law only considers the non-deformed state of the leg. Moreover,

Laplace's law does not consider any interactions between the bandage and the leg, expect normal pressure.
This study evaluated the feasibility and reliability of a numerical simulation and showed that improving the simulation complexity, by taking bandage-to-bandage friction into account, for example, is promising.
This patient-specific simulation could then be used to assess pressure distribution over a patient's leg in order to adapt his treatment, by choosing a specific bandage or application technique, and to prevent localized overpressures, which could improve the compliance with the treatment.

3.4 Conclusion

The preliminary experimental study (Chapter 3.2, page 38) showed that interface pressure varies with bandage mechanical properties, application technique and leg morphology. Although strong correlations were observed between the pressure and the application technique but also between the pressure and the bandage mechanical properties, pressure was not found to be directly proportional to the bandage tension, which contradicts Laplace's Law.
In the meantime, the first numerical simulation (Chapter 3.3, page 52) showed the role of soft tissue deformation in pressure generation. However, the simulation of bandage application (inflation and relaxation of the bandage) was too simplified compared to the actual bandage application, which consists in wrapping a stretched bandage over the leg.

Consequently, these studies led to the following projects:

- the development of a methodology to identify the mechanical properties of calf tissue, as soft tissue deformation impacts interface pressure
- the design of a new method to characterize bandage-to-bandage frictional properties, to investigate the potential impact of such friction in pressure generation
- a new simulation of bandage application, modelling the actual bandage application (i.e. wrapping a stretched bandage around the leg).

Chapter 4

Méthodes de caractérisation - *Characterization Methods*

The first experimental and numerical studies led to the design of two characterization methods which are described in this chapter. The first one consists in a finite element model updating method for the in vivo identification of the calf soft tissue mechanical properties. This study was a collaboration with Fanny Frauziols, who worked on the mechanical characterization of the lower limb soft tissues. The development of the characterization device and method was the result of our collaboration. However, Fanny Frauziols performed the sensitivity analysis to show that the method was suitable for the identification of deep soft tissues mechanical properties. This characterization method, which was later used in a clinical study, was published in Strain (vol. 52, no. 5, pp. 400-411, Oct. 2016).
Also, a method was developed to characterize the fabric-to-fabric frictional properties of medical compression bandages. This method was based on the adaptation of the Kawabata Evaluation System. This article was submitted to the Textile Research Journal in January 2016.

Contents

4.1 Résumé

Les deux premières études expérimentale et numérique ont soulevé plusieurs interrogations quand à l'influence du frottement bande-bande et des propriétés mécaniques des tissus mous de la jambe sur les pressions d'interface. Cela a mené au développement de deux outils de caractérisation.

Le premier outil a été conçu pour caractériser *in vivo* les propriétés mécaniques des tissus mous de la jambe. L'identification de ces propriétés mécaniques est basée sur l'association d'un essai mécanique non invasif et d'un modèle éléments-finis. Un dispositif a été construit afin de compresser l'arrière du mollet avec un cylindre métallique (Figure 4.3). Cet essai permet d'obtenir la force nécessaire pour comprimer le mollet en fonction du déplacement du cylindre. Un modèle 2D de l'expérience est ensuite créé. Cette modélisation 2D de la jambe différencie les tissus superficiels (entourant le *fascia cruris*) et les tissus profonds (entourés par le *fascia cruris*) (Figure 4.2). Ainsi les propriétés des tissus mous sont modifiées dans la simulation, via un algorithme d'optimisation, jusqu'à ce que le modèle donne la même réponse (courbe force = f(déplacement)) que l'expérience.

L'efficacité de cette méthodologie inverse pour l'identification des propriétés mécaniques des tissus mous profonds a été évaluée grâce à un plan d'expériences numériques (Figure 4.5).
Ensuite, cette méthode a été testée pour 4 sujets sains. Les propriétés mécaniques des tissus mous de ces 4 sujets ont été identifiées pour deux lois de comportement hyperélastiques différentes, Néo-Hookéenne (Équation 4.1) et polynomiale d'ordre 2 (Équation 4.2) (moins linéaire que la première). Les résultats obtenus montrent que la loi de comportement la moins linéaire (polynomiale) est plus proche du comportement mécanique des tissus mous de la jambe (Figure 4.14).
Cette méthode de caractérisation, non-invasive et rapide pour le patient, a ensuite été utilisée sur une plus large cohorte dans le cadre d'une étude clinique (Chapitre 6.3, page 132).

Une deuxième méthode de caractérisation a été développée afin de mesurer le coefficient de frottement textile-textile. Ce paramètre joue un rôle important dans de nombreux dispositifs médicaux textiles de compression, tels que les ceintures lombaires ou les bandes de compression. Il était donc important de pouvoir procéder à la mesure du coefficient de frottement dans des conditions, pression appliquée et allongement du textile, proches des conditions d'utilisation du dispositif médical.

Pour cela, une nouvelle méthode de caractérisation a été développée, en adaptant le Kawabata Evaluation System [Kawabata 80]. Ce système est régulièrement utilisé pour caractériser le coefficient de frottement entre un textile et un doigt métallique, en vue d'évaluer le *toucher* d'un textile. Un nouveau palpeur de frottement textile a été développé afin de pouvoir faire varier la pression appliquée ainsi que l'allongement du textile (Figures 4.9 et 4.10).

Cette méthode, simple et reproductible, a d'abord été testée pour plusieurs bandes de compression. Les coefficients de frottement mesurés étaient relativement élevés, entre 0.5 et 0.7 (Figure 4.11).

Ensuite, l'étude s'est focalisée sur les deux bandes de compression déjà évoquées (Biflex® 16 et Biflex® 17 (Thuasne)), qui ont des structures similaires mais des propriétés mécaniques différentes. Il a été observé, dans les gammes de variation testées, que l'allongement et la pression appliquée n'avaient que très peu d'effet sur le coefficient de frottement mesuré (Figures 4.12 et

4.13).

Cette méthode simple peut être mise en œuvre pour la mesure du cœfficent de frottement d'autres dispositifs textiles de compression.
Les valeurs des cœfficients de frottement obtenues grâce à ce dispositif ont ensuite été utilisées dans une deuxième simulation numérique de l'application d'une bande sur la jambe (Chapitre 5.2, page 104).

4.2 In vivo identification of the passive mechanical properties of soft tissues in the human leg

Co-authored with Fanny Frauziols, Pierre Badel, Laurent Navarro, Jérôme Molimard, Nicolas Curt and Stéphane Avril, from [Frauziols 16]

4.2.1 Introduction

4.2.1.1 Motivations

Different draining mechanisms prevent blood from stagnating in the legs of healthy subjects, such as the effect of muscular contraction, the activity of the sympathetic nervous system or the venous valve system [Marieb 10]. In case of default in one of these mechanisms, chronic venous insufficiency (CVI) may appear. Symptoms of CVI range from "heavy leg" feelings to development of ulcers. CVI affects about thirty percent of the French population [Floury 96]. Compression of the limb using medical compression stockings or bandages is a widely used treatment and is efficient for almost all forms of CVI [Partsch 07]. The benefits of these treatments are not to be proven, but still, for some patients, the therapeutic goal is not reached and generally, there is a need to improve their comfort. To understand the mechanisms of this treatment and to be able to better design and size the stockings or bandages, biomechanical numerical models have been developed [Avril 10] [Dubuis 12] [Rohan 13] [Wang 13].
A challenging step to develop these models is to identify the material properties of soft tissues. To that extent, several characterization methods have been established. A first approach to characterize the mechanical properties of soft tissues is to perform in vitro tensile or compression tests on tissue sample [Fung 93] [Ottenio 15]. A second and more recent approach is by direct measurements of the mechanical properties of soft tissues *in vivo* with different techniques. For example, ultrasound elastography [Bercoff 04] and magnetic resonance elastography [Bensamoun 08] techniques both map the elasticity of soft tissues. A third approach is to combine experimental data acquisitions with finite element (FE) model updating through an inverse method. This approach can address experimental data that could not be analysed directly to identify material parameters of different constitutive models. Previously, FE model updating has been used *in vivo* on arterial tissue [Franquet 12], brain tissue [Miller 00], skin [Boyer 13] and adipose tissues [Livarinen 11] or musculo-skeletal tissues [Avril 10] [Dubuis 12] [Bouten 09] [Affagard 15].

4.2.1.2 Problem definition and proposed approach

The leg is composed of several compartments made of soft tissues (Figure 4.1):

- the compartment composed of adipose tissue and skin which, in this study, is referred to as superficial soft tissues;
- the *Fascia cruris* which is a collagenous membrane separating both compartments;
- the compartment of soft tissues surrounded by the *fascia cruris*, mainly composed of muscular tissue which, in this study, is referred to as deep soft tissue compartment.

It is believed that the transmission of pressure through soft tissues plays an important role in the treatment of venous insufficiency by elastic compression [Avril 10]. Therefore, modelling the biomechanical effects of elastic compression requires a precise identification of the constitutive behaviour of this medium through which the pressure is transmitted.
Also, a large inter-subject variability in the efficacy of the compressive treatments has been

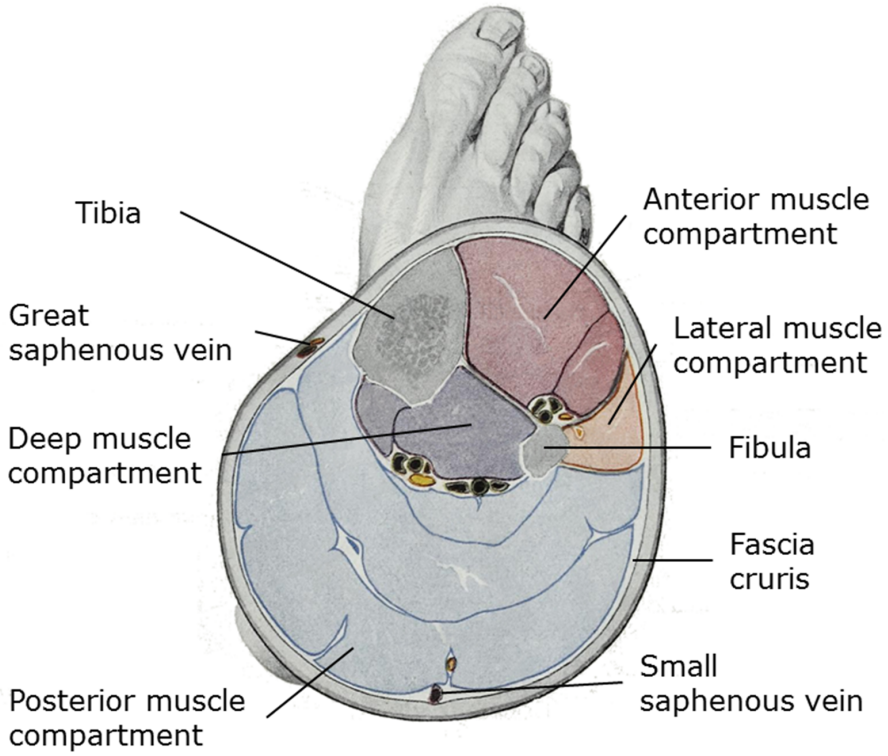

Figure 4.1: Anatomy of the human leg - Cross-section of the human right leg. The *fascia cruris* makes a separation between the superficial tissues, composed by the adipose tissue, the skin and the superficial veins, and the deep tissues, composed by the muscular compartments and the deep veins. Adapted from [Braus 21]

observed previously [Chassagne 15]. Therefore, the identification of mechanical properties must be patient-specific and could later be performed for clinical studies with large cohorts.

In this context, a fast and non-invasive method to identify passive mechanical properties of deep soft tissues is proposed and evaluated. Using an inverse method, subject-specific FE models and experimental localized compression data sets are combined to identify material parameters on four healthy subjects. The related assumptions are discussed to assess the accuracy of this approach.

4.2.1.3 General outline of the paper

The *material and methods section* details the methodology used to retrieve subject-specific material properties by acquiring localized compression data on the leg and implementing an inverse method. Then, in the *results section*, accuracy of the methodology is assessed and the material parameters of each subject are reported. Finally, in the *discussion section*, the experimental set-up and the assumptions of the FE model are thoroughly discussed to present their domain of validity and limitations.

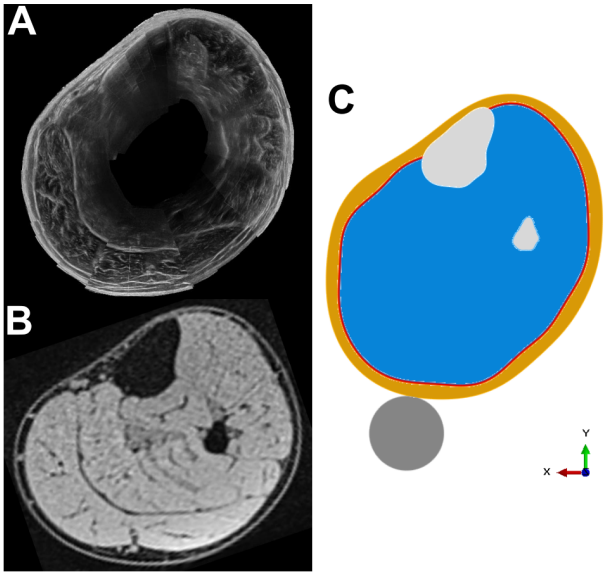

Figure 4.2: Finite element (FE) model implementation - B-mode ultrasound reconstruction of the leg (A), MRI of the leg (B), bi-dimensional FE model (C) composed by the bones (tibia and fibula); the deep soft-tissue compartment, the superficial soft-tissues compartment and the fascia cruris separating them

4.2.2 Material and methods

4.2.2.1 Data acquisition and processing

Four volunteers (3 males, 1 female, mean age: 27 y.o.) underwent MRI scans, ultrasound acquisitions and localized compression data acquisition on the calf of the right hand-side of the leg, following informed consent. The ultrasound acquisitions (Figure 4.2 - A) and the MRI scans (Figure 4.2 - B) provide the subject-specific geometry used for the implementation of a FE model (Figure 4.2 - C). An ultrasound elastographic device (Aixplorer®; Super-Sonic Imagine, Aix-en-Provence, France) was used in a previous study [Frauziols 15b] to reconstruct the fields of elastic modulus in the superficial tissues. B-mode scans acquired all around the leg were stitched together to reconstruct the anatomy of superficial soft tissues of the subject.

In the present study, an experimental setup has been designed to identify the passive mechanical properties of deep soft tissues. More specifically, displacements and reaction forces were measured after compressing the calf with a 30 mm diameter cylinder (Figure 4.3). Since these experimental data were aimed at being combined to a bi-dimensional finite element (FE) model, a cylinder was chosen rather than a sphere. More, it is worth noting that with such geometrical arrangement, material with linear elastic behaviour would give a linear force/displacement curve.
During data acquisition, the subject was seated in a chair allowing a relaxed state of the calf muscles. The subject's foot was fixed with straps and the knee was supported by rubber buffers avoiding motions of the leg during the acquisition. Double-sided adhesive tape was used at the leg-cylinder contact in order to avoid sliding. This adaptation reduces the number of unknowns in the inverse approach (i.e. no friction coefficient to identify), lowering the computation time. An in-house LabVIEW® (National Instruments, Austin, TX, USA) code was used to display and record the reaction forces given by the 100 N load cell (LCMKD-100N, Omega engineering

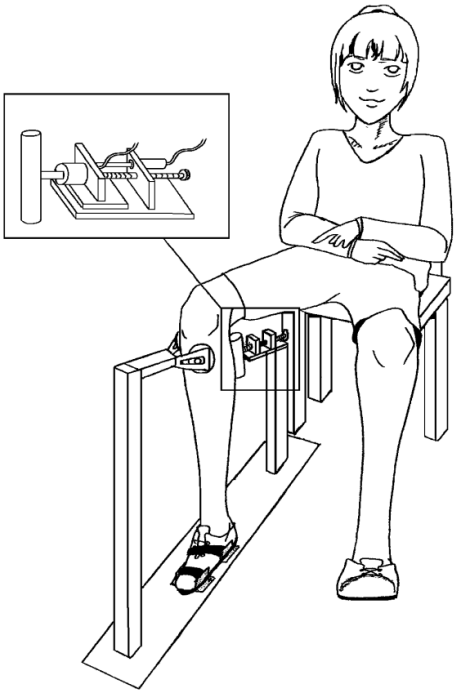

Figure 4.3: Experimental setup - The subject is seated on a chair. The straps around the foot and the rubber buffers behind the knee lead to minimum motion of the leg during data acquisition. A 30 mm diameter cylinder is applied parallelly to the leg axis. A force sensor and a displacement sensor record the desired data

INC) with an accuracy of ± 0.25% and the displacements given by the 50 mm displacement sensor (MTN/EUG025-10, Monitran) with an accuracy of ± 0.25 mm. Three sets of localized compression were acquired per subject at a rate of 0.4 mm/s. The compression was increased until a displacement of 30 mm of the cylinder was reached. Only the loading part of the curve was further analysed for the inverse analysis. This choice will be commented in the *discussion section*.

4.2.2.2 Implementation of a subject-specific FE model

The aim of the paper is to identify the deep soft tissue material parameters using an inverse FE analysis through an iterative process. Two imaging modalities were used to create the subject-specific FE model: ultrasound (Figure 4.2 - A) and MRI (Figure 4.2 - B). To register both images, the bones edges visible in both images were segmented and used to perform a rigid body registration. The external geometry of the leg was segmented from the ultrasound images [Frauziols 15b] as well as the position of the *fascia cruris*. Since the thickness of the *fascia cruris* shows high inter-individual variability [Stecco 09] and cannot be precisely determined from ultrasound images, a sensitivity analysis was performed about this parameter.

In a **first model**, the behaviour of soft tissues was described with a Neo-Hookean hyper-elastic

Material	Behavior law	Parameters	Source
Deep soft tissues	Hyper-elastic Neo-Hookean	C_{10} $D_1 = 28\ MPa^{-1}$	Identified [Bouten 09]
	Hyper-elastic reduced polynomial	C_{10}, C_{20} $D_1 = D_2 = 28\ MPa^{-1}$	Identified [Bouten 09]
Superficial soft tissues	Hyper-elastic Neo-Hookean	$C_{10} = 2\ kPa$ $D_1 = 22.5\ MPa^{-1}$	[Bouten 09] [Bouten 09]
Fascia cruris	Hyper-elastic Neo-Hookean	$C_{10} = 100\ kPa$ $D_1 = 22.5\ MPa^{-1}$	[Bouten 09] [Bouten 09]

Table 4.1: Material properties of the biomechanical model

constitutive equation. The strain energy density function was defined such as [Hibbit 09]:

$$U = C_{10}^{H}(\bar{I}_1 - 3) + \frac{1}{D_1}(J^{el} - 1)^2 \tag{4.1}$$

where $\bar{I}_1$ is the first invariant of the isochoric deformation; J^{el} the elastic volume ratio; C_{10}^{H} and D_1 the material parameters to identify.

In a **second model**, the behaviour of deep soft tissues (i.e. below the *fascia cruris*) was modeled with a 2$^{\text{nd}}$ order reduced polynomial strain energy density function defined such as [Hibbit 09]:

$$U = C_{10}^{P}(\bar{I}_1 - 3) + C_{20}(\bar{I}_1 - 3)^2 + \frac{1}{D_1}(J^{el} - 1)^2 + \frac{1}{D_2}(J^{el} - 1)^4 \tag{4.2}$$

where C_{10}^{P}, C_{20}, D_1 and D_2 are the material parameters to identify.

Material parameters are summarized in Table 4.1. D_1 and D_2 were not identified in this study, common values were assigned to them [Bouten 09]. This choice is discussed in the *discussion section.*

The iterative process to identify the material parameters requires a low computation time of the FE simulation. This is why it was chosen, in accordance with previous studies [Avril 10] [Rohan 13] [Bouten 09] to implement a bi-dimensional FE model to mimic the 3D experiments. The construction of the bi-dimensional FE model whose purpose is to replicate the 3D experiment required several assumptions. Considering the chosen geometrical arrangement, the bi-dimensional FE model is based on a classical plane-strain model combined with correction functions in order to take into account the 3D effects.

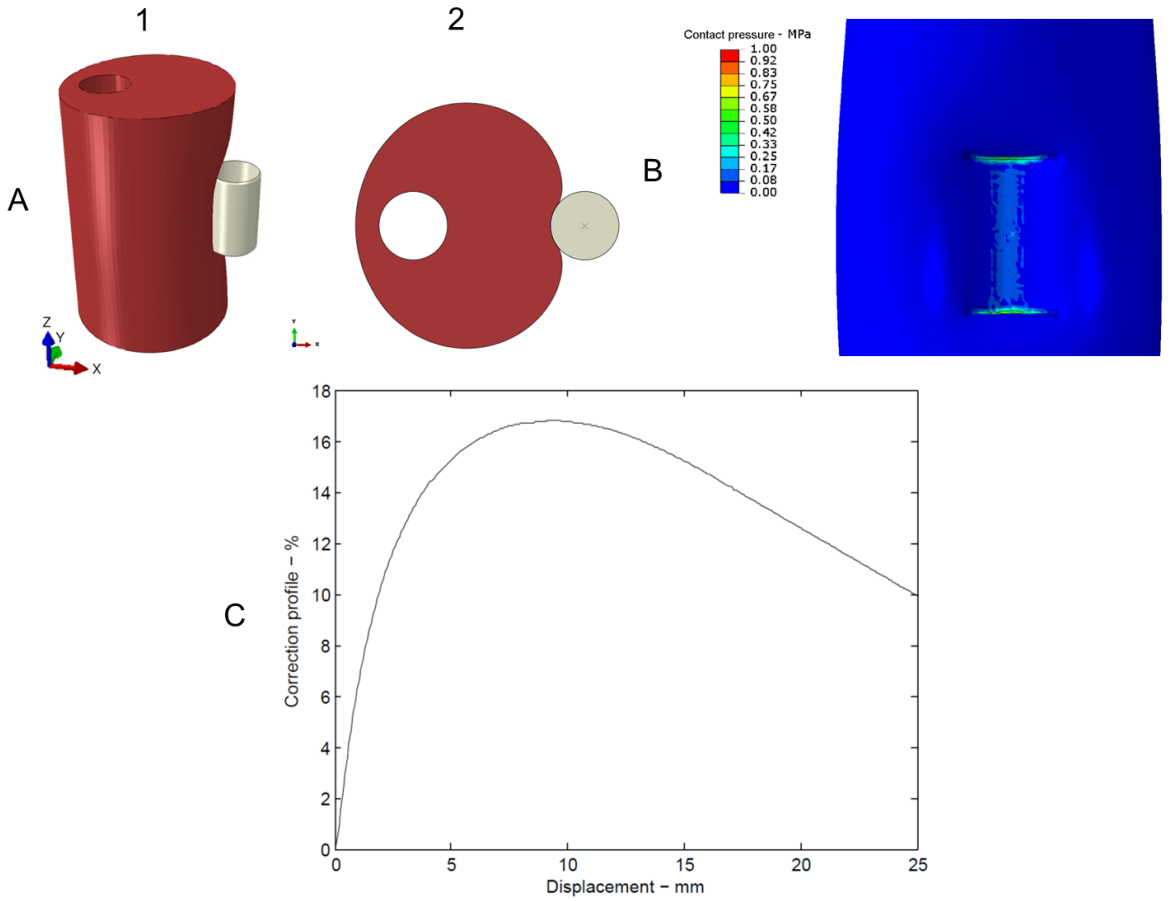

Figure 4.4: A - Computations of an idealized leg under a localized compression using a 30 mm diameter cylinder of different lengths. 1: 3 dimensional simulation; 2: bi-dimensional simulation. B - Pressure distribution applied onto the leg by the cylinder. C - Function defined by Equation 4.3 to compensate the underestimation of the reaction forces made with a 2D plane-strain model

As the soft tissues compression test was performed thanks to a 50 mm long cylinder, edge effects may occur due to a non-uniform pressure distribution on the leg (Figure 4.4 - B).

In order to assess the influence of the change from a 3D experiment to a plane-strain FE model, a 3D model representing the experimental 3D problem was implemented and compared to a plane-strain model. Idealized leg geometry was used to create the 3D FE mesh, made of first order tetrahedral elements, using the meshing tools available in Abaqus®. The material behaviour was described by a Neo-Hookean constitutive equation (Equation 4.1).
Two computations were performed. In the first one, named 3D simulation, the compression of the idealized leg is modeled in 3D with a 30 mm diameter and 50 mm long cylinder (Figure 4.4 - A - 1). The external surface of the idealized bone was pinned and the top and bottom faces of the idealized leg segment were unconstrained. In the second one, named plane-strain simulation, the compression of the idealized leg is modeled in plane strain with a 30 mm diameter circle (Figure 4.4 - A - 2). Plane-strain results being calculated for a unit transverse length, reaction forces were multiplied by the length of the compression cylinder (i.e. 50 mm). In order to evaluate the error due to edge effects (Figure 4.4 - B) made with a plane strain

FE model, a correction function, P, was defined as the difference between force/displacement curves from the two previous computations as follows:

$$P(d) = 1 - \frac{RF^{3D}(d)}{L^{cylinder}} \frac{1}{RF^{2D}(d)} \tag{4.3}$$

with, $RF^{3D}(d)$ and $RF^{2D}(d)$ being the reaction forces obtained respectively from the 3D and 2D simulations, as a function of the displacement of the cylinder d, $L^{cylinder}$, the length of the cylinder. The results were used to apply a correction function (Figure 4.4 - C) on the force/displacement curves in the bi-dimensional FE models for the 4 subjects.

Eventually, the bi-dimensional reconstruction comprising the bones, the compartment of superficial soft tissues and the compartment of deep soft tissues, separated by the fascia cruris (Figure 4.2 - C) was meshed with 3-node and 4-node linear plane strain finite elements with hybrid formulation, using the meshing tools available in Abaqus®.
The compression cylinder was modeled as a 30 mm diameter circle (Figure 4.2 - C). Its initial position and its translation direction were defined in agreement with each experiment. The two bones and the cylinder were implemented as rigid bodies. The bones were pinned and a 30 mm radial displacement was assigned as boundary condition of the FE model for the cylinder. In this study, the interaction between the leg and the cylinder was managed using contact algorithms from those available in the Abaqus® library. In the tangential direction, a rough behaviour was chosen (i.e. infinite coefficient of friction) to satisfy the experimental conditions (i.e. double-sided adhesive tape at the cylinder/leg interface). In the normal direction, an exponential contact pressure/over-closure relationship was used.

4.2.2.3 Evaluation of the FE model sensitivity

A sensitivity analysis of the FE model response to parameters of interest has been performed for one subject through a design of experiments approach [Tinsson 10]. This methodology allowed determining the sensitivity of the FE model to each parameter (material parameters or thickness of the fascia cruris for example) and defining whether this bi-dimensional FE model can be used to identify the material parameters of deep soft tissues. For this sensitivity analysis, the behaviour of deep soft tissues was modeled with a 2nd order reduced polynomial strain energy density function (Equation 4.2), as it was observed that this constitutive law better fits the experimental results.

Parameter selection

5 parameters were taken into consideration, the C_{10}^P and C_{20} material parameters of deep soft tissues, the thickness of the fascia cruris, the C_{10} material parameter of the fascia cruris and the C_{10}^H material parameter of the superficial soft tissues (Figure 4.1). To compare the sensitivities, the parameters were scaled and centred from -1 to 1 in their respected domain as reported in Table 4.2.

Sampling method

The set of numerical simulations performed was defined using a full factorial design with interactions and resulted in 33 simulations ($n = 2^5 + 1$).

Selection of metrics from the FE analysis

Parameter	Domain
C_{10}^{P} Deep soft tissues	from 0.5 to 30.0 kPa
C_{20} Deep soft tissues	from 0.5 to 30.0 kPa
C_{10}^{H} Superficial soft tissues	from 1.0 to 30.0 kPa
C_{10} *Fascia cruris*	from 0.1 to 10.0 MPa
Thickness *Fascia cruris*	from 0.2 to 1.0 mm

Table 4.2: Parameters studied in the sensitivity analysis

Two types of metrics were studied in order to capture the non-linearity of the response. The first one is the mean slope of the force/displacement curve. The second one is the mean curvature of the force/displacement curve. For each metrics, 3 parts of the force/displacement curve were analysed to study the influence of the parameters at different stages of the compression test: from 0 mm to 5 mm; from 5 mm to 20 mm; from 20 mm to 30 mm (Figure 4.5 - A).

Response surface definition

A response surface was then fitted on the metrics values obtained from the 33 numerical simulations. This surface response was modeled with a first order polynomial (Equation 4.4) including interactions (5 studied parameters coefficients + 10 interaction coefficients + 1 constant term).

$$Y = \beta_0 + \sum_{i=1}^{p} \beta_i \; x_i + \sum_{i,j=1,\; j>i}^{p} \beta_{ij} \; x_i \; x_j \tag{4.4}$$

where $p = 5$ is the number of parameters; Y is the output of the model and x the parameter value in its coded space. Except for β_0, the absolute value of the coefficients β will reflect the sensitivity of the FE model to the corresponding parameters.

Statistical analysis of the response surface

To assess the quality of the fitted response surface, a statistical analysis was used. After ensuring that the outputs of the 33 simulations followed a Normal law, an analysis of variance (ANOVA) was performed [Tinsson 10]. The sum of squares due to the error (SSE) and the sum of squares due to the regression (SSR) were calculated as follows:

$$SSE = \sum_{i=1}^{n} (Y_i - \hat{Y}_i)^2 \tag{4.5}$$

$$SSR = \sum_{i=1}^{n} (\hat{Y}_i - \bar{Y}_i)^2 \tag{4.6}$$

where $n = 33$ is the number of simulations; Y_i are the outputs of the simulation; $\bar{Y}_i$ are the means of the outputs and $\hat{Y}_i$ are the estimated outputs computed from the fitted model.

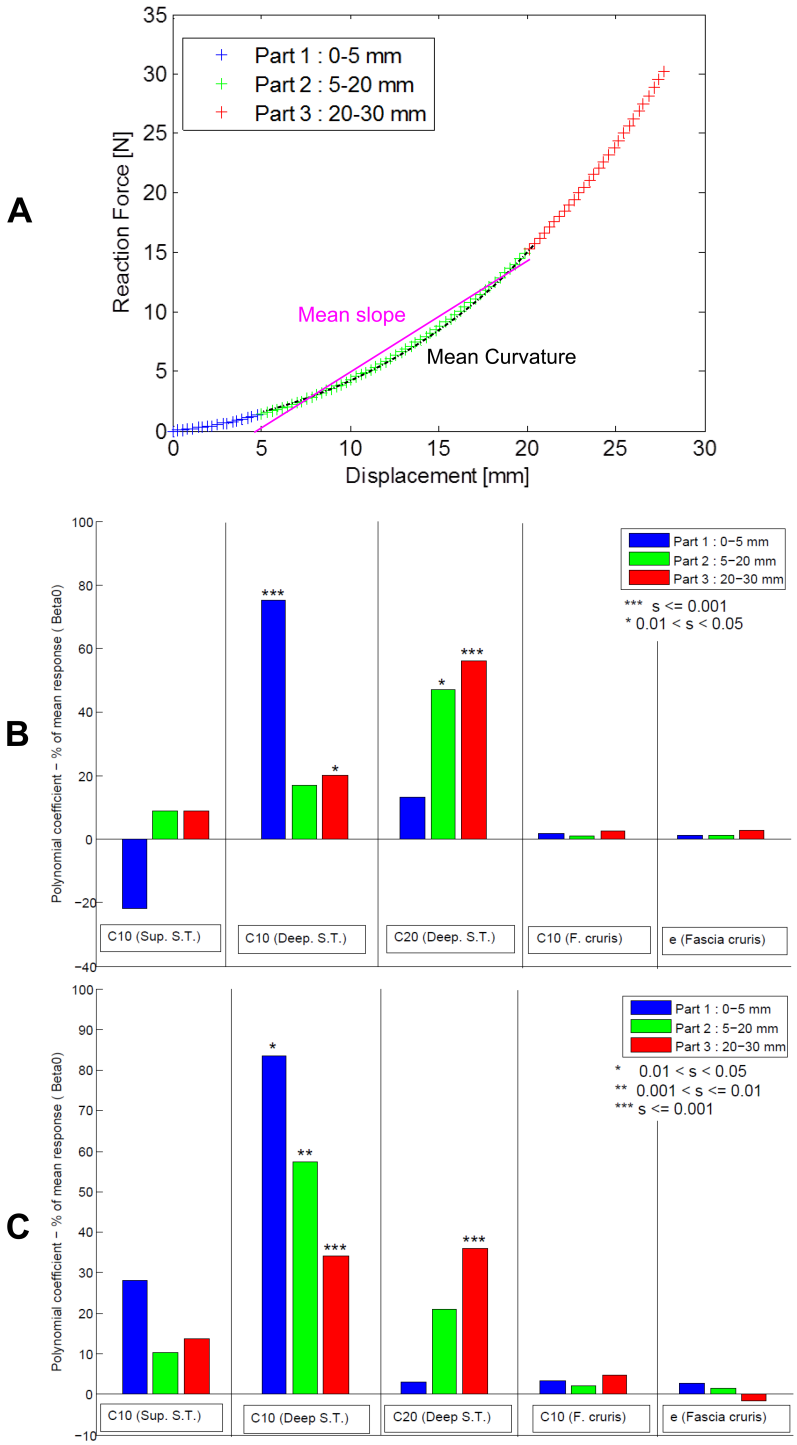

Figure 4.5: Illustration of a force/displacement curve (A); Sensitivities - 2nd order polynomial coefficients adjusted on the model for the mean curvature response (B) and mean slope response (C) on the 3 stages of the force/displacement curve
From left to right: C_{10}^{H} of superficial soft tissues, C_{10}^{P} of deep soft tissues, C_{20} of deep soft tissues, C_{10} of the *fascia cruris* and thickness of the *fascia cruris*
s stands for significance

From these values the mean sum of squares due to the error (MSE) and the mean sum of squares due to the regression (MSR) were deduced. Then, the linear coefficient of regression was calculated.

$$MSE = \frac{SSE}{n-p} \tag{4.7}$$

$$MSR = \frac{SSR}{p-1} \tag{4.8}$$

$$R^2 = \frac{SSR}{SST} \tag{4.9}$$

where $n = 33$ is the number of simulations and $p = 5$ the number of parameters.

The global validity of the model was then assessed by applying a Fisher test with $p-1$ and $n-p$ degrees of freedom to the following quantity:

$$T^{model} = \frac{MSR}{MSE} \tag{4.10}$$

Finally, the significance of the sensitivity of each parameters with respect to the experimental variance, $\hat{\beta}_i$, was assessed by applying a Student test with $n-p$ degrees of freedom to the quantity:

$$T^{parameter} = \frac{\hat{\beta}_i}{\sqrt{Var(\beta_{experimental})}} \tag{4.11}$$

The results of this design of experiments applied to the FE model are presented in the results section.

4.2.2.4 Identification method

To identify the material parameters of both constitutive models (C_{10}^H for Equation 4.1; C_{10}^P and C_{20} for Equation 4.2), an inverse method was implemented.

Several steps were necessary:

1. Extraction of force-displacement curves from the bi-dimensional model
2. Definition of a cost function quantifying the mismatch between numerical and experimental force-displacement curves
3. Minimization of the cost function with the genetic algorithm implemented in Matlab®.

To estimate the mismatch between numerical and experimental force-displacement curves, the reaction forces from the numerical simulations and the experiments were sampled on an identical displacement range and the cost function was defined in the least square sense:

$$E = \sum_{i=1}^{l} (Y_{sim}(i) - Y_{exp}(i))^2 \tag{4.12}$$

where l is the number of points, Y_{sim} the reaction forces predicted by the numerical simulation and Y_{exp} the obtained experimental reaction forces.

The stopping criterion of the genetic algorithm was the tolerance on the cost function, which was set to 10^{-3}. Reaction forces were of the order of magnitude 10^0.

Indicator	Regression		Error		R^2
	Sum of squares	Mean of squares	Sum of squares	Mean of squares	
Curvature from 0 to 5 mm*	$9.4\ 10^{-5}$	$6.3\ 10^{-6}$	$6.7\ 10^{-7}$	$4.0\ 10^{-8}$	0.9929
Curvature from 5 to 20 mm*	$3.2\ 10^{-5}$	$2.1\ 10^{-6}$	$1.2\ 10^{-7}$	$6.9\ 10^{-9}$	0.9964
Curvature from 20 to 30 mm*	$1.8\ 10^{-4}$	$1.7\ 10^{-5}$	$3.2\ 10^{-7}$	$1.9\ 10^{-8}$	0.9982
Slope from 0 to 5 mm*	$2.2\ 10^{-2}$	$1.5\ 10^{-3}$	$2.1\ 10^{-4}$	$1.2\ 10^{-5}$	0.9907
Slope from 5 to 20 mm*	$5.7\ 10^{-2}$	$3.8\ 10^{-3}$	$1.1\ 10^{-4}$	$6.7\ 10^{-6}$	0.9980
Slope from 20 to 30 mm*	0.19	$1.3\ 10^{-2}$	$1.4\ 10^{-2}$	$8.0\ 10^{-4}$	0.9336

Table 4.3: Statistical analysis (ANOVA) of the response surface - Fisher's test probability: * ≤ 0.001

4.2.3 Results

4.2.3.1 FE model sensitivity

A design of experiments approach was used to evaluate the sensitivity of the FE model to different parameters. The aim was to ensure that this simulation can be used to identify deep soft tissue mechanical parameters (i.e. that the response of the simulation is sensitive enough to deep soft tissue mechanical parameters).

Statistical analysis of the response surface

The results of the ANOVA test concerning the surface response evaluation (Equation 4.5 to Equation 4.11) are reported in Table 4.3. The coefficients of determination, R^2, are above 99% for all tested metrics except for the mean slope for depth of compression in the 20-30 mm range. This indicates that the first order surface response (Equation 4.4) provides a very good agreement with the simulation sets.

Parameters sensitivity

The 1st order polynomial coefficients (Equation 4.4) calibrated against the mean curvature values are shown in Figure 4.5 - B. They represent the sensitivity of the FE model response to each parameter: the higher the absolute value of the coefficient, the more sensitive the FE model response to a change in this parameter. These coefficients were derived from simulations at 3 different stages of the force/displacement curves. Those adjusted on the mean slope are shown in Figure 4.5 - C. Coefficients characterizing the combined effects of the different parameters (β_{ij} - Equation 4.4) were derived but they are not significant, so they are not reported here.

The values of the sum of squares due to the regression are higher for the second and third parts

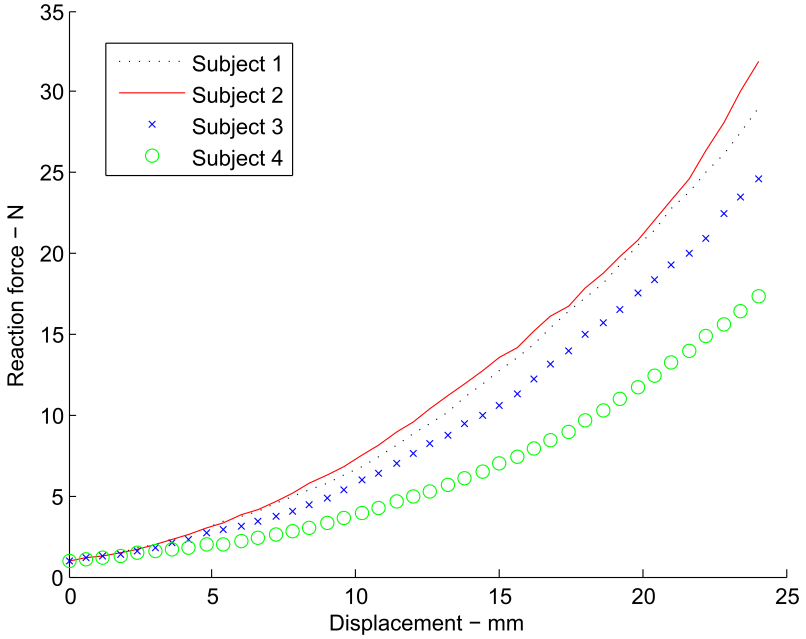

Figure 4.6: Experimental data - Response of 4 subjects to a localized compression of 25 mm depth with a 30 mm diameter cylinder

of the force/displacement curves, for all studied metrics (Table 4.3). This indicates that the identification of the material parameters of the constitutive equations for deep soft tissues is more relevant as the compression progresses.
For both types of analysed metrics (i.e. mean curvature and mean slope of the force/displacement curves), the sensitivities are significantly higher for the material properties of the deep soft tissues, which means that they have a greater impact on the response.
This result confirms that the proposed combination of experimental and numerical approaches permits identifying the mechanical properties of *deep* soft tissues.

4.2.3.2 Identified material properties of 4 subjects

Experimental data

For the four subjects, the responses to a 25 mm deep localized compression with a 30 mm diameter cylinder were acquired according to the methodology described before. The results are shown in Figure 4.6.

Identification: Neo-Hookean strain energy density function

An example of the experimental and numerical force/displacement curves after identification of the C_{10}^H material parameter (Equation 4.1) is shown in Figure 4.7 - A. The results of the identified parameter C_{10} for 4 subjects and the related cost function values are reported in Table 4.4.

Identification: 2^{nd} order reduced polynomial strain energy density function

An example of the experimental and numerical force/displacement curves after identification of C_{10}^P and C_{20} (Equation 4.2) is shown in Figure 4.7 - B. The C_{10} and C_{20} values for four

subjects and the related cost function values are reported in Table 4.5.

Subject	C_{10}^H identified $[kPa]$	Cost function value $[N^2]$
1	2.11	0.45
2	1.72	0.48
3	1.21	0.23
4	0.51	0.16

Table 4.4: Identification of C_{10}^H of deep soft tissues for 4 subjects

Subject	C_{10}^P identified $[kPa]$	C_{20} identified $[kPa]$	Cost function value $[N^2]$
1	0.82	2.61	$6.5\ 10^{-3}$
2	0.80	2.00	$2.5\ 10^{-2}$
3	0.70	0.80	$3.5\ 10^{-1}$
4	0.19	0.24	$4.3\ 10^{-1}$

Table 4.5: Identification of C_{10}^P and C_{20} of deep soft tissues for 4 subjects

4.2.4 Discussion

4.2.4.1 Contribution of the study

The methodology developed in this study is a fast and efficient tool to identify the passive mechanical properties of deep soft tissues in the leg of several subjects, taking into account the non-linear behaviour of these tissues. In the literature, only a few non-invasive methods have already been developed to identify the passive mechanical properties of deep soft tissues and it is the first time that a thorough analysis is conducted to really separate the contribution of deep and superficial tissues in the response to compression tests or indentation tests.
A method combining an axisymmetric multi-layer (i.e. skin, adipose tissue) FE model with an indentation experiment was used to identify the mechanical properties of the forearm soft tissues [Livarinen 11]. A small indentor allowed recruiting the behaviour of superficial soft tissues only. An interesting point of this technique was to identify separately each type of soft tissues.
Also, the characterization of the soft tissues of the leg has been performed for several subjects [Dubuis 12] [Bouten 09]. FE models of the leg in a relaxed initial state and a compressed state with stocking were compared to MRI scans of the legs in the same two states. The identification was performed between two loading states and could not capture the non-linear

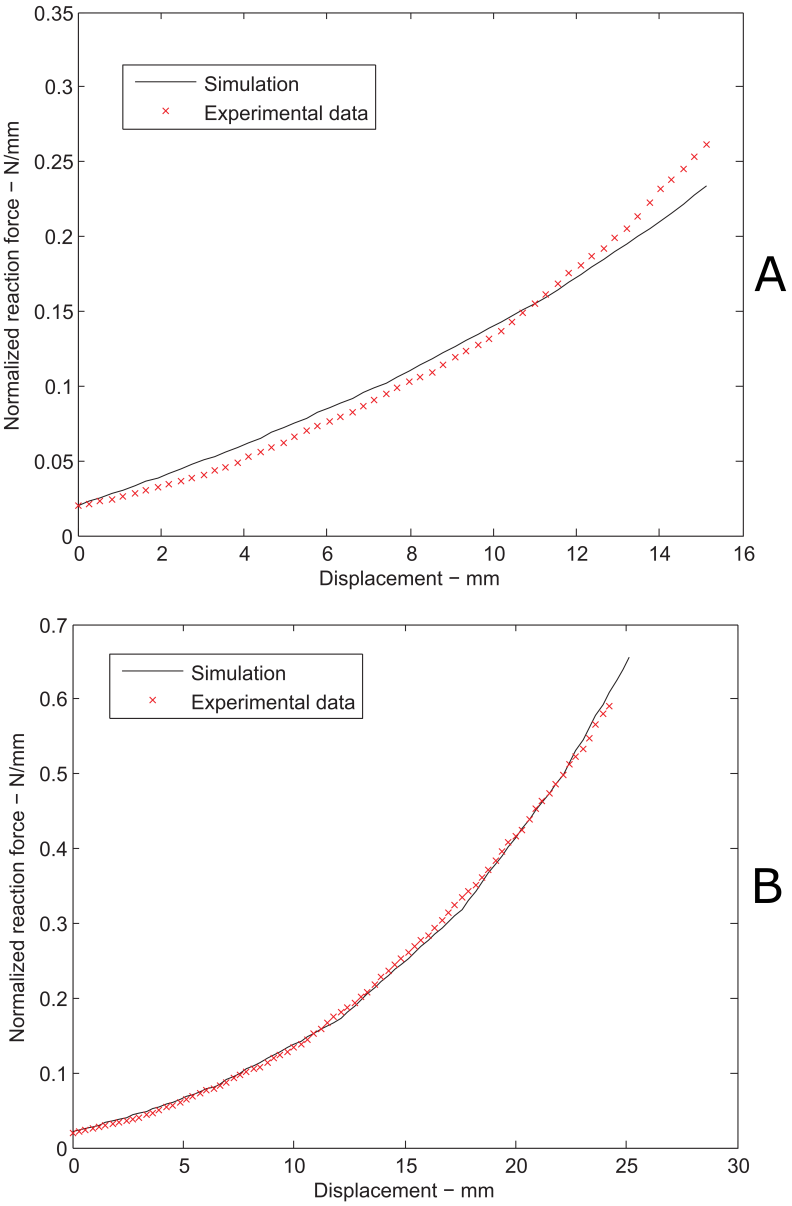

Figure 4.7: Numerical (solid line) and experimental (dash line) force/displacement curves for one subject; A - Result with the Neo-Hookean constitutive equation. B - Result of the 2nd order reduced polynomial constitutive equation

behaviour of soft tissues. However, the FE model was composed of two compartments of soft tissues, allowing a distinction between the mechanical properties of adipose tissue and muscular tissue.
Finally, a study similar to the one presented here identified mechanical properties of soft tissues of the calf [Vannah 96]. An inverse method combined a subject-specific FE model with the indentation of the leg at the calf location by 8 mm or 19 mm diameters cylinders. In this case, the cylinders were applied perpendicularly to the leg axis. Nevertheless, this FE model was composed of only one compartment of soft tissues, without any distinction between skin, fat and muscle.

4.2.4.2 Limitations of the experiments

The leg geometry in the FE model was defined from the ultrasound reconstruction and might differ from the actual leg geometry during the acquisition of the compression data. Indeed, both data sets were not acquired on the same day but also, the leg position differed between both data acquisitions: prone position for the ultrasound image acquisition; sitting position for the compression test.

The effects of these geometrical differences and their impact on the identification of mechanical properties still need to be investigated. This matter could be prevented if the leg geometry acquisition was performed right before the compression of the calf soft tissues, with a 3D optical scanner for example. A 3D scanner will provide the external geometry of the leg, but also the exact location of the cylinder before the compression as well as the direction of the cylinder displacement. Nevertheless, the bones location and the different soft tissue compartments are not available with this imaging modality. As the aim of the study was to identify deep soft tissues mechanical properties, it would have been impossible to use the 3D scanner to implement the simulation, as it only provides the external geometry of the leg.

4.2.4.3 Numerical assumptions

The subject-specific FE model of the leg implemented in this study is based on several assumptions discussed here.

Bi-dimensional FE model

The identification process compares the 3D experimental curves with that of the bi-dimensional FE model. The bi-dimensional FE model is built on a classical plane-strain model combined with correction factors taking into account 3D effects. As a matter of fact, a plane-strain model would be insufficient, the 3D effects corresponding to about 15% of the reaction force (Figure 4.4 - C). This reduction of the 3D model may be questionable for small displacements. Indeed, in the first millimeters of the localized compression, the contact length is smaller than the length of the applied cylinder because the leg is not a perfect cylinder. Not surprisingly, the design of experiments showed that the identification of material parameters is more significant for a displacement larger than 5 mm.

Material compressibility

It is fairly common to assume soft tissues as nearly incompressible *in vivo* because they are mainly composed of water [Fung 93]. However, a preliminary study showed that a fully incompressible strain energy density function raised numerical issues. Consequently, a slightly

compressible model was chosen and D values for both constitutive equations (Equation 4.1 and Equation 4.2) were selected from a previous study [Bouten 09]. In the latter study, a difference of leg cross-section area of about 5% was observed in MRI transverse scans between wearing and not wearing compression stockings (Class II delivering averagely a 20 mmHg pressure to the calf).
Two phenomena could explain this observation of tissue loss of volume. First, when the leg is under compression, the venous system is drained compared to the uncompressed state and second, soft tissues can move upwards when a compression stocking is worn. Thus, the loss of area occupied by the leg in the MRI transverse planes could be the combined result of blood draining and 3D deformations. Assigning the D values reported in Table 4.1 was sufficient to take these effects into account in the models. An improvement could be to identify a subject-specific compressibility parameter, but this would require precise volume measurements of soft tissues during the test.

Viscoelasticity

The methodology described in this paper presents the identification of soft tissues elastic properties. However, human soft tissues are often considered as viscoelastic materials [Sengeh 16]. The experimental setup was designed to compress soft tissue with a very low displacement rate. It was checked that displacement rate variation (within the range being possible with this setup) had negligible influence on the response. This confirms that for the time scales of the experiments, viscoelastic effects remain negligible and hence an identification on the loading curve is convenient.

4.2.4.4 Design of experiments

Several studies raised questions about the mechanical role of the *fascia cruris* in the biomechanics of elastic compression, one of them being the contention of muscular tissues [Bergqvist 99] [Papadopoulos 81]. However, the sensitivity analysis performed here showed no significant effect of its mechanical properties or of its thickness. It is still possible that the *fascia cruris* plays a biomechanical role but that this role is marginally involved in the localized compression applied here. Other investigations should be proposed in the future to answer the questions regarding the biomechanical role of this tissue and how it participates to the response in other modes of loading.

4.2.4.5 Identified material parameters

Material parameters of a Neo-Hookean strain energy density function have already been identified for the soft tissues of the human leg [Dubuis 12] [Bouten 09]. In those studies, C_{10} was identified between 1 kPa and 15 kPa. Here, the C_{10}^H are between 0.5 kPa and 2.1 kPa.
Although material properties of the *fascia cruris* have no significant impact on the response of the current FE model, the presence of this tissue seems to stiffen the leg, likely due to a structural effect. This may explain why the identified values of C_{10}^H identified here are in the lower range of the values found in the literature [Dubuis 12] [Bouten 09].

Due to the large deformations of the leg during localized compression, the Neo-Hookean strain energy density function appeared limited since it could not capture the non-linear behaviour observed experimentally (Figure 4.7 - A). However, a 2$^{\text{nd}}$ order reduced polynomial equation described well the behaviour of deep soft tissues of the leg (Figure 4.7 - B).

In this bi-dimensional FE model, muscular tissues were considered as transversally isotropic, which is fairly common when assuming muscular fibers to be distributed perpendicular to the transversal plane. In the future, it would be interesting to investigate localized compression in several directions to study the anisotropic behaviour of muscular tissue.
Also, the identified mechanical properties here were those of a relaxed muscular state. Other investigations with a controlled muscular contraction would allow identifying the mechanical properties at an active muscular state.
Finally, this methodology applied to a larger population could shed a light on inter-subject variability.

4.2.5 Conclusion

This paper presented a fast and non-invasive novel methodology to identify the mechanical properties of deep soft tissues of the human leg, using conventional ultrasound imaging and a simple mechanical test. To do so, an inverse method was used, combining a subject-specific bi-dimensional FE model with localized compression tests. After the evaluation of this method on one healthy subject, it was performed on three other subjects to identify the material parameters of two constitutive equations of the deep soft tissues.
The methodology takes into account the non-linear behaviour of deep soft tissues by identifying the material properties on a large range of deformations rather than comparing two states (i.e. initial and final). This study showed that a 2^{nd} order reduced polynomial strain energy density function should be used over a Neo-Hookean model for deep soft tissues of the leg.
Also, the differentiation of materials (i.e. skin, fat, *fascia cruris*, and muscle) allowed separating the contributions of each tissue. It is the first time that a thorough analysis is conducted to really separate the contribution of deep and superficial tissues in the response to compression tests and this permitted to estimate the passive material properties of deep soft tissues for four subjects independently of the response of their other tissues.

4.3 Characterization of fabric-to-fabric friction: application to medical compression bandages

Co-authored with Emilie Benoist, Pierre Badel, Reynald Convert, Laurence Schacher and Jérôme Molimard, from [Chassagne a]

4.3.1 Introduction

Fabric-to-fabric friction is involved as one of the underlying mechanisms in many medical devices. In these applications, friction is sometimes only a negligible phenomenon, whereas in others, it is a salient feature directly impacting the function of the device. In such cases, an accurate understanding and characterization of friction is of highest importance and deserves specific studies. One of these applications is medical compression bandage therapy in which a textile bandage is wrapped with two or three overlaps around a limb within the aim to apply controlled pressure to the limb. Pressure itself is the active principle of the therapy; however, when wrapped around a leg for instance, friction prevents the bandage to fall down on the ankle [Ghosh 08], and is likely to influence the final pressure distribution on the limb, hence being a key feature to secure the desired function.
Friction between two materials was, and is still, very widely studied in conventional material science, like metallic material science. Literature and experimental equipment dedicated to textile material friction properties are slightly less abundant [Gupta 08].
Friction is most usually characterized with the simple Amonton's law (which includes Coulomb's) stating that $|F| = \mu|N|$ where F and N are respectively the tangential and normal contact forces. The friction coefficient, μ, is generally different in static situation, prior to movement initiation and in dynamic situation when sliding between both surfaces occurs. Though other more refined but more complex, friction laws exist, this simple law is very widely used in modelling and especially numerical simulation.
Interest in studying the geometry of fabric surfaces by developing experimental characterization of the friction coefficient can be dated to 1955, when Butler et al. described their "cloth profile recorder" [Butler 55]. Development of numerous methods involving most often a linear planar motion of a body on another one are named "contact measurement method" [Gupta 08].
For measuring static coefficient, the inclined plane is the simplest method. To obtain the dynamic coefficient, sled-type techniques, based on a planar body surface and a device to control the displacement of the other body surface are the most common. Note that alternative techniques exist like Capstan's method in which a fabric is wrapped and rolled around a cylindrical surface, or the twist method in which two fabrics are twisted together [Gupta 08]. The choice of the characterization technique and associated equipment should ideally depend on the nature of the studied contact (point, line, surface), the environment (air, water, etc.) [Das 05], the type of fabric, and the method used to control the normal force and the displacement, and to measure the friction force [Gupta 08].
Characterizing the touch of fabrics or fabric-to-fabric friction was another motivation that led to several previous studies. A work by Ramkumar et al. [Ramkumar 03] aimed at developing a polymeric human finger sensor used in a sled-type friction measurement device. Similarly, though more simple, one of the modules of the system developed by Kawabata [Kawabata 80] was designed to characterize friction related to the hand of fabrics and was used in previous studies [Bertaux 07]. This module relies upon a point-plane friction principle in which a metallic sensor devised to reproduce a fingertip is rubbed over a plane fabric while applying a constant pre-defined pressure. Fabric-to-fabric friction usually yields different, higher, friction coefficients. Moorthy et al. [Moorthy 15] used a plane-plane system to determine static and dynamic friction coefficients between fabrics made of nonconventional fibers, and focused on the

influence of the fibers, their blend and proportion. Because fabric-to-fabric friction coefficient also depends on the geometrical structure of the fabric (e.g. yarn structure, crimp height, etc.), the studies by Ajayi [Ajayi 92a] [Ajayi 92b] aimed at detailing such relationships. An in-house plane-plane friction bench test was used to shed light on precise mechanisms underlying fabric friction properties. In particular, the evolution of hairiness and its influence on friction coefficients were studied, showing that hairiness decreased with increased contact pressure and with increased number of movements, hence reducing the friction coefficient. Relationships between fabric structure and friction properties could also be addressed demonstrating, for instance, that yarn density directly influences the friction coefficient of a fabric due to protruding yarns effects.
To sum up this short overview of the literature, each method was specifically designed for either measurements related to an application or for characterizations of friction mechanisms. However, none of them addressed the problem of fabric-to-fabric friction characterization in use conditions, like use under tension which is typical of many medical applications, for instance. To address this lack, the objective of the present study was to develop an experimental technique based on the existing and recognized equipment of Kawabata. The system presented in this paper includes adjustment of both fabric tension and contact pressure to evaluate their respective influence on the measured fabric-to-fabric friction coefficient. An application is proposed through an experimental campaign carried out on medical compression bandages.

4.3.2 Methods

Tests were conducted under standard conditions: $20°C \pm 2°C$ and $65\% \pm 2\% R.H.$ according to ISO standard 139:2005 [139:2005 05].

4.3.2.1 Compression bandages

Compression bandages are textile medical devices designed for the treatment of some venous or lymphatic pathologies. The treatment consists in wrapping the stretched bandages around the limb, hence applying an interface pressure on the limb thanks to the tension in the fabric. The interface pressure, which is the active principle of the therapeutic treatment, depends on several parameters such as the bandage tension, the leg geometry, the number of layers and other parameters such as bandage-to-bandage contact interactions [Chassagne 15]. Moreover, bandage-to-bandage frictional properties prevent the bandage to fall down and are thought to also have an impact on the interface pressure variation between rest state and exercise.
First, the frictional properties of several medical compression bandages were investigated under conditions close to their use conditions. The chosen bandages were the Biflex® 16, the Biflex® 17, the Flexideal®, the Biflexideal® and the Cotton bandages, all manufactured by Thuasne®, but also the bandage Rosidal® K, manufactured by L&R. Their characteristics are given in Table 4.6. These bandages consisted in a small representative sample of commercially available bandages, with different textile structures. The characterization of their frictional properties provided a range of friction coefficient.

In a second phase, the impact of applied pressure and stretch on frictional properties was evaluated for only two bandages: the Biflex® 16 (B16) and the Biflex® 17 (B17) (Figure 4.8). These two bandages were selected because they have a very similar structure but different mechanical properties. They mainly differ in their core elastic yarn, whose strength at stretch = 1.3 is higher for the B17 (12.3 cN) than for the B16 (5.7 cN). According to the manufacturers' recommendations these bandages should be applied on the lower limb with a 1.3 stretch ($stretch = L/L_0$, with L the post-application length of the bandage and L_0 its initial length).

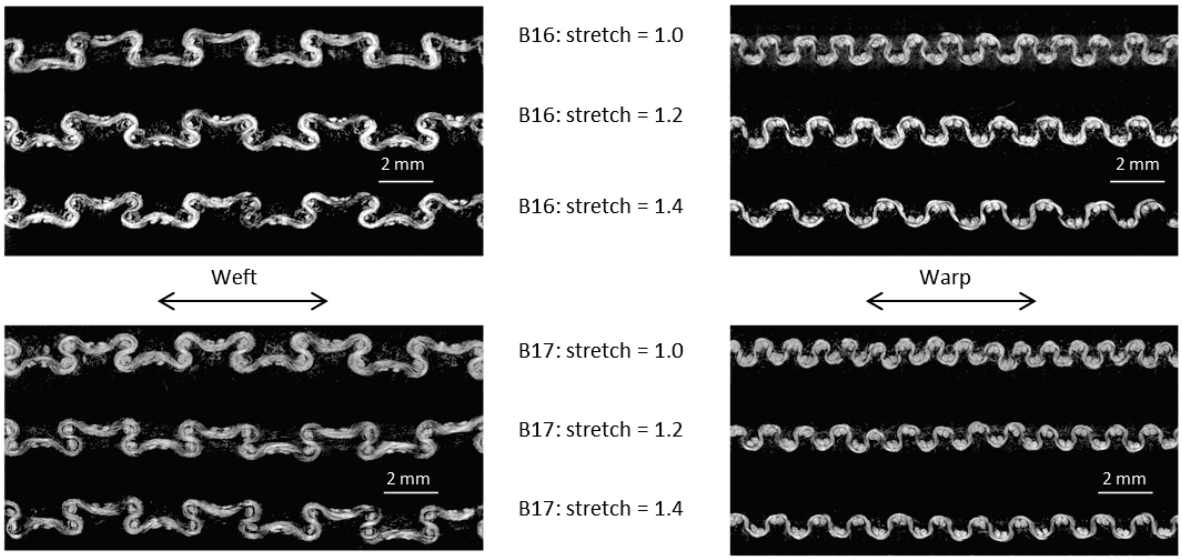

Figure 4.8: Cross-sectional images of bandages B16 (top) and B17 (bottom) obtained in X-ray micro-tomography (Phoenix Nanotom® S) in the weft (left) and warp (right) planes and at 3 different stretch levels (1.0, 1.2 and 1.4)

	Biflex® 16	Biflex® 17	Flexideal®	Biflexideal®	Cotton Bandage	Rosidal® K
Type of weave	Leno weave	Leno weave	Plain weave	Plain weave	Tubular knitted Jersey	Plain weave
Composition*	51/40/5/4 Vi/PES/Pa/El	54/31/3/12 Vi/PES/Pa/El	47/35/17/1 Pa/Vi/PES/El	65/33/2 Co/Vi/El	100 Co	100 Co
Area density $[g/m^2]$	389	511	223	248	200	350
Yarn density Warp	22	22	20	16	14 courses/cm	17
$[yarn/cm]$ Weft	15	20	9	11		14
Force to stretch a 10 cm bandage width at stretch = 1.3 [N]	7	13	3.2	1.3	19	2.2 at stretch=1.3 27 at stretch=1.7
Elastic warp yarn count [Tex]	135	125	8	29	N/A	N/A
Non elastic warp yarn 1 count [Tex]	26	26	16	N/A	20	40
Non elastic warp yarn 2 count [Tex]	16	16	N/A	N/A	N/A	N/A
Weft yarn count [Tex]	40	40	33	71	N/A	72

Table 4.6: Characteristics of the bandages - *Composition: Vi = Viscose, PES = Polyester, Pa = Polyamide, El = Elastane, Co = Cotton

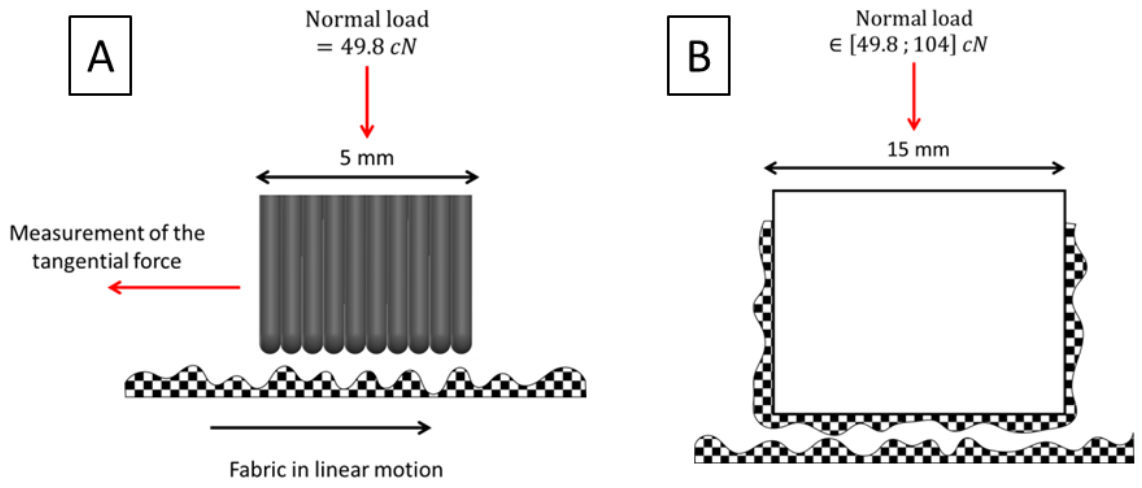

Figure 4.9: Illustration of the two friction contactors: A - the initial one from the KES, B - the one designed for fabric to fabric friction characterization

4.3.2.2 Kawabata evaluation system (KES)

The Kawabata Evaluation System was designed for the standard evaluation of a fabric hand [Kawabata 80]. It is composed of four instruments [Harwood 08]. Six characterization tests can be performed thanks to these different devices: tensile and shear tests, pure bending test, compression test and friction and roughness measurements. The last of these four systems was of interest in the present study: the KES-FB4. This system, which was customized in this study, helps to characterize the roughness and the frictional behaviour of the fabric.

Characterization of fabrics frictional properties

KES-FB4

The fourth module of the Kawabata Evaluation system (KES-FB4) was designed to characterize the fabric roughness and its frictional properties. Its purpose was to mimic a human finger touching the fabric. For this, a 5 mm long friction contactor, composed of piano strings which were tied together, was in contact with the fabric (Figure 4.9). This contactor was linked to the frictional force sensor and a normal load (49.8 cN) was applied on the contactor (equivalent to a 50 g weight). Then the fabric underwent a 3 cm translation motion, with return, under the friction contactor, at a constant speed equal to 1 mm/s. The instantaneous dynamic friction coefficient was computed thanks to the following equation (Amonton's law):

$$\mu(displacement) = \left| \frac{\text{frictional force}}{\text{normal force}} \right| \tag{4.13}$$

It was then averaged over the fabric displacement, the first and last half centimeter of the translation motion (i.e. the acceleration and deceleration phases) being not taken into account for this computation (Figure 4.14). Consequently, the friction coefficient obtained and provided by the device was the dynamic friction coefficient.
The Kawabata Evaluation System was only suitable for fabrics to metal friction characterization. Moreover, the contact area of the sensor could be quite small with respect to the fabric pattern. However it was a reliable and simple measurement tool [Hu 04], hence the idea to use

Applied Weight [g]	Normal Force [cN]	Pressure [hPa]	Pressure [mmHg]
50.8	49.8	22.2	16.6
65.4	64.2	28.5	21.4
80.5	79.0	35.1	26.3
95.2	93.4	41.5	31.1
106.1	104.1	46.3	34.7

Table 4.7: Different normal loads applied for the characterization of friction coefficient

this module but to design a new friction contactor.

Fabric-to-fabric friction contactor

Within the aim to propose a simple characterization method of fabric-to-fabric friction, a new friction contactor was designed (Figure 4.9 - B and Figure 4.10 - B). It was composed of a metal cube on which the fabric was taped, with the required stretch. Different weights could be set on the contactor in order to adapt the normal load within the experimentally observed range of pressure [Chassagne 15] (Table 4.7).
The contactor was linked to the KES-FB4 frictional force transducer. However, the automatic data post-processing was based on the assumption that the normal load was 48.9 cN (corresponding to a 50 g weight). Therefore a correction of the data given by the KES-FB4 was required (Equation 4.14):

$$\mu \; = \; k * \mu_{KES-FB4} \text{ with } k \; = \; \frac{\text{regular normal load (48.9 cN)}}{\text{applied normal load}} \tag{4.14}$$

Tensioning and holding frames

The pressure applied on the limb by compression bandages is a direct consequence of the fabric stretch, and it is the active principle of the therapeutic treatment. Thus it was primordial to perform the experiments on stretched bandages. For that purpose, a stretching frame was designed to set the fabric with a homogeneous stretch (Figure 4.10 - A). The fabric was set with no stretch then pinned with a pair of jaws, one of which can translate. The translation of the jaw stretched the fabrics, in a homogeneous way, until the expected stretch was reached. Then the fabric was fixed in the holding frame (Figure 4.10 - A and B), which maintained the fabric at the desired stretch. The fabric was then removed from the jaws and the frame was set on the KES moving platform.

4.3.2.3 Experimental protocols

Measurement precision

Repeatability conditions of measurements were chosen among the classical specified conditions for the estimation of the measurement precision. They are defined as: "condition of measurement, out of a set of conditions that includes the same measurement procedure, same operators, same measuring system, same operating conditions and same location, and replicate measurements on the same or similar objects over a short period of time" [BIPM 08].

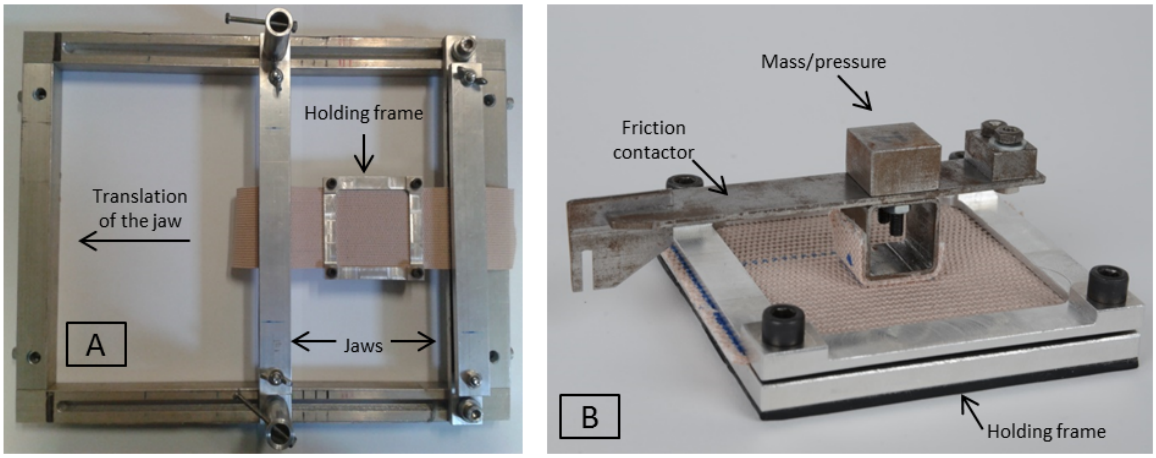

Figure 4.10: A - Stretching frame: the fabric is set in the jaws with no stretch, then the translation of the jaw stretches in an homogeneous way the fabric. Once stretched, the fabric is fixed in the holding frame and removed from the jaws; B - Holding frame and friction contactor used for the measurement of fabric to fabric friction coefficient

The frictional test could slightly degrade the contact area of the fabric, thus frictional measurements were performed by the same operator using the same equipment and measuring facility within a short interval of time, but on different measurement items. Ten tests were run for each bandage B16 and B17, with no stretch and along the warp direction. The applied load was 49.8 cN (50 g), which corresponded to a pressure equal to 16.6 mmHg (within the range of pressure in use).
From the 10 test repetitions, the mean value $\bar{\mu}$, the standard deviation σ and the coefficient of variation $CV[\%]$ were computed:

$$CV[\%] = \frac{\sigma}{\bar{\mu}} * 100 \tag{4.15}$$

The coefficient of variation $CV[\%]$ was respectively equal to 2.4% and 4.3% for the B16 and the B17. The repeatability was considered as acceptable if the coefficient of variation $CV[\%]$ was lower than 5%. Consequently, the measure of bandage to bandage frictional coefficient can be considered as "repeatable".

Frictional properties of different medical compression bandages

The friction coefficient was measured for six different commercially available medical compression bandages with various structures (Table 4.6). The aim of these measurements was to provide a variation range for friction coefficients of bandages. The applied stretch was chosen to be in accordance with the actual bandage application:

- stretch = 1.3 for the Biflex® 16 and Biflex® 17
- stretch = 1.5 for the Flexideal®, Biflexideal® and Rosidal® K
- no stretch for the Cotton bandage.

The Cotton Bandage is not a compression bandage but a padding layer (applied under a compression bandage) and is usually applied with very little stretch. The applied load was set to

28.5 hPa (21.4 mmHg, i.e. similar to use conditions) and friction was measured along the warp direction. Five measurements were performed for each bandage.

Influence of applied pressure

A previous study investigated the level of interface pressure (onto the skin) applied by both compression bandages, with different application techniques and on different subject's morphologies [Chassagne 15]. The pressure investigated in the present study ranged from 22.2 hPa to 46.3 hPa (16.6 mmHg to 32.3 mmHg), in accordance with the actual pressure applied by medical compression bandages measured in this previous study. In order to modulate the applied pressure, different masses could be set up onto the friction contactor (Table 4.7 and Figure 4.10 - B).
For all frictional tests performed to evaluate the influence of applied pressure, the bandage sample taped on the friction contactor and the one in the holding frame had a 1.3 stretch. The tests were repeated five times in a row with different bandage samples.

Influence of fabric stretch

The actual stretch of applied bandages may vary significantly [Chassagne 15]. Thus it was essential to address the influence of stretch value on frictional properties. In the case of bandages Biflex® 16 and Biflex® 17, the stretch recommended by the manufacturer is 1.3. For both bandages, the friction coefficient was measured for five different stretches varying from 1.1 to 1.5.
To evaluate the impact of fabric stretch on bandage frictional properties, the stretch of the bandage taped on the friction contactor was kept to 1.3 whereas the stretch of the bandage in the holding frame varied. The applied pressure was set to 28.5 hPa (21.4 mmHg).
All frictional tests were performed five times in a row.

4.3.2.4 Statistical analysis

All mean results are given with their 95% interval of confidence.
The significance of the difference between the friction coefficient at different stretch levels or pressure levels was assessed with the Kruskal-Wallis non parametric test, as the samples were very small ($n = 5$). Then the individual effects were tested with a Mann-Withney U-test corrected with the Bonferroni method ($\alpha = \frac{0.05}{\text{Number of tests}}$). Difference was considered as significant if $p < 0.05$.

4.3.3 Results

4.3.3.1 Friction coefficient for different bandages

The bandage-to-bandage friction coefficient was measured for six commercially available bandages (Figure 4.11). The variation range of the measured friction coefficient was between 0.5 and 0.7. For bandages with similar structures, Biflex® 16 and Biflex® 17 but also Biflexideal® and Flexideal®, increasing the fabric density tended to increase the friction coefficient. Indeed, the friction coefficient was higher for the Biflex® 17 (0.57 ± 0.03) than for the Biflex® 16 (0.53 ± 0.02) and the same trend was observed for the Biflexideal® (0.51 ± 0.01) and the Flexideal® (0.63 ± 0.03). The maximum friction coefficient was observed for the bandage Rosidal® K (0.65 ± 0.03).

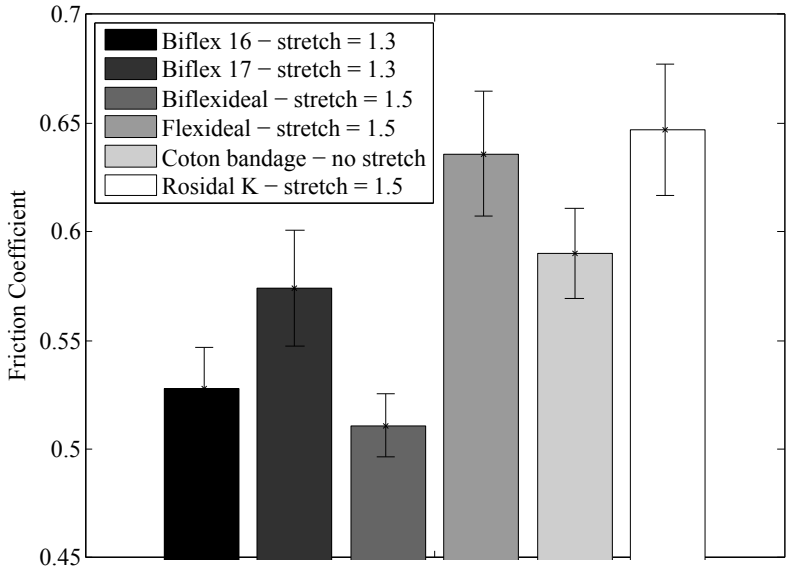

Figure 4.11: Bandage-to-Bandage friction coefficient for different medical compression bandages (mean value ± CI)

4.3.3.2 Influence of applied pressure

Friction coefficient μ was measured with varying applied pressure for two bandages with very similar structures, Biflex® 16 (B16) and Biflex® 17 (B17). The results are presented in Figure 4.12. For bandage Biflex® 16, the friction coefficient tended to decrease at the initiation of pressure increase and then was stable. For bandage Biflex® 17, a trend of decrease in the friction coefficient was also observed when pressure increased. Significant differences were observed in friction coefficient for varying pressure ($p = 0.03$ for the B16 and $p = 0.01$ for the B17), only between applied pressures equal to 22.2 hPa and 41.5 hPa (Figure 4.12).

4.3.3.3 Influence of stretch

Frictional behaviour of both bandages B16 and B17 was characterized at different level of stretch. The results, presented in Figure 4.13, showed that stretch had no significant impact on friction coefficient of bandage B17 ($p = 0.58$) but it had a significant impact for the bandage B16 ($p = 0.006$) between stretches equal to 1.2 and 1.3.

4.3.4 Discussion

A new and simple method was developed to characterize fabric-to-fabric frictional behaviour, adapted from the Kawabata Evaluation System. Thanks to this methodology, the impact of fabric stretch and applied pressure on the friction coefficient can be investigated.
This method showed a good repeatability for the measurement of bandage-to-bandage friction coefficient. Despite the fact that only six types of compression bandage were tested, this methodology could very likely be used for a wide range of fabric.

4.3.4.1 Bandages structure

Following the KES protocol, the friction coefficient was the mean of that measured for a 20 mm displacement forward and backward. This friction coefficient varied quite periodically

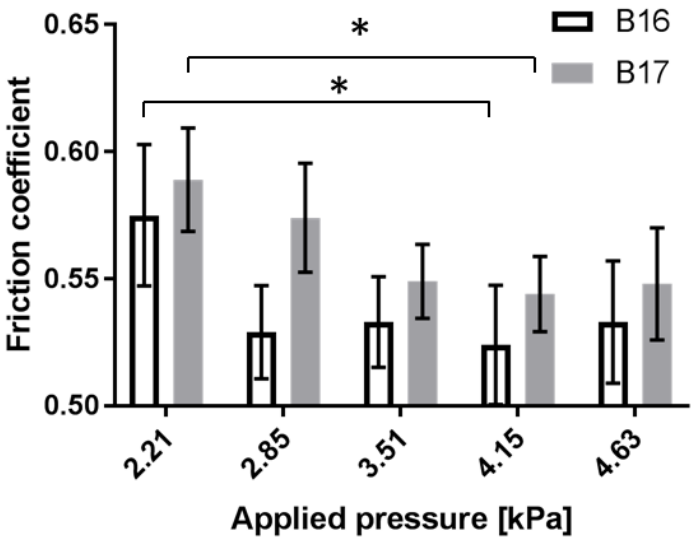

Figure 4.12: Evolution of friction coefficient with regards to applied pressure (* = significant difference)

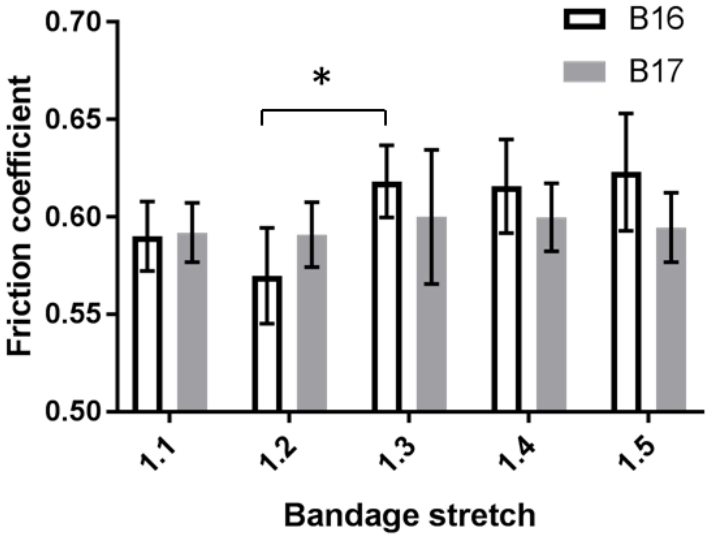

Figure 4.13: Evolution of friction coefficient with regards to bandage stretch (* = significant difference)

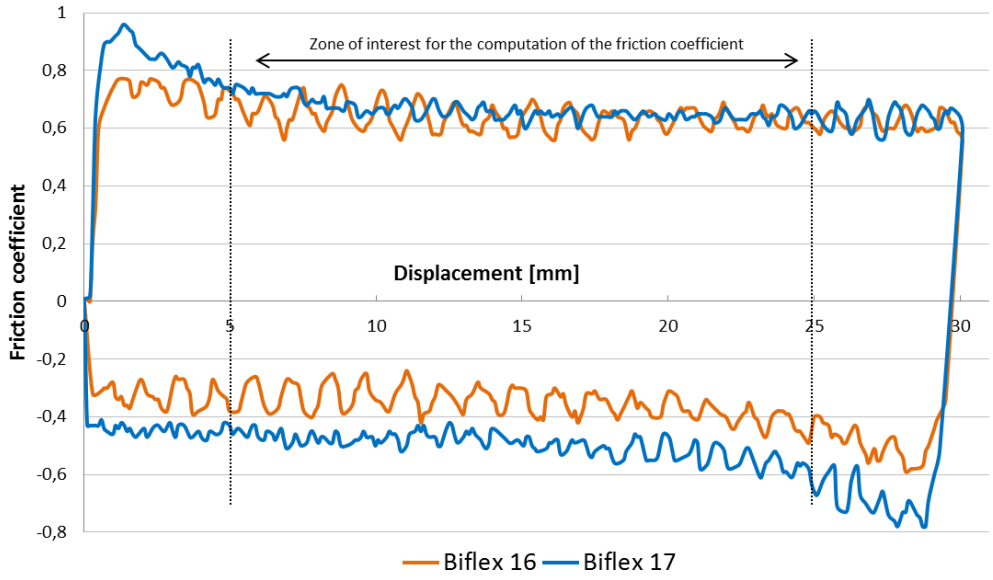

Figure 4.14: Examples of curves for two bandages samples B16 and B17, along the warp direction

within the displacement range (Figure 4.14). As it was previously observed by Ajayi et al. [Ajayi 92b], the peaks which could be observed in Figure 4.14 corresponded to the weft yarns. These experiments were not designed to investigate the impact of fabric structure on frictional properties. However, the measurements performed for the six bandages tend to be in agreement with a previous study [Ajayi 97] which noticed that an increase in fabric construction (i.e. the number of weft yarn per centimeter) led to an increase in the friction coefficient. Further investigations would be needed to conclude about a real impact of fabric structure on friction coefficient.

4.3.4.2 Influence of applied pressure

In the range of the tested applied pressure, very little changes in the friction coefficient have been observed. Even if most of the changes were non-significant, increasing normal load seemed to result in decreasing friction coefficient. This has already been observed by Ajayi [Ajayi 92b] and Das et al. [Das 05], where the relationship between the normal load and the frictional was found to be logarithmic. Here, the variability in the friction coefficient makes this logarithmic model impossible to verify and friction coefficient must be considered as constant.
This result supported the use of Amonton's law (Equation 4.13) to describe the frictional behaviour of these fabrics in this range of pressure.

4.3.4.3 Influence of stretch

Contrary to applied pressure, stretch impacted the bandages thickness. According to the tomographic images (Figure 4.8), the structure of the fabrics was subject to important changes along the warp direction but did not vary along the weft direction. Indeed, these bandages showed no Poisson effect once stretched (i.e. the width of the bandage remains stable whatever its stretch). However, stretching the fabric tended to decrease its density. It could have been expected that the friction coefficient decreased when stretch increased, as the number of weft

yarn per cm decreased, but it was not the case. Figure 4.8 clearly shows that stretching the fabric changed the period of the structure, but did not change the pattern. A simple geometrical model based on moiré description was built to quantify the average interaction area between the 1.3 stretch fabric (on the movable pad) and the varying stretch fabric. This model shows that, because of the small pad dimension, the interaction area is almost constant independently of the stretch.

4.3.4.4 Limitations

To compute the friction coefficient, the KES removed the first and last 5 mm of the translation (which corresponds to the initiation of the translation motion). So the computed friction coefficient was the dynamic friction coefficient. This system did not permit to characterize the static fabric-to-fabric friction coefficient. Another limitation of the KES was the translation speed. Even though previous studies did not observe significant effect of sliding speed on the dynamic friction coefficient [Ajayi 92b] [Hermann 04] it was not possible to characterize the frictional properties at varying speeds with the KES.
The area of the friction contactor should be designed with regards to the weaving pattern of the fabric. If the pattern is too large, the friction contactor area has to be enlarged. This may be the cause of difficulty depending on the required normal load for the characterization. Indeed, increasing the area means also increasing the applied weight, which might disturb the translation motion of the KES.
Eventually, the fabrics tested in the present study were mostly woven fabrics. But it was proven that the fabric structure and its fibers components impacts on the friction coefficient [Ajayi 92a] [Moorthy 15].

4.3.5 Conclusion

A simple and reliable method was designed to characterize the fabric-to-fabric friction coefficient, based on the surface tester of the Kawabata Evaluation System. The coefficient could be measured for varying fabric stretches and normal load. This method provided the frictional properties of compression bandages in use conditions and is suitable for the friction characterization of other compression textiles.

Chapter 5

Simulation numérique de l'action des bandes de compression - *Numerical simulation of the action of medical compression bandages*

Two preliminary studies (Chapter 3.2, page 38 and Chapter 3.3, page 52) showed the limitations of the use of Laplace's law and highlighted the need of new tools for interface pressure computation. Moreover, the simulation of bandage application designed in the first numerical study (Chapter 3.3, page 52) was too simplified and should be more realistic.
Consequently, a new method to predict interface pressure applied by a single compression bandage was developed and is described in this chapter. This methodology was based on the model reduction of a new finite element simulation, which mimicked the wrapping of the bandage on the leg. This numerical simulation was combined with the parametrization of the lower leg geometry, obtained from 35 legs from previous studies.
The model reduction approach helped to compute patient-specific interface pressures as a linear combination of 5 leg geometrical parameters, the bandage tension and the skin-to-bandage friction coefficient. The results of this computation were found to be in agreement with experimental pressure values measured on 66 legs.
This article was submitted to IEEE Transactions for Biomedical Engineering.

Contents

5.1 Résumé

Les deux premières études préliminaires (Chapitre 3.2, page 38 et Chapitre 3.3, page 52) ont montré les limites de la loi de Laplace pour la prédiction des pressions exercées par les bandes de compression. De nouveaux outils sont donc nécessaires pour prédire la pression appliquée par une bande de compression.

Ainsi, l'objectif de ce chapitre est de proposer une nouvelle méthodologie pour la prédiction personnalisée des pressions d'interface. Cette méthodologie est basée sur la réduction d'une nouvelle simulation éléments finis de la pose d'une bande, construite à partir de la géométrie personnalisée de la jambe.

Afin d'obtenir un modèle réduit de cette simulation numérique, la géométrie de la jambe a été paramétrisée. Le but était de pouvoir décrire la géométrie avec un faible nombre de paramètres, tout en ayant une erreur de reconstruction acceptable. Cette paramétrisation géométrique a été développée à partir de 35 géométries de jambes obtenues dans les deux études préliminaires (Chapitre 3.2, page 38 et Chapitre 3.3, page 52). En décrivant la jambe avec seulement 4 paramètres géométriques et la longueur de la jambe, 95% des erreurs de reconstruction étaient inférieures à 2 mm. Cette paramétrisation de la jambe a ensuite été utilisée dans la simulation numérique.

Parallèlement, la modélisation éléments finis de l'enroulement d'une bande sur la jambe a été développée, basée sur une géométrie de la jambe issue de la paramétrisation. Pour cette simulation, l'application de la bande était donc plus proche de la réalité. La bande était d'abord étirée jusqu'à l'allongement souhaité (ici 1.3) puis enroulée sur la jambe (Figure 5.4). Cette cinématique d'enroulement a été adaptée à chaque géométrie de jambe. Les interactions de frottement entre la peau et la bande, mais aussi celles entre les différentes couches de bandes, ont été prises en compte dans le modèle.
Pour confronter les résultats de cette simulation aux résultats expérimentaux, le résultat de cette simulation correspondait à la pression moyenne exercée au niveau du point B1 sur un disque de 50 mm de diamètre (correspondant à la taille du Picopress®, capteur utilisé pour les mesures de pression) (Figure 5.5 - A).

Un modèle réduit a été construit à partir de cette simulation. Il a été considéré que les paramètres pouvant impacter la pression étaient :

- la géométrie de la jambe
- les propriétés mécaniques des tissus mous de la jambe
- la tension de la bande
- le coefficient de frottement entre la peau et la bande
- le coefficient de frottement entre les différentes couches de bande

Une étude préliminaire, réalisée sur une géométrie de jambe moyenne (Équation 5.7) a montré que, dans la gamme de variation testée (Table 5.1), deux paramètres étaient responsables de plus de 93% de la variation de pression observée : la tension de la bande et le coefficient de frottement bande-peau. Les deux paramètres restants, les propriétés mécaniques des tissus mous et le coefficient de frottement bande-bande, ont donc été retirés de la définition du problème.
L'impact sur la pression de la tension de la bande, du coefficient de frottement bande-peau et

de la géométrie de la jambe, décrite par 4 paramètres géométriques et la longueur de la jambe, a été évalué grâce à un plan d'expériences numériques.
Cette approche a permis d'exprimer la pression au point B1 comme une combinaison linéaire de ces différents paramètres (Équation 5.9 et Table 5.3).
Les résultats de ce modèle réduit sont globalement en accord avec les mesures de pressions réalisées sur 66 jambes, mais restent dispersés.

Ce modèle réduit permet de calculer en quelques minutes et de manière personnalisée la pression appliquée au point B1 alors qu'il faudrait plusieurs jours pour la simulation numérique.

5.2 Numerical model reduction for the prediction of interface pressure applied by compression bandages on the lower leg

Co-authored with Jérôme Molimard, Reynald Convert, Pascal Giraux and Pierre Badel, from [Chassagne d]

5.2.1 Introduction

Compression bandages applies a pressure onto the skin, called interface pressure, which is then transmitted to the vessels through soft tissues (mainly adipose and muscle tissues) [Partsch 05a]. The target interface pressure, which is a key aspect of the treatment [Partsch 14], may vary with the pathology to be treated. Indeed, the pressure required for severe pathologies such as venous leg ulcers may be over 40 mmHg [Blair 88] whereas other pathologies would require lower interface pressures [Vicaretti 10]. More than the success of the treatment, this target pressure can also impact the treatment observance [Milic 10], hence an important need to control it. Interface pressure generated by compression bandages results from complex phenomena [Clark 03] [Melhuish 00] which remain poorly understood [Partsch 03a]. On the one hand, this pressure is impacted by the fabric material: its mechanical properties (stiffness characterizing the tension needed to stretch the bandage), its stretch once applied on the leg, the application technique (spiral pattern, figure-of-eight, ...) and the interaction between the bandage layers (i.e. the frictional properties of the fabric) [Ghosh 08]. On the other hand, the pressure varies with the lower leg morphology and its mechanical properties, both dependent on body position. Eventually, once applied on the leg, the bandage interacts with the skin through friction phenomena.
Among the large diversity of commercially available bandages [Partsch 14], practitioners have to select the one best suited to the patient's morphology and pathology. However, for now, the only method to compute interface pressure is Laplace's law, which states that interface pressure P is directly proportional to the bandage tension T [N/mm] and the number of layers n but inversely proportional to the local radius of curvature r_C:

$$P = \frac{n\,T}{r_C}\ ,\ T > 0\ ,\ r_C > 0 \tag{5.1}$$

Though it was adapted to compression bandage therapy [Al Khaburi 12] [Thomas 03a], the relevance of the use of this law was called into question [Schuren 08]. First, the measure of interface pressure applied on 30 healthy subjects' legs by two bandages with similar fabric structure but different tension showed that pressure was not directly proportional to bandage tension T [Chassagne 15]. Moreover, the use of this Law often considers a cylindrical approximation of the leg geometry (considering only the leg circumference) and an homogeneous bandage tension [Williams 99]. Eventually, this law does not take into account all parameters impacting interface pressure, like soft tissue deformation induced by bandage application for instance [Chassagne 16].
Another mean to predict interface pressure is finite element simulation. This method was shown to be efficient for the computation of pressure applied by compression stockings, with 2D [Rohan 15] or 3D models [Dai 07], but was rarely implemented to compute pressure applied by compression bandages [Chassagne 16].
Therefore, a new method for fast interface pressure computation, based on a finite element modelling, is proposed in this study. A 3D simulation of bandage application, based on a personalized leg geometry, was designed. Then a model reduction technique was developed, including a novel global geometrical description of the lower leg, to predict personalized pressure values, which were then confronted to experimental pressure values.

5.2.2 Methods

5.2.2.1 Geometrical parametrization of the lower leg

To compute interface pressure with Laplace's law, the leg is geometrically described by its local radius of curvature. For subsequent model reduction, another parametrization of the global leg geometry was needed in the present study. This parametrization should require as few parameters as possible for the leg description within an acceptable reconstruction error. This objective was reached thanks to the Proper Orthogonal Decomposition (POD) of 35 leg geometries.
These geometries were obtained from the 3D optical scans of the right leg (in standing position) of 35 patients (20 women - 15 men) from previous studies [Chassagne 15] [Chassagne 16]. They were all set in the same reference frame, then normalized to their lengths and divided into 100 sections (in the transverse plane). Each section was then approximated with Fourier polynomials:

$$r(\theta) = r_0 + \sum_{m=1}^{n} a_m * cos(m\theta) + + \sum_{m=1}^{n} b_m * sin(m\theta). \tag{5.2}$$

with $n = 5$ the degree of the polynomials and $r(\theta, z)$ the radius for a given angle θ and a given height z (cylindrical coordinates system). For $n = 5$, each section was describe with 11 Fourier polynomials coefficients and the coordinates of the centre (x_0, y_0). Thereby, each leg geometry $\{U^i\}_{i=1..N}$, previously normalized to its length, was described with 1300 parameters. The same methodology as described by Gogu et al. [Gogu 13] was followed to build the POD basis. The $N = 35$ leg geometries could then be approximated as a linear combination of the vectors of the orthogonal basis:

$$\tilde{U}^i = \sum_{k=1}^{K} \alpha_{i,k}\ \phi_k = \sum_{k=1}^{K} < U^i, \phi_k > \phi_k, \quad K < N \tag{5.3}$$

with $\tilde{U}^i$ the approximated leg geometry, ϕ_k the vectors of the orthogonal POD basis, K the size of the basis and N the number of leg geometries U^i. The median reconstruction error ($\|U^i - \tilde{U}^i\|$) with regards to the basis dimension K is presented in Figure 5.1. With the first 4 POD vectors, 95% of the reconstruction errors of all measuring points of the 35 legs were found to be smaller than 2 mm (Figure 5.1 - left).

5.2.2.2 Numerical Simulation

A finite element simulation of bandage application was designed with Abaqus®. This simulation was based on a 3D lower leg geometry on which a 10 cm wide stretched bandage was wrapped in a spiral pattern. The output of the simulation was the interface pressure measured over a 50 mm diameter disk located at measurement point B1 on the medial side of the leg (corresponding the Picopress® sensor area (Microlab, Padua, Italia), used in the experimental measurements [Chassagne 15] [Chassagne c]) (Figure 5.5 - A).

Leg geometry and mechanical properties

The external leg geometry was given thanks to the geometrical parametrization previously described and was then converted to a 3D volume. The geometry of bone holes (tibia and fibula) was obtained from anatomical slices of the 'Visible Human Server' (Computer Science Department, Peripheral Systems Lab., Ecole Polytechnique Fédérale de Lausanne), then scaled to the 3D leg geometry and implanted in the leg volume with the software Solidworks®. A

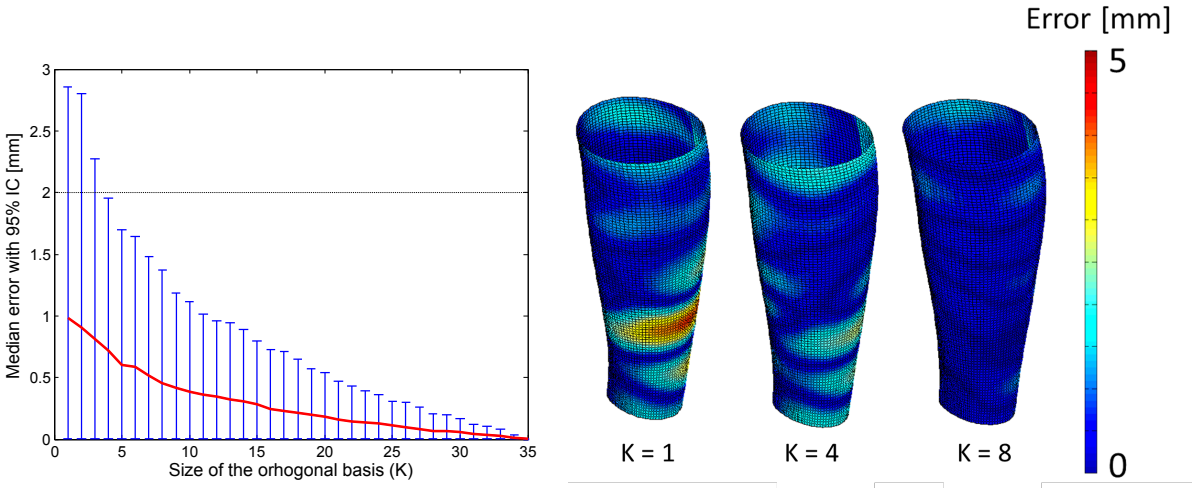

Figure 5.1: Median absolute error between the initial and the approximated leg geometry, as a function of the dimension of the orthogonal POD basis K (left) and illustration of the reconstruction error with regards to the size of the basis K (right)

preliminary study showed that considering one large hole surrounding the two bones (red dotted line in Figure 5.2 - B) had negligible impact on interface pressure. Thus, as a simplification, the envelope of the two bones geometries was used, whose edge was pinned to mimic a non-deformable material. After a mesh convergence study, the leg volume was meshed in Abaqus® with 4-node linear tetrahedron hybrid elements (about 450,000 elements depending on the leg geometry).
Leg soft tissues were modeled with one single homogeneous material whose behaviour was described by a Neo-Hookean constitutive law:

$$U = c_{10}\ (\bar{I}_1 - 3) + \frac{\kappa}{2}\ (J^{el} - 1)^2 \tag{5.4}$$

with $\bar{I}_1$ the first invariant of the isochoric deformation, J^{el} the elastic volume ratio, c_{10} the shear modulus and κ the bulk modulus, whose value was taken from the literature ($\kappa = 14.3\ MPa$ [Dubuis 12]). Even though it was shown in Chapter 4.2 that soft tissues mechanical behaviour was better modeled with a 2$^{\text{nd}}$ order reduced polynomial strain energy density function, soft tissue deformation induced by bandage application were small enough to consider the use of a Neo-Hookean model as relevant in this study (mean strain ≈ 0.001).

Bandage geometry and mechanical properties

Compression bandage was modeled as a 10-cm wide shell geometry, whose length was adapted to the leg length (Figure 5.2 - C). It was meshed with 4-node shell elements with reduced integration (about 40,000 elements, depending on the leg geometry).
Compression bandages material was described as an orthotropic linear elastic material. All material parameters are linked by the following equations:

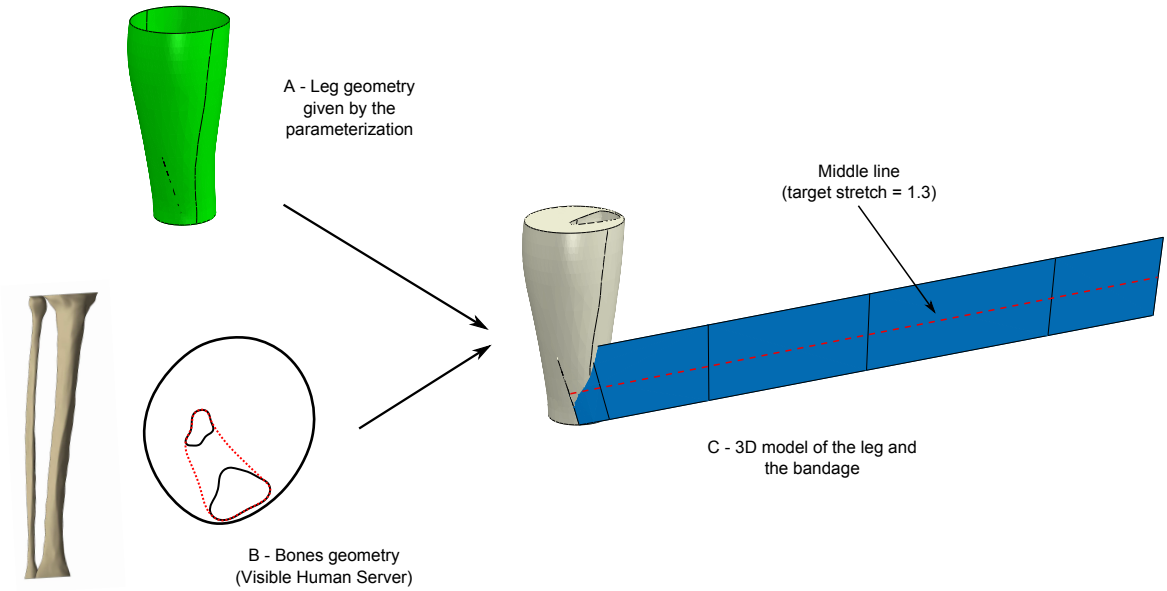

Figure 5.2: Design of the 3D model: first the leg external geometry is given by the geometrical parametrization (A) and converted to a 3D volume in which bones are implanted (B); eventually, a flat bandage is added to the model (C)

$$\begin{bmatrix} \epsilon_{11} \\ \epsilon_{22} \\ \gamma_{12} \end{bmatrix}_{\perp} = \begin{bmatrix} \frac{1}{K_1} & -\frac{\nu_{12}}{K_1} & 0 \\ -\frac{\nu_{12}}{K_2} & \frac{1}{K_2} & 0 \\ 0 & 0 & \frac{1}{G} \end{bmatrix}_{\perp} \begin{bmatrix} N_{11} \\ N_{22} \\ N_{12} \end{bmatrix}_{\perp} \quad (5.5)$$

$$\begin{bmatrix} M_{11} \\ M_{22} \\ M_{12} \end{bmatrix}_{\perp} = \begin{bmatrix} F_1 & \tilde{0} & 0 \\ \tilde{0} & F_2 & 0 \\ 0 & 0 & \tau_{12} \end{bmatrix}_{\perp} \begin{bmatrix} \kappa_{11} \\ \kappa_{22} \\ \kappa_{12} \end{bmatrix}_{\perp} \quad (5.6)$$

with ϵ_{11} and ϵ_{22} the strains in the in-plane longitudinal and transverse directions (i.e. the warp and weft directions), N_{11} and N_{22} the section forces in the in-plane longitudinal and transverse directions, γ_{12} and N_{12} the in-plane shear strain and section force, K_1 and K_2 the elastic moduli in the in-plane directions, ν_{12} the Poisson's ratio and G the shear modulus, M_{11}, M_{22} and M_{12} the section moments and κ_{11}, κ_{22} and κ_{12} the bending strains.
The material parameter of interest in the study was the elastic modulus in the longitudinal direction K_1. The other parameters K_2, ν_{12} , G, F_1, F_2 and τ_{12} were set to the values measured in a previous study [Chassagne 16].
The elastic modulus in the longitudinal direction K_1 was given by the tension of the bandage T at a 1.3 stretch (circle in Figure 5.3) (secant modulus, ensuring the correct tension value at the prescribed 1.3 stretch).

Simulation strategy

The edge of the bones hole was pinned. The bandage was tied to the leg close to the ankle, then stretched to a 1.3 stretch (following manufacturer's recommendations) and wrapped on the leg in a 50% overlapping spiral-pattern application technique (Figure 5.4). The kinematics of bandage application (i.e. wrapping the bandage around the leg) was computed with an

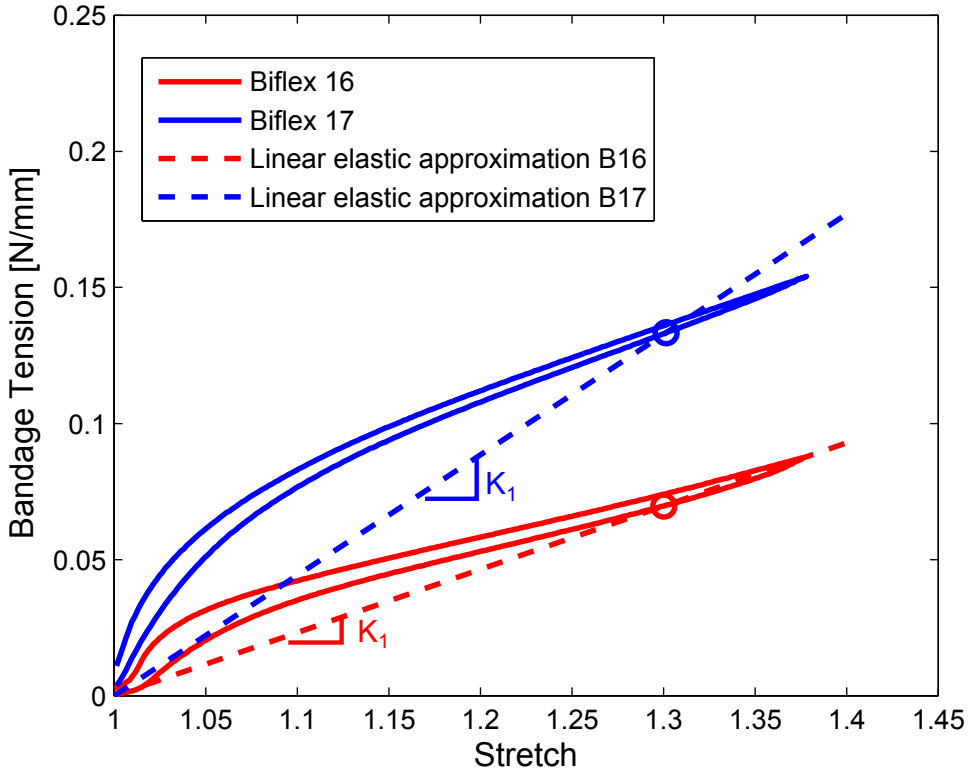

Figure 5.3: Illustration of two secant elastic moduli from two tension-stretch curves

in-house Matlab® code for each leg geometry. The aim of these kinematic boundary conditions was to wrap the bandage, in a 2-layer spiral pattern, with a stretch equal to 1.3 at the midline of the bandage (Figure 5.2 - C), as the operator would do in the experiments.
The contact between the leg and the bandage but also the contact between the different bandage layers allowed no penetration and were modeled with the Coulomb's friction law. Depending on the size of the leg, computation time varied from 1 to 3 days on 12 CPUs.

Output of the simulation

Within the aim to later compare the values from the simulation with the experimental pressure values, the output of the simulation was the mean pressure over an area corresponding to the sensor Picopress® located at measurement point B1 (Figure 5.5 - A). This area of interest was determined from the curvature of the posterior part of the leg (in blue in Figure 5.5). Starting from the top of the zone of interest (the top of the leg was not taken into account), in green in Figure 5.5, the height of measurement point B1 was the first point with a curvature derivative lower than ϵ (very close to 0) (in red in Figure 5.5). This methodology was used to determine the location of measurement point B1 for all legs.

5.2.2.3 Numerical model reduction

From this numerical simulation, a model reduction approach was used to assess the impact of different parameters on interface pressure. This approach helps to model a complex phenomenon, in this case interface pressure at measurement point B1, depending on a large number

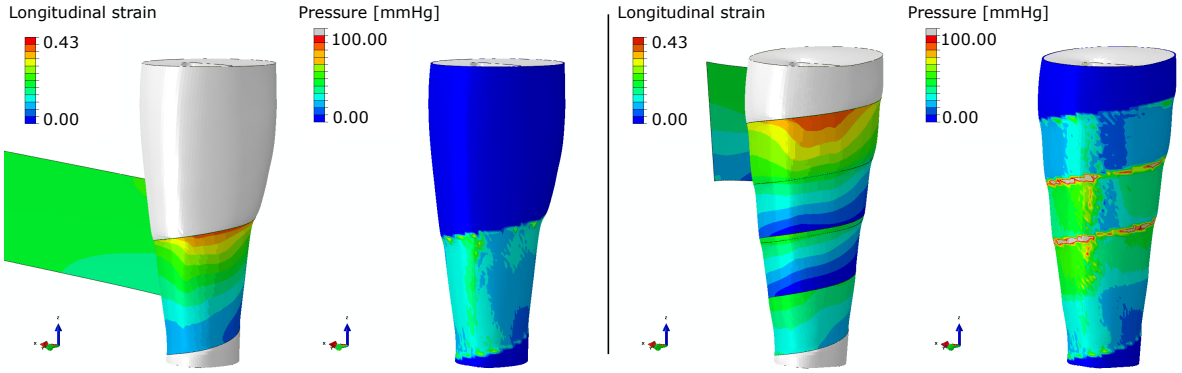

Figure 5.4: Illustration of the simulation - bandage application on the leg and resulting interface pressure distribution (left: first turn, right: end of simulation)

of parameters, with a very few repetitions of the simulation [Tinsson 10].
The parameters possibly impacting interface pressure were:

- the leg geometry,
- the leg soft tissue mechanical properties (c_{10} - (Equation 5.4))
- the bandage tension (T)
- the skin-to-bandage friction coefficient ($\mu_{skin-bandage}$)
- the bandage-to-bandage friction coefficient ($\mu_{bandage-bandage}$).

First, a study was performed on a mean leg geometry in order to evaluate the impact of the four remaining parameters on interface pressure (soft tissue mechanical properties, bandage tension and the two friction coefficients). The mean leg geometry was obtained by setting all the geometrical parameters to their mean value $\bar{\alpha}_k$:

$$U^{mean\ leg} = \sum_{k=1}^{35} \bar{\alpha}_k\ \phi_k \tag{5.7}$$

The impact of the variation of the four parameters was evaluated within the ranges given in Table 5.1. A preliminary numerical study was performed to evaluate the variation of interface pressure induced by a variation of skin-to-bandage friction coefficient within the range found in the literature [Gerhardt 09] [Gerhardt 08]. The lowest value was obtained from the literature (0.10) and the maximum one corresponded to complete adhesion (0.3) (higher values would not lead to lower sliding).
A similar methodology was followed for the range of variation of leg soft tissue mechanical properties, going from 2 to 8 kPa (higher values led to no difference in interface pressure). Minimum and maximum bandage tensions were chosen with regards to the tension of bandages Biflex® 16 and Biflex® 17 (Figure 5.3) and the experimental stretches measured in a previous study [Chassagne 15]. The bandage-to-bandage friction coefficient range of variation was given by previous experimental measurements [Chassagne a].
The evaluation of the impact of these four parameters, in the ranges of variation summarized in Table 5.1, showed that two parameters, skin-to-bandage friction coefficient and bandage tension, were responsible for more than 93% of interface pressure variation. Consequently, the bandage-to-bandage friction coefficient and the leg soft tissues material parameter were

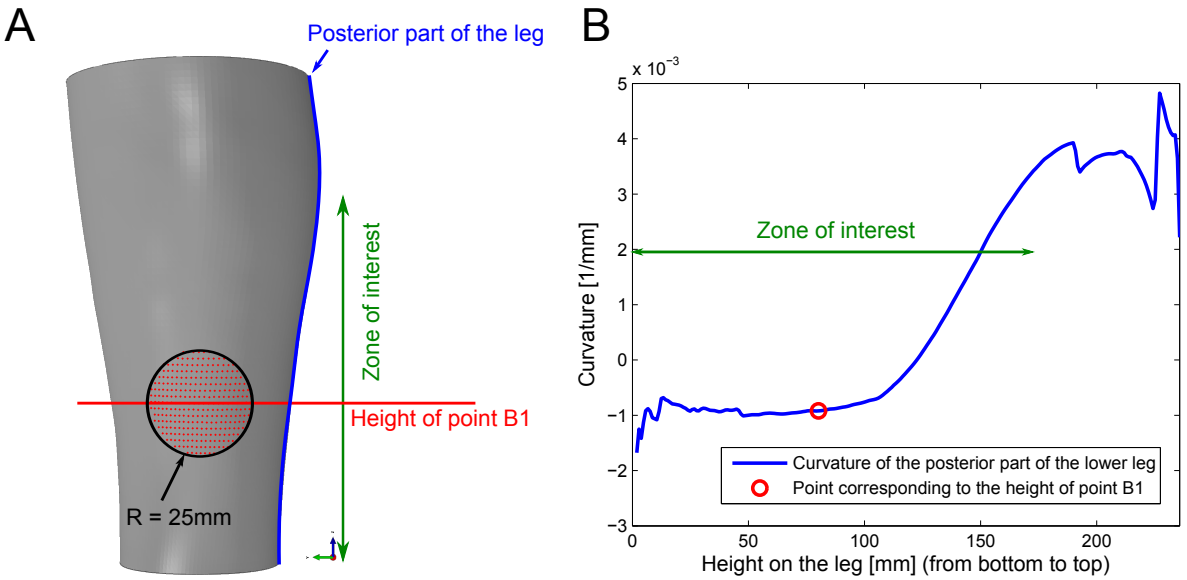

Figure 5.5: A - Location of the output of the simulation on the mean leg geometry, i.e. a 50-mm diameter area around measurement point B1; B - Determination of the height of measurement point B1 from the curvature of the posterior part of the leg

Parameter	**Lowest value**	**Highest value**
Skin-to-bandage friction coefficient $\mu_{skin-bandage}$	0.10	0.30
Bandage-to-bandage friction coefficient $\mu_{bandage-bandage}$	0.50	0.70
Bandage tension T [N/mm]	0.059	0.137
Leg soft tissue mechanical properties c_{10} [kPa]	2.00	8.00

Table 5.1: Ranges of variation for the skin-to-bandage friction coefficient ($\mu_{skin-bandage}$), the bandage-to-bandage friction coefficient ($\mu_{bandage-bandage}$), the bandage tension (T) and the soft tissue material parameter (c_{10})

removed from the problem definition and set to their mean values: $\mu_{bandage-bandage} = 0.6$ and $c_{10} = 5kPa$.

The second step consisted in the evaluation of the impact of skin-to-bandage friction coefficient, bandage tension and leg geometry on interface pressure. The leg geometry was given with 4 geometrical parameters (Equation 5.3) and the leg length L. The ranges of variation of the morphological parameters, presented in Table 5.2, were obtained from the 35 leg geometries.

Parameter	**Lowest value**	**Highest value**
Skin-to-bandage friction coefficient $\mu_{skin-bandage}$	0.10	0.30
Bandage tension T [N/mm]	0.059	0.137
Lower leg length L [mm]	184.86	290.43
1st geometrical parameter α_1	-0.920	-0.503
2nd geometrical parameter α_2	-0.109	0.119
3rd geometrical parameter α_3	-0.092	0.068
4th geometrical parameter α_4	-0.081	0.095

Table 5.2: Ranges of variation for the skin-to-bandage friction coefficient ($\mu_{skin-bandage}$), the bandage tension (T), the leg length (L) and the four geometrical parameters ($\alpha_{1..4}$)

From the ranges of variation defined in Table 5.2, the parameters were coded between -1 and 1:

$$X^* = 2 * \frac{X - X_{min}}{X_{max} - X_{min}} - 1 \tag{5.8}$$

with X^* the value of X in the coded space, X_{min} and X_{max} the minimum and maximum value of the parameter X.
A fractional factorial design was built [Tinsson 10] to select the different combinations of the 7 parameters of interest. Each combination was used to run one simulation and eventually compute the response surface of the model. Here, 9 simulations were run for this model reduction.
From the output of these 9 simulations, i.e. the interface pressure at measurement point B1 on the medial side of the leg, it was possible to compute this interface pressure $\hat{P}$ at measurement point B1 as a linear combination of skin-to-bandage friction coefficient $\mu^*_{skin-bandage}$, bandage tension T^*, leg length L^* and 4 geometrical parameters $\alpha^*_{1..4}$:

$$\hat{P} = \bar{P} + \beta_\mu \ \mu^*_{skin-bandage} + \beta_T \ T^* + \beta_L \ L^* + \beta_1 \ \alpha^*_1 + \beta_2 \ \alpha^*_2 + \beta_3 \ \alpha^*_3 + \beta_4 \ \alpha^*_4 \tag{5.9}$$

with all parameters coded between -1 and 1 (Equation 5.8). The coefficients β were obtained from the model reduction approach.

5.2.2.4 Comparison between numerical pressure, pressure computed with Laplace's law and experimental pressure values

Experimental pressure measurements applied by two bandages (Biflex® 16 and Biflex® 17) were previously performed on the legs of 35 subjects, whose geometry was used for the geometrical parametrization [Chassagne 15] [Chassagne 16]. Other pressure measurements applied by the Biflex® 16 were performed on both legs of 25 patients [Chassagne c], whose leg geometry was obtained with a 3D optical scanner (Artec^{tm} MHT 3D scanner, Artec^{tm} Group) in sitting and standing positions. Among these scans, 38 represented the complete lower leg and thus were suitable for this study. Once normalized to their length, these 38 leg geometries were decomposed in the orthogonal basis $\{\phi_k\}_{k=1..4}$ obtained from the geometrical parametrization. From the 38 sets of geometrical parameters seven were found to be out of the range of variation studied in the model reduction and were discarded.
Eventually, 66 leg geometries and 101 experimental pressure values (two bandages for 35 legs and one bandage for 31 legs) were kept for the comparison.
The pressure applied at measurement point B1 was computed thanks to the linear combination given by the reduced model (Equation 5.9). As no measurements were performed for the skin-to-bandage friction, this parameter was set to its mean value. In addition, interface pressure applied on the 66 leg geometries was computed thanks to Laplace's Law (Equation 5.1), following the same methodology described in a previous study [Chassagne 16].
For both computations, bandage tension was computed from the experimental stretch measurements:

$$Tension = (stretch - 1) * bandage\ elastic\ modulus\ (K) \tag{5.10}$$

Interface pressure values computed with these two methods, reduced model and Laplace's Law, were confronted to experimental values. Note that a previous work showed that the presence of the pressure sensor induced little measurement error, which was previously evaluated thanks to a numerical approach providing a methodology to correct this error [Chassagne 16]. The same methodology was implemented here for the correction of experimental pressure values.

5.2.3 Results

A new simulation of bandage application was built, within the aim to wrap the bandage around the leg with a 1.3 stretch. The mean stretch measured at the midline of the bandage (Figure 5.2 - C) was equal to 1.282 ± 0.001, but this stretch was very variable over the bandage width: 1.411 ± 0.004 at the top edge of the bandage and 1.139 ± 0.002 at its bottom edge.

5.2.3.1 Model reduction

Thanks to the model reduction approach it was possible to compute interface pressure applied at measurement point B1 as a linear combination of seven parameters (Equation 8). The coefficients β of the linear combination are reported in Table 5.3.
The overall significance of the linear model obtained from the model reduction was tested with the Fischer test ($p = 0.02$). Moreover, in light of the very high coefficient of determination $R^2 = 0.99$, it can be considered that this seven parameter reduced model gave a relevant description of the variation of interface pressure.

5.2.3.2 Comparison of the data computed with the numerical model reduction, Laplace's law and the experimental data

Pressure was computed from two equations, the reduced model (Equation 5.9 and Table 5.3) and Laplace's law (Equation 5.1), for 66 legs, as a function of the experimentally measured

Parameter (coded between -1 and 1)	**Coefficient**	**Value**
Mean pressure	$\bar{P}$	32.73
Skin-to-bandage friction coefficient $\mu^*_{bandage-bandage}$	β_μ	2.70
Bandage tension T^*	β_T	11.54
Lower leg length L^*	β_L	2.85
1^{st} geometrical parameter α_1^*	β_1	4.54
2^{nd} geometrical parameter α_2^*	β_2	3.92
3^{rd} geometrical parameter α_3^*	β_3	-1.74
4^{th} geometrical parameter α_4^*	β_4	-0.51

Table 5.3: Coefficients of the linear model β obtained from the model reduction approach (Equation 5.9)

bandage stretch. For 35 of them, pressure values applied by two different bandages (Biflex® 16 and Biflex® 17) were measured at measurement point B1 [Chassagne 15], whereas for the 31 remaining legs, only the pressure applied by the Biflex® 16 was measured [Chassagne c]. 101 pressure values computed from the model reduction equation (Equation 5.9 and Table 5.3) and Laplace's law (Equation 5.1), are plotted as a function of the experimental pressure values in Figure 5.6.
Though the data from the model reduction were scattered, they were in agreement with the experimental data ($slope = 1.04$), with a mean error equal to $9.7 \pm 5.0\%$. For Laplace's Law, the slope was further to 1 ($slope = 0.87$) and the mean error was equal to $-11.6 \pm 4.0\%$. Data from the model reduction were more scattered than the one given by Laplace's law because this model took into account more experimental parameters (seven) than Laplace's Law (two).

5.2.4 Discussion

A new method, based on the reduction of a numerical simulation, was designed to compute interface pressure applied by compression bandages at measurement point B1.
This method was based on a deformable 3D leg geometry described by 4 geometrical parameters and its length. Other influencing parameters were the bandage tension and the skin-to-bandage friction coefficient. The results obtained from this methodology were in agreement with previous experimental pressure measurements.

The simulation of bandage application was designed to apply the bandage in a spiral pattern with a 1.3 stretch. The stretch of the numerically applied bandage was found to be slightly lower (1.28). This could be explained by the little compression of the leg soft tissues induced by bandage application, and the cross-section becoming rounder. Even though the stretch at the

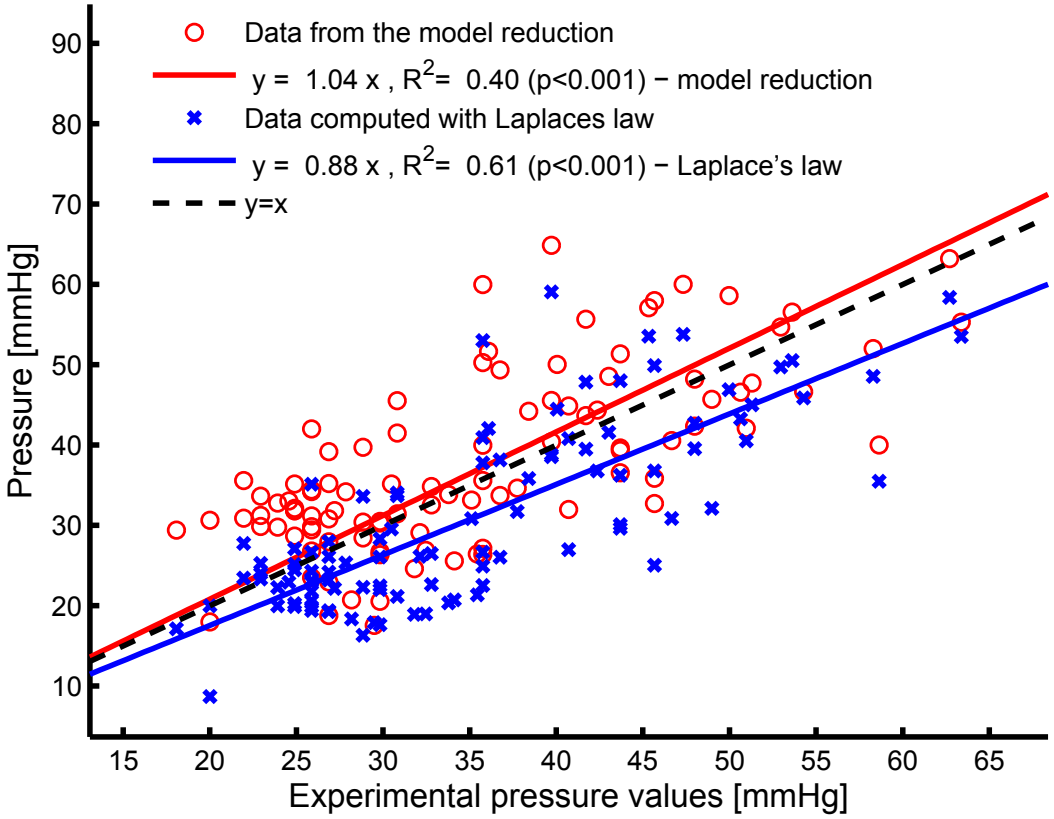

Figure 5.6: Pressure computed from the model reduction and Laplace's law as a function of the experimental pressure values

midline was close to the targeted value, it was found to be heterogeneous over the leg (Figure 5.4 and Figure 5.7). This stretch heterogeneity was the consequence of the "conical" shape of the leg (stretch is higher in the upper half of the bandage layer and lower in the lower half).
Usually, leg geometry is locally described by its radius of curvature. This new global geometrical parametrization, based on 35 right leg geometries, resulted in very low reconstruction error with only 5 parameters (4 geometrical parameters and the leg length) and was suitable to geometrically describe other leg geometries (31 among the 38 available leg geometries). The model reduction approach showed that the last parameters α_4 had lower effect than the three other geometrical parameters $\alpha_{1..3}$ (about 2% of the mean pressure) (Table 5.3).
The impact of several parameters on interface pressure was evaluated thanks to this model reduction approach. First it was observed that the mechanical properties of soft tissues had not much influence on interface pressure, even though it was shown in a previous numerical study [Chassagne 16] that the deformability of the soft tissue was to be considered to understand pressure generation. Nonetheless, it was previously shown that soft tissue mechanical properties influence the transmission of interface pressure to the vessels [Rohan 15].
The second parameter with very low impact on interface pressure was bandage-to-bandage friction. The values of this friction coefficient, provided by experimental measurements [Chassagne a], was very high (from 0.5 to 0.7) and did not result in any sliding motion between the different layers, hence its very low impact on pressure. However, bandage layers are in interactions with each other, but also with the skin.
Skin-to-bandage friction coefficient was found to be more influencing than bandage-to-bandage

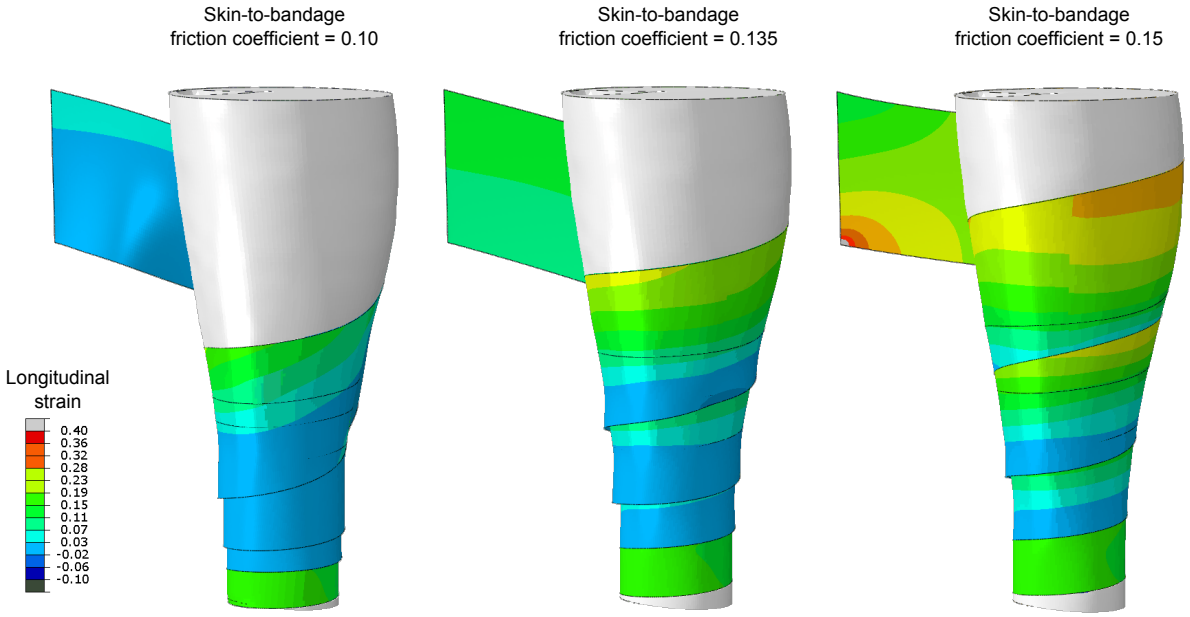

Figure 5.7: Illustration of the influence of the skin-to-bandage friction coefficient on a very conical leg geometry

friction in the preliminary study on the mean leg geometry. The values were much lower than for the other frictional parameter. Thus, for the lowest value (0.10) the bandage tended to slide down over the leg (Figure 5.7), whereas for the highest value (0.3), the bandage did not. While sliding down, the stretch of the bandage decreased and so did interface pressure. Nonetheless, as expected considering Coulomb's friction law, it was observed that the impact of skin-to-bandage friction coefficient was influenced by the leg morphology and more especially by the slope of the leg shape. This is the reason why a friction coefficient equal to 0.1 did not lead to much sliding for some leg geometries and led to complete sliding of the bandage for others (Figure 5.7). This lower value was in the lowest range of skin-to-textile friction coefficient reported in the literature.
The last parameter impacting interface pressure was, as expected, the tension, which in the study was a function of the bandage elastic modulus and the stretch (Equation 5.10). However, note that the reduced model is slightly more sensitive to the stretch than reality because the secant elastic modulus is higher than the tangent modulus (Figure 5.3).

In a second time, the pressure was computed for 66 legs and compared to experimental results. Though predicted pressure values were in agreement with experimental measured values, they sometimes showed large discrepancies. Four possible sources of error were identified.
First, due to the non-cylindrical shape of the leg, wrapping the bandage in a spiral pattern resulted in high pressure areas (in red in Figure 5.4) induced by the overlapping of the bandage which is not perfectly equal to 2 layers all over the leg (being, sometimes, very locally one or three layers). Whether the sensor is located under such an overlapping zone or not will change the interface pressure. The source of variability was evaluated using the FE model, by moving the center of the area of interest on a 1 cm radius circle around its initial position and led to a mean absolute pressure variation of 1.27 ± 0.38 mmHg.
The second source of error is the location of the sensor. In the simulation, it was determined from the curvature of the posterior part of the leg (Figure 5.5). However, experimentally, it is

likely that this location slightly differs from the one numerically determined, which may lead to a small pressure variation, of the same order as that evaluated right above.
Also, as it is not possible to patient-specifically characterize the skin-to-bandage friction coefficient, this parameter was set to its mean value. Thus all pressure values computed from the model reduction are given with a ± 2.70 mmHg uncertainty.
The last source of error is body position. Indeed, the bandage is applied in supine position, but it was not possible to scan the leg in this position. So the leg geometries were either obtained in sitting or standing position. These geometries were neither the one on which the bandage was applied, nor the one corresponding to the measured stretch. Due to gravity, muscle groups fall down and bandage stretch may be increased and thus interface pressure may vary.

Limitations

This methodology was based on the lower leg geometrical parametrization. However, this parametrization was obtained from 35 legs of healthy subjects. Even though these subjects showed a wide range of morphologies, the parametrization should be enriched with more leg geometries, from patients with leg oedema for instance.
For the numerical simulation, the kinematics of bandage application was based on the non-deformed shape of the leg and was not updated during the simulation (to take into account bandage sliding or leg deformation for example). An improvement of the simulation would be to update wrapping boundary conditions during the simulation, after each bandage turn for instance, as an operator does in reality.
Also, modelling bandage material as an elastic material tended to increase the influence of stretch on interface pressure (secant elastic modulus considered (Figure 5.3)). Next step would be to consider the non-linear mechanical behaviour of fabric materials in the simulation. Another important parameter was the skin-to-bandage friction coefficient. This study did not investigate the coupled effect of the leg geometry and this frictional parameter on interface pressure. Further mechanical studies would be needed for a better understanding of the effect of this frictional parameter.
The output of the simulation was only the pressure value at measurement point B1. However, the complete pressure distribution was provided by the simulation and could be further investigated.
Eventually, it seems crucial to be able to scan the leg geometry in the same position in which bandage is applied, to eliminate the uncertainty about the leg geometry.

5.2.5 Conclusion

A new method to compute interface pressure applied by compression bandages at measurement point B1 was proposed. This methodology was based on the parametrization of the leg geometry and the numerical simulation of bandage application. In addition to the leg morphology, the bandage tension and the skin-to bandage friction coefficient impacted interface pressure. Thanks to this approach, it is possible to compute patient-specific pressure values in a few minutes when it would take a few days with numerical simulation.
The pressure values computed for 66 legs were found to be in agreement with experimental pressure values. This methodology could later be enriched to compute pressure applied by multi-layer bandages.

Chapter 6

Etude clinique - *Clinical study*

The previous studies aimed to investigate the pressure applied by single component bandages. However, in clinical practice, different single bandages are often superimposed to form multi-component bandages. Therefore, the objective of this study was to investigate the pressure applied by superimposed bandages.
The first part of the clinical study was focused on the variations of interface pressure and Static Stiffness Index for different single and multi-layer bandages composed of elastic and/or non-elastic bandages. A part of the pressure measurements performed in this study was also used for the validation of the reduced model described in Chapter 5. This study was submitted to the Journal of Vascular Surgery. The second part investigated the impact of calf soft tissues mechanical properties on interface pressure. This short report was submitted to Phlebology.

Contents

6.1 Résumé

Une étude clinique a été réalisée au sein du Service de Médecine Physique et de Réadaptation du CHU de Saint-Étienne. Le but de cette étude était de mieux comprendre la pression exercée par la superposition de bandes de compression.
En effet, en pratique clinique, il est très courant de superposer plusieurs bandes de compression. Cela permet d'atteindre des niveaux de pression plus élevés mais aussi de faire varier les propriétés mécaniques des bandages en associant des bandes dites élastiques et inélastiques. Le but était d'étudier les pressions exercées par la superposition de deux bandages, élastiques et inélastiques.

Pour cela, la pression exercée par six bandages différents (mono ou multi couches) a été mesurée sur les deux jambes de 25 patients en position allongée, assise et debout dans un verticalisateur (Figure 6.1 - B). Les six bandages étaient composés d'une bande élastique (Biflex® 16, Thuasne) et/ou d'une bande inélastique (Rosidal® K, L & R):

- une bande élastique seule,
- une bande inélastique seule,
- une bande élastique posée sur une autre bande élastique,
- une bande inélastique posée sur une autre bande inélastique,
- une bande inélastique posée sur une bande élastique,
- une bande élastique posée sur une bande inélastique.

Tous les bandages ont été posés en spirale à 2 recouvrements (c'est à dire, recouvert à la moitié de la hauteur de la bande) par un seul opérateur. La pression a été mesurée en 4 points sur la jambe, à hauteur des points de mesure B1 et C sur les faces médiale et latérale de la jambe (Figure 6.1 - B). Les pressions exercées par la superposition de deux bandages ont ensuite été comparées à la pression exercée par chacune des bandes individuellement.

Les deux bandages simples (composés d'une seule bande) appliquaient des pressions similaires en position allongée (Figure 6.3), mais la bande inélastique avait un *Static Stiffness Index* (i.e. la variation de pression entre la position allongée et la position debout) plus élevé (Figure 6.4 - B). Cependant, les deux bandages multi-couches composés d'une bande élastique et d'une bande inélastique exerçaient des pressions différentes ($p < 0.05$) suivant l'ordre dans lequel étaient appliquées les bandes (Figure 6.3), bien que leurs *SSI* étaient égaux (Figure 6.4 - B).
Les mesures de pression en quatre points (B1 et C sur les faces médiale et latérale) ont permis de montrer que tous les bandages étaient dégressifs (la pression au point C était inférieure à celle au point B), sauf la bande inélastique appliquée seule sur la jambe. Il a aussi été observé que le maximum de variation de pression entre la position allongée et la position debout était situé au niveau du point B1 médial, renforçant donc son utilisation comme point de référence pour la mesure du *SSI*.
La pression exercée par la superposition de deux bandes a ensuite été exprimée comme une combinaison linéaire (avec un terme constant nul) de la pression exercée par chacune des bandes composant le bandage, appliquées seules sur la jambe. A part pour la superposition de deux bandes élastiques, les combinaisons linéaires n'étaient pas en accord avec les résultats expérimentaux (Équation 6.2).
Cette étude expérimentale a permis de montrer l'impact de l'ordre d'application des bandes sur la pression d'interface. Néanmoins, la faible corrélation entre la pression exercée par un

bandage multi-couches et celle appliquée par chacune de ses composantes a aussi mis en lumière la faible compréhension des mécanismes mis en jeux dans la superposition des bandes. Une étude mécanique plus poussée est donc nécessaire pour une meilleure compréhension des phénomènes impactant la génération de pression.

Au cours du même protocole expérimental, les propriétés mécaniques des tissus mous (tissus musculaires et adipeux ainsi que la peau) du membre inférieur des patients ont été caractérisées selon une méthodologie très proche de celle décrite dans le Chapitre 4.2, page 72. Cette caractérisation, couplée aux mesures de pression décrites précédemment, avait pour but d'évaluer l'impact de la variation des propriétés mécaniques des tissus mous sur les pressions d'interface. En effet, la pression d'interface augmente de la position allongée à la position debout, mais aussi de la position assise à la position debout. L'hypothèse a été faite que cette augmentation était consécutive à une variation de volume de la jambe (sang et tissus mous qui tombent du fait de la gravité) mais aussi à un changement de propriétés mécaniques des tissus mous (contraction des muscles en position debout). Cette étude avait donc pour but d'évaluer le lien entre la variation de pression et la variation de propriétés mécaniques des tissus mous.

Pour cela, un test de compression de la jambe par un cylindre métallique a été effectué sur les deux jambes de 24 patients, en position assise et debout (Figure 6.7). Avant le test de compression, la géométrie de la jambe avait été obtenue grâce à un scanner optique.
Ensuite, un modèle éléments-finis 2D du test de compression a été construit sur la base de la géométrie obtenue par le scanner 3D, permettant l'identification des propriétés mécaniques des tissus mous par méthode inverse. Ici, un modèle néo-Hookéen a été jugé pertinent car les déformations des tissus mous induites par l'application de la bande restent faibles. Le module d'élasticité E a été calculé à partir du paramètre Néo-Hookéen c_{10} identifié pour les 24 jambes (approximation pour les petites déformations, Équation 2.13, page 29).

Une augmentation significative du module d'élasticité linéaire des tissus mous des mollets a été observée de la position assise à debout, respectivement 10.4 kPa [6.1; 18.5] et 18.0 kPa [8.4; 52.1] (Tableau 6.1). Cependant, aucune corrélation entre la variation de pression d'interface et cette variation de propriétés mécaniques n'a été observée. Il est donc fort probable que l'augmentation de pression de la position assise à debout ne soit que la conséquence de la variation de volume de la jambe. Néanmoins, bien que les propriétés mécaniques des tissus mous de la jambe ne semblent pas impacter les pressions d'interface, elles influent sur la transmission de cette pression vers les veines [Rohan 15].

6.2 Superimposition of elastic and non-elastic compression bandages

Co-authored with Clothilde Helouin-Desenne, Jérôme Molimard, Reynald Convert, Pierre Badel and Pascal Giraux, from [Chassagne c]

6.2.1 Introduction

Compression therapy remains the cornerstone of severe venous pathologies such as ulcers [Association 03]. This treatment, whose efficacy is admitted [Amsler 09] [Lattimer 14] [Agu 99], can be performed thanks to stockings or bandages. Bandages are preferred at the early stages of the treatment [Allaert 15] and/or for the most severe pathologies. Compression bandages can be differentiated, being either *short-stretch* or *long-stretch* [Partsch 08], with regards to their maximal stretch. Another terminology classifies the bandages with regards to their elastic properties, being either *elastic* or *non-elastic*. The difference in mechanical properties will lead to different behaviours once applied on the leg. Elastic bandages result in lower pressure variation from supine to standing position (and also between resting and working pressure) as they can more easily accommodate the change in leg morphology [Dissemond 16]. On the other hand, the pressure increase induced by non-elastic bandages is much higher. From a clinical point of view this differentiation is possible thanks to the *Static Stiffness Index* (*SSI*), which is the pressure increase, at measurement point B1 (Figure 6.1 - A), from supine to standing position [Partsch 05b]. This index helps to characterize the behaviour of multi-component bandages combining elastic and non-elastic bandages. The superimposition of compression bandages is very common in clinical practice [Hafner 00a] and showed a positive impact on ulcer healing [Nelson 12] [Milic 10]. Multi-layer bandages are often composed of a padding layer (to homogenize the leg geometry), one to two compression layers and possibly a fixation layer (cohesive bandage). Even though the most representative illustration of multi-layer bandages is the so-called 4-layer bandage [Moffatt 02], a large diversity of multi-layer bandages is commercially available [Hanna 08] [Wong 12a].
Interface pressure is one of the key parameters of compression treatment. Pressure generated by one single bandage was extensively investigated. The impact of several parameters such as fabric materials [Danielsen 98b] [Rimaud 14] [Hirai 98], application technique [Coull 06] [Benigni 08] or body positions [Lee 06] was assessed. However, whether there is a direct relationship between the pressure applied by a single bandage and the one applied by the superimposition of bandages remains an open question.
The pressure applied by two-layer bandages composed of short-stretch and long-stretch bandages as well as their *stiffness* (i.e. the pressure increase per 1 centimeter increase in leg circumference [Prestandard 01]) was investigated *in vitro* [Hirai 11a]. This pressure applied by superimposed bandages was then compared with the pressure applied by each component separately. Furthermore, *in vivo* interface pressure measurements were performed to evaluate the *stiffness* of commercially available multi-component bandages [Mosti 07]. It was also observed that superimposing bandages led to an increase in *Static stiffness Index* even with elastic bandages [Mosti 08b]. However, a study performed with the 4-layer bandage, showed that the pressure resulting from the superimposition of bandages was not the sum of the pressure applied by each single bandages [Dale 04].
Consequently, the objective of this study was to investigate the pressure applied by the superimposition of elastic and/or non-elastic compression bandages. These pressures were compared to the pressures applied by each single bandage with the aim to evaluate the possible linear correlation between the pressure applied by single and multi-component bandages. The impact of the order of bandage application was also addressed. Interface pressure measurements were

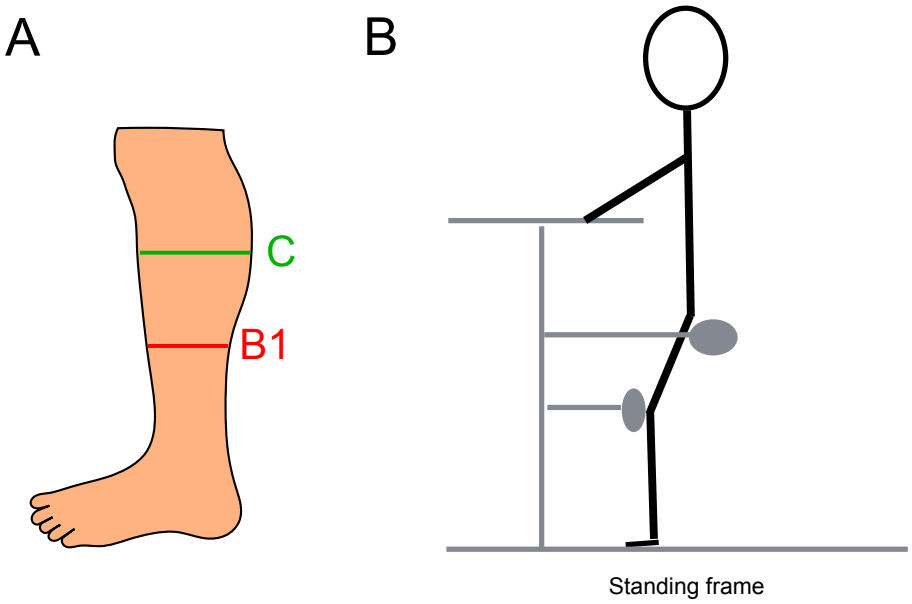

Figure 6.1: A - Location of measurement points B1 and C; B - Patient's position in the standing frame

performed in 3 positions to assess the pressure variation and the *Static Stiffness Index* of the bandages.

6.2.2 Methods

This protocol was approved by the local *Ethical Committee* (CPP Sud-Est I - 2015-34) (NCT 02803398).

6.2.2.1 Population

26 patients (16 women - 10 men; mean age = 48 [19 - 72]) were included in the study, but one left after the first visit for medical reasons unrelated to this study. These patients were at risk of venous thrombosis and were treated with compression therapy (stockings or bandages). This risk was the consequence of walking impairment or very limited walking distance induced by a central or peripheral motor deficiency. They were hospitalized in the Physical Medicine and Rehabilitation Department of the University Hospital of Saint-Etienne, France. To take part in the study, they had to be able to stand for at least 10 min in a standing frame (Figure 6.1 - B). Patients with venous thrombosis history or with any contraindication to compression therapy were not included in the study. Among the 26 patients included in the study, 13 suffered from post-stroke hemiplegia (partial or complete), 3 suffered from paraplegia (consecutive to a trauma (2) or a surgery (1)) and 2 had a cerebellar stroke. The 8 remaining patients were treated for motor deficiency or impaired balance resulting from various pathologies.

6.2.2.2 Bandages

The pressure applied by two different bandages was investigated in the study: Biflex® 16 (Thuasne) and Rosidal® K (L & R). Both were 10-cm wide bandages but differed in their mechanical properties. Biflex® 16 (B16) is an elastic and long-stretch bandage composed of

elastic yarns, whereas Rosidal® K (RK) is a non-elastic and short-stretch bandage only composed of cotton yarns (thus non-elastic yarns). The pressure applied by the different possible combinations of these two bandages was measured, even though these bandages were never associated in regular practice. This resulted in six possible combinations:

- B16: a single Biflex® 16 bandage,
- RK: a single Rosidal® K bandage,
- B16+B16: a Biflex® 16 was applied on top of another Biflex® 16,
- RK+RK: a Rosidal® K was applied on top of another Rosidal® K,
- B16+RK: a Rosidal® K was applied on top of a Biflex® 16,
- RK+B16: a Biflex® 16 was applied on top of a Rosidal® K.

All bandages were applied in a spiral pattern with a 50% overlapping technique (i.e. a 2-layer bandaging technique) by a single experienced operator. Biflex® 16 was applied on the lower limb with a target stretch equal to 1.3 (Equation 6.1) and Rosidal® K with a maximum stretch, following their manufacturers' recommendations.

$$stretch = \frac{actual\ bandage\ length\ (L)}{initial\ bandage\ length\ (L_0)} \tag{6.1}$$

Following the methodology described in a previous study [Chassagne 15], the stretch of the applied bandage was then measured thanks to marks drawn every 10-cm on the non-stretched bandage. The six bandages were applied on the leg in a randomized order.

6.2.2.3 Interface pressure measurements

Interface pressure measurements were performed at 4 measurement points: 2 at the height of measurement point B1 (where the Achilles tendon turns into the gastrocnemius muscle [Partsch 06]) on the medial and lateral side of the leg and 2 at the height of measurement point C (at the calf largest circumference [Partsch 06]) (Figure 6.1 - A). Four probes were kept in place during the 6 bandage applications. The pressure was measured thanks to the sensor Picopress®(MicroLab Elettronica, Ponte S. Nicolo, Italy), which was used in several previous studies [Lattimer 14] [Rimaud 14] [Damstra 13].

6.2.2.4 Interface pressure measurements protocol

Pressure measurements were performed on both legs. The first leg on which bandages were applied was randomly selected for each patient. The order in which the six bandages were applied was also randomized and was the same for both patient's legs. All randomizations were performed with the software Matlab®.
The protocol was divided into three visits. The time between 2 visits could not exceed 5 days. Informed consents were signed by the patients before their inclusion.
1st visit
This visit consisted in the inclusion visit.
2nd and 3rd visits
These two visits, which consisted in interface pressure measurements, were identical: the 2nd visit was performed on the first leg and the 3rd visit on the second leg.
First the patient lied on an examination bed and 4 sensors were taped on her/his leg. Then the first bandage (selected from the randomization) was applied on the leg. The bandage stretch

was measured around measurement points B1 and C after each bandage application and for both bandages in the case of multi-component bandages. Pressure measurement was taken one minute after bandage application. Then the patient sat on the edge of the bed, her/his feet on the ground with a 90 ° angle between the thigh and the lower leg. Pressure was measured one minute later. Eventually, the patient stood in a standing frame (Figure 6.1 - B) and the last pressure measurement was taken after waiting for one minute. This waiting time was chosen in order to reach a stationary state of leg venous system [Meissner 07]. Eventually the patient lied on the examination bed and the same protocol was repeated for the 5 remaining bandages.

6.2.2.5 Statistical analysis

144 pressure values were measured for each patient, hence a total of 3600 pressure values (105 missing values). Bar graphs represent the mean value and 95% confidence interval. The normality of the distribution was tested with the Shapiro-Wilk test. Most of the comparison tests were paired tests. For only two groups, the comparison was performed with the non-parametric Wilcoxon test (or the paired T test with regards to the data distribution) and for more than two groups, with the Friedman test. The Nemenyi post-hoc test was used to test the multiple paired comparisons.
The coefficient of determination R^2 was computed as an evaluation of the linear correlation between two samples (the experimental data and the one given by the linear regression for example).
The statistical analysis was performed thanks to XLSTAT and Matlab®.

6.2.3 Results

6.2.3.1 Interface pressure measurements

Stretch of the applied bandage was measured in the area of measurement point B1 and C for all bandage applications. Mean stretches, measured at both areas and for all bandages combinations, were equal to 1.347 ± 0.005 for the RK and 1.294 ± 0.005 for the B16 (whose target stretch was 1.3) (Figure 6.2). Stretch was higher at measurement point C than at B1.
Pressures applied by the B16 and the RK at measurement point B1 (medial) in supine position were found to be very similar, respectively 25.69 ± 1.16 and 25.94 ± 1.13 mmHg (Figure 6.3). Two-component bandages resulted in much higher pressures: 49.64 ± 1.94 mmHg for 2B16, 47.98 ± 2.24 mmHg for 2RK. The superimposition of two different bandages applied significantly different pressures depending on the order of bandages application ($p < 0.05$): 52.38 ± 2.34 mmHg for a RK applied on top of a B16 (B16+RK) and 48.10 ± 1.59 mmHg for a B16 applied on top of a RK (RK + B16).

6.2.3.2 SSI

Pressure was measured in three positions, supine then sitting and eventually standing, in a very short time (about 5 minutes). For all bandages, pressure increased from supine to sitting position and then to sitting to standing position (Figure 6.4 - A). The pressure increase at measurement point B1 (medial) from supine to standing position is the so called *Static Stiffness Index* (*SSI*), which helps to characterize the mechanical properties of the whole bandage [Partsch 05b].

The minimum *SSI* was observed for a single elastic bandage (4.18 ± 0.75 mmHg) (Figure 6.4 - B). However, the superimposition of two of these bandages resulted in an increased SSI

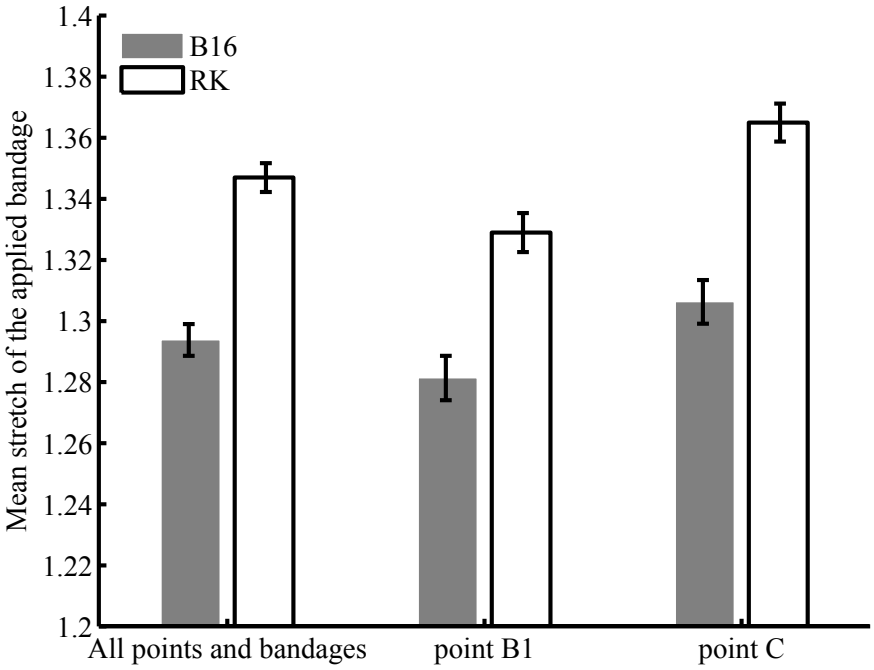

Figure 6.2: Stretch of the applied bandages; for all measurement points and bandages; at measurement point B1; at measurement point C;

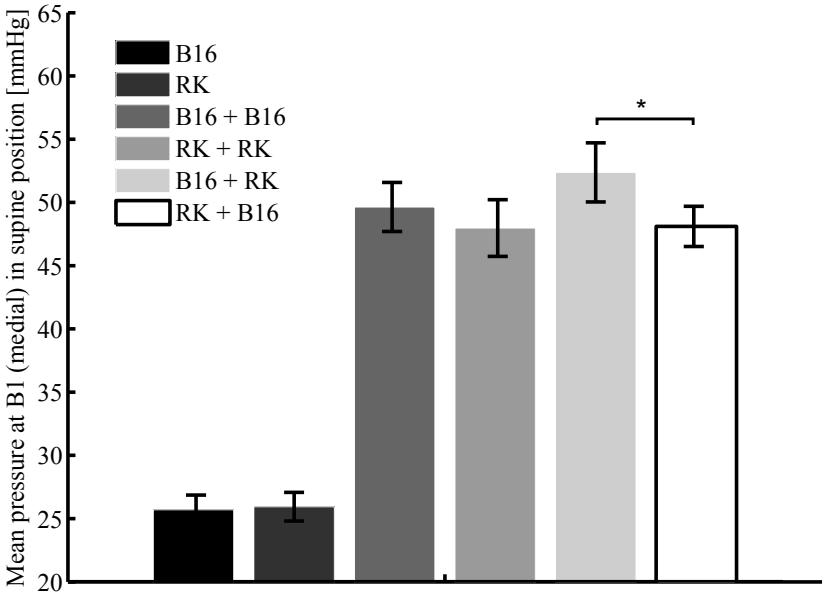

Figure 6.3: Mean pressure applied by the 6 different bandages at measurement point B1 (medial) in supine position; * states for significant difference

(6.48 $\pm$ 0.82 mmHg). The maximum *SSI* was obtained for the superimposition of two non-elastic bandages (13.60 ± 2.29 mmHg). As expected, a single non-elastic bandage showed a high *SSI* (7.35 ± 1.55 mmHg). Eventually the two combinations of elastic and non-elastic bandages

have similar SSI: 9.54 ± 1.32 mmHg for B16 + RK and 9.98 ± 1.48 mmHg for RK + B16.
Interface pressure was measured at 4 points on the leg: at the height of measurement point B1 and C on the medial and lateral side of the leg (B1 med, B1 lat, C med and C lat). In supine position, all bandages were found to be degressive (i.e. the pressure applied at measurement point B1 (medial) was higher than at point C (medial)), except the RK (Figure 6.5 - A). For most bandages, pressures on the lateral side of the leg were lower than on the medial side.
The highest interface pressure was always measured at B1 on the medial side of the leg (Figure 6.5 - A, B, C). This measurement point also showed the largest pressure increase from supine to standing position (Figure 6.5 - D): 8.52 ± 0.68 mmHg for B1 medial, 5.43 ± 0.65 mmHg for B1 lateral, 6.42 ± 0.65 mmHg for C medial and 3.63 ± 0.57 mmHg for C lateral.

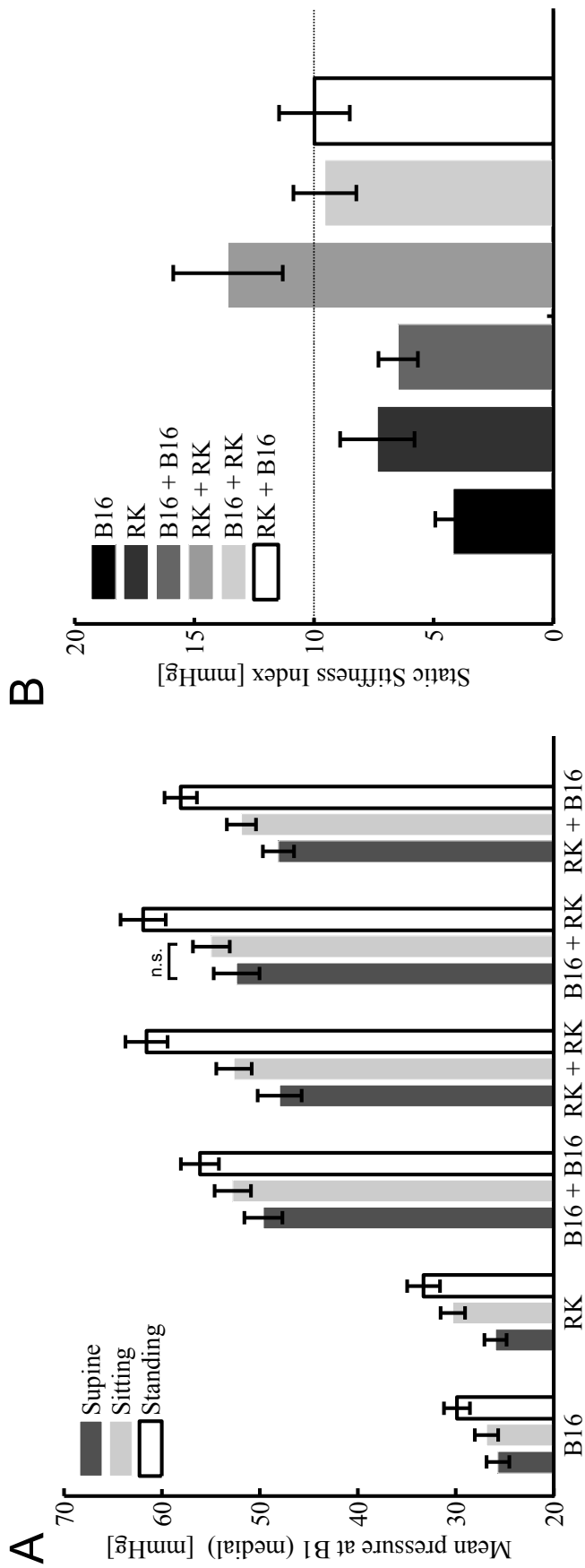

Figure 6.4: A - Mean pressures applied by the 6 bandages at measurement point B1 (medial) in supine, sitting and standing positions; n.s. states for non-significant difference; B - Static Stiffness Index for the 6 bandages

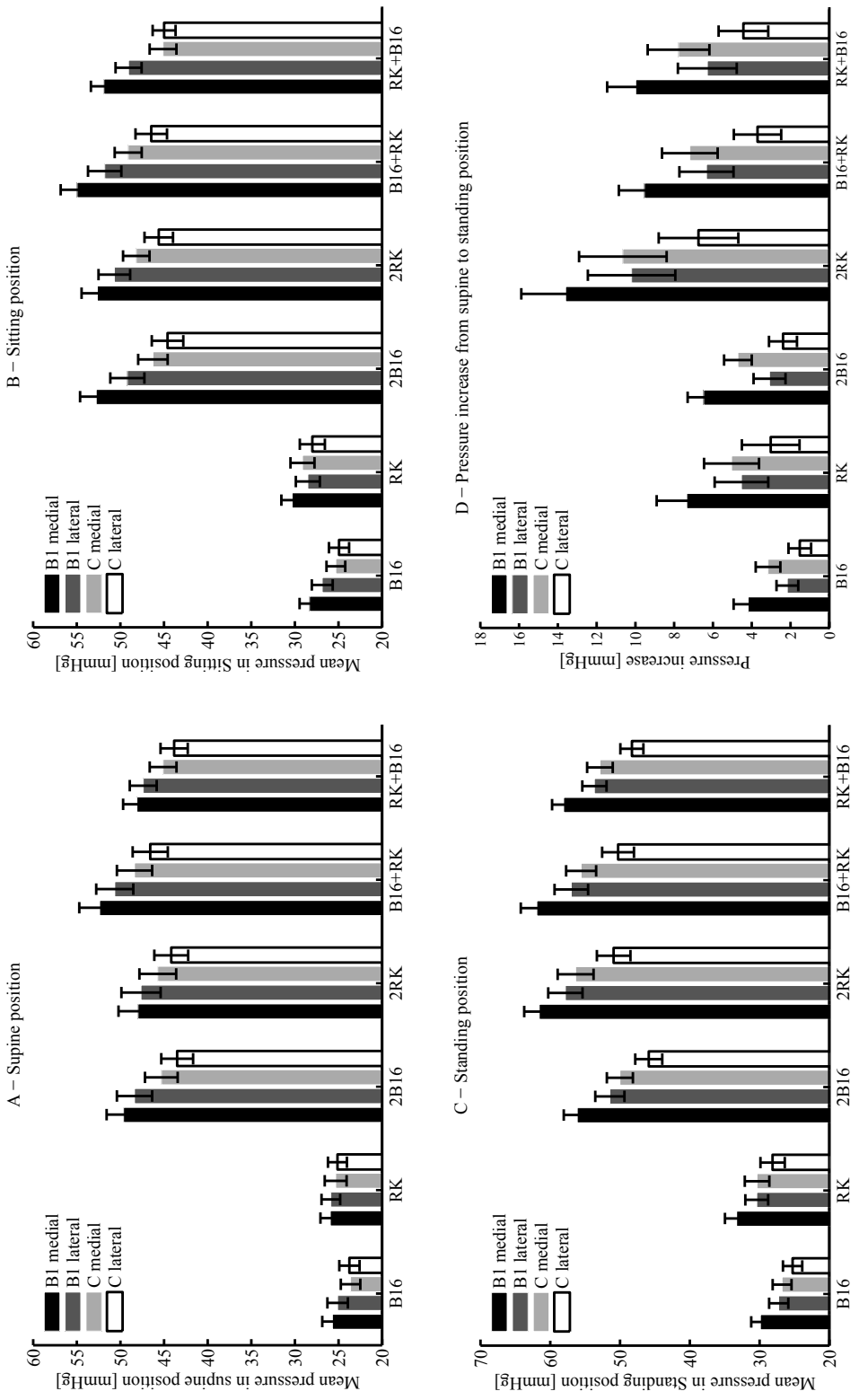

Figure 6.5: Mean pressure for the four measurement points and the six bandages in the three positions, supine (A), sitting (B) and standing (C); Pressure increase from supine to standing position for the six bandages and the four measurement points (D)

6.2.3.3 Pressure applied by a 2-component bandage with regards to the one applied by each component

Interface pressure applied by the 6 possible combinations of elastic and non-elastic bandages was measured within the aim to better understand the superimposition of compression bandages. The assumption was made that the pressure applied by the superimposition of two bandages would be a linear combination of the pressure applied by both single bandages (with a constant term set to 0).
First, the ratio between the pressure applied by the superimposition of two identical bandages and the pressure applied by a single bandage was computed (for all measurement points, in supine position). This ratio was equal to 1.89 for the B16 and 1.80 for the RK (Equation 6.2 (a) and (b)). However, the coefficient of determination R^2 was very low for the RK. Then the pressure applied by the combination of two different bandages was computed as a linear combination of the pressure applied by both single bandages. By comparing the two equations (Equation 6.2 (c) and (d)), it can be noticed that the order of bandage application tends to impact interface pressure, despite the low coefficient of determination.

$$\begin{aligned}
&P_{2B16} = 1.89\ P_{B16} && (R^2 = 0.48,\ p < 0.001)\ (a)\\
&P_{2RK} = 1.88\ P_{RK} && (R^2 = 0.06,\ p < 0.001)\ (b)\\
&P_{B16+RK} = 1.31\ P_{B16} + 0.67\ P_{RK} && (R^2 = 0.37,\ p < 0.001)\ (c)\\
&P_{RK+B16} = 0.91\ P_{RK} + 0.92\ P_{B16} && (R^2 = 0.10,\ p < 0.001)\ (d)
\end{aligned} \tag{6.2}$$

Equation 6.2: Pressure applied by multi-component bandages as a linear combination of the pressure applied by a single component bandage; P_{B16} and P_{RK} are the pressures applied by a single B16 and RK, P_{2B16} and P_{2RK} are the pressures applied by the superimposition of two B16 and two RK, P_{B16+RK} was the pressure applied by a RK over a B16 and P_{RK+B16} was the pressure applied by a B16 over a RK

6.2.4 Discussion

Interface pressure applied by 6 different single or multi component bandages was measured at 4 measurement points on the leg and in 3 positions. These 6 bandages, whose SSI was evaluated, resulted from the combination of one elastic (B16) and one inelastic (RK) bandage. The pressure varied with the bandage components but also with the order in which the components were applied on the leg. Eventually, the pressure applied by the 4 multi-component bandages was computed as a linear combination of the pressure applied by the two single component bandages.

6.2.4.1 Interface pressure measurements

The design of this study was very close to an *in vitro* study by Hirai *et al.* [Hirai 11a]. The pressure and the *stiffness* (i.e. the pressure increase for a 1 cm leg circumference increase) of different combinations of short and long stretch bandage were measured, as well as the pressure applied by the single bandages. The two single bandages (short-stretch and long-stretch) applied very similar pressure levels (about 30 mmHg) but had very different *stiffnesses*: 4 mmHg for the long-stretch bandage and 17 mmHg for the short-stretch bandage.
However, their observations contradicted the present study. Indeed, for the range of pressure measured in the present study (about 50 mmHg), Hirai *et al.* observed no significant impact

of the order of bandage application on *in vitro* interface pressure and *stiffness*. In the present study, B16 + RK exerted a higher pressure than RK + B16, even though the pressure applied by B16 and RK were similar. Nonetheless the *SSI* of these two bandages were equal, which was in agreement with the *in vitro* study of Hirai *et al.*.

This *SSI* is an usual tool for the classification of compression bandages [Partsch 08]. The *SSI* of inelastic bandages is usually higher than 10 mmHg and the one of elastic bandages is lower. However, it was found here that the *SSI* of RK, which is a non-elastic bandage, was lower than 10 mmHg. This was previously observed for a low-pressure bandaging technique [Partsch 05c]. According to this classification, in the present study, all multi-component bandages composed of at least one non-elastic bandage are inelastic bandages. This result corroborated the fact that adding at least one non-elastic component to the bandage has a pronounced effect on *SSI* [Hafner 00a] [Hirai 11a]. However, the superimposition of bandages (either elastic or non-elastic) increased the *SSI*, which led to think that bandage-to-bandage friction can play a role in the *SSI*. Indeed, by superimposing bandages, the bandage-to-bandage contact surface is highly increased. In standing position, the increase in leg volume is limited by the mechanical resistance of the bandage but also by the friction between the different layers.

Bandage degressivity was assessed thanks to interface pressure at 4 different measurement points (points B1 and C on the medial and lateral side of the leg). All bandages were found to be significantly degressive except the RK. This can be explained by the fact that stretch was higher at measurement point C than at point B1 (Figure 6.2). As a consequence, as it can be noticed in Figure 6.6, this stretch increase (in green in Figure 6.6) led to a larger tension increase for the RK than for the B16, respectively 48.3 % and 9.0 % of the tension for the mean stretch (in black in Figure 6.6). This larger tension increase may compensate the increase in circumference from measurement point B1 to C, hence the fact that the bandage was not degressive. Nonetheless, all the trends observed here about the bandage stretch cannot be generalized, as they are the results of only one bandager.

Eventually, measuring the pressure at two heights on the leg and on the medial and lateral sides of the leg showed that the maximum pressure increase from supine to standing position was observed at measurement point B1 which confirmed the relevance of the use of this point for the characterization of the stiffness of the bandage [Partsch 05c]. Also, pressures measured on the medial side of the leg were higher than those measured on the lateral side. This can easily be explained by the anatomy of the leg: the radii of curvature are lower on the medial than on the lateral side.

6.2.4.2 Pressure applied by a 2 component bandage with regards to the one applied by each component

The pressure applied by two-component bandages was computed as a linear combination of the one applied by each single component. However, except for the superimposition of two elastic compression bandages, this linear model did not properly fit the experimental data. Moreover, it could have been expected that the pressure applied by a two-component bandage would be the sum of the pressures applied by each single component bandage. A possible explanation could be the thickness of the bandage [Al Khaburi 11b]. Moreover, the second bandage was applied on a deformed leg shape induced by the application of the first bandage.
For the computation of the pressure applied by two-component bandages, setting the constant term to 0 for the linear model might be a too strong hypothesis. Also, the low correlation between the pressure applied by a two-component bandage, composed of at least one non-

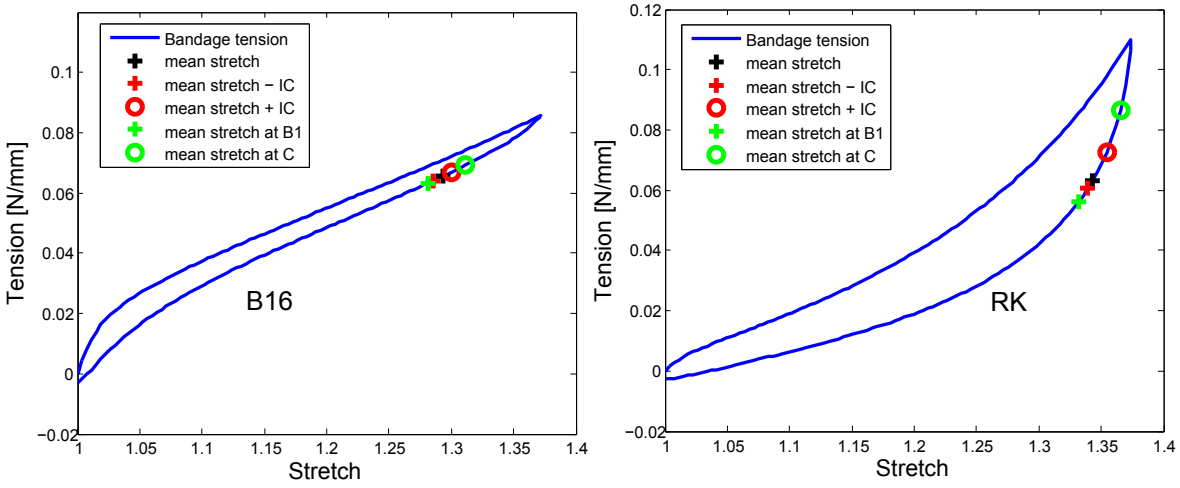

Figure 6.6: Tension as a function of the stretch for both bandages B16 and RK

elastic bandage, and the one applied by a single component bandage might be due to the mechanical properties of the fabrics. As it can be observed in Figure 6.6, the stretch variation in between the confidence interval (in red in Figure 6.6) induced a much larger tension variation for the non-elastic bandage (about 19% of the mean value) than for the elastic bandage (about 4% of the mean value).

6.2.4.3 Limitations

The pressure measurements were taken in a very short time after bandage application. However pressure tends to vary over time [Wong 12b], because the bandage slides down on the leg and because of fabric relaxation [Kumar 13b] (loss of tension over time). Relaxation tests (performed in our laboratory, results not shown here) showed that after 10 minutes, the B16 lost about 7% of its nominal tension whereas the RK lost about 22%. It could be interesting to perform these measurements within a longer period of time to reach a stationary state for bandage materials, although it would hardly be sustainable for the patients. Moreover, these measurements were static measurements. Even though pressure was measured in three positions, this study did not investigate the working pressure of these bandages (i.e. the interface pressure applied while walking).
The two bandages were chosen as representative bandages of elastic and non-elastic bandages, even though they are not routinely combined in usual clinical practice. Thereby measurements of pressure applied by other commercially available multi-component bandages would be of high interest.

6.2.5 Conclusion

This study consisted in static interface pressure measurements applied by 6 different bandages, all composed of elastic and/or non-elastic bandages. First, it was observed that the components of the bandage but also the order in which they are applied on the leg significantly impact interface pressure. Second, the very low correlation between the pressure applied by multi-component bandages and the one applied by the single-component highlighted the poor understanding of the mechanisms involved in bandages superimposition. Further mechanical studies would be needed to better understand the pressure generation resulting from such superimposition.

Following a similar protocol, it would be clinically relevant to characterize the performance of commercially available multi-component bandages, and also to investigate their dynamic behaviour, while walking for instance.

6.3 Investigation of the impact of calf soft tissue mechanical properties on the variation of interface pressure applied by compression bandages in different body positions

Co-authored with Clothilde Helouin-Desenne, Jérôme Molimard, Reynald Convert, Pierre Badel and Pascal Giraux, from [Chassagne b]

6.3.1 Introduction

Interface pressure is one of the key aspects of compression bandages therapy [Partsch 14]. This pressure depends on the bandages mechanical properties [Partsch 08], but also on the patient morphology [Chassagne 15] and her/his body position [Partsch 05c]. Bandages can be differentiated with regards to the interface pressure variation from supine to standing position, the so-called Static Stiffness Index [Partsch 05b]. From supine to standing position, calf muscles and blood tend to fall down, but also, muscles contract to stabilize the standing position [Loram 04]. Consequently, the leg geometry is modified, as well as the calf soft tissue mechanical properties. Moreover, a previous numerical study showed the role of soft tissues deformation induced by bandage application in pressure generation [Chassagne 16]. This result questions the influence of soft tissue mechanical properties on interface pressure.
Therefore this study aimed to investigate the possible impact of calf soft tissue mechanical properties on interface pressure. Calf soft tissue mechanical properties of both legs of 24 patients were characterized in sitting and standing position. In addition, pressure applied by six different bandages was measured in supine, sitting and standing position. The correlation between the variation of soft tissue mechanical properties and interface pressure was then investigated.

6.3.2 Methods

This protocol was approved by the local *Ethical Committee* (CPP Sud-Est I - 2015-34) (NCT 02803398).

6.3.2.1 Characterization of the lower leg soft tissue mechanical properties

The leg geometry of the patients in sitting and standing position (in a standing frame (Figure 6.7)) was obtained with a 3D optical scanner (Artec^{tm} MHT 3D scanner, Artec^{tm} Group). This 3D scan was combined with the compression of the lower leg soft tissues (Figure 6.7 - C), on the posterior side of the leg, within the aim to characterize the mechanical properties of these soft tissues. The methodology used for the identification of material properties was adapted from a previous study [Frauziols 16].

6.3.2.2 Interface pressure measurements

After the compression test of the calf soft tissues, interface pressure applied by six different bandages was measured for both patients' legs thanks to the pressure sensor Picopress®(MicroLab Elettronica, Ponte S. Nicolo, Italy). These bandages, composed of elastic (Biflex® 16, Thuasne) and/or inelastic (Rosidal® K, L & R) bandages, were applied on the patients' legs, following a previously described protocol [Chassagne c]. The pressure they applied was measured at 4 measurement points (B1 and C [Partsch 06] on the medial and lateral side of the leg) and in 3 positions: supine, sitting and standing.

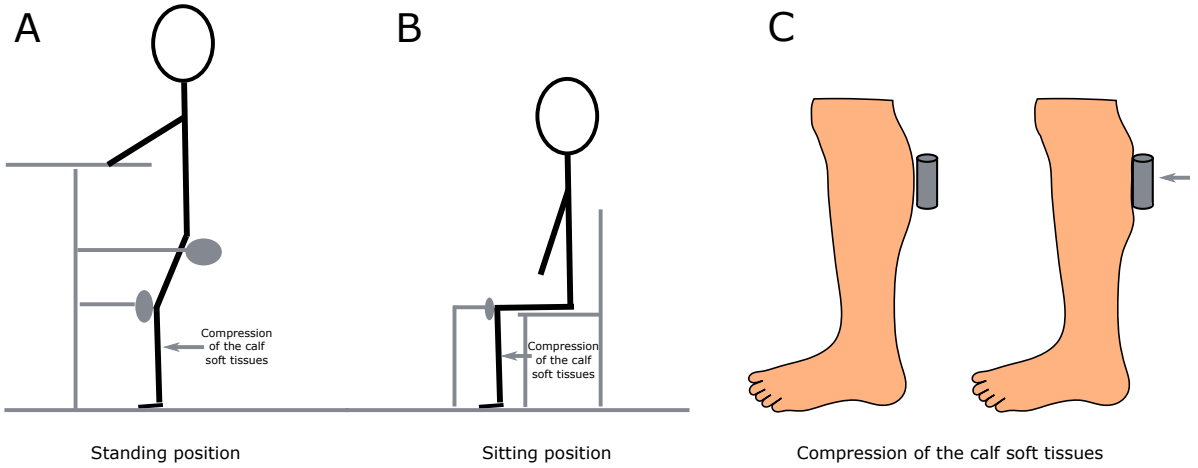

Figure 6.7: Patient's position for the compression test of the calf soft tissue and pressure measurements: A - in a standing frame, B - sitting; C - Illustration of the compression test of soft tissues

6.3.2.3 Statistical analysis

The normality of the distribution of soft tissues mechanical properties was tested with the Shapiro-Wilk test. The significance of the difference in soft tissue mechanical properties, but also interface pressure, between sitting and standing position was then tested thanks to the Wilcoxon paired-test.
The correlation between the variation of interface pressure and calf soft tissue mechanical properties was evaluated thanks to Pearson's correlation coefficient.

6.3.3 Results

Calf soft tissue mechanical properties were identified for both legs of each patient in sitting and standing positions, thanks to an inverse identification method [Frauziols 16] and are presented in Table 6.1. The elastic modulus (E), which represents the global stiffness of calf soft tissues, was computed from the Neo-Hookean constitutive parameters c_{10} given by the identification (approximation for small strain, Equation 2.13, page 29).
The elastic modulus (E) significantly increased from sitting to standing position, respectively 10.4 kPa [6.1; 18.5] and 18.0 kPa [8.4; 52.1]. The compression test was followed by pressure measurements applied by 6 different bandages in supine, sitting and standing positions. Interface pressure significantly increased from sitting to standing position ($p<0.0001$) (Figure 6.8 - A). This pressure variation from sitting to standing position was plotted as a function of the variation of calf soft tissue elastic modulus in Figure 6.8 - B. However, no significant correlation was found between the variation in soft tissue mechanical properties and the pressure variation between sitting and standing positions (for the 6 bandages: $max(R^2) = 0.071, p = 0.09$).

6.3.4 Discussion and conclusion

The mechanical properties of the leg soft tissues were characterized in sitting and standing positions for both legs of 24 patients and were combined with interface pressure measurement applied by 6 compression bandages. It was hypothesized that the pressure increase from supine to standing position was the consequence of two phenomena: a change in leg geometry (muscles and blood falling down) and a change in the muscle mechanical properties induced by muscle

	E [kPa]			
# patient	Right leg - Sitting position	Left leg - Sitting position	Right leg - Standing position	Left leg - Standing position
1	8.0	6.7	15.2	13.4
2	8.2	12.0	11.9	8.8
3	10.2	11.8	20.4	13.9
4	7.9	6.8	9.6	10.3
5	7.4	6.7		8.4
6	7.0	10.4	28.4	20.7
7	12.6	8.8	15.2	15.8
8	6.1	9.1	9.8	9.1
9	11.2	12.6	10.5	11.9
10	16.7	13.1	13.4	31.9
11	11.6	9.9	10.2	12.3
12	7.6	8.6	15.5	17.5
13	18.5	16.1	52.1	45.4
14	9.7	9.1	16.1	35.2
15	7.3	9.7	9.7	13.2
16	6.5	6.4	14.3	15.0
17	13.4	12.5	19.9	14.0
18	7.4	10.3	10.9	19.4
19	8.5	15.1		8.8
20	13.1	12.8	26.2	32.8
21	8.3	8.9	14.4	12.1
22	14.6	15.9	23.8	20.9
23	9.5	10.9	23.5	
24	10.0	8.9	26.0	15.7

Table 6.1: Calf soft tissue mechanical properties identified for 24 patients - E is the elastic modulus

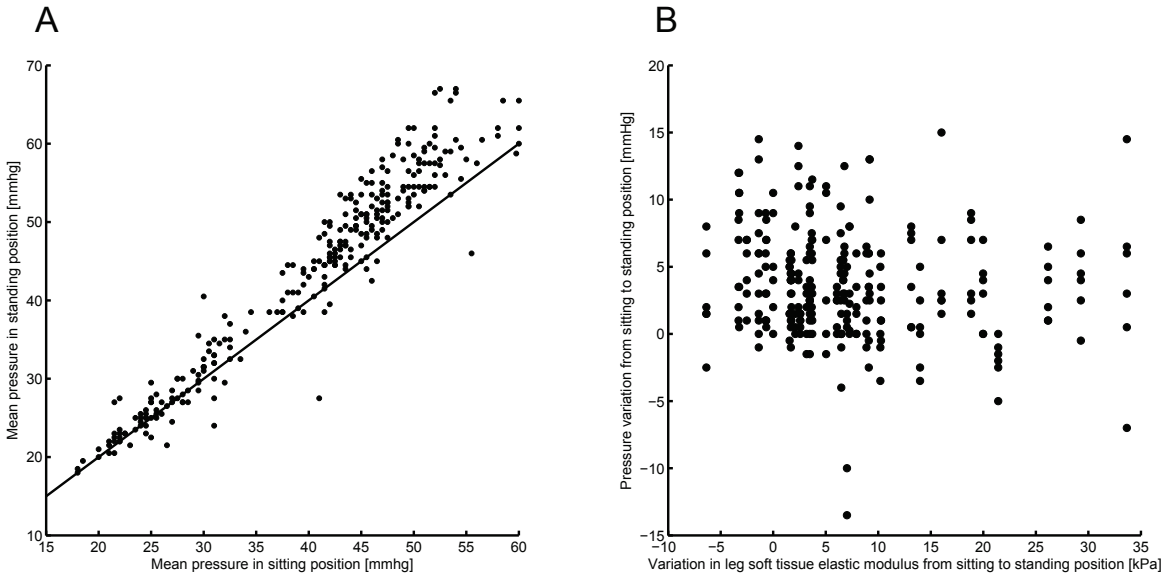

Figure 6.8: A - Mean pressure in standing position as a function of the mean pressure in sitting position; B - Interface pressure variation from sitting to standing position as a function of the variation in leg soft tissue elastic modulus from sitting to standing position

contraction. A significant change in mechanical properties from sitting to standing was observed but was not correlated to pressure variation. Consequently, it is likely that this pressure variation is mostly due to the geometrical changes of the leg (volume for instance). However, even though soft tissue mechanical properties do not seem to impact interface pressure, they may impact its transmission though soft tissues to the veins [Rohan 15].

Chapter 7

Conclusion Générale - *Conclusion*

Synthèse

La pression exercée par une bande de compression résulte de phénomènes complexes et encore mal compris. Cette étude, mêlant approche expérimentale et simulation éléments-finis, avait pour but de mieux comprendre les mécanismes impliqués dans la génération de pression.

D'abord, deux études préliminaires, expérimentale et numérique, ont permis de montrer les limites de l'utilisation de la loi de Laplace. L'étude expérimentale a montré que la pression n'était pas directement proportionnelle à la tension de la bande et a soulevé des interrogations concernant l'éventuel impact des interactions entre les différentes couches de bande (frottement bande-bande). L'étude numérique, quant à elle, a souligné l'impact des déformations de la jambe induites par l'application d'une bande sur la pression d'interface.

Ces deux études préliminaires ont mené vers le développement de deux méthodes de caractérisation : la première pour l'identification des propriétés mécaniques des tissus mous de la jambe et la deuxième pour la mesure du coefficient de frottement bande-bande.

Une nouvelle simulation éléments finis de l'application d'une bande, avec une cinématique d'enroulement plus réaliste, a été développée. Cette simulation, couplée à la paramétrisation géométrique de la jambe, a permis de concevoir une nouvelle méthode pour prédire, de manière personnalisée, les pressions exercées par une bande de compression. Les valeurs de pression obtenues avec cette méthodologie pour 66 jambes étaient en accord avec les résultats expérimentaux.

La suite de l'étude s'intéresse à la pression exercée par la superposition de deux bandes (méthode courante en pratique clinique). Cette étude clinique a permis de montrer l'influence de l'ordre dans lequel étaient appliquées les bandes sur la pression d'interface. L'étude avait pour but de faire le lien entre la pression exercée par la superposition de deux bandes et celle exercée par chacune des bandes appliquées séparément. Cependant, les faibles corrélations observées entre ces pressions montrent que d'autres études mécaniques seront nécessaires pour comprendre les mécanismes mis en jeu dans cette superposition.

Finalement, la méthode de caractérisation des propriétés mécaniques des tissus mous de la jambe a été mise en œuvre pour 24 sujets de l'étude clinique. Les propriétés mécaniques des tissus mous des deux jambes des patients ont été identifiées en position assise et debout. Cette

caractérisation a été couplée aux mesures de pression d'interface. Cela a permis de montrer qu'il n'y avait pas de corrélation entre la variation de propriétés mécaniques des tissus mous de la position assise à debout (dues à la contraction des muscles pour maintenir la position debout) et la variation de pression correspondante. Ce résultat tend à conclure que la variation de pression entre ces positions est uniquement due à la variation de volume de la jambe (effet de la gravité sur les muscles et afflux sanguin).

Limites

Un des premiers choix de cette étude fut de se limiter à l'étude des pressions de manière statique. Même si les pressions ont été mesurées dans différentes positions, cela était réalisé de manière statique et dans un temps très court. Les pressions à long terme (rendant compte de la relaxation des bandes, du glissement de la bande sur la jambe ou de la réduction de l'œdème) ou lors de la marche n'ont pas été étudiées.

De même, la modélisation éléments-finis est quasi-statique. Toutefois, une des principales limites de cette modélisation est de considérer les tissus mous comme un seul et même matériau, sans différencier la peau, les tissus adipeux et les différents groupes musculaires. Le fait de ne travailler que sur le scan optique des jambes, c'est à dire leur surface externe, est très simple d'un point de vue expérimental. Cependant, nombre d'informations anatomiques sont manquantes, comme la forme et la position des os. Bien qu'une étude numérique ait montré qu'une variation sur la forme ou la position des os n'avait que très peu d'influence sur la pression d'interface, cela représente une limite de la modélisation. En plus de la simulation, cette problématique est aussi présente pour la méthodologie d'identification inverse des propriétés mécaniques des tissus mous de la jambe.
Cette simulation assez simplifiée de la jambe résulte de la décision de se concentrer, dans un premier temps, sur la cinématique de l'application de la bande, déjà complexe (conditions limites et contact) et de n'observer que les pressions d'interface.

La simulation numérique de l'application d'une bande permet d'obtenir la distribution complète des pressions sur la jambe. Or pour l'instant, le modèle réduit développé dans cette étude ne considère que la pression au niveau du point B1. Il serait donc pertinent d'utiliser cette distribution complète dans un autre modèle. L'intérêt, en plus de l'effet thérapeutique, serait de pouvoir prédire les zones de surpression et donc d'inconfort, ce qui pourrait permettre d'anticiper les défauts d'observance du traitement.

Il a été observé que le capteur utilisé pour les mesures de pression modifiait localement la pression. Une méthode, basée sur une étude numérique, a été proposée pour corriger cette erreur. Cette modification locale ne représente pas un problème majeur pour les études expérimentales, mais devient plus problématique lors de la comparaison entre les valeurs données par la simulation, où le capteur n'est pas simulé, et les mesures expérimentales. D'autres études approfondies seraient donc nécessaires afin de mieux évaluer la modification locale de pression induite par la présence de ce capteur.

Expérimentalement, une des limites de cette étude, mais plus généralement de l'application des bandes, réside dans la reproductibilité de la pose. En mesurant l'allongement des bandes une fois appliquées sur la jambe, la variabilité de la pose a été évaluée. Cependant, cela ne permet pas de mieux contrôler la pose. En plus de la faible reproductibilité, une hétérogénéité de l'allongement des bandes sur la jambe a été observée. Or, pour la simulation, la bande est

appliquée avec un allongement théorique constant sur la jambe. Une des améliorations serait donc de pouvoir faire varier, dans la simulation, l'allongement de la bande pour pouvoir se rapprocher de la réalité.

Perspectives

D'un point de vue numérique, une évolution nécessaire est le développement d'un modèle de jambe plus complet. Ce modèle différencierait la peau, les tissus adipeux, les différents groupes musculaires et les vaisseaux sanguins. Il permettrait de rendre compte, de manière plus réaliste, de la déformation de la jambe lors de l'application d'une bande, mais surtout, il permettrait d'évaluer l'effet de la compression sur les vaisseaux.
Mieux comprendre quel est le niveau de pression exercé sur la peau est un premier pas, mais afin de bien comprendre l'effet thérapeutique d'un tel traitement, il est essentiel de comprendre comment cette pression d'interface est transmise aux vaisseaux.
Cela peut se faire numériquement, par le développement d'un modèle 3D complexe ou expérimentalement, en évaluant le flux sanguin avant et pendant le port de la compression (Doppler). Cela pourrait être couplé avec l'identification des propriétés mécaniques des tissus mous, car il a été montré que ces propriétés impactaient la transmission de la pression d'interface vers les vaisseaux sanguins [Rohan 15].

Un outil pour cette nouvelle modélisation pourrait être la paramétrisation géométrique. Celle mise en œuvre pour cette étude reste limitée car elle ne repose pas sur des critères anatomiques simples à repérer. Une perspective intéressante serait d'améliorer cette paramétrisation en la basant sur des critères anatomiques mesurables simplement, comme la circonférence du mollet à différentes hauteur sur la jambe. Une paramétrisation plus simple permettrait une utilisation encore plus rapide de la méthode prédictive développée dans cette étude. A plus long terme, une paramétrisation plus complète, comprenant l'intérieur de la jambe (os et tissus mous), représenterait un réel atout pour la modélisation personnalisée.

Le développement d'une méthodologie prédictive et personnalisée pour les pressions d'interface a mis en lumière le rôle des interactions bande-peau. Le développement d'une méthode de mesure de ce coefficient de frottement semble donc nécessaire. Cette méthode devrait être rapide et pourrait être mise en œuvre pour chaque patient en même temps que les mesures de pression. Pour les mesures statiques, l'impact de ce paramètre est peut être limité, mais pour les mesures dynamiques, son rôle est vraisemblablement accru. En effet, lors de la marche, le mouvement du pied tend à faire glisser la bande sur la jambe, pouvant mener à une forte diminution de pression.
Aussi, lors de l'enroulement de la bande sur la jambe, la bande applique un effort de cisaillement sur la peau. Cet effort peut être source d'inconfort pour le patient. De nouvelles études mécaniques pour mieux caractériser ces interactions et comprendre leur rôle dans la génération de pression paraissent donc essentielles.

La pression exercée par une seule bande de compression a fait l'objet d'un très grand nombre d'études expérimentales. Cependant, cette technique ne représente qu'une partie du traitement par compression. La pression résultant de la superposition de bandes de compression, ayant des propriétés mécaniques différentes, reste mal comprise. Il parait donc important de poursuivre l'étude de cette pression d'interface avec une approche mécanique. En plus des paramètres influant sur la pression exercée par une bande seule, les interactions bande-bande jouent un rôle important lors de la superposition. La bande appliquée interagit avec celle déjà posée sur la

jambe. L'effet de l'application de cette bande reste peu compris (la deuxième bande vient-elle augmenter ou réduire la tension dans la première bande?). Ici, en plus de la poursuite des études expérimentales, la simulation numérique pourrait permettre de répondre à certaines de ces interrogations.

Bibliography

[139:2005 05] ISO 139:2005. *Textiles – Standard atmospheres for conditioning and testing*, January 2005.

[21748:2010 10] ISO 21748:2010. *Guidance for the use of repeatability, reproducibility and trueness estimates in measurement uncertainty estimation*, 2010.

[61632 09] DIN 61632. *Verbandmittel – Idealbinden*, 2009.

[Affagard 15] Jean-Sébastien Affagard, Pierre Feissel & Sabine F. Bensamoun. *Identification of hyperelastic properties of passive thigh muscle under compression with an inverse method from a displacement field measurement.* Journal of Biomechanics, vol. 48, no. 15, pages 4081–4086, November 2015.

[Afnor 86] Afnor. *NF G30-102 - Articles de bonneterie - Détermination de la pression de contention*, 1986.

[Agu 99] O. Agu, G. Hamilton & D. Baker. *Graduated compression stockings in the prevention of venous thromboembolism.* British Journal of Surgery, vol. 86, no. 8, pages 992–1004, August 1999.

[Ajayi 92a] J. O. Ajayi. *Effects of Fabric Structure on Frictional Properties.* Textile Research Journal, vol. 62, no. 2, pages 87–93, February 1992.

[Ajayi 92b] J. O. Ajayi. *Fabric Smoothness, Friction, and Handle.* Textile Research Journal, vol. 62, no. 1, pages 52–59, January 1992.

[Ajayi 97] Jo Ajayi & Hm Elder. *Effects of Surface Geometry on Fabric Friction.* Journal of Testing and Evaluation, vol. 25, no. 2, page 182, 1997.

[Al Khaburi 11a] J. Al Khaburi, A.A. Dehghani-Sanij, E.A. Nelson & J. Hutchinson. *The effect of multi-layer bandage on the interface pressure applied by compression bandages.* Engineering and technology, vol. 54, pages 868–873, 2011.

[Al Khaburi 11b] J. Al Khaburi, E. A. Nelson, J. Hutchinson & A. A. Dehghani-Sanij. *Impact of multilayered compression bandages on sub-bandage interface pressure: a model.* Phlebology, vol. 26, no. 2, pages 75–83, March 2011.

[Al Khaburi 12] J. Al Khaburi, A. A. Dehghani-Sanij, E. A. Nelson & J. Hutchinson. *Effect of bandage thickness on interface pressure applied by compression bandages.* Medical Engineering & Physics, vol. 34, no. 3, pages 378–385, 2012.

[Allaert 15] F. Allaert. *Différentes indications de la compression élastique.* Actualités Pharmaceutiques, vol. 54, no. 547, pages 14–20, June 2015.

[Amsler 09] F. Amsler, T. Willenberg & W. Blättler. *In search of optimal compression therapy for venous leg ulcers: A meta-analysis of studies comparing divers bandages with specifically designed stockings.* Journal of Vascular Surgery, vol. 50, no. 3, pages 668–674, September 2009.

[Andreozzi 05] G. Andreozzi, R. Cordova, M. Scomparin, R. Martini, A. D'eri & F. Andreozzi. *Quality of life in chronic venous insufficiency.* International Angiology: A Journal of the International Union of Angiology, vol. 24, pages 272–7, 2005.

[Arshi 12] A. Arshi, A. Jeddi & A. Katbab. *Frictional behavior of plan woven fabrics constructed from polyester and cotton yarns in different environmental conditions.* Journal of Engineered Fabrics & Fibers, vol. 7, no. 2, page 99, June 2012.

[Association 03] European Wound Management Association. *Position document: Understanding compression therapy*, 2003.

[Avril 10] S. Avril, L. Bouten, L. Dubuis, S. Drapier & J.-F. Pouget. *Mixed Experimental and Numerical Approach for Characterizing the Biomechanical Response of the Human Leg Under Elastic Compression.* Journal of Biomechanical Engineering, vol. 132, no. 3, page 031006, 2010.

[Basford 02] J. R. Basford. *The Law of Laplace and its relevance to contemporary medicine and rehabilitation.* Archives of Physical Medicine and Rehabilitation, vol. 83, no. 8, pages 1165–1170, August 2002.

[Beebe-Dimmer 05] J. L. Beebe-Dimmer, J. R. Pfeifer, J. S. Engle & D. Schottenfeld. *The epidemiology of chronic venous insufficiency and varicose veins.* Annals of epidemiology, vol. 15, no. 3, pages 175–184, March 2005.

[Begarin 14] L. Begarin, A. Beaujour, P. Fainsilber, J.-L. Hermil, H. Lévesque & Y. Benhamou. *Compression et ulcère veineux en pratique de ville : une étude observationnelle en médecine générale.* Journal des Maladies Vasculaires, June 2014.

[Benigni 08] J. P. Benigni, J. F. Uhl, A. Cornu-Thénard & E. Blin. *Compression bandages: influence of techniques of use on their clinical efficiency and tolerance.* International Angiology, vol. 27, no. 1, pages 68–73, February 2008.

[Bensamoun 08] S. Bensamoun, L. Wang, L. Robert, F. Charleux, J.-P. Latrive & M.-C. Ho Ba Tho. *Measurement of liver stiffness with two imaging techniques: Magnetic resonance elastography and ultrasound elastometry.* Journal of Magnetic Resonance Imaging, vol. 28, no. 5, pages 1287–1292, November 2008.

[Bercoff 04] J. Bercoff, M. Tanter & M. Fink. *Supersonic shear imaging: a new technique for soft tissue elasticity mapping*. IEEE transactions on ultrasonics, ferroelectrics, and frequency control, vol. 51, no. 4, pages 396–409, April 2004.

[Bergqvist 99] D. Bergqvist, C. Lindholm & O. Nelzén. *Chronic leg ulcers: The impact of venous disease*. Journal of Vascular Surgery, vol. 29, no. 4, pages 752–755, April 1999.

[Bertaux 07] E. Bertaux, M. Lewandowski & S. Derler. *Relationship between Friction and Tactile Properties for Woven and Knitted Fabrics*. Textile Research Journal, vol. 77, no. 6, pages 387–396, June 2007.

[Bhattacharya 12] S. Bhattacharya, T. Shaikh & R. Purushottam Solao. *Development of prototype bandage lapper for constant tension bandaging required for effective medical-clinical treatments*. Journal of Tissue Viability, vol. 21, no. 2, pages 54–63, May 2012.

[BIPM 08] BIPM. *International vocabulary of metrology — Basic and general concepts and associated terms (VIM)*, 2008.

[Blair 88] S.D. Blair, D.D. Wright, C.M. Backhouse, E. Riddle & C.N. Mc Collum. *Sustained compression and healing of chronic venous ulcers*. BMJ, vol. 297, pages 1159–1161, November 1988.

[Bonnaire 14] R. Bonnaire, M. Verhaeghe, J. Molimard, P. Calmels & R. Convert. *Characterization of a pressure measuring system for the evaluation of medical devices*. Proceedings of the Institution of Mechanical Engineers, Part H: Journal of Engineering in Medicine, vol. 228, no. 12, pages 1264–1274, December 2014.

[Bonnaire 15] R. Bonnaire. *Caractérisation mécanique des orthèses : Application aux ceintures de soutien lombaire dans le cadre de la lombalgie*. PhD thesis, Mines Saint-Etienne, 2015.

[Bouten 09] L. Bouten. *Identification des propriétés mécaniques des tissus constitutifs du mollet pour l'étude mécanique de la contention*. PhD Thesis, Ecole Nationale Supérieure des Mines de Saint-Etienne, 2009.

[Boyer 13] G. Boyer, J. Molimard, M. Ben Tkaya, H. Zahouani, M. Pericoi & S. Avril. *Assessment of the in-plane biomechanical properties of human skin using a finite element model updating approach combined with an optical full-field measurement on a new tensile device*. Journal of the Mechanical Behavior of Biomedical Materials, vol. 27, pages 273–282, November 2013.

[Braus 21] H. Braus & C. Elze. Anatomie des Menschen: ein Lehrbuch für Studierende und ärzte, volume 1. J. Springer, 1921.

[Brizzio 10] E. Brizzio, F. Amsler, B. Lun & W. Blättler. *Comparison of low-strength compression stockings with bandages for the treatment of recalcitrant venous ulcers*. Journal of Vascular Surgery, vol. 51, no. 2, pages 410–416, February 2010.

[Butler 55] K.J. Butler, W.T. Cowhig & W.J. Morris. *A Cloth Profile Recorder*. Silk and Rayon Record, July 1955.

[Callam 87] M. J. Callam, D. R. Harper, J. J. Dale & C. V. Ruckley. *Chronic ulcer of the leg: clinical history.* British Medical Journal (Clinical Research Ed.), vol. 294, no. 6584, pages 1389–1391, May 1987.

[Carpentier 04] P. H. Carpentier, H. R. Maricq, C. Biro, C. O. Ponçot-Makinen & A. Franco. *Prevalence, risk factors, and clinical patterns of chronic venous disorders of lower limbs: A population-based study in France.* Journal of Vascular Surgery, vol. 40, no. 4, pages 650–659, October 2004.

[Chassagne a] F. Chassagne, E. Benoist, P. Badel, R. Convert, L. Schacher & J. Molimard. *Characterization of fabric-to-fabric friction: application to medical compression bandages.* Textile Research Journal (submitted).

[Chassagne b] F. Chassagne, C. Helouin-Desenne, J. Molimard, R. Convert, P. Badel & P. Giraux. *Investigation of the impact of calf soft tissue mechanical properties on the variation of interface pressure applied by compression bandages in different body positions.* Phlebology (submitted).

[Chassagne c] F. Chassagne, C. Helouin-Desenne, J. Molimard, R. Convert, P. Badel & P. Giraux. *Superimposition of elastic and non-elastic compression bandages.* Journal of Vascular Surgery (submitted).

[Chassagne d] F. Chassagne, J. Molimard, R. Convert, P. Giraux & P. Badel. *Numerical model reduction for the prediction of interface pressure applied by compression bandages on the lower leg.* IEEE Transactions on Biomedical Engineering (submitted).

[Chassagne 15] F. Chassagne, F. Martin, P. Badel, R. Convert, P. Giraux & J. Molimard. *Experimental Investigation of Pressure Applied on the Lower Leg by Elastic Compression Bandage.* Annals of Biomedical Engineering, vol. 43, no. 12, pages 2967–2977, December 2015.

[Chassagne 16] F. Chassagne, J. Molimard, R. Convert, P. Giraux & P. Badel. *Numerical Approach for the Assessment of Pressure Generated by Elastic Compression Bandage.* Annals of Biomedical Engineering, vol. 44, no. 10, pages 3096–3108, October 2016.

[Chawla 08] A. Chawla, S. Mukherjee & B. Karthikeyan. *Characterization of human passive muscles for impact loads using genetic algorithm and inverse finite element methods.* Biomechanics and Modeling in Mechanobiology, vol. 8, no. 1, pages 67–76, February 2008.

[Christopoulos 88] D. Christopoulos, A. N. Nicolaides & G. Szendro. *Venous reflux: quantification and correlation with the clinical severity of chronic venous disease.* The British Journal of Surgery, vol. 75, no. 4, pages 352–356, April 1988.

[Chung 08] J.-H. Chung, V. Rajagopal, P. M. F. Nielsen & Martyn P. Nash. *Modelling mammographic compression of the breast.* Medical image computing and computer-assisted intervention: MICCAI ... International Conference on Medical Image Computing and Computer-Assisted Intervention, vol. 11, Pt 2, pages 758–765, 2008.

[Clark 03] M. Clark. *Compression bandages : principles and definition.* European Wound Management Association, pages 5–7, 2003.

[Coleridge-Smith 09] P. D. Coleridge-Smith. *Leg ulcer treatment.* Journal of Vascular Surgery, vol. 49, no. 3, pages 804–808, March 2009.

[Cornu-Thenard 94] A. Cornu-Thenard, P. Boivin, J. M. Baud, I. De Vincenzi & P. H. Carpentier. *Importance of the familial factor in varicose disease. Clinical study of 134 families.* The Journal of Dermatologic Surgery and Oncology, vol. 20, no. 5, pages 318–326, May 1994.

[Coull 06] A. Coull, D. Tolson & J. McIntosh. *Class-3c compression bandaging for venous ulcers: comparison of spiral and figure-of-eight techniques.* Journal of Advanced Nursing, vol. 54, no. 3, pages 274–283, May 2006.

[Couzan 09] S. Couzan, C. Assante, S. Laporte, P. Mismetti & J.-F. Pouget. *Étude booster : évaluation comparative d'un nouveau concept de compression élastique dans l'insuffisance veineuse chronique légère et modérée.* La Presse Médicale, vol. 38, no. 3, pages 355–361, March 2009.

[Couzan 12] S. Couzan, A. Leizorovicz, S. Laporte, P. Mismetti, J.-F. Pouget, C. Chapelle & I. Quéré. *A randomized double-blind trial of upward progressive versus degressive compressive stockings in patients with moderate to severe chronic venous insufficiency.* Journal of Vascular Surgery, vol. 56, no. 5, pages 1344–1350, November 2012.

[Dai 07] X.Q. Dai, R. Lui, M. Abel & Y.L. Kwok. *Numerical simulation and prediction of skin pressure distribution applied by graduated compression stockings.* Computaional textile, vol. 55, pages 301–309, 2007.

[Dale 04] J.J. Dale, C.V. Ruckley, B. Gibson, D. Brown, A.J. Lee & R.J. Prescott. *Multi-layer Compression: Comparison of Four Different Four-layer Bandage Systems Applied to the Leg.* European Journal of Vascular and Endovascular Surgery, vol. 27, no. 1, pages 94–99, January 2004.

[Damstra 08] R. J. Damstra, E. R. Brouwer & H. Partsch. *Controlled, comparative study of relation between volume changes and interface pressure under short-stretch bandages in leg lymphedema patients.* Dermatologic surgery, vol. 34, no. 6, pages 773–778; discussion 778–779, June 2008.

[Damstra 13] R. J. Damstra & H. Partsch. *Prospective, randomized, controlled trial comparing the effectiveness of adjustable compression Velcro wraps versus inelastic multicomponent compression bandages in the initial treatment of leg lymphedema.* Journal of Vascular Surgery: Venous and Lymphatic Disorders, vol. 1, no. 1, pages 13–19, January 2013.

[Danielsen 98a] L. Danielsen, S. M. Madsen & L. Henriksen. *Healing of venous leg ulcers. A randomized prospective study of a long-stretch versus short-stretch compression bandage.* Phlebology, vol. 13, no. 2, pages 59–63, June 1998.

[Danielsen 98b] L. Danielsen, S. Munk Madsen, L. Henriksen, J. Sindrup & L.J. Petersen. *Subbandage pressure measurements comparing a long-stretch with a short-stretch compression bandage.* Acta Derm Venerol., vol. 78, pages 201–204, 1998.

[Das 05] A. Das, V. K. Kothari & N. Vandana. *A study of frictional characteristics of woven fabrics.* AUTEX Research Journal, vol. 5, no. 3, September 2005.

[De Bruyne 76] P. De Bruyne & T. Dvorak. *The pressure exerted by an elastic stocking and its measurement.* Medical & biological engineering & computing, vol. 14, pages 94–96, January 1976.

[Demanget 12] N. Demanget, S. Avril, P. Badel, L. Orgéas, C. Geindreau, J.-N. Albertini & J.-P. Favre. *Computational comparison of the bending behavior of aortic stent-grafts.* Journal of the Mechanical Behavior of Biomedical Materials, vol. 5, no. 1, pages 272–282, January 2012.

[Derler 11] S. Derler & L.-C. Gerhardt. *Tribology of Skin: Review and Analysis of Experimental Results for the Friction Coefficient of Human Skin.* Tribology Letters, vol. 45, no. 1, pages 1–27, October 2011.

[Derler 13] S. Derler & G.-M. Rotaru. *Stick–slip phenomena in the friction of human skin.* Wear, vol. 301, no. 1-2, pages 324–329, April 2013.

[Dissemond 16] J. Dissemond, B. Assenheimer, A. Bültemann, V. Gerber, S. Gretener, E. Kohler-von Siebenthal, S. Koller, K. Kröger, P. Kurz, S. Läuchli, C. Münter, E.-M. Panfil, S. Probst, K. Protz, G. Riepe, R. Strohal, J. Traber & H. Partsch. *Compression therapy in patients with venous leg ulcers: Compression in leg ulcers.* Journal der Deutschen Dermatologischen Gesellschaft, vol. 14, no. 11, pages 1072–1087, November 2016.

[Dubuis 11] L. Dubuis. *Biomécanique des tissus mous de la jambe sous compression élastique.* PhD Thesis, Mines Saint-Etienne, 2011.

[Dubuis 12] L. Dubuis, S. Avril, J. Debayle & P. Badel. *Identification of the material parameters of soft tissues in the compressed leg.* Computer Methods in Biomechanics and Biomedical Engineering, vol. 15, no. 1, pages 3–11, January 2012.

[Eklöf 04] B. Eklöf, R. B. Rutherford, J. J. Bergan, P. H. Carpentier, P. Gloviczki, R. L. Kistner, M. H. Meissner, G. L. Moneta, K. Myers, F. T. Padberg, M. Perrin, C. V. Ruckley, P. C. Smith & T. W. Wakefield. *Revision of the CEAP classification for chronic venous disorders: Consensus statement.* Journal of Vascular Surgery, vol. 40, no. 6, pages 1248–1252, December 2004.

[Ferguson-Pell 00] M. Ferguson-Pell, S. Hagisawa & D. Bain. *Evaluation of a sensor for low interface pressure applications.* Medical engineering & physics, vol. 22, no. 9, pages 657–663, November 2000.

[Flaud 10] P. Flaud, S. Bassez & J.-L. Counord. *Comparative In Vitro Study of Three Interface Pressure Sensors Used to Evaluate Medical Compression Hosiery: interface pressure sensors and medical compression hosiery.* Dermatologic Surgery, vol. 36, no. 12, pages 1930–1940, December 2010.

[Floury 96] N.C. Floury, N. Guignon & A. Pinteaux. *Données sociales 1996, la société française.* Edition INSEE, Paris, 1996.

[Franquet 12] A. Franquet, S. Avril, R. Le Riche & P. Badel. *Identification of heterogeneous elastic properties in stenosed arteries: a numerical plane strain study.* Computer Methods in Biomechanics and Biomedical Engineering, vol. 15, no. 1, pages 49–58, January 2012.

[Frauziols 15a] F. Frauziols. *Elastographie ultrasonore des tissus mous du membre inférieur en vue de la caractérisation des effets mécaniques de dispositifs médicaux textiles.* PhD Thesis, Mines Saint-Etienne, 2015.

[Frauziols 15b] F. Frauziols, J. Molimard, L. Navarro, P. Badel, M. Viallon, R. Testa & S. Avril. *Prediction of the biomechanical effects of compression therapy by finite element modeling and ultrasound elastography.* IEEE transactions on bio-medical engineering, vol. 62, no. 4, pages 1011–1019, April 2015.

[Frauziols 16] F. Frauziols, F. Chassagne, P. Badel, L. Navarro, J. Molimard, N. Curt & S. Avril. *In vivo Identification of the Passive Mechanical Properties of Deep Soft Tissues in the Human Leg: In vivo Identification of Passive Mechanical Properties of Leg Soft Tissues.* Strain, vol. 52, no. 5, pages 400–411, October 2016.

[Fung 93] Y. C. Fung. Biomechanics: mechanical properties of living soft tissues. Springer New York, New York, NY, 1993.

[Fung 01] Y. C. Fung & P. Tong. Classical and computational solid mechanics. Numeéro v. 1 in Advanced series in engineering science. World Scientific, Singapore ; River Edge, NJ, 2001.

[Gardon-Mollard 06] C. Gardon-Mollard & A.-A. Ramelet. La compression médicale. 2006.

[Gerhardt 08] L.-C Gerhardt, V Strassle, A Lenz, N.D Spencer & S Derler. *Influence of epidermal hydration on the friction of human skin against textiles.* Journal of The Royal Society Interface, vol. 5, no. 28, pages 1317–1328, November 2008.

[Gerhardt 09] L.-C. Gerhardt, A. Lenz, N. D. Spencer, T. Münzer & S. Derler. *Skin-textile friction and skin elasticity in young and aged persons.* Skin Research and Technology, vol. 15, no. 3, pages 288–298, August 2009.

[Ghosh 08] S. Ghosh, A. Mukhopadhyay, M. Sikka & K.S. Nagla. *Pressure mapping and performance of the compression bandage/garment for venous leg ulcer treatment.* Journal of Tissue Viability, vol. 17, no. 3, pages 82–94, August 2008.

[Gogu 13] C. Gogu, W. Yin, R. Haftka, P. Ifju, J. Molimard, R. Le Riche & A. Vautrin. *Bayesian Identification of Elastic Constants in Multi-Directional Laminate from Moiré Interferometry Displacement Fields.* Experimental Mechanics, vol. 53, no. 4, pages 635–648, April 2013.

[Gupta 08] B. S. Gupta & Textile Institute, editeurs. Friction in textile materials. Woodhead publishing in textiles. CRC Press, 2008.

[Hafner 00a] J. Hafner, I. Botonakis & G. Burg. *A comparison of multilayer bandage systems during rest, exercise, and over 2 days of wear time.* Archives of dermatology, vol. 136, no. 7, pages 857–863, July 2000.

[Hafner 00b] J. Hafner, W. Lüthi, H. Hänssle, G. Kammerlander & G. Burg. *Instruction of Compression Therapy by Means of Interface Pressure Measurement.* Dermatologic Surgery, vol. 26, no. 5, pages 481–488, May 2000.

[Hanna 08] R. Hanna, S. Bohbot & N. Connolly. *A comparison of interface pressures of three compression bandage systems.* British Journal of Nursing (Mark Allen Publishing), vol. 17, no. 20, pages S16–24, November 2008.

[Harwood 08] R J Harwood, P J Weedall & C Carr. *The use of the Kawabata Evaluation System for product development and quality control.* Journal of the Society of Dyers and Colourists, vol. 106, no. 2, pages 64–68, October 2008.

[HAS 10] HAS. *La compression médicale dans les affection veineuses chroniques - Bon usage des technologie de santé*, 2010.

[Hermann 04] D. Hermann, S. S. Ramkumar, P. Seshaiyer & S. Parameswaran. *Frictional study of woven fabrics: The relationship between the friction and velocity of testing.* Journal of Applied Polymer Science, vol. 92, no. 4, pages 2420–2424, May 2004.

[Hibbit 09] K. Hibbit. ABAQUS Theory and User Manuals Version 6.9. USA ABAQUS Inc, 2009.

[Hirai 98] M. Hirai. *Changes in interface pressure under elastic and short stretch bandages during posture changes and exercises.* Phlebology - Venous Forum of the Royal Society of Medicine, vol. 13, pages 25–28, 1998.

[Hirai 09] M. Hirai, K. Niimi, H. Iwata, I. Sugimoto, H. Ishibashi, T. Ota & H. Nakamura. *A comparison of interface pressure and stiffness between elastic stockings and bandages.* Phlebology, vol. 24, no. 3, pages 120–124, June 2009.

[Hirai 11a] M. Hirai, A. Koyama, K. Miyazaki, H. Iwata & Y. Kominami. *Interface pressure and stiffness in different combinations of compression material.* Phlebology, vol. 27, no. 2, pages 82–89, September 2011.

[Hirai 11b] M. Hirai, K. Niimi, K. Miyazaki, H. Iwata, I. Sugimoto, H. Ishibashi, T. Ota & Y. Kominami. *Development of a device to determine the stiffness of elastic garments and bandages.* Phlebology, vol. 26, no. 7, pages 285–291, April 2011.

[Hu 04] J. Hu. Structure and mechanics of woven fabrics. Numeéro 35 in Woodhead Publishing series in textiles. CRC Press [u.a.], Boca Raton, Fla., 2004.

[Huston 08] R. L. Huston. Principles of biomechanics. Mechanical engineering. CRC Press, 2008.

[Int. L. F. 12] Int. L. F. *Best practice for the management of lymphoedema - 2nd edition - Compression therapy: a position document on compression bandaging.* International lymphoedema framework, 2012.

[Jünger 09] M. Jünger, A. Ladwig, S. Bohbot & H. Haase. *Comparison of interface pressures of three compression bandaging systems used on healthy volunteers.* Journal of wound care, vol. 18, no. 11, pages 474, 476–480, November 2009.

[Kamina 09] P. Kamina. Anatomie clinique. Maloine, Paris, 2009.

[Kawabata 80] S. Kawabata. The Standardization and Analysis of Hand Evaluation. Textile Machinery Society of Japan, 2nd edition edition, 1980.

[Keller 09] A. Keller, M. L. Müller, T. Calow, I. K. Kern & H. Schumann. *Bandage pressure measurement and training: simple interventions to improve efficacy in compression bandaging.* International wound journal, vol. 6, no. 5, pages 324–330, October 2009.

[Kothari 94] V. K. Kothari & M. K. Gangal. *Assessment of frictional properties of some woven fabrics.* Indian Journal of Fibre and Textile Research, vol. 19, pages 151–5, September 1994.

[Kumar 13a] B. Kumar, A. Das & R. Alagirusamy. *Characterization of compression bandage.* Science of compression bandage, pages 20–40, 2013.

[Kumar 13b] B. Kumar, A. Das & R. Alagirusamy. *Effect of material and structure of compression bandage on interface pressure variation over time.* Phlebology - Venous Forum of the Royal Society of Medicine, April 2013.

[Kumar 13c] B. Kumar, A. Das & R. Alagirusamy. *Study on interface pressure generated by a bandage using in vitro pressure measurement system.* Journal of the Textile Institute, vol. 104, no. 12, pages 1374–1383, December 2013.

[Kyriacou 98] S. K. Kyriacou & C. Davatzikos. *A biomechanical model of soft tissue deformation, with applications to non-rigid registration of brain images with tumor pathology.* In W. M. Wells, A. Colchester & S. Delp, editeurs, Medical Image Computing and Computer-Assisted Intervention — MICCAI'98, volume 1496, pages 531–538. Springer Berlin Heidelberg, Berlin, Heidelberg, 1998.

[Lafuma 94] A. Lafuma, F. Fagnani, F. Peltier-Pujol & A. Rauss. *Venous disease in France: an unrecognized public health problem.* Journal des Maladies Vasculaires, vol. 14, no. 3, pages 185–9, 1994.

[Lattimer 14] C.R. Lattimer, E. Kalodiki, M. Kafeza, M. Azzam & G. Geroulakos. *Quantifying the Degree Graduated Elastic Compression Stockings Enhance Venous Emptying.* European Journal of Vascular and Endovascular Surgery, vol. 47, no. 1, pages 75–80, January 2014.

[Lee 06] A. J. Lee, J. J. Dale, C. V. Ruckley, B. Gibson, R. J. Prescott & D. Brown. *Compression therapy : effects of posture and application techniques on initial pressures delivered by bandages of different physical properties.* European journal of vascular and endovascular surgery: the official journal of the European Society for Vascular Surgery, vol. 31, no. 5, pages 542–552, May 2006.

[Linder-Ganz 07] E. Linder-Ganz, N. Shabshin, Y. Itzchak & A. Gefen. *Assessment of mechanical conditions in sub-dermal tissues during sitting: a combined experimental-MRI and finite element approach.* Journal of Biomechanics, vol. 40, no. 7, pages 1443–1454, 2007.

[Liu 06] R. Liu, Y.-L. Kwok, Y. Li, T.-T. Lao, X. Zhang & X. Q. Dai. *A three-dimensional biomechanical model for numerical simulation of dynamic pressure functional performances of graduated compression stock-*

ing (GCS). Fibers and Polymers, vol. 7, no. 4, pages 389–397, December 2006.

[Livarinen 11] J. T. Livarinen, R. K. Korhonen, P. Julkunen & J. S. Jurvelin. *Experimental and computational analysis of soft tissue stiffness in forearm using a manual indentation device.* Med. Eng. Phys., vol. 33, no. 10, pages 1245–1253, 2011.

[Logan 92] R.A. Logan, S. Thomas & E.F. Harding. *A comparison of sub bandage pressures produced by experienced and inexperienced bandagers.* Journal of Wound Care, no. 1, pages 23–26, 1992.

[Loram 04] Ian D. Loram, Constantinos N. Maganaris & Martin Lakie. *Paradoxical muscle movement in human standing: Paradoxical muscle movement in standing.* The Journal of Physiology, vol. 556, no. 3, pages 683–689, May 2004.

[Marieb 10] E. N. Marieb & K. Hoehn. Anatomie et physiologie humaines. ERPI, 2010.

[Meissner 07] M. H. Meissner, G. Moneta, K. Burnand, P. Gloviczki, J. M. Lohr, F. Lurie, M. A. Mattos, R. B. McLafferty, G. Mozes, R. B. Rutherford, F. Padberg & D. S. Sumner. *The hemodynamics and diagnosis of venous disease.* Journal of Vascular Surgery, vol. 46, no. 6, pages S4–S24, December 2007.

[Melhuish 00] J. M. Melhuish, M. Clark, R. Williams & K. G. Harding. *The physics of sub-bandage pressure measurement.* Journal of wound care, vol. 9, no. 7, pages 308–310, July 2000.

[Milic 10] D. J. Milic, S. S. Zivic, D. C. Bogdanovic, M. M. Jovanovic, R. J. Jankovic, Z. D. Milosevic, D. M. Stamenkovic & M. S. Trenkic. *The influence of different sub-bandage pressure values on venous leg ulcers healing when treated with compression therapy.* Journal of Vascular Surgery, vol. 51, no. 3, pages 655–661, March 2010.

[Miller 00] K. Miller, K. Chinzei, G. Orssengo & P. Bednarz. *Mechanical properties of brain tissue in-vivo: experiment and computer simulation.* Journal of Biomechanics, vol. 33, no. 11, pages 1369–1376, November 2000.

[Moffatt 02] C. Moffatt. *Four-layer bandaging: from concept to practice.* The international journal of lower extremity wounds, vol. 1, no. 1, pages 13–26, March 2002.

[Moorthy 15] R. Rathina Moorthy. *Surface Friction Characteristics of Woven Fabrics with Nonconventional Fibers and their Blends.* Journal of Textile and Apparel, Technology and Management, vol. 9, no. 3, 2015.

[Mosti 07] G. Mosti & V. Mattaliano. *Simultaneous changes of leg circumference and interface pressure under different compression bandages.* European journal of vascular and endovascular surgery, vol. 33, no. 4, pages 476–482, April 2007.

[Mosti 08a] G. Mosti, V. Mattaliano & H. Partsch. *Inelastic compression increases venous ejection fraction more than elastic bandages in patients with superficial venous reflux.* Phlebology, vol. 23, no. 6, pages 287–294, December 2008.

[Mosti 08b] G. Mosti, V. Mattaliano & H. Partsch. *Influence of Different Materials in Multicomponent Bandages on Pressure and Stiffness of the Final Bandage.* Dermatologic Surgery, vol. 34, no. 5, pages 631–639, May 2008.

[Mosti 10a] G. Mosti & H. Partsch. *Inelastic bandages maintain their hemodynamic effectiveness over time despite significant pressure loss.* Journal of Vascular Surgery, vol. 52, no. 4, pages 925–931, October 2010.

[Mosti 10b] G. Mosti & H. Partsch. *Is low compression pressure able to improve venous pumping function in patients with venous insufficiency?* Phlebology - Venous Forum of the Royal Society of Medicine, vol. 25, no. 3, pages 145–150, June 2010.

[Mosti 11] G. Mosti & H. Partsch. *Compression Stockings with a Negative Pressure Gradient Have a More Pronounced Effect on Venous Pumping Function than Graduated Elastic Compression Stockings.* European Journal of Vascular and Endovascular Surgery, vol. 42, no. 2, pages 261–266, August 2011.

[Mosti 12a] G. Mosti. *Compression and Venous Surgery for Venous Leg Ulcers.* Clinics in Plastic Surgery, vol. 39, no. 3, pages 269–280, July 2012.

[Mosti 12b] G. Mosti & H. Partsch. *High Compression Pressure over the Calf is More Effective than Graduated Compression in Enhancing Venous Pump Function.* European Journal of Vascular and Endovascular Surgery, vol. 44, no. 3, pages 332–336, September 2012.

[Mosti 13] G. Mosti & H. Partsch. *Bandages or Double Stockings for the Initial Therapy of Venous Oedema? A Randomized, Controlled Pilot Study.* European Journal of Vascular and Endovascular Surgery, vol. 46, no. 1, pages 142–148, July 2013.

[Mosti 14] G. Mosti & H. Partsch. *Improvement of Venous Pumping Function by Double Progressive Compression Stockings: Higher Pressure Over the Calf is More Important Than a Graduated Pressure Profile.* European Journal of Vascular and Endovascular Surgery, vol. 47, no. 5, pages 545–549, May 2014.

[Musani 10] M. H. Musani, F. Matta, A. Y. Yaekoub, J. Liang, R. D. Hull & P. D. Stein. *Venous Compression for Prevention of Postthrombotic Syndrome: A Meta-analysis.* The American Journal of Medicine, vol. 123, no. 8, pages 735–740, August 2010.

[Narracott 09] A.J. Narracott, G.W. John, R.J. Morris, J.P. Woodcock, D.R. Hose & P.V. Lawford. *A Validated Model of Calf Compression and Deep Vessel Collapse During External Cuff Inflation.* IEEE Transactions on Biomedical Engineering, vol. 56, no. 2, pages 273–280, February 2009.

[Nelson 12] E. A. Nelson & S. E. M. Bell-Syer. *Compression for preventing recurrence of venous ulcers.* In The Cochrane Collaboration & E. A. Nelson, editeurs, Cochrane Database of Systematic Reviews. John Wiley & Sons, Ltd, Chichester, UK, August 2012.

[Nicolaides 93] A. Nicolaides & D. Christopoulos. *Quantification of venous reflux and outflow obstruction with air-plethysmography.* In Vascular Diagnosis, pages 915–21. Bernstein EF, 1993.

[O'Meara 12] S. O'Meara, N. Cullum, E. A. Nelson & J. C. Dumville. *Compression for venous leg ulcers.* In The Cochrane Collaboration, editeur, Cochrane Database of Systematic Reviews. John Wiley & Sons, Ltd, Chichester, UK, November 2012.

[Ottenio 15] M. Ottenio, D. L. Bader, A. Ní Annaidh, M. D. Gilchrist & K. Bruyère. *Strain rate and anisotropy effects on the tensile failure characteristics of human skin.* Journal of the Mechanical Behavior of Biomedical Materials, vol. 41, pages 241–250, January 2015.

[Papadopoulos 81] N. J. Papadopoulos, M. F. Sherif & E. N. Albert. *A fascial canal for the great saphenous vein: gross and microanatomical observations.* Journal of Anatomy, vol. 132, Pt 3, pages 321–329, May 1981.

[Partsch 99] H. Partsch, G. Menzinger & A. Mostbeck. *Inelastic leg compression is more effective to reduce deep venous refluxes than elastic bandages.* Dermatologic surgery, vol. 25, no. 9, pages 695–700, September 1999.

[Partsch 03a] H. Partsch. *Evidence based compression therapy.* VASA, vol. 62 (S/63), pages 1–39, December 2003.

[Partsch 03b] H. Partsch. *Understanding the pathophysiological effect of compression.* EWMA Position Document. Understanding compression therapy, pages 2–4, 2003.

[Partsch 05a] B. Partsch & H. Partsch. *Calf compression pressure required to achieve venous closure from supine to standing positions.* Journal of vascular surgery, vol. 42, no. 4, pages 734–738, October 2005.

[Partsch 05b] H. Partsch. *The static stiffness index: a simple method to assess the elastic property of compression material in vivo.* Dermatologic surgery, vol. 31, no. 6, pages 625–630, June 2005.

[Partsch 05c] H. Partsch. *The use of pressure change on standing as a surrogate measure of the stiffness of a compression bandage.* European journal of vascular and endovascular surgery, vol. 30, no. 4, pages 415–421, October 2005.

[Partsch 06] H. Partsch, M. Clark, S. Bassez, J.-P. Benigni, F. Becker, V. Blazek, J. Caprini, A. Cornu-Thénard, J. Hafner, M. Flour, M. Jünger, C. Moffatt & M. Neumann. *Measurement of lower leg compression in vivo: recommendations for the performance of measurements of interface pressure and stiffness: consensus statement.* Dermatologic surgery, vol. 32, no. 2, pages 224–232; discussion 233, February 2006.

[Partsch 07] H. Partsch. *Chapter 10 -Mechanism and effects of compression therapy.* In The Vein Book, pages 103–109. Elsevier, 2007.

[Partsch 08] H. Partsch, M. Clark, G. Mosti, E. Steinlechner, J. Schuren, M. Abel, J.-P. Benigni, P. Coleridge-Smith, A. Cornu-ThéNard, M. Flour, J. Hutchinson, J. Gamble, K. Issberner, M. Juenger, C. Moffatt, H. A. M. Neumann, E. Rabe, J.-F. Uhl & S. Zimmet. *Classification of Compression Bandages: Practical Aspects.* Dermatologic Surgery, vol. 34, no. 5, pages 600–609, May 2008.

[Partsch 10] H. Partsch & G. Mosti. *Comparison of three portable instruments to measure compression pressure.* International angiology, vol. 29, no. 5, pages 426–430, October 2010.

[Partsch 14] Hugo Partsch. *Compression for the management of venous leg ulcers: which material do we have?* Phlebology, vol. 29, 1 suppl, pages 140–145, May 2014.

[Partsch 16] H. Partsch, J. Schuren, G. Mosti & J.P. Benigni. *The Static Stiffness Index: an important parameter to characterise compression therapy in vivo.* Journal of Wound Care, vol. 25, no. Sup9, pages S4–S10, September 2016.

[Portnoy 08] S. Portnoy, Z. Yizhar, N. Shabshin, Y. Itzchak, A. Kristal, Y. Dotan-Marom, I. Siev-Ner & A. Gefen. *Internal mechanical conditions in the soft tissues of a residual limb of a trans-tibial amputee.* Journal of Biomechanics, vol. 41, no. 9, pages 1897–1909, January 2008.

[Prestandard 01] CEN European Prestandard. *Medical compression hosiery*, August 2001.

[Rabe 08] E. Rabe, H. Partsch, M. Jünger, M. Abel, I. Achhammer, F. Becker, A. Cornu-Thenard, M. Flour, J. Hutchinson, K. Ißberner, C. Moffatt & F. Pannier. *Guidelines for Clinical Studies with Compression Devices in Patients with Venous Disorders of the Lower Limb.* European Journal of Vascular and Endovascular Surgery, vol. 35, no. 4, pages 494–500, April 2008.

[Rabe 13] E. Rabe, S. Hertel, E. Bock, B. Hoffmann, K.-H. Jöckel & F. Pannier. *Therapy with compression stockings in Germany - results from the Bonn Vein Studies.* Journal der Deutschen Dermatologischen Gesellschaft = Journal of the German Society of Dermatology, vol. 11, no. 3, pages 257–261, March 2013.

[Raj 80] T. B. Raj, M. Goddard & G. S. Makin. *How long do compression bandages maintain their pressure during ambulatory treatment of varicose veins?* The British journal of surgery, vol. 67, no. 2, pages 122–124, February 1980.

[Ramkumar 03] S.S. Ramkumar, D.J. Wood, K. Fox & S.C. Harlock. *Developing a Polymeric Human Finger Sensor to Study the Frictional Properties of Textiles: Part I: Artificial Finger Development.* Textile Research Journal, vol. 73, no. 6, pages 469–473, June 2003.

[Rimaud 14] D. Rimaud, R. Convert & P. Calmels. *In vivo measurement of compression bandage interface pressures: The first study.* Annals of Physical and Rehabilitation Medicine, vol. 57, no. 6-7, pages 394–408, August 2014.

[Robertson 08] L. Robertson, C. Evans & F. G. R. Fowkes. *Epidemiology of chronic venous disease.* Phlebology, vol. 23, no. 3, pages 103–111, June 2008.

[Rohan 13] C.P-Y. Rohan, P. Badel, B. Lun, D. Rastel & S. Avril. *Biomechanical response of varicose veins to elastic compression: A numerical study.* Journal of Biomechanics, vol. 46, no. 3, pages 599–603, February 2013.

[Rohan 15] P.-Y. Rohan, P. Badel, B. Lun, D. Rastel & S. Avril. *Prediction of the Biomechanical Effects of Compression Therapy on Deep Veins Using Finite Element Modelling.* Annals of Biomedical Engineering, vol. 43, no. 2, pages 314–324, February 2015.

[Sackett 96] D. L. Sackett, W. M. Rosenberg, J. A. Gray, R. B. Haynes & W. S. Richardson. *Evidence based medicine: what it is and what it isn't.* BMJ (Clinical research ed.), vol. 312, no. 7023, pages 71–72, January 1996.

[Schuren 08] J. Schuren & K. Mohr. *The efficacy of Laplace's equation in calculating bandage pressure in venous leg ulcers.* WOUNDS UK, vol. 4, no. 2, pages 38–47, 2008.

[Schuren 13] J. Schuren & J. Bichel. *Sub-bandage dynamics: stiffness unravelled.* Veins and Lymphatics, vol. 2, no. 1, March 2013.

[Sengeh 16] D. M. Sengeh, K. M. Moerman, A. Petron & H. Herr. *Multi-Material 3-D Viscoelastic Model of a Transtibial Residuum from In-vivo Indentation and MRI Data.* Journal of the Mechanical Behavior of Biomedical Materials, vol. 59, pages 379–392, June 2016.

[Shepherd 16] Jan Shepherd. *Progressive compression versus graduated compression for the management of venous insufficiency.* British Journal of Community Nursing, vol. 21, Sup 9, pages S13–S18, September 2016.

[Stecco 09] C. Stecco, P. G. Pavan, A. Porzionato, V. Macchi, L. Lancerotto, E. L. Carniel, A. N. Natali & R. De Caro. *Mechanics of crural fascia: from anatomy to constitutive modelling.* Surgical and Radiologic Anatomy, vol. 31, no. 7, pages 523–529, August 2009.

[Stolk 04] R. Stolk, C. P. M. Wegen van der Franken & H. A. M. Neumann. *A method for measuring the dynamic behavior of medical compression hosiery during walking.* Dermatologic surgery, vol. 30, no. 5, pages 729–736; discussion 736, May 2004.

[Takaza 13] M. Takaza, K. M. Moerman & C. K. Simms. *Passive skeletal muscle response to impact loading: Experimental testing and inverse modelling.* Journal of the Mechanical Behavior of Biomedical Materials, vol. 27, pages 214–225, November 2013.

[Thomas 03a] S. Thomas. *The use of the Laplace equation in the calculation of sub-bandage pressure.* European Wound Management Association, no. 3, pages 21–23, 2003.

[Thomas 03b] S. Thomas & P. Fram. *Laboratory-based evaluation of a compression-bandaging system.* Nursing Times, vol. 99, no. 40, pages 24–28, October 2003.

[Thomas 14] S. Thomas. *Practical limitations of two devices used for the measurement of sub-bandage pressure: Implications for clinical practice.* Journal of Wound Care, vol. 23, no. 6, pages 300–313, June 2014.

[Tinsson 10] W. Tinsson. Plans d'expérience: constructions et analyses statistiques, volume 67 of *Mathématiques et Applications*. Springer Berlin Heidelberg, Berlin, Heidelberg, 2010.

[Uhl 05] J-F. Uhl, S. Drapier, I. Gaied & B. Lun. *Pression théorique et pression mesurée in-situ des BMC : apport de l'imagerie médicale et des techniques de simulations numériques.* Phlébologie, vol. 58, no. 2, pages 131–138, 2005.

[Van Der Heide 13] E. Van Der Heide, X. Zeng & M. A. Masen. *Skin tribology: Science friction?* Friction, vol. 1, no. 2, pages 130–142, June 2013.

[Van Loocke 06] M. Van Loocke, C.G. Lyons & C.K. Simms. *A validated model of passive muscle in compression.* Journal of Biomechanics, vol. 39, no. 16, pages 2999–3009, January 2006.

[Vannah 96] W. M. Vannah & D. S. Childress. *Indentor tests and finite element modelling of bulk muscular tissue in vivo.* Journal of Rehabilitation Research and Development, vol. 33, no. 3, pages 239–252, July 1996.

[Veraart 97] J. C. Veraart, G. Pronk & H. A. Neumann. *Pressure differences of elastic compression stockings at the ankle region.* Dermatologic Surgery, vol. 23, no. 10, pages 935–939, October 1997.

[Vicaretti 10] M. Vicaretti. *Compression therapy for venous disease.* Australian prescriber, vol. 33, pages 186–90, 2010.

[Vinckx 90] L. Vinckx, W. Boeckx & J. Berghmans. *Analysis of the pressure perturbation due to the introduction of a measuring probe under an elastic garment.* Medical & Biological Engineering & Computing, vol. 28, no. 2, pages 133–138, March 1990.

[Wang 13] Y. Wang, S. Downie, N. Wood, D. Firmin & X. Y. Xu. *Finite element analysis of the deformation of deep veins in the lower limb under external compression.* Medical Engineering & Physics, vol. 35, no. 4, pages 515–523, April 2013.

[Wiklander 16] K. Wiklander, A. E. Andersson & U. Källman. *An investigation of the ability to produce a defined 'target pressure' using the PressCise compression bandage: An investigation of the ability to produce a target pressure using the PressCise compression bandage.* International Wound Journal, vol. 13, no. 6, pages 1336–1343, December 2016.

[Williams 99] R. J. Williams, D. Wertheim, J. Melhuish & K. G. Harding. *How compression therapy works.* Journal of Wound Care, vol. 8, no. 6, pages 297–298, June 1999.

[Wolsley 00] C. J. Wolsley & P. D. Hill. *Review of interface pressure measurement to establish a protocol for their use in the assessment of patient support surfaces.* Journal of tissue viability, vol. 10, no. 2, pages 53–57, April 2000.

[Wong 12a] I. K. Y. Wong, A. Andriessen, H. E. Charles, D. Thompson, D. T. F. Lee, W. K. W. So & M. Abel. *Randomized controlled trial comparing treatment outcome of two compression bandaging systems and standard care without compression in patients with venous leg ulcers.* Journal of the European Academy of Dermatology and Venereology, vol. 26, no. 1, pages 102–110, January 2012.

[Wong 12b] I.K.Y. Wong, M.B.L. Man, O.S.H. Chan, F.C. Siu, M. Abel & A. Andriessen. *Comparison of the interface pressure and stiffness of four types of compression systems.* Journal of Wound Care, vol. 21, no. 4, pages 161–167, April 2012.

[WUWHS 08] WUWHS. *Principes de bonne pratique : la compression dans les ulcères veineux de jambe. Document de consensus*, 2008.

École Nationale Supérieure des Mines
de Saint-Étienne

NNT : 2017LYSEM015

Fanette CHASSAGNE

BIOMECHANICAL STUDY OF THE ACTION OF COMPRESSION BANDAGES ON THE LOWER LEG

Speciality: Mechanics and Engineering

Keywords: Compression bandages, Interface pressure, Finite element analysis, Clinical study

Abstract:

Compression bandages are commonly used for the treatment of chronic venous insufficiency. They apply a pressure onto the leg, called interface pressure, which is one of the key aspects of the treatment. The objective was to better understand the mechanisms impacting interface pressure applied by compression bandage on the lower leg.

In collaboration with clinicians and a medical devices manufacturer, a biomechanical approach was proposed. This approach was composed of experimental pressure measurements and the numerical simulation of bandage application.

Two preliminary studies, experimental and numerical, showed the limitations of the use of Laplace's Law (current standard) for interface pressure computation. These studies also questioned the possible impact of bandage surface properties (bandage-to-bandage friction coefficient) on interface pressure. They also showed the need to consider soft tissues deformation induced by bandage application.

Two characterization methods were designed for the identification of patient-specific soft tissue mechanical properties and the measurement of bandage-to-bandage friction coefficient.

A new methodology for the prediction of interface pressure was developed thanks to the combination of the numerical simulation of bandage application and the leg geometry parametrization. The results were then confronted to experimental measurements.

Finally, a clinical study was designed to investigate the pressure applied by superimposed compression bandages (very common in clinical practice for the treatment of venous ulcers).

École Nationale Supérieure des Mines
de Saint-Étienne

NNT : 2017LYSEM015

Fanette CHASSAGNE

ÉTUDE BIOMÉCANIQUE DE L'ACTION DES BANDES DE COMPRESSION SUR LE MEMBRE INFÉRIEUR

Spécialité: Mécanique et Ingénierie

Mots clefs : Bandes de compression, Pression d'interface, Modélisation éléments-finis, Etude clinique

Résumé :

Les bandes de compression, couramment utilisées pour le traitement de l'insuffisance veineuse, appliquent une pression sur la jambe, appelée pression d'interface, qui est le principe actif du traitement. L'objectif était de mieux comprendre les mécanismes influençant la pression exercée par une bande de compression sur le membre inférieur.
En lien avec des médecins et un industriel, l'approche biomécanique proposée était composée d'une part expérimentale (mesures de pression d'interface) et d'une part numérique (modélisation éléments-finis de la pose d'une bande).
Deux études préliminaires, expérimentale et numérique, ont montré la limite de l'utilisation de la Loi de Laplace (standard actuel) pour le calcul des pressions d'interface. Ces études ont soulevé des interrogations concernant l'éventuel impact des propriétés de surface des bandes (coefficient de frottement bande-bande) sur la pression. Elles ont aussi montré l'importance des déformations des tissus mous de la jambe induite par l'application de la bande.
Deux méthodes de caractérisation mécanique ont donc été mises en place pour l'identification personnalisée des propriétés mécaniques des tissus mous de la jambe et la mesure du coefficient de frottement bande-bande.
Un nouvel outil de prédiction des pressions d'interface a été développé grâce à la combinaison de la simulation numérique de la pose d'une bande et de la paramétrisation géométrique de la jambe puis il a été confronté aux mesures expérimentales.
Finalement, une étude clinique a été réalisée pour étudier la pression exercée par la superposition de deux bandes de compression (pratique clinique très courante pour le traitement de l'ulcère veineux).